UNIVERSITY OF CALIFORNIA
RIVERSIDE

# GABAergic Remodeling and Astrocyte Dysfunction in Demyelination-Induced Neuronal Hyperexcitability

A Dissertation submitted in partial satisfaction
of the requirements for the degree of

Doctor of Philosophy

in

Biomedical Sciences

by

Andrew S. Lapato

December 2020

Dissertation Committee:
Dr. Seema K. Tiwari-Woodruff, Chairperson
Dr. Devin K. Binder
Dr. Monica J. Carson

The Dissertation of Andrew S. Lapato is approved:

---

---

---

Committee Chairperson

University of California, Riverside

ABSTRACT OF THE DISSERTATION

GABAergic Remodeling and Astrocyte Dysfunction in Demyelination-Induced Neuronal Hyperexcitability

by

Andrew S. Lapato

Doctor of Philosophy, Graduate Program in Biomedical Sciences
University of California, Riverside, December 2020
Dr. Seema Tiwari-Woodruff, Chairperson

## ABSTRACT

Epileptic seizures are diagnosed in patients with the autoimmune demyelinating disease multiple sclerosis (MS) at a rate three times higher than the population overall. Despite prognosticating fulminant course of disease and early mortality, scientific understanding of seizures in MS remains significantly limited. In this series of experiments, we observe electrographic, cellular, and molecular changes engendered by demyelinating disease that may feed into neuronal hyperexcitability and seizures using animal models and postmortem human brain tissue.

We report that mice given 0.2% dietary Bis(cyclohexanone)oxaldihydrazone for up to twelve weeks display electrographic and behavioral seizures. Epileptiform discharges are observed in lateral cortical areas of these mice. In addition, differential changes to electroencephalogram spectral power in cortex and hippocampus in chronically demyelinated mice, suggesting regional heterogeneity in response. Electrographic changes occurred concomitant to GABAergic PV+ cell loss and remodeling of inhibitory synapses, upregulation of hippocampal glutamate receptors, and perturbation of

molecules crucial for astrocyte metabolite handling. Loss of glutamate transporters and water channels were observed in postmortem human hippocampal tissue, bolstering the translational relevance of murine findings. These data suggest poorly constrained glutamatergic signaling pursuant to loss of parvalbumin+ GABAergic innervation, aberrant GluA2+ glutamate receptor expression, and altered astrocytic handling of potassium and glutamate may contribute to demyelination-induced seizures.

TABLE OF CONTENTS

## LIST OF FIGURES

## LIST OF TABLES

## BACKGROUND & INTRODUCTION

Multiple sclerosis (MS) is an autoimmune demyelinating disease of the central nervous system (CNS) that affects roughly 913,925 in the United States (1). Disease onset frequently occurs between ages 20-50 and is diagnosed in women at a rate three times greater than men (2), however pediatric . Neurological symptomology in MS is multifarious and cumulative, owing to the largely non-stereotyped distribution of leukocytic lesions throughout the brain and spinal cord of MS patients (3, 4). Regularly reported complaints include sensorimotor deficit, cognitive & affective impairment, and autonomic dysfunction, but can include more exotic manifestations, such as seizures (1, 2, 5, 6).

Although largely permanent, the rate at which disability in MS is accrued depends on disease phenotype. Relapsing-remitting (RR)MS is the most commonly observed disease course, affecting roughly 85% of patients (2). In this form, periods of relatively little demyelinating activity (remittance) are punctuated by acute flares of multifocal inflammatory lesion deposition (relapse) (2). Among RRMS patients, 65% will undergo conversion into secondary progressive (SP)MS, which is characterized by reduced frequency and intensity of relapses, but ongoing clinical deterioration (7). Roughly 15% of MS patients are diagnosed with primary progressive (PP)MS, which, similar to SPMS, involves fewer relapse-like events, but is associated with more rapid acquisition of disability and does not require a previous RRMS diagnosis (8).

Diagnosing MS can be challenging due to the variety of forms the disease can take at presentation and the requirement of temporal dissemination of demyelinating plaques (2). Magnetic resonance imaging (MRI) is the gold standard used in MS diagnosis in combination with clinical examination (9). According to the widely accepted McDonald criteria, at a minimum, MS diagnosis requires appearance of two or more enhancing

lesions in different CNS sites that correlate with episodes of clinical disease lasting for ≥24 (9). Although lesions can form within any myelinated area, although the white matter tracts surrounding the ventricles and adjacent to the meninges are often attacked, thereby holding some diagnostic value (10). These findings are frequently validated by additional paraclinical measures. In combination with clinical examination, observation of oligoclonal bands when patient cerebrospinal fluid (CSF) is electrophoresed across an agarose gel, which indicates a high degree of immunoglobulin production within the CNS (3).

Etiologically, the factors driving MS predisposition are poorly understood, but likely involve both genetic risk variants & environmental exposure. Genetic risk factors for MS have remained elusive despite strong evidence for familial clustering of the disease. People with an affected immediate family member develop MS 20-40 times more often than someone without such a relation, while concordance among monozygotic twins ranges from 30-50% (4). Perhaps lending credence to the notion that MS arises at the confluence of genetic and risk factors, many of the >200 genetic variants associated with MS are in genes that participate in antigen presentation and lymphocyte function (11).

Of the genetic factors identified, the most significant risk for developing MS comes from the human leukocyte antigen (HLA)-DRB1*1501 variant of the class II major histocompatibility complex (MHC) (12, 13). MHC class II HLA alleles are co-expressed constitutively by professional antigen presenting cells (APCs), such as dendritic cells, B cells, and macrophages (14, 15). Once phagocytosed, cathepsins cleave exogenous peptides and HLA-DM chaperones ready nascent MHC class II molecules for antigen loading before returning to the cell surface (15). Once there, APCs bearing epitope laden MHC class II activate CD4+ T lymphocytes bearing cognate T cell receptors (TCRs) through MHC and co-stimulatory molecule interactions (16, 17).

The strong association between MS & HLA-DRB1*1501 has led some to speculate that HLA-DRB1*1501 bearing a yet-unknown peptide fragment forms a molecular complex similar enough to myelin to cause expansion of autoreactive T cells (18, 19). Lending credence to this model, translational study in mice expressing limited TCR repertoires and the human HLA-DRB1*1501 allele spontaneously develop a form of experimental autoimmune encephalomyelitis (EAE) (20). However, structural analysis of differences in MHC-peptide moieties have not supplied clear answers regarding their involvement in MS pathogenesis: other HLA-DRB1 alleles are indistinguishable at the sequence level at sites known to interact with immunoregulatory molecules (11, 13, 18). Furthermore, the sheer complexity of MHC class II regulation and signaling has led some to question whether HLA-DRB1*1501 may increase MS risk independent of its role in antigen binding (12, 18, 21). While no clear answers exist pertaining to the role of HLA-DRB1*1501 in MS, research is ongoing to determine whether changes to epigenetic or other regulatory elements participate in MS pathogenesis.

Beyond antigen presentation, several immunoregulatory genes display variants associated with enhanced MS risk. Though myriad minor links between MS and a constellation of such genes have been noted, major variants associated with MS are observed in interleukin (IL)-2 receptor(R)A (also called CD25), IL-7R, and TNFRSF1A, the gene that encodes tumor necrosis factor (TNF) receptor 1 (TNFR1) (22-25). Broadly, the products of these genes influence leukocyte survival and response to inflammation but also participate in highly nuanced lymphocyte biology.

Among the most robust findings in genome-wide association studies (GWAS) probing genetic susceptibility to MS is polymorphisms in IL-2 signaling pathways, specifically within the *IL2RA* locus (26). IL-2 is a highly pleiotropic cytokine involved in

both immunological development and immunity, acting on heteromultimeric IL-2 receptors composed of α (IL-2Rα/CD25), β (IL-2Rβ/CD122), & common γ chain subunits (IL-2Rγ/CD132) (27). During T cell maturation, stromal IL-2 mediates negative selection of double-positive thymocytes (28, 29). CD4+ cells secrete low basal levels of IL-2, which it is thought to support regulatory T cell (30) survival and facilitate early T cell expansion, but is rapidly upregulated in response to TCR stimulation (31, 32).

*IL2RA* (the gene encoding CD25/IL-2Rα) polymorphisms linked to MS are associated with elevated concentrations of the soluble form of the receptor (sIL-2Rα) in peripheral blood (24). Although soluble sIL-2Rα is able to neutralize circulating IL-2, the IL-2/CD25 complex formed may retain the ability to signal through membrane bound IL-2Rs or *trans* pathways, offering one possible pathophysiological mechanism for myelin-reactive T cell expansion in the context of MS (33-36). Furthermore, the IL-2Rα polymorphisms observed in MS are associated with enhanced IL-2/STAT5-dependedent granulocyte-macrophage colony stimulating factor (GM-CSF) secretion by CD4+ T cells, which itself comprises a key component of myeloid cell recruitment and proliferation during inflammation (35, 37, 38). IL-2Rα risk alleles may also contribute to Treg hypofunction in MS, whose immunosuppressive effector action issues from IL-2R/STAT5 responsive genes (31, 39, 40). Similarly, variants in the APC-expressed costimulatory molecule CD58 are associated with poor engagement of its receptor CD2 present on Tregs, likely also contributing to poor immunosuppression (41)

Polymorphisms in *IL7R*, which encodes the receptor for IL-7, are also correlated with enhanced MS risk (23). IL-7 is a lymphoid tissue-derived interleukin that signals to lymphocytes through IL-7Rα/CD132 heterodimers, which together comprise the IL-7R (42). In addition to providing survival cues during T & B cell receptor recombination,

ongoing IL-7/IL-7R pathway engagement is required for T cell survival as well as expansion in the context of lymphopenia (42). *IL7R* alleles associated with MS risk increase soluble IL-7Rα, which sequesters and extends the signaling efficacy of IL-7 (43). As the pool of available IL-7 is thought to be significantly restricted and invariant in its production, mutations that enhance IL-7ergic signaling may allow myelin-reactive T cells to evade thymic selection and persist until exposure to their cognate antigen (44).

Although GWAS consistently implicate the TNF pathway in harboring MS risk factors, recent data indicate one possible mechanism contributing to immune dysfunction in MS (45). *TNFRSF1A* variants associated with MS limit the ability of TNF to induce apoptosis by releasing excessive TNF-neutralizing soluble TNFR1 (22). Ongoing research seeks to place the relevance of this finding within the constellation of genetic factors predisposing to MS.

In addition to the immunogenetic variants described above, several factors tied to environmental exposure also correlate strongly with risk of developing MS. Both increasing distance from the equator and little exposure to ultraviolet light are associated with increasing probability of developing MS and may be exacerbated by MS risk alleles that further depress 1,25-dihydroxycholecalciferol (vitamin D) biosynthesis (46-49). Supporting an environmental influence over this risk category, while MS prevalence is low among people living close to the equator, their offspring born in northern latitudes exhibit MS risk closer to that of the population where they live (47). As vitamin D is an essential regulator of immune function, reducing its availability may favor autoimmunity (49).

Infection by Epstein-Barr virus (EBV), a human herpes virus that is a common cause of infectious mononucleosis due to its B cell tropism, may render a susceptible person more likely to develop MS (50-52). The connection between these phenomena is

not wholly described, but is thought to involve training long-lived EBV-infected memory B cells to recognize autoantigens (53). Again highlighting the additive confluence between environmental and genetic risks, HLA-DRB*1501 carriers may be at exceptionally high risk of developing MS after EBV exposure (54).

A theme common to many of the MS risks identified above is insufficient control of inflammatory status — which itself may be a risk factor for MS, especially in conjunction with HLA haplotype. Conditions characterized by multi-organ inflammation, such as adolescent obesity, cigarette smoke exposure, and air pollution, are increasingly recognized as predisposing to MS (55-57). How these environmental stressors specifically raise MS risk is uncertain, but may promote expansion of autoimmune lymphocytes in affected tissues that results in MS progression (58). Support for this hypothesis is bolstered by the multiplicative effect these elements have on MS risk in combination with MS-associated HLA haplotypes, but specific mediators remain elusive (58). Of note, while smoking contributes to MS risk, oral tobacco may be protective, as MS rates are lower among Swedish people that chew tobacco (59). This is potentially mediated by nicotine, which agonizes α7 nicotinic acetylcholine receptors present on activated CD4+ T cells and suppressors their effector function (30). Overall, risk factors contributing to MS are diverse, but conditions that allow evasion of immunoregulatory frameworks or promote lymphocyte proliferation favor development of autoimmune diseases such as MS.

Perhaps owing to its polyfactorial origins, neurological manifestations of MS are diverse, largely unpredictable, and some are poorly understood, such as in the case of MS-induced seizures (60, 61). MS patients are diagnosed with seizure disorders at a rate roughly three times higher than the overall population but the pathophysiology driving their

appearance has not been identified (62, 63). MS with seizures (MS+S) is approximately similar to MS at the level of cellular actors involved in demyelinating lesion formation.

Some debate surrounds the degrees to which autoimmunity and neurodegeneration drive MS pathology, but the result of these processes is foci of lost or thinning myelination with T, B, and phagocytic cell infiltration (64). During early lesion formation, demyelination radiates outward from small post-capillary venous tissue sites, which eventually converge and expand into surrounding white matter as “Dawson’s fingers” (64, 65). During periods of remission, lesions may become inactive, in which lymphocytic invasion subsides despite ongoing decline of axon health (66). Oligodendrocyte precursor cells (OPCs) are attracted to inflammatory demyelination by various chemokine receptors and persist to some extent even in chronic plaques (67, 68). Despite their presence, however, OPC differentiation into remyelinating oligodendrocytes is limited due to reasons encompassing poor penetration into sites of remyelination and direct cytotoxic T cell mediated killing (69, 70). As a result, acute lymphocyte-mediated damage is exacerbated as ongoing loss of homeostatic support mechanisms contribute to protracted neurodegeneration.

While axons are spared to varying levels in individual lesions, profound dysfunction is commonly observed in remaining fibers. In addition to loss of myelin at the site of autoimmune attack, denuded intralesional axons within the lesion undergo various deleterious changes, producing deficits in autonomic, cognitive, motor, sensory, and visual function (6, 71-73). Loss of oligodendrocyte-supplied trophic support, axonal transection, and derangement of internodal voltage gated cation channels all contribute to functional deficits and degeneration of demyelinated neurons (71, 72, 74-76). Further injury arises from energetic deficits as exposure to inflammatory mediators released during

autoimmune attack, such as reactive oxide species & proinflammatory cytokines (IL-1β, TNF, IL-6, IL-17, interferon (IFN)γ, etc), and reduced metabolic support from oligodendrocytes and astrocytes yields mitochondrial dysfunction (77, 78). Thus, the pathophysiology of MS is likely a result of variegated neurodegenerative processes working in parallel.

Despite the breadth of scientific understanding pertaining to MS, seizures that arise during the disease receive little attention. This is despite epidemiological data estimating that the risk of developing a seizure disorder is higher among MS patients than the general population (5, 63, 79, 80). Although classically disregarded clinically as a benign manifestation of MS, the appearance of seizures prognosticates earlier need for mobility devices and mortality (79, 81, 82). Complicating their management, many anti-epileptic drugs exacerbate MS-induced neurological disability, with a significant fraction of patients with seizures displaying pharmacoresistant epilepsies (83, 84). However, despite the deleterious sequelae tied to seizures in MS (MS+S), mechanistic insight regarding their etiology is finite and confined largely to paraclinical study.

MS patients with seizures exhibit a variety of electroencephalographic (EEG) abnormalities that localize to structures demonstrating changes in temporal lobe epilepsy (TLE), hinting at convergent pathology between the two (83-88). In addition to the appearance of diffuse slowing across monitored sites, EEG recordings from MS+S patients display epileptiform spike/wave complexes, high amplitude delta waves, and rhythmic interictal discharges in frontotemporal areas (84-87). Together, these studies confirm that seizures in MS patients are electrographically identifiable and may occur following a recognizable pattern.

Magnetic resonance imaging (MRI) of structures showing EEG aberrations have been edifying in characterizing how lesion distribution differentially partitions in MS+S. More numerous grey matter lesions (GMLs) are seen in MS+S as well as large cortical lesions that extend across adjacent gyri (89, 90). Furthermore, limbic structures that frequently serve as epileptic foci in TLE display significant damage in MS+S, including accumulation of enhancing lesions in the hippocampal formation, cingulate cortex, and insula (91). In addition to accelerated temporal lobe atrophy, MS+S hippocampi and abutting structures harbor nearly four times as many MRI-identified GMLs than MS only (91). These reports bolster a role for inflammatory infiltration in MS epileptogenesis, however, their ability to clarify the cellular mechanism driving seizures in MS is limited.

Direct histological examination of MS+S postmortem tissue is rare and only specifically indicated in a 2016 study by Nicholas et al. (82). Analyzing entorhinal cortex, enhanced thinning of middle temporal gyrus and loss of deep inhibitory GABAergic interneurons not explained by leukocyte infiltration or mitochondrial dysfunction in MS+S specimens (82). Epileptic hippocampi exhibit similar neurodegeneration, with sclerosis and loss of GABAergic cells both commonly identified throughout the hippocampal formation (92, 93). Thus, MS+S pathophysiology has been infrequently probed and significant work remains to fully elucidate its pathophysiology.

In the following chapters, we contribute to scientific apprehension regarding the cellular and functional correlates of seizures in MS. Utilizing functional, in vivo, and ex vivo methodologies, we evaluate how chronic demyelination produces seizures in mice using the cuprizone model of MS. Additionally, we evaluate the translational relevance of data obtained in mice by probing postmortem human hippocampi for biomarkers identified in animal studies. Our data indicate that seizures in MS involve perturbation to

excitatory/inhibitory (E/I) balance issuing from loss of GABAergic cells and synapses. Glutamatergic drive is also putatively enhanced in these animals due to postsynaptic glutamate sensitization as well as dysregulated presynaptic and astroglial control of synaptic glutamate release. Lastly, in addition to reduced glutamate transporter expression, astrocyte-mediated $K^+$ and water homeostasis is putatively altered in demyelinated mice, suggesting neuronal greater excitability and energy demands. In summary, demyelination-induced seizures likely result from polyfactorial E/I imbalance.

**CHAPTER 1 | Chronic demyelination-induced seizures**

Andrew S Lapato[1,3,#], Jennifer I Szu[2,3,#], Jonathan PC Hasselmann[1], Anna J Khalaj[1], Devin K Binder[1,2,3], & Seema K Tiwari-Woodruff[1,2,3]

1. Division of Biomedical Sciences, UCR School of Medicine, Riverside, CA 92521
2. Neuroscience Graduate Program, UCR, Riverside, CA 92521
3. Center for Glia-Neuronal Interaction, UCR School of Medicine, Riverside, CA 92521

# Co-first authors

A version of this chapter is published in *Neuroscience*.

Lapato, A. S. *et al.,* Chronic demyelination-induced seizures. *Neuroscience* **346**, 409-422, doi:10.1016/j.neuroscience.2017.01.035 (2017).

## 1.1 | ABSTRACT

Multiple sclerosis (MS) patients are three to six times more likely to develop epilepsy compared to the rest of the population. Seizures are more common in patients with early onset or progressive forms of the disease and prognosticate earlier disability and death. Grey matter atrophy, hippocampal lesions, interneuron loss, and elevated juxtacortical lesion burden have been identified in MS patients with seizures; however, translational studies aimed at elucidating the pathophysiological processes underlying MS epileptogenesis are limited. Here, we report that cuprizone-mediated chronically demyelinated (9-12 weeks) mice exhibit marked changes in electroencephalography (EEG) and evidence of overt seizure activity. Subsequently, histopathological correlates were probed by immunohistochemistry, revealing extensive demyelination, loss of parvalbumin inhibitory interneurons in the hippocampus CA1 subregion, widespread gliosis and changes to astrocytic aquaporin-4 expression. Our results suggest that chronically demyelinated mice are a valuable model with which we may begin to understand the mechanisms underlying demyelination-induced seizures.

## 1.2 | INTRODUCTION

Multiple sclerosis (MS) is an autoimmune demyelinating disorder of the central nervous system (CNS) that affects roughly 2.3 million people worldwide (94). In the United States, MS prevalence is estimated at 40-177 people per 100,000 (80) and varies with sex, ethnicity, and distance from the equator (95). While MS clinical presentation is multifarious, epidemiological studies show that MS patients are three to six times more likely to develop epileptic seizures than the overall population, with incidence rising with time since MS diagnosis (62, 96-98). Seizures in MS may signal disease onset or relapse in a subset of patients (99, 100) and are associated with diminished cognitive function (90), fulminant disease course, and accelerated time to disability (82, 83). However, despite increased occurrence of seizures among MS patients, little research exists probing their pathogenesis.

Electroencephalography (EEG) recordings from MS patients have revealed aberrant low-amplitude cortical alpha waves and the appearance of delta waves in awake patients, while MS with seizures (MS+S) patients display these changes and exhibit waking theta frequencies and paroxysmal discharges (85, 101). Magnetic resonance imaging (MRI) of MS+S patients demonstrates abundant temporal leukocortical lesions, and hippocampal accumulation of demyelinating foci (86, 91, 102, 103) in addition to findings common to MS, such as global cortical thinning and ventricular hypertrophy (104).

Examining postmortem MS+S entorhinal cortex, Nicholas *et al.* reported augmented middle temporal gyrus thinning relative to other cortical regions and loss of layer IV & VI GABAergic interneurons not explained by leukocyte infiltration or mitochondrial dysfunction (82). This is analogous to findings from epileptic hippocampi, which show loss of pyramidal neurons and GABAergic interneurons throughout the

hippocampal formation (92, 93). Interestingly, MS+S cortical atrophy and neuron loss is localized to structures associated with mesial temporal lobe epilepsy (MTLE) (82, 90), suggesting convergent pathology between MTLE and MS with seizures. However, while the development of seizures secondary to MS has been probed by a limited number of EEG, MRI, and *postmortem* histological studies, little is known regarding its etiology or neuropathology. Furthermore, translational research examining this phenomenon and its origins is restricted to a single 2008 study (105).

Although several well-established mouse models of MS are available (106, 107), the cuprizone (bis-cyclohexanone-oxalyldihydrazone; CPZ) diet was utilized by this study to probe seizures secondary to demyelination. CPZ symptomology is highly reproducible and is thought to be an excellent model of progressive MS (108-110). CPZ neuropathology includes axon damage (111, 112), mitochondrial stress (8, 108), motor deficits primarily relegated to gait ataxias (113), and easily identified tonic-clonic seizures (105, 108).

Early reports examining CPZ intoxication noted convulsions in Swiss mice fed ≥0.3% CPZ for ≥7, but did not investigate their pathogenesis (114, 115). To our knowledge, only one group has previously characterized seizures induced by the lower 0.2% concentration of CPZ currently used to model MS (105). This group observed unusual spiking in intracortical EEG recordings from chronically (≥9 weeks) CPZ demyelinated C57BL/6 mice and degenerating hippocampal neurons but did not identify vulnerable populations or address glial involvement. To elucidate specific cellular involvement, our group examined CA1 electrophysiology and histopathology of mice subject to chronic CPZ-induced demyelination. The hippocampal formation frequently exhibits profound changes in MS (116) and MTLE, and has been implicated as a focus of

seizure initiation (92) and maintenance (117, 118). These changes include loss of inhibitory interneuron populations, degeneration of CA1 principle neurons, and derangement of dentate gyrus projections into CA regions (92, 119). For these reasons, we probed CA1 neuronal pathology, including parvalbumin $(PV)^+$ inhibitory interneurons due to this population's vulnerability in demyelination and seizure models (119-121).

Glia were also assessed, since CPZ induces astrogliosis and phagocyte infiltration at intervals shorter than the chronic model utilized in this study (108, 122-125). In addition, both human postmortem tissue and animal models of seizure show reactive astrocytes, which exhibit increased expression of the intermediate filament glial fibrillary acidic protein (GFAP) and alteration of astrocyte channels, including the water channel aquaporin-4 (AQP4) and the inward rectifying potassium channel Kir4.1, both of which are central to epileptogenesis (92, 126-130).

In this study, we characterize EEG waveforms recorded from within the dorsal hippocampus of chronically demyelinated mice with seizures. Our findings indicate that theta and beta frequency power differ with duration of CPZ administration. Additionally, we describe CA1 neuronal and glial histopathology, including infiltration of microglia/macrophages, appearance of reactive astrocytes, changing AQP4 expression with CPZ duration, pyramidal layer atrophy, and loss of $PV^+$ interneurons. These results lay a solid foundation for the study of seizure development secondary to demyelination and highlight the necessity of additional research into the pathogenesis of this phenomenon.

## 1.3 | MATERIALS & METHODS

*Animals* B6.Cg-Tg(Thy1-YFP)16Jrs/J mice backcrossed to wild type C57BL/6 mice for more than five generations (hereafter referred to as Thy1-YFP mice) were obtained from the Jackson Laboratory (Bar Harbor, ME) and maintained at the University of California Riverside (UCR) animal facility. Originally described by Feng *et al.* (131), Thy1-YFP mice express yellow fluorescent protein (YFP) under the control of a modified mouse *Thy1* promoter construct at high levels, resulting in YFP expression in axons, dendrites, and soma of sensory, motor, and some central neurons with no detectable expression in other cell types. Thy1-YFP mice are healthy and have no distinguishable phenotype aside from neuronal YFP expression. All procedures and experiments were conducted in accordance with the National Institutes of Health (NIH) Guide for the Care and Use of Laboratory Animals and approved by the Institutional Animal Care and Use Committee at UCR.

*Cuprizone treatment* Eight week old male Thy1-YFP mice were assigned to groups that received standard chow (normal; n=10) or 0.2% cuprizone (CPZ)-milled chow (Harlan Teklad, Madison, WI) as detailed in Crawford *et al.* (132) for 9 or 12 weeks—hereafter referred to as 9 wk CPZ (n=10) and 12 wk CPZ (n=9), respectively. Normal mice received standard chow (Picolab, St. Louis, MO) following the same timeline. All groups had access to food and water *ad libidum* and were housed on a 12 hr light/dark cycle under pathogen-free conditions at the UCR animal facility.

*Electroencephalography (EEG) probe preparation* A 3-channel twisted bipolar stainless steel electrode was used for all EEG experiments (Plastics One, Roanoke, VA). The bipolar wires were cut to 2 mm in length for intrahippocampal recordings. Similarly, an epidural ground electrode was cut to 0.5 mm and placed during stereotactic surgery (133).

Approximately 0.5 mm of the insulating coat was removed at the distal tip of the bipolar recording electrode using a scalpel to ensure high-fidelity EEG recordings. Implants were sterilized with 70% ethanol and the ground position on top of the implant pedestal was marked to ensure proper placement of the pins during data acquisition prior to insertion.

*EEG implantation* Unilateral indwelling EEG electrodes were chronically implanted in the right dorsal hippocampus after 8 weeks of CPZ or control chow for longitudinal recordings as detailed in (134). Mice were anesthetized by intraperitoneal (IP) injection of 80 mg/kg ketamine (Phoenix Pharmaceuticals, Burlingame, CA) and 10 mg/kg xylazine (Akron Inc., Lake Forest, IL). Anesthesia was continuously monitored by testing hind limb paw pinch reflex and additional anesthetics were administered as needed. Body temperature was maintained at 37°C using a homeothermic pad. Scalp hair was removed using clippers and depilatory cream (Nair; Church Dwight Company, Inc., Trenton, NJ), then disinfected with betadine solution (Purdue Products, Stamford, CT) and cleaned with 70% ethanol.

Mice were immobilized within a stereotaxic frame (Stoelting, Wood Dale, IL) and a midline incision was made and reflected to expose the skull, which was then cleaned with sterile saline and cotton swabs. Etching gel (Kuraray America, New York, NY) was applied to the skull for 10 s, then washed 2-3 times with sterile saline.

EEG electrodes were implanted 1.8 mm caudal and 1.6 mm lateral to bregma to position probe at the right dorsal hippocampus. A 2 mm diameter craniotomy was performed to accommodate the distance between the recording and ground wires using a high-speed surgical hand drill (Foredom, Bethel, CT) equipped with a 1/4-HP sized carbide bur (SS White, Lakewood, NJ). The skull was cleaned again with sterile saline and the dura was carefully removed using a 27G needle to prevent laceration of the pia or

underlying cortex. Bonding agent (Clearfil photo bond; Kuraray America) was prepared according manufacturer instructions and carefully applied on the skull by microbrush to avoid the brain, then cured until completely set. The EEG implant was then secured onto a probe holder with a side clamp and lowered into the hippocampus until the implant pedestal contacted the top of the skull (2 mm per the length of the probe). After verifying that the implant was in place, permanent cement (Panavia SA Cement; Kuraray America) was applied caudal to the implant and skull, then light cured until set. The side clamp was carefully released and the probe holder was raised. Remaining cement was applied in even layers to the exposed skull and the margins of the scalp to ensure a strong hold.

*Video-EEG recordings* Treatment groups were separated into two subgroups for staggered video-EEG (vEEG) recordings, which were obtained at weeks 9 and 12 for 4 hours per day. Animals 1-3 were recorded on Days 1 and 3, and animals 4-5 were recorded on Days 2 and 4. Control animals were recorded one week after probe implantation. Animals were connected to a tethered EEG recording system via a commutator (Plastics One) connected to a digital EEG acquisition system (MP150, AcqKnowledge 4.4 software) to allow them freedom of motion during data acquisition. Normal EEG output was filtered at 35 Hz (low pass) and 0.1 Hz (high pass) at a gain of 20,000 with a sample rate of 5,000 samples/s. Behavioral activity was recorded using a Sony FDR-AX33 digital video camera (New York, NY) placed in front of the animals' home cages capable of infrared dark phase recording.

*EEG analysis* Mice that had no EEG signal due to poor contact of electrodes resulting from chronic recording were excluded from analysis. One mouse was excluded from the normal group (final n=9) and 3 mice were excluded from the 9 week demyelinated

group (final n=7). No mice were excluded from the 12 wk CPZ group (n=10). Resting EEG data were analyzed using BrainVision Analyzer 2.1 (Brain Products GmbH, Gilching, Germany). Mice were recorded for 4 hrs and the entire recording period was analyzed to avoid bias. Artifacts were removed with semi-automatic procedure in BrainVision Analyzer 2.1 software based on gradient, max-min, and low activity criteria. Resting EEG signals were divided into 1 s segments and Fast Fourier Transform (FFT) was performed on each segment at 1Hz resolution from 1-29 Hz to generate frequency values for each animal in the groups analyzed. Predetermined frequency ranges [Delta (1-4 Hz), Theta (4-7 Hz), Alpha (7-15 Hz), and Beta (15-29 Hz)] were compared by one-way ANOVA with Tukey's post test for multiple comparisons.

*Immunohistochemistry (IHC)* After concluding EEG recordings, all mice, regardless of EEG contract strength (Normal n=10, 9 wk CPZ n=10, 12 wk CPZ n=9), were perfusion fixed and processed for immunohistochemistry (135). Briefly, mice were deeply anesthetized by isoflurane inhalation (Piramal Healthcare, Mumbai, India) and perfused transcardially with cold phosphate buffered saline (PBS, Thermo Fisher Scientific, Waltham, MA) then 10% formalin (Thermo Fisher Scientific). Brains were dissected and post-fixed in 10% formalin (Thermo Fisher Scientific) for 24 hrs, cryoprotected in 30% sucrose (EMD Millipore, Darmstadt, Germany) for 48 hrs, and embedded in gelatin for sectioning. 40 µm coronal sections were cut using a HM525 NX cryostat (Thermo Scientific). Sections containing rostral corpus callosum or dorsal hippocampus were stained by IHC following a previously described protocol (136, 137).

Myelination, gliosis, and CA1 pyramidal cell layer neuron densities were visualized by the following primary antibodies at a concentration of 1:500 in PBS unless otherwise noted: chicken anti-myelin basic protein (MBP; polyclonal, EMD Millipore), rabbit anti-olig2

(polyclonal, Thermo Fisher Scientific), mouse anti-cleaved caspase 3 (1:400, clone AM1.31-11, EMD Millipore), mouse anti-glial fibrillary acidic protein (GFAP; clone 1B4, BD Biosciences, San Diego, CA), rabbit anti-aquaporin 4 (AQP4; polyclonal, EMD Millipore), mouse anti-NeuN (clone A60, EMD Millipore), mouse anti-parvalbumin (PV; 1:400, clone PARV-19, EMD Millipore), mouse anti-adenomatous polyposis coli (CC-1; clone CC-1, Genetex, Irvine, CA), rabbit anti-Ki-67 (1:250, polyclonal, EMD Millipore), and guinea pig anti-doublecortin (DCX; polyclonal, EMD Millipore).

Secondary staining was performed using these polyclonal fluorophore-conjugated antibodies from ThermoFisher Scientific diluted 1:500 unless otherwise noted: goat anti-rabbit IgG (H+L) Cy3 (EMD Millipore), goat anti-mouse IgG (H+L) Alexa Fluor®647 (AF647), goat anti-mouse IgG2a AF647, rabbit anti-goat IgG (H+L) AF647, goat anti-rabbit (H+L) AF647, goat anti-mouse IgG2b AF647, goat anti-guinea pig IgG (EMD Millipore), and donkey anti-chicken IgY Cy3 (EMD Millipore). Nuclei were stained with 4′,6-diamidino-2-phenylindole (DAPI, 2 ng/ml; Molecular Probes) for 15 min after incubation with secondary antibodies and sections were mounted onto positively charged glass slides, allowed to dry, and coverslipped using Fluoromount G mounting medium (Thermo Fisher Scientific).

*Confocal microscopy and analysis* Corpus callosum (CC) and hippocampal CA1 contralateral to probe were imaged using an Olympus BX61 confocal microscope (Olympus America Inc., Center Valley, PA) at 10X or 40X magnification. ≤20 µm thick z-stack projections were compiled using SlideBook 6 software (Intelligent Imaging Innovations, Inc., Denver, CO). Whole coronal section images were acquired at 10X magnification and stitched with Olympus cellSens Software (Olympus America Inc.). Immunostaining was quantified using Fiji version 2.2.0-rc-46/1.50g (NIH). One data point

per stain per animal was entered for each brain region analyzed. To avoid experimenter bias, auto-adjustment of brightness and contrast, as well as threshold of staining signal, was carried out by NIH software. $NeuN^+$, $PV^+$, $GFAP^+$, $Olig2^+$, $CC\text{-}1^+$, Thy1-$YFP^+$ blebs, and Ki-$67^+$ cells were quantified by drawing a region of interest (ROI) around a brain structure to be analyzed (CC, CA1 subfields), measuring the area delineated by the ROI, counting immunoreactive cells within the ROI, then counts were normalized to area measured. GFAP, MBP, and DCX immunoreactive signal intensity was determined by Fiji and normalized to area of ROI. Iba1, AQP4, and $MBP^+$ % area was measured as percent positive immunoreactivity within ROIs.

*Statistical analysis* Statistical analysis was carried out per previously published work (136, 138). All statistics were performed using Prism 6 software (GraphPad Software, La Jolla, CA). Differences were considered significant at $p \leq .05$. P values are represented by the following: *$p \leq 0.05$, **$p \leq 0.01$, ***$p \leq 0.001$, ****$p \leq 0.0001$. Effect size ($\eta^2$) is reported as the fraction of the overall variance of all groups pooled attributable to differences among the group means. EEG and IHC data are presented as mean ± SEM and were analyzed by ordinary one-way ANOVA with Tukey's post test for multiple comparison test to generate p-values. Number of animals in each group ranged from 7-10/group for EEG analysis and 8-12/group for IHC analysis.

## 1.4 | RESULTS

### Chronic cuprizone demyelination-induced behavioral seizures and changes to hippocampal EEG

Thy1-YFP mice fed CPZ diet for 9 weeks (9 wk CPZ) and 12 weeks (12 wk CPZ) appeared somewhat more active to experimenters when undisturbed in their home cages relative to standard diet-fed control (normal) mice, but activity level was not quantified. Overall, non-seizure behavioral changes between groups were minimal and have been described previously (108, 113). Overt seizure-like behavior (**Figure 1.1A**) was observed during handling in approximately 30.0% of 8 wk CPZ mice. Seizure behavior increased to 57.5% in 9 wk CPZ mice and 66.25% in 12 wk CPZ mice (n=20-45 total mice observed over 4 experiments, **Figure 1.1B**). Spontaneous seizures were also seen in mice unperturbed in their home cages during both light and dark cycles by vEEG (Supplemental Video 1 – available online).

Verification and characterization of seizure waveforms in chronically demyelinated mice was performed by intrahippocampal EEG recording. The dorsal hippocampus was selected as the site of implant for its role in seizure initiation and maintenance (92, 117, 118). One week after EEG electrodes were placed, resting state EEG waveforms were acquired to determine if electrical signals corresponded with behavior observed. Mice were awake and freely moving during vEEG recordings (**Figure 1.1A**).

Significant changes to EEG power were observed with chronic demyelination (**Figure 1.1C—D**). 9 wk CPZ mice (n=7) displayed suppressed EEG waveform power compared to normal mice (n=9), but 12 wk CPZ group (n=10) waveform power was equivalent to normal (**Figure 1.1C—D**). Theta, alpha, and beta frequencies were significantly increased in 12 wk CPZ mice compared to 9 wk CPZ mice and delta power

also trended toward increase (**Figure 1.1E**; delta p=0.0573, $\eta^2$=0.2320; theta *p≤0.05, $\eta^2$=0.2928; alpha *p≤0.05 $\eta^2$=0.2571; beta *p≤0.05 $\eta^2$=0.3203). EEG data were analyzed by one-way ANOVA with Tukey's post test for multiple comparisons.

**Demyelination occurs in the corpus callosum and hippocampus of chronically cuprizone-fed mice**

Cuprizone diet causes demyelination throughout the CNS by induction of apoptotic pathways in post-mitotic oligodendrocytes (OLs) secondary to mitochondrial dysfunction and accumulation of reactive oxygen species (108, 139). Montages of coronal brain slices immunostained for myelin basic protein (MBP-green) with nuclei counterstained by 4′,6-diamidino-2-phenylindole (DAPI-red) from normal, 9 wk CPZ and 12 wk CPZ groups showed extensive demyelination in the corpus callosum-CC, cortical hemispheres, and hippocampus-hipp (**Figure 1.2A**). A detailed analysis of CC (**Figure 1.2Bi**) and CA1 SR/SLM subregions contralateral to EEG implant (**Figure 1.2Bii**) revealed a significant decrease in myelin density in the CC (**Figure 1.2C**; 9 wk CPZ vs normal **p≤0.01, 12 wk CPZ vs normal **p≤0.01, $\eta^2$=0.4373) and CA1 SR/SLM subregions (**Figure 1.2G**; 9 wk CPZ vs normal ****p<0.0001, 12 wk CPZ vs normal ****p<0.0001, $\eta^2$=0.7453) of CPZ fed groups.

To investigate the status of OLs in the CNS after chronic demyelination, brain sections were immunostained for the OL lineage-specific transcription factor olig2 (140). No difference was observed in the number of OLs immunostained with olig2 in the CC of any group (**Figure 1.2Bi—D**). Olig2$^+$ OLs were significantly decreased in the CA1 of 12 wk CPZ mice versus normal (**Figure 1.2Bii—H**, *p≤0.05, $\eta^2$=0.2725).

Post-mitotic OLs were identified by positive immunostaining for both olig2 and adenomatous polyposis coli (CC-1), a negative regulator of Wnt/β-catenin signaling in myelinating OLs in the CNS (141). The number of olig2$^+$CC1$^+$ post-mitotic OLs, were decreased by >75% in the CC of 9 wk CPZ and 12 wk CPZ groups (**Figure 1.2E**, 9 wk CPZ vs normal ****p<0.0001, 12 wk CPZ vs normal ****p<0.0001, $\eta^2$=0.8933). Similarly, decreased olig2$^+$CC-1$^+$ OL numbers were observed in the CA1 of 9 wk CPZ and 12 wk CPZ mice relative to normal (**Figure 1.2Biv, I;** 9 wk CPZ vs normal **p≤0.01, 12 wk CPZ vs normal ****p<0.0001, $\eta^2$=0.5471).

To assess the status of ongoing apoptosis in OLs due to CPZ diet, immunostaining for cleaved caspase 3 was performed. In the CC of 9 wk CPZ mice, 46.70±1.784% of olig2$^+$ OLs exhibited cleaved caspase 3 staining, indicating cells committed to apoptosis (142) (**Figure 1.2F**, 9 wk CPZ vs normal ****p<0.0001, $\eta^2$=0.9784). Similarly, apoptotic cells comprised 46.39±1.661% of total olig2$^+$ OL lineage cells in the CC of 12 wk CPZ mice (**Figure 1.2F**, 12 wk CPZ vs normal ****p<0.0001, $\eta^2$=0.9784). Interestingly, although MBP reactivity and olig2$^+$ OL lineage cells were reduced in the CA1 of 9 wk CPZ and 12 wk CPZ mice, significant cleaved caspase 3 immunoreactivity was not observed in either group (**Figure 1.2J**), indicating that olig2$^+$ cell loss was caspase 3 independent. IHC data were analyzed by one-way ANOVA with Tukey's post test for multiple comparisons.

**Microglia/macrophage infiltration, astrogliosis, and dysregulation of AQP4 expression**

Microglia/macrophages expressing ionized calcium-binding adaptor molecule 1 (Iba1), a cytoplasmic protein constitutively expressed by macrophages and microglia

(143), occupied 10.44±1.254% of imaged CA1 in normal mice and 13.26±3.270% in 9 wk CPZ mice (**Figure 1.3C**). Iba1$^+$ immunoreactive area increased more than three-fold in the CA1 of 12 wk CPZ mice to 47.29±10.98% of imaged fields (**Figure 1.3C**, 12 wk CPZ vs normal **p≤0.01, 12 wk CPZ vs 9 wk CPZ **p≤0.01, $\eta^2$=0.5128).

Upregulation of the intermediate filament glial fibrillary acidic protein (GFAP) by reactive astrocytes occurs in the context of inflammatory demyelination and MTLE, confining damage and inflammatory mediators to the area behind the resulting glial scar (144, 145). GFAP$^+$ cells in the CA1 of both 9 and 12 wk CPZ groups displayed hypertrophic morphology characteristic of reactive astrocytes, membrane varicosities, and loss of non-overlapping process domains (**Figure 1.3B**; arrowheads), but these parameters were not quantified. The number of GFAP$^+$ astrocytes significantly increased in the CA1 of 9 wk CPZ (***p≤0.001) and 12 wk CPZ (***p≤0.001) groups compared to normal mice (**Figure 1.3D**, $\eta^2$=0.5658). GFAP staining intensity per astrocyte increased in 12 wk CPZ mice compared to normal, indicating increased GFAP expression per cell in the chronically demyelinated CA1 (**Figure 1.3E**, *p≤0.05, $\eta^2$=0.2514).

The astrocytic water channel aquaporin-4 (AQP4) plays a crucial role in maintaining CNS water and ion homeostasis (129, 146). Perturbations in AQP4 expression and localization has been identified in postmortem sclerotic hippocampal tissue from epileptic donors (147) and translational models of epilepsy (134). In normal mice, AQP4 reactivity covered 8.628±0.6162% of the imaged CA1 and followed vasculature (**Figure 1.3B**). AQP4 immunoreactive area decreased to 4.281±0.4782% in 9 wk CPZ mice, approximately 49% of normal controls (**p≤0.01, $\eta^2$=0.5668), but recovered to 10.64±1.297% in 12 wk CPZ mice (**Figure 1.3F**, 12 wk CPZ vs 9 wk CPZ

****p<0.0001, $\eta^2$=0.5668). IHC data were analyzed by one-way ANOVA with Tukey's post test for multiple comparisons.

**Callosal axon damage, reduced CA1 pyramidal cell layer thickness and loss of parvalbumin$^+$ interneurons in the CA1**

To assess the potential demyelination-induced axon damage blebbing of axonal plasma membranes that is associated with toxic protein accumulation (148) was analyzed in chronically demyelinated brain. The coherent linear morphology of Thy1-YFP$^+$ axons observed in the CC of normal mice was lost with chronic demyelination. Thy1-YFP$^+$ axon varicosities, indicative of transected axons or impaired transport, were observed in 9 wk CPZ and 12 wk CPZ groups (**Figure 1.4A**; arrowheads). Quantification of axon blebs in the CC (**Figure 1.4E**) showed a significant increase in 9 wk CPZ mice (9 wk CPZ vs normal ****p<0.0001, $\eta^2$=0.9258) and 12 wk CPZ compared to normal mice (12 wk CPZ vs normal *p≤0.05, $\eta^2$=0.9258). Blebbing in 9 wk CPZ mice was significantly higher compared to 12 wk CPZ mice (12 wk CPZ vs 9 wk CPZ ****p<0.0001, $\eta^2$=0.9258), possibly reflecting loss of Thy1-YFP$^+$ axons. However, no axon or dendrite swelling/blebbing was observed in the SLM or SR) of any group (**Figure 1.4B**). CA1 stratum oriens (SO) projection blebbing was not quantified due to its proximity to the CC which made distinguishing the two fiber tracts unclear.

Degeneration of hippocampal pyramidal neurons is a feature commonly observed in sclerotic epileptic and MS hippocampi (92, 149). CA1 pyramidal cell layer thickness, measured as height of pyramidal layer nuclei reactive for NeuN, a neuron-specific epitope found on the FOX-3 transcription factor (150), was significantly reduced in the brains of 12 wk CPZ mice relative to normal (**Figure 1.4C & F**; *p≤0.05, $\eta^2$=0.2458). However, total

NeuN$^+$ pyramidal layer neurons did not change between groups (**Figure 1.4C & G**) and did not co-localize with cleaved caspase 3 in groups examined (not shown), suggesting atrophy of neuronal cell bodies and/or dendrites.

The effect of chronic demyelination on neuronal regeneration was assessed by immunostaining for doublecortin (DCX), a microtubule associated protein expressed by newly generated neurons (151) and Ki-67, a nuclear protein expressed by proliferating cells (152). DCX$^+$ cells were not observed in the CA1 of normal mice. However, DCX$^+$ cells with stellate morphology resembling astrocytes or appeared in the CA1 SO and overlying white matter tract of 9 wk CPZ (****$p<0.0001$) and 12 wk CPZ (**$p\leq0.001$) mice, but did not penetrate the pyramidal cell layer (**Figure 1.5A—B)**, $\eta^2=0.6077$). Ki-67$^+$ nuclei were rarely observed in all group analyzed and did not co-localize with DCX$^+$ cells. These data indicate that new neurons did not account for unchanged pyramidal cell numbers despite pyramidal layer thinning during chronic demyelination.

Loss of inhibitory interneuron populations occurs in a variety of disease states, including experimental autoimmune encephalomyelitis (EAE), an autoimmune mouse model of MS, chemical/traumatic seizure induction, MTLE, and human MS lesions (82, 93, 149, 153). Parvalbumin (PV) is expressed by subset of GABAergic interneurons, including basket, axo-axonic, bistratified, and oriens-lacunosum moleculare cells in the hippocampus (119, 120). Quantification of PV$^+$ inhibitory interneuron soma in the CA1 revealed significantly fewer cell bodies in 12 wk CPZ mice compared to normal (**Figure 1.4D & H** *$p\leq0.05$, $\eta^2=0.4372$). IHC data were analyzed by one-way ANOVA with Tukey's post test for multiple comparisons.

## 1.5 | DISCUSSION

Despite increased seizure incidence in MS patients (80), little is known regarding the pathophysiology or risk factors that contribute to epileptogenesis in these patients. We have for the first time demonstrated that long-term CPZ administration reproduces facets of neuropathology observed in human MS patients with seizures (82, 154). We observed changes in intrahippocampal EEG recordings from demyelinated mice that experienced spontaneous seizures during chronic CPZ treatment. Specifically, we found a reduction in EEG power at the 9-week time point, which may reflect the electrophysiological effects of widespread cortical demyelination. Interestingly, we observed recovery of EEG power at the 12-week time point. Future studies will need to assess the timing of onset of spontaneous electrographic seizures in this model as well as the relationship of seizure onset to demyelination and other cellular and molecular changes.

While the pathophysiology leading to seizures in chronic demyelination remains to be elucidated, our results indicate several possibilities. Loss of CA1 $PV^+$ cell bodies suggests impaired inhibition may contribute to seizures during demyelination. $PV^+$ inhibitory interneurons comprise an essential component of the hippocampal timing circuitry crucial to maintaining physiologic seizure resistance (93, 120, 155). Our results mirror models of seizure disorders (93, 119, 156, 157) and autoimmune inflammatory demyelination (149), where drop-out of $PV^+$ immunoreactivity is also observed. Future studies will examine whether CA1 inhibitory interneuron loss is confined to $PV^+$ cells, or extends to other GABAergic populations, such as cholecystokinin octapeptide$^+$ cells which are thought to represent a distinct inhibitory network (158).

CPZ intoxication does not contribute to neuronal pathology directly (108). Neuron sparing in the face of mitochondrial stress imposed by CPZ has been explained by

metabolic coupling to astrocytes, which augment neuronal resilience by carrying out glycolysis in response to energetic deficits (108, 159, 160). In addition to increased numbers of $GFAP^+$ reactive astrocytes, astrocytes displayed crossed domains, membrane blebbing, upregulation of GFAP, and altered AQP4 expression with chronic demyelination concurrent with changes to theta and beta frequency power and spontaneous seizure. Membrane blebbing of astrocyte processes has been shown to precede apoptotic cell death following oxygen-glucose deprivation (161), and is associated with impaired ATP metabolism in other cell types (162). However, whether blebbing observed reflects impaired metabolism or pre-apoptotic astrocytes requires additional investigation.

Recent research illustrates the importance of astrocyte-astrocyte and astrocyte-oligodendrocyte gap junction coupling in maintaining astrocyte homeostatic function and survival (163). Genetic ablation of connexin-30 and connexin-43, two connexin proteins responsible for oligodendrocyte-astrocyte gap junction pairing, leads to marked astrogliosis, myelin vacuolation, and tonic-clonic seizures (163). While astrogliosis begins early with CPZ administration (123), in the chronically demyelinated CNS, loss of astrocyte-oligodendrocyte coupling via gap junctions could feasibly contribute to the seizures and pathological astrocyte morphology that our group observed. In addition, increased expression of the astrocyte gap junction protein connexin-43 and more rapid decay of inward glutamate currents in astrocytes have been shown to accompany kainic acid-induced seizures (164). These changes occur prior to alteration of astrocyte inward potassium currents, indicating that changes in astrocyte coupling with other glia and glutamate buffering may herald the onset of spontaneous seizures in that model. Future studies will probe the extent to which changes in astrocyte-oligodendrocyte gap junctions

are featured in the genesis of seizures in chronic CPZ-mediated demyelination and what consequences these changes may have on glutamate and potassium handling.

Mounting evidence suggests that downregulation of AQP4 is observed in seizure models and may play a role in hyperexcitability leading to seizures (129, 165, 166). Specifically, AQP4 appears to be downregulated during the epileptogenic period in which spontaneous seizures emerge (134, 165, 166). Our results showed a similar pattern, with transient decrease in CA1 AQP4 expression at 9 weeks of demyelination at the earliest onset of observable seizures, then rising at 12 weeks once seizures were well established. Changes in aquaporin expression may be significant as their expression has been shown to trace Kir4.1 localization in astrocytes, implicating the co-involvement of these two molecules in regulating osmolarity that could contribute to perturbation of resting membrane potential and hyperexcitability (129) by increasing extracellular potassium concentration. Additional study is necessary to identify whether alterations in Kir4.1/AQP4 homeostasis contributes to seizure genesis in chronic demyelination. In addition, chronic video-EEG monitoring will be needed to determine the exact time course of onset of spontaneous seizures in the CPZ model, and the site of seizure genesis (hippocampus *vs.* cortex) (105).

The appearance of augmented Iba1$^{+}$ immunoreactivity coinciding with seizures and changes to EEG theta and beta frequency power is congruous with findings from both translational models of epilepsy and analysis of postmortem human tissue (167, 168). Infiltration of microglia/macrophages peaks at 4.5 weeks of CPZ intoxication as is mediated by the chemokines CCL2, CCL3, and CXCL10 (125). However, to the best of our knowledge, no studies have addressed microglia/macrophage behavior in the chronic CPZ model utilized in this study. In mouse models of epilepsy, microglia/macrophages

express so-called M1 pro-inflammatory cytokines such as inducible nitric oxide synthase, tumor necrosis factor α, interleukin (IL)-1β, IL-6, and IL-12 as well as lymphocyte co-stimulatory molecules cluster of differentiation (CD) 80, CD86, and major histocompatibility complex II at high levels (168). M1 polarization may be attributable to signaling by TLR4/MYD88 and purinergic receptors, which play a prominent role in many neuroinflammatory states (169, 170). Determining the phenotype of microglia/macrophages that appear in CA1 during chronic demyelination may help clarify their role in seizures secondary to MS.

Additional research is required to elucidate the pathophysiology underpinning inhibitory cell loss in chronic demyelination with seizures. However, based on our data, it is conceivable that chronic demyelination-induced metabolic dysfunction arising in astrocytes due to oxidative stress or uncoupling from post-mitotic oligodendrocytes could preclude their ability to execute neuroprotective functions such as maintaining physiologic osmolarity and metabolite buffering, thereby leading to loss of vulnerable $PV^+$ neuron and seizures. The resulting release of ATP and inflammatory mediators from hippocampal neurons susceptible to excitotoxic death may then attract microglia/macrophages. Future studies will address the functional correlations of our results, while brain tissue from MS+S patients will be evaluated for markers observed in the present study to establish translational relevance.

Understanding the pathophysiology contributing to seizures in chronic demyelinating disease has implications extending beyond the treatment of MS with epilepsy. Oligodendrocyte death and dysmyelination are frequently noted features of seizure disorders. If a relationship exists between these phenomena and hippocampal GABAergic neuron survival, exposing this framework could inform investigation into novel

therapeutic targets in epilepsy and MS that could prevent seizure-induced demyelination and/or demyelination-induced seizures.

## 1.7 | FIGURES & LEGENDS

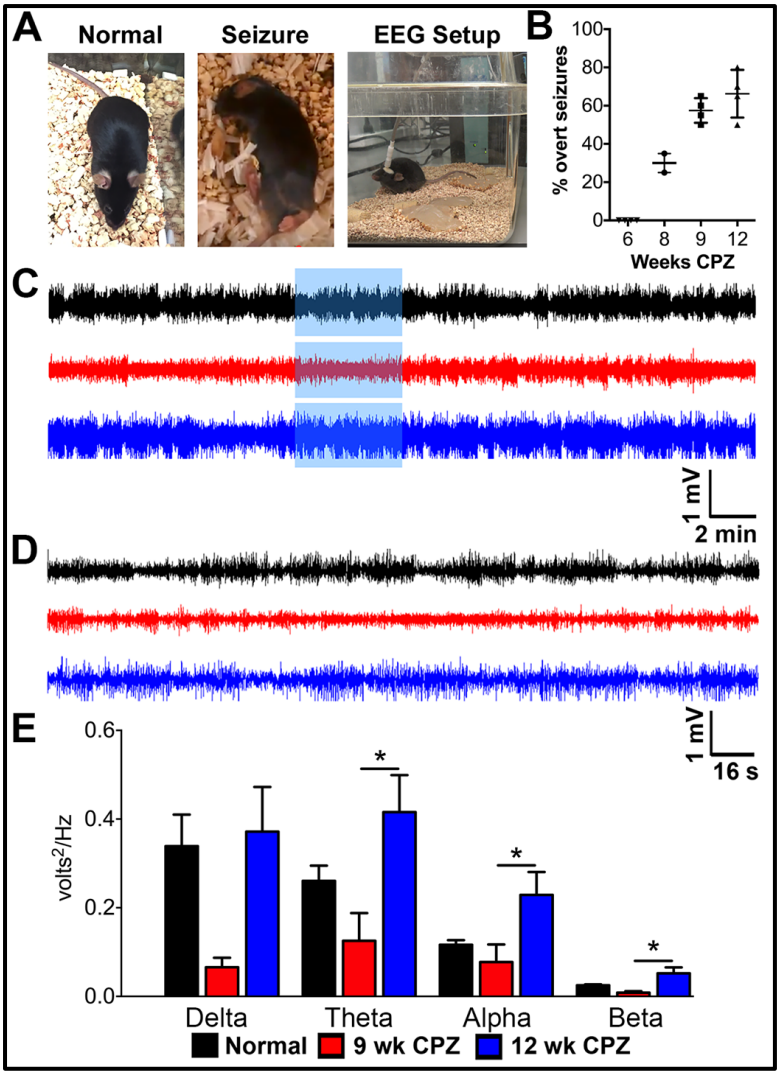


**Figure 1.1 |** *Hippocampal electroencephalogram (EEG) changes occur in chronically demyelinated mice.* **A)** Representative images of a control mouse fed normal diet (normal), an experimental mouse that was fed cuprizone (CPZ) diet for nine weeks (9 wk CPZ) undergoing seizure-like behavior during handling (seizure), and an image of a normal mouse with an intrahippocampal probe tethered to an external EEG recording setup to allow freedom of movement (EEG setup). **B)** Nearly 30% of mice on CPZ diet for 8 weeks presented overt seizure during handling. Seizure activity increased to 55% in 9

wk CPZ mice and 65% in 12 wk CPZ mice (total of 20-45 mice observed over 3 different experiments). **C)** Representative 30 min recordings from a normal, 9 wk CPZ, & 12 wk CPZ animal are shown. **D)** Recording period highlighted in blue box from A was magnified to better assess changes in activity. **E)** Frequency analysis was performed on 4 hours of EEG recordings from the same period in normal [n=9], 9 wk CPZ [n=7], and 12 wk CPZ [n=10] groups. No significant changes were observed in any frequency between normal and 9 wk CPZ groups. Similarly, 12 wk CPZ mice showed power equivalent to normal across all frequencies, but exhibited increased theta, alpha, and beta frequency power compared to 9 wk CPZ (theta *$p \leq 0.05$, $\eta 2 = 0.2928$; alpha *$p \leq 0.05$ $\eta 2 = 0.2571$; beta *$p \leq 0.05$ $\eta 2 = 0.3203$, one-way ANOVA with Tukey's post test for multiple comparisons.

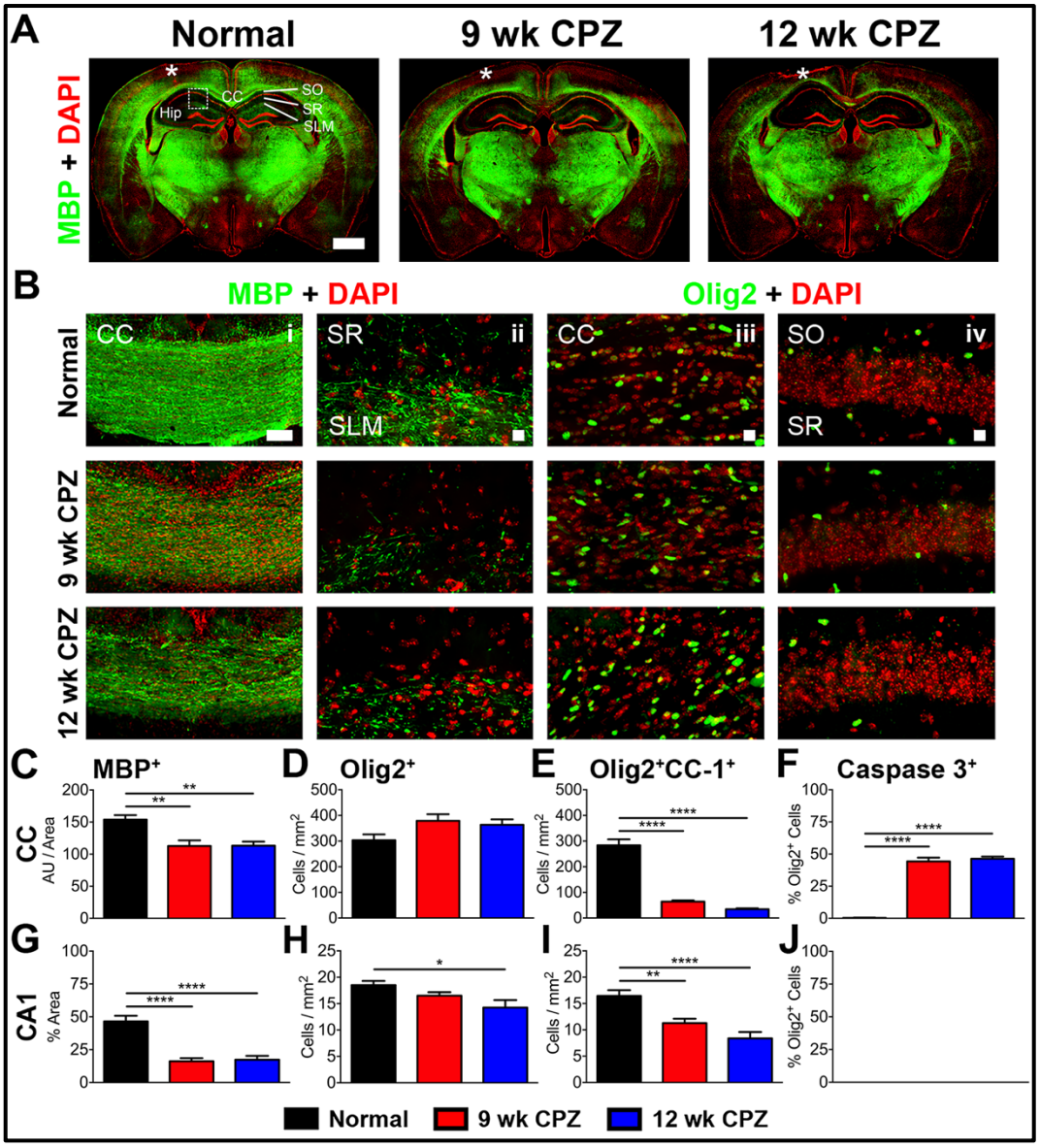


**Figure 1.2 |** *Demyelination in the corpus callosum (CC) and hippocampus (Hip) during chronic cuprizone diet.* **A)** Representative 10X montages of coronal brain section immunostained for myelin basic protein (MBP-green) and double-stranded DNA (DAPI-red) from normal, 9 wk CPZ and 12 wk CPZ mice show decreased MBP staining in the CC and hippocampi of 9 wk CPZ and 12 wk CPZ group. Scale bar: 1 mm, * indicates injury at the site of EEG probe implant. **B)** Representative 10X magnified image of CC,

scale bar 100 μm (i) and 40X magnified image of hippocampus area showing the stratum radiatum (SR) and stratum lacunosum-moleculare (SLM) (ii) immunostained for MBP (green) and DAPI (red) antibodies. A decrease in myelinated fibers was observed in 9 wk and 12 wk CPZ panels. 40X magnified images of the CC (iii) and CA1 (iv) immunostained for olig2 (green) and DAPI (red) were analyzed for olig2$^+$ oligodendrocyte (OL) lineage cell numbers. Scale bar in ii, iii, and iv is 10 μm. **C)** Quantification of MBP staining intensity in the CC normalized to area measured showed a significant decrease in 9 wk CPZ (**p≤0.01) and 12 wk CPZ groups (**p≤0.01) compared to normal mice. 8-10 animals/ group, one-way ANOVA with Tukey's post test for multiple comparisons, $\eta^2$=0.4373. **D)** No difference was identified in the number of olig2$^+$ nuclei counted in the CC of normal, 9 wk CPZ, and 12 wk CPZ mice. 7-10 animals/group, one-way ANOVA with Tukey's post test for multiple comparisons. **E)** Fewer post-mitotic olig2$^+$CC-1$^+$ OLs were counted in the CC of 9 wk CPZ (****p<0.0001) and 12 wk CPZ (***p<0.0001) groups as compared to normal mice. 7-10 animals/group, one-way ANOVA with Tukey's post test for multiple comparisons, $\eta^2$=0.8933. **F)** Apoptotic olig2$^+$caspase 3$^+$ cells accounted for 44.29±2.879% of all olig2$^+$ OL lineage cells in the CC of 9 wk CPZ mice (9 wk CPZ vs normal ****p<0.0001) and 46.39±1.661% of total olig2$^+$ OL lineage cells in the CC of 12 wk CPZ mice (12 wk CPZ vs normal ****p<0.0001). No difference was observed between 9 wk CPZ and 12 wk CPZ groups. 7-10 animals/group, one-way ANOVA with Tukey's post test for multiple comparisons, $\eta^2$=0.9784. **G)** MBP immunostained areas of CA1 SR/SLM subregions were significantly reduced in 9 wk CPZ (****p<0.0001) and 12 wk CPZ groups (****p<0.0001) compared to normal mice. 8-10 animals/group, one-way ANOVA with Tukey's post test for multiple comparisons, $\eta^2$=0.7453. **H)** No significant change was observed in olig2+ OLs between normal and 9wk CPZ mice, but a 20% decrease of olig2$^+$

OLs was observed in 12 wk CPZ compared to normal (*p≤0.05). 8-10 animals/group, one-way ANOVA with Tukey's post test for multiple comparisons, $\eta^2$=0.2725. **I)** Post-mitotic olig2$^+$CC-1$^+$ OLs counted in the CA1 were significantly decreased in 9 wk CPZ mice (**p≤0.01) and 12 wk CPZ mice (****p<0.0001) compared to normal. 9-10 animals/group, one-way ANOVA with Tukey's post test for multiple comparisons, $\eta^2$=0.5471. **J)** Cleaved caspase 3 labeled olig2$^+$ OL lineage cells were not observed in any groups analyzed. 8-10 animals/group, one-way ANOVA with Tukey's post test for multiple comparisons.

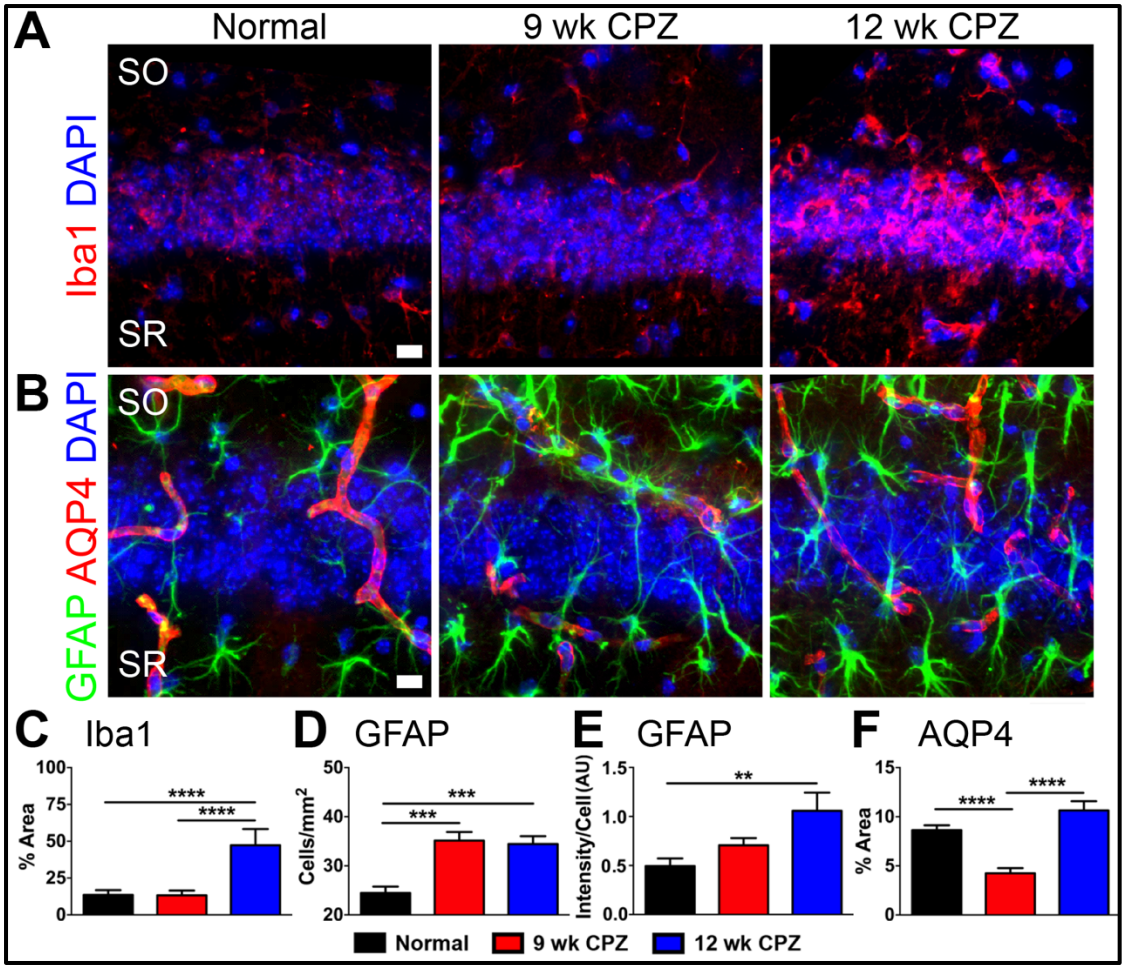


**Figure 1.3 |** *Macrophage/microglia infiltration, reactive astrocytes, and altered AQP4 expression are observed in the CA1 of chronically cuprizone-fed mice with seizures.* **A)** Representative 40X magnification images of Iba1 (red) and DAPI (blue) immunostained CA1 SO/SR from normal, 9 wk CPZ, and 12 wk CPZ mouse coronal brain sections showing increased Iba1 reactivity in 12 wk CPZ mice. Scale bar: 10 μm. **B)** Representative 40X magnification images of GFAP (green), AQP4 (red) immunostaining, and DAPI (blue) stained CA1 SO/SR of normal, 9 wk CPZ, and 12 wk CPZ mice. The number of $GFAP^+$ astrocytes and staining intensity per cell increased in the CA1 of 9 wk and 12 wk CPZ mice and displayed hypertrophic morphology characteristic of reactive

astrocytes, membrane varicosities, and loss of non-overlapping process domains (arrowheads). In normal mice, $AQP4^+$ staining followed vasculature and co-localized with GFAP at the site of astrocyte end foot processes contacting blood vessels. AQP4 staining decreased in 9 wk CPZ mice, but GFAP staining increased proximal to vasculature. AQP4 reactive area returned to normal levels in 12 wk CPZ mice and $GFAP^+$ reactive astrocytes did not accumulate near blood vessels. Scale bar: 10 μm. **C)** $Iba1^+$ immunostaining in the CA1 was quantified as a percent of imaged field in normal, 9 wk CPZ, and 12 wk CPZ mice. $Iba1^+$ microglia/macrophages occupied approximately 10—13% of the imaged CA1 in normal and 9 wk CPZ mice, but increased more than three-fold in 12 wk CPZ mice to 47.29±10.98% (12 wk CPZ vs normal, **p≤0.01; 12 wk CPZ vs 9 wk CPZ **p≤0.01). 7-9 animals/group, one-way ANOVA with Tukey's post test for multiple comparisons, $\eta^2$=0.5128. **D—E)** Astrocytes were quantified by counting number of $GFAP^+$ cells/area. A significant increase was observed in the CA1 of 9 wk CPZ (***p≤0.001) and 12 wk CPZ (***p≤0.001) groups compared to normal mice. Staining intensity per astrocyte also rose significantly in 12 wk CPZ mice compared to normal mice *p≤0.05), indicating increased GFAP expression per cell. 8-10 animals/group, one-way ANOVA with Tukey's post test for multiple comparisons, $GFAP^+$ cells/$mm^2$ $\eta^2$=0.5658; GFAP intensity per cell $\eta^2$=0.2514. **F)** AQP4 reactive area was significantly decreased in the CA1 of 9 wk CPZ mice compared to normal (**p≤0.01) and 12 wk CPZ groups (****p<0.0001). 7-10 animals/group, one-way ANOVA with Tukey's post test for multiple comparisons, $\eta^2$=0.5668.

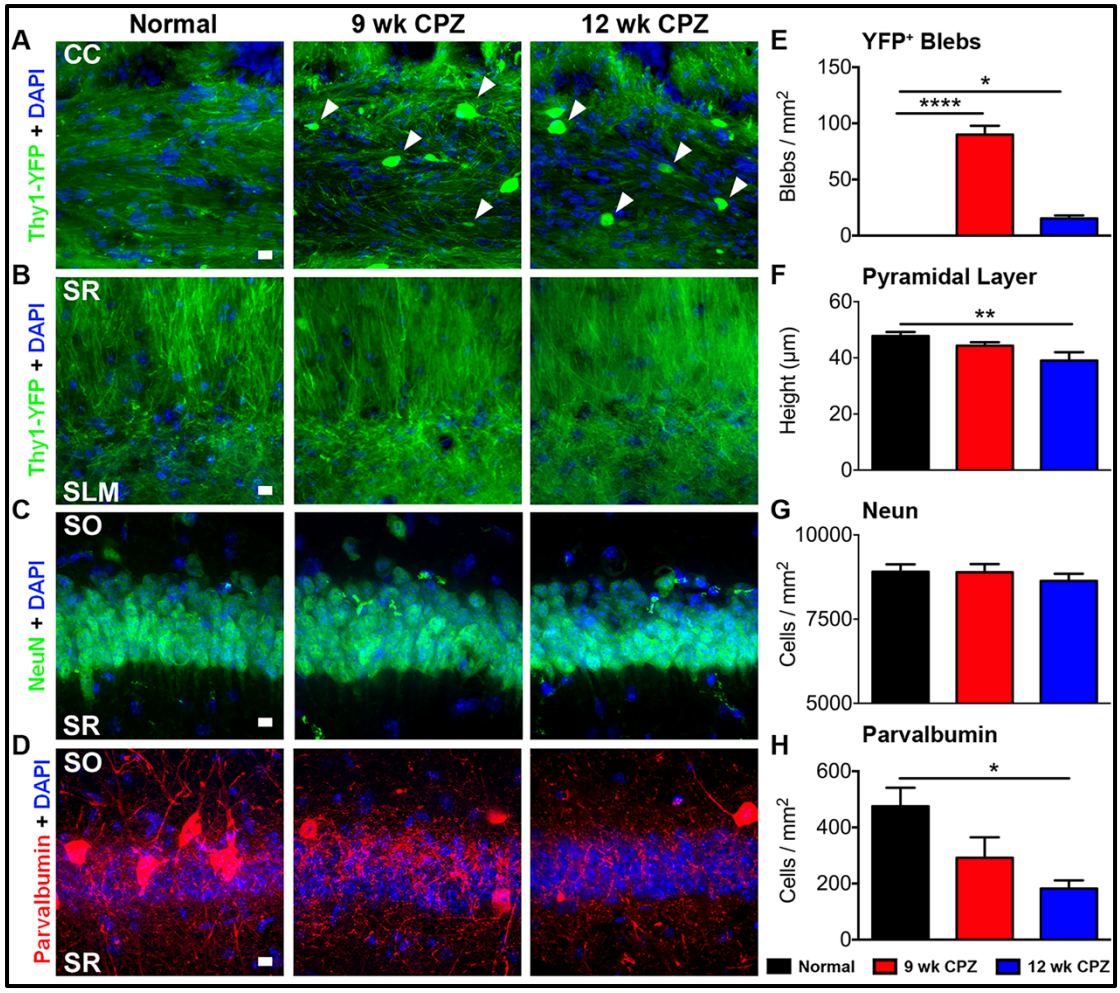


**Figure 1.4 |** *CC axon pathology, reduced CA1 pyramidal cell layer thickness and loss of PV immunostaining in the CA1 of chronically demyelinated mice with seizures.* **A—B)** Representative 40X magnification images from normal, 9 wk CPZ, and 12 wk CPZ coronal brain sections showing the CC and the SR/SLM regions of the CA1. The coherent linear morphology of Thy1-YFP$^{+}$ axons in the normal CC was lost with chronic demyelination. Thy1-YFP$^{+}$ axon varicosities (arrowheads), indicative of transected axons or impaired protein transport, were observed in 9 wk and 12 wk CPZ groups. No axon or dendrite swelling/blebbing was observed in SR or SLM. Scale bar: 10 µm. **C—D)** Representative 40X magnification images of CA1 pyramidal layer immunostained for NeuN+ (green),

DAPI, (blue), and parvalbumin (PV; red) from normal, 9wk CPZ and 12 wk CPZ groups. A decrease in overall CA1 pyramidal neuron layer thickness and loss of $PV^+$ neurons was observed in 9 wk CPZ and 12 wk CPZ CA1 pyramidal layer. Scale bars: 10 μm. **E)** Quantification of axon blebs in the CC showed a significant increase in both 9 and 12 wk CPZ groups compared to the normal group (9 wk CPZ vs normal ****$p<0.0001$; 12 wk CPZ vs normal *$p\leq0.05$). Blebbing in the CC of 9 wk CPZ mice was significantly higher than 12 wk CPZ mice (****$p<0.0001$), reflecting fewer Thy1-YFP callosal axons. 8-10 animals/group, one-way ANOVA with Tukey's post test for multiple comparisons, $\eta^2=0.9258$. **F—G)** Quantification of pyramidal cell layer thickness was determined by measuring the total height of $NeuN^+$ nuclei in the pyramidal cell layer. Compared to normal, a significant decrease was observed in pyramidal cell layer thickness of 12 wk CPZ mice (*$p\leq0.05$). However, total pyramidal layer NeuN+ neurons were not statistically different between groups. 8-10 animals/group, one-way ANOVA with Tukey's post test for multiple comparisons; pyramidal layer height $\eta^2=0.2458$. **H)** Quantification of $PV^+$ interneuron soma in the CA1 region pyramidal cell layer showed a significant decrease in only 12 wk CPZ mice *$p\leq0.05$) as compared to normal group. 8-10 animals/group, one-way ANOVA with Tukey's post test for multiple comparisons, $\eta^2=0.4372$.

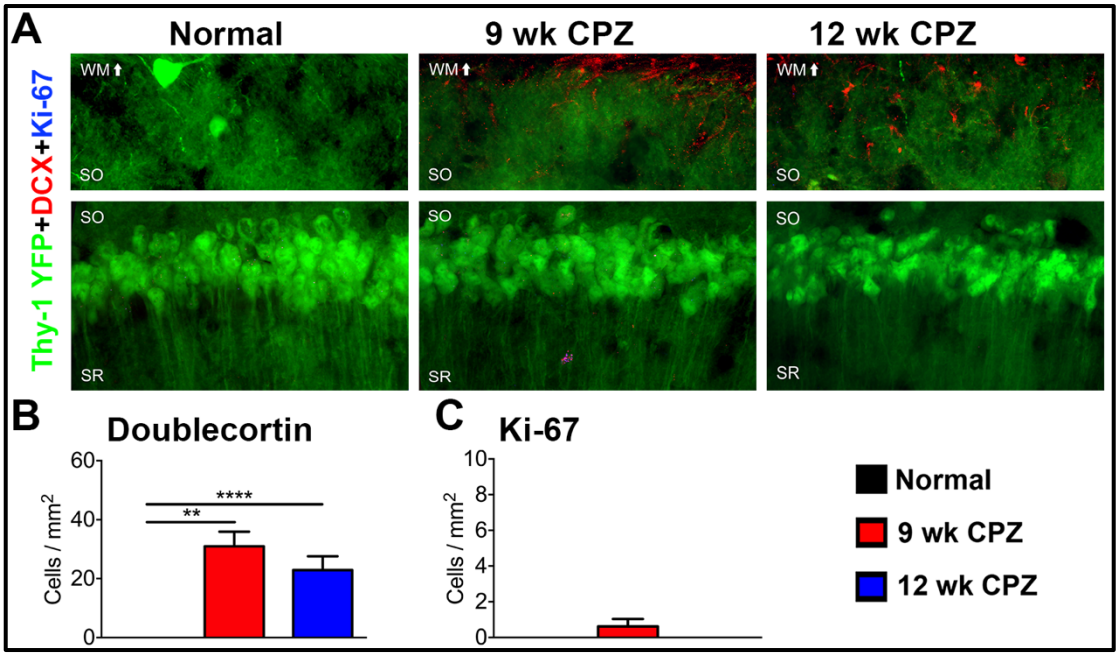


**Figure 1.5 |** *Status of Ki-67$^+$ doublecortin$^+$ cell population in the CA1 of chronically demyelinated mice with seizures.* **A)** Representative 40X magnified images of CA1 pyramidal cell layer immunostained for doublecortin (DCX) and Ki-67 in normal, 9 wk CPZ, and 12 wk CPZ mice. DCX$^+$ cells with stellate morphology resembling astrocytes or microglia were observed in the CA1 SO and overlying white matter tract of 9 wk CPZ and 12 wk CPZ mice. Ki-67$^+$ nuclei were rarely detected in the CA1 of any group, and did not co-localize with DCX. Scale bar: 10 μm. **B)** DCX$^+$ cells were significantly increased in the CA1 SO of 9 wk CPZ (****$p<0.0001$) and 12 wk CPZ mice mice (**$p\leq0.01$). 8-9 animals/group, one-way ANOVA with Tukey's post test for multiple comparisons, $\eta^2=0.6077$. **C)** Ki-67$^+$ nuclei counted were not significantly different between groups. 8-9 animals/group, one-way ANOVA with Tukey's post test for multiple comparisons.

**CHAPTER 2 | Astrocyte glutamate uptake and water homeostasis are dysregulated in the hippocampus of multiple sclerosis patients with seizures**

Andrew S Lapato[1,3], Sarah M. Thompson[3,4], Karen Parra[3,4], Seema K Tiwari-Woodruff[1,2,3]

1. Division of Biomedical Sciences, UCR School of Medicine, Riverside, CA 92521
2. Neuroscience Graduate Program, UCR, Riverside, CA 92521
3. Center for Glia-Neuronal Interaction, UCR School of Medicine, Riverside, CA 92521
4. Undergraduate Programs, UCR, Riverside, CA 92521

A version of this chapter has been accepted for publication pending revision.

Lapato, A. S., Thompson, S. M., Parra, K. & Tiwari-Woodruff, S. K. Astrocyte glutamate uptake and water homeostasis are dysregulated in the hippocampus of multiple sclerosis patients with seizures. ASN Neuro (accepted) (2020).

## 2.1 | ABSTRACT

While seizure disorders are more prevalent among multiple sclerosis (MS) patients than the population overall and prognosticate earlier disability and death, their etiology remains unclear. Translational data indicate perturbed expression of astrocytic molecules contributing to homeostatic neuronal excitability, including water channels (AQP4) and synaptic glutamate transporters (EAAT2) in a mouse model of MS with seizures (MS+S). However, astrocytes in MS+S have not been examined. To assess the translational relevance of astrocyte dysfunction observed in a mouse model of MS+S, demyelinated lesion burden, astrogliosis, and astrocytic biomarkers (AQP4/EAAT2/CX43) were evaluated by immunohistochemistry in postmortem hippocampi from MS (n=5) & MS+S (n=13) donors. Relative to MS only, hippocampal astrocytes from MS+S patients display regional differences in expression of molecules associated with glutamate buffering and water homeostasis that could exacerbate neuronal hyperexcitability. Importantly, mislocalization of CA1 perivascular AQP4 seen in MS+S is analogous to epileptic hippocampi without a history of MS, suggesting convergent pathophysiology.

## 2.2 | INTRODUCTION

Multiple sclerosis (MS) is an autoimmune demyelinating disease of the central nervous system (CNS) that affects roughly 913,925 in the United States (1). Neurological symptomology in MS is multifarious owing to the largely non-stereotyped distribution of leukocytic lesions throughout the brain and spinal cord of MS patients. In addition to the loss of myelin at the site of autoimmune attack, denuded axons within the lesion undergo various deleterious changes (71, 72), producing deficits in autonomic, cognitive, motor, sensory, and visual function (6). While these outcomes are well-characterized, epileptic seizures are observed at a rate three times higher in MS patients than the population overall but the pathophysiology driving their appearance is poorly understood (62, 63).

Both partial and generalized seizures are commonly identified in MS patients with seizure disorders (MS+S), although primary and secondary generalized subtypes account for approximately 67% of cases (5, 87, 171-173). Unusual seizure manifestations are also reported by these patients, including dysphasic/aphasic status epilepticus and musicogenic seizures (174-176). Seizures may herald or occur concomitant to relapse in a subset of MS+S patients (63, 96, 100, 172, 177) and rise in incidence with disease duration (83, 84, 96, 178). Although their etiology remains unclear, seizures in MS are associated with poor response to traditional anti-epileptic drugs (AEDs) which include worsening of MS-induced neurological dysfunction, aggressive disease, and accelerated time to disability and death (63, 87, 178-180). While seizures in MS produce significantly worse health outcomes and are poorly controlled by current AEDs, their pathophysiology and risk factors are poorly understood.

Though limited in number, paraclinical studies examining MS+S have yielded some insight into distinguishing features of seizures arising during MS. MS patients with

seizures exhibit a variety of electroencephalographic (EEG) abnormalities that localize to structures associated with seizure in temporal lobe epilepsy, suggesting commonality between the two disorders. In addition to a varying degree of diffuse slowing across monitored sites, EEG recordings from MS+S patients display sharp- and slow-wave complexes, high amplitude delta waves, and rhythmic interictal discharges in frontotemporal areas (84-87). In addition to possessing possible diagnostic value, these studies confirm that seizures in MS patients are electrographically identifiable and may follow a similar course of disease.

Magnetic resonance imaging (MRI) studies examining cortical structures showing EEG irregularities in MS+S patients have identified differences in lesion phenotype and distribution relative to MS patients without seizures. Along with abundant grey matter lesions (GMLs), large cortical lesions that extend across adjacent gyri are observed in MS+S more frequently that other MS patients (89, 90). Subcortical areas are similarly affected in MS+S: limbic structures implicated as seizure foci in patients with temporal lobe epilepsy display significant damage, including accumulation of enhancing lesions in the hippocampal formation, cingulate cortex, and insula (91). In addition to showing temporal lobe atrophy that outpaces other cortical areas, MS+S hippocampi harbor nearly four times as many MRI-identified GMLs than MS only, with similarly high ratios observed in abutting structures (91). While these studies support a role for enhanced inflammatory lesion burden in MS patients with seizures, their ability to clarify the cellular mechanism driving seizures in MS is limited. Thus, direct observation of possible cellular and molecular players in the etiology of MS+S is warranted.

## 2.3 | MATERIALS & METHODS

*Human postmortem hippocampal specimens* Human tissue was acquired from the NIH NeuroBioBank/HBSFRC at UCLA with a history of MS preceding seizure disorder diagnosis. Tissues arrived with limited cause of death and neuropathology reports with all identifying patient data removed. EDSS scores or frequency of seizures was not disclosed in specimen information provided. Donor age at death, autolysis time, and cohort gender composition is presented in **Table 1**. Due to anatomical variability in HBSFRC samples, not all sections contained all hippocampal subregions analyzed, leading to *n* values below cohort totals.

*Brain Slice integrity and identifications of structures to compare* Initially, slices from all postmortem specimens were Nissl stained to assess tissue integrity and delineate anatomical boundaries of subregions. Most, but not all, slices displayed coronally sectioned hippocampal formation with abutting structures as depicted in **Figure 2.1**. Cornu Ammonis (CA)1, CA3 and dentate gyrus (DG) were identified based on cytoarchitecture (**Figure 2.1A—C**) and mapped for subsequent analysis and comparison. These subregions were chosen as they represent most major functionally distinct gray matter structures participating in the hippocampal trisynaptic circuit (181) and frequently display pathological changes in epilepsy (92). In nearly 1/3$^{rd}$ of brain slices, DG was either only partially represented or absent. CA1 & CA3 were analyzed in these specimens but no data was acquired for DG comparisons.

*Immunohistochemistry (IHC)* Tissues were received from HBSFRC frozen, whereupon they were gradually thawed at 4 °C followed by two hours fixation in 10% neutral buffered formalin (Fisher Scientific, Hampton, NH) at the same temperature.

Following incubation, specimens were cryoprotected in 30% w/v sucrose in phosphate buffered saline (PBS) with 0.2% w/v $NaN_3$ (both Millipore Sigma, St. Louis, MO) and incubated at 4 °C until tissue density exceeded the sucrose solution. Once cryoprotection was complete, specimens were embedded in Tissue-Tek Cryo-OCT compound (Andwin Scientific, Los Angeles, CA) and 40 µm sections were cut using an HM525 cryostat (Thermo Fisher Scientific, Waltham, MA) and stored in PBS with 0.1% w/v $NaN_3$ 4 °C until use.

40 µm free floating postmortem hippocampal specimens were immunostained following a previously described procedure (136, 137). All antibodies & dilutions used in the present study are denoted in **Table 2** (obtained from Millipore Sigma & Invitrogen, Carlsbad, CA). Primary antibodies were diluted in PBS and detection antibodies were diluted in tris-buffered saline (TBS). For chromogen myelin labeling, after incubation with horseradish peroxidase (HRP)-conjugated detection antibody, MOG immunoreactivity was visualized using the 3,3'-diaminobenzidine (DAB) Peroxidase (HRP) Substrate Kit (Vector Laboratories, Burlingame, CA), mounted to slides, counterstained with Hematoxylin QS (Vector Laboratories), then cover-slipped using Permount non-aqueous medium (Fisher Scientific). For fluorescent microscopy, after incubation with fluorophore-conjugated antibodies, sections were counterstained in TBS containing 4',6-diamidino-2-phenylindole (DAPI, 2 ng/ml; Molecular Probes), mounted on glass slides, and cover-slipped in Fluoromount G aqueous medium (Thermo Fisher Scientific).

*Imaging and Quantification* Chromogen-stained hippocampi were imaged using a Leica DM5500 B upright transmitted light microscope (Leica Microsystems Inc., Buffalo Grove, IL) at 5X magnification, then stitched into segments using a pairwise-stitching algorithm (182) included with the Fiji ImageJ package (183), and segments were

assembled in Adobe Illustrator (Adobe Inc., San Jose, CA). Fluorescence micrographs were acquired on an Olympus BX61 confocal microscope (Olympus America Inc., Center Valley, PA) at 20X magnification. ≤20 μm thick z-stack projections were compiled using SlideBook 6 software (Intelligent Imaging Innovations, Inc., Denver, CO) or Olympus cellSens software (Olympus America Inc.).

Image analysis was carried out in Fiji software. Data points represent average values for two fields of view per area per donor sample. Fields were selected away from active lesions and large white matter tracts to assess normal appearing gray matter, equating to stratum radiatum in CA1 & CA3 and hilus in DG. Lesion density was calculated by delineating rough lesion borders in stitched images then normalizing lesion counts to total area within each of the 3 subregions analyzed. Signal intensity (mean gray value) was measured in regions of interest containing CA1/CA3 stratum radiatum and pyramidal cell layer or hilus/CA4 for DG and normalized to minimum/maximum values for the entire HBSFRC cohort.

*Statistical analysis* Statistical analysis was carried out per previously published work (136, 184). All statistics were performed using Prism 8 software (GraphPad Software, La Jolla, CA). Differences were considered significant at $p \leq 0.05$ and denoted by the addition of an asterisk (*) above the statistically different data sets. All statistical tests used to determine significance are noted in corresponding figure legends. *N* values included in each analysis are represented as individual points in scatter plots shown. Anatomical variation within HBSFRC tissues circumscribed the number of specimens available for DG analysis, leading to reduced data points within those plots.

## 2.4 | RESULTS

### HBSFRC cohort demographic data

Hippocampi from 21 MS and 7 MS+S donors were obtained from the HBSFRC (**Table 2.1**). The MS only cohort was 57.1% female and 42.9% male and was composed of donors with relapsing-remitting MS (RRMS; 23.8%), secondary progressive (SPMS; 33.3%), and non-specified MS (42.9%) disease phenotypes. Average age at death for this group was 64.6±10.5 & 66.9±7.9 years for female and male donors, respectively, and a cohort average of 65.6±9.3. Autolysis time was comparable between male (14.7±8.9 hours) and female (27.6±6.3 hours) specimens, with an aggregate average of 16.4±7.5 hours. Neither age at death (p=0.5871) or autolysis time (p=0.3807) were statistically different between male and female donors within the MS only group.

The MS+S cohort was divided equally between female and male donors, with 42.9% of donors diagnosed with SPMS and 57.1% having an unspecified MS phenotype. Female donors were aged 59.8±15.9 years at time of death and male donors 64.8±11.6, for a cohort average of 61.9±13.4 years. On average, female specimens waited 14.6±3.6 hours and male specimens 27.9±11.6 hours until cryopreservation (cohort average=20.3±10.1 hours). No differences were identified in age at death (p=0.6722) or autolysis time (p=0.0763) between male and female specimens in the MS+S cohort.

No differences were observed in age at death (p=0.4195) or autolysis time (p=0.2829) when comparing MS and MS+S groups overall or when divided by sex (male: age at death p=0.7112, autolysis time p=0.0636; female: age at death p=0.4912, autolysis time p=0.3727).

**HBSFCR MS & MS+S hippocampi display similar demyelinated lesion burden**

Imaging studies have reported greater accumulation of demyelinating lesions in the hippocampi of MS+S patients relative to MS patients without seizures(91). To establish whether the HBSFRC cohort displays similar differences in myelination, immunolabeling for myelin oligodendrocyte glycoprotein (MOG) was performed and the density of lesions in CA1, CA3, and DG were measured (**Figure 2.2**). Demyelinated lesions were observed in both MS & MS+S groups that varied in their size and involvement of adjacent structures (**Figure 2.2A**). Quantification of lesion density in hippocampal subregions revealed no difference in lesion burden in CA1, CA3, or DG between MS & MS+S specimens in the HBSFRC cohort (**Figure 2.2B—D**).

**Enhanced astrogliosis in the HBSFRC MS+S CA1**

Seizure-induced reactive astrocytes undergo various metabolic and physiologic changes that exacerbate disease severity and vulnerability to additional seizures(185). Thus, to identify differences in the extent of astrogliosis between MS & MS+S specimens, $GFAP^+$ immunoreactivity was assessed in CA1, CA3, and DG subfields. $GFAP^+$ intensity was elevated in MS+S CA1 (**Figure 2.3A—B**). No difference in $GFAP^+$ signal intensity was observed in CA3 or DG subfields (**Figure 2.3C—F**). No difference was observed in the total $GFAP^+$ immunoreactive area fraction between MS & MS+S in any region (not shown), suggesting increased signal intensity was not due to differences in number of $GFAP^+$ cells or coverage of $GFAP^+$ processes.

**Reduced AQP4 expression in MS+S CA1/CA3 with loss of perivascular localization**

The glial water channel AQP4 is thought to play a role in maintenance of extracellular space volume and facilitation of ion movement throughout cytoplasmically linked glial networks(185). Perturbation of AQP4 expression and localization away from its normal perivascular distribution is commonly observed in hippocampal CA1 of epileptic patients(186). To assess whether MS+S involves similar changes to AQP4, its expression was evaluated in MS & MS+S hippocampi. Relative to MS only, MS+S CA1 and CA3 exhibited reduced AQP4 staining intensity (**Figure 2.4A-B/D-E**). No statistically significant difference was observed in MS+S DG (**Figure 2.4C/F**), although AQP4 immunoreactive area fraction trended toward increase in MS+S DG (not shown, p=0.0605). Of interest, while AQP4 signal was enriched proximal to putative blood vessels in MS CA1, perivascular AQP4 staining was infrequent in MS+S CA1 (**Figure 2.4A**). No differences were noted in perivascular AQP4 in CA3 and DG.

**CA1 synaptic glutamate clearance is likely impaired in HBSFRC MS+S CA1**

The glial glutamate/aspartate transporter EAAT2 is the most widely distributed glutamate transporter in the adult mammalian brain(187). As loss of glutamate transporters and accumulation of extracellular glutamate is observed in both MS and temporal lobe epilepsy(188, 189), EAAT2 was assessed. EAAT2 intensity dereased in MS+S CA1 vs MS (**Figure 2.5A/D**), but not statistically significant in CA3 (**Figure 2.5B/E**) or DG (**Figure 2.5C/F**). However, while EAAT2 immunoreactive area fraction was not statistically different in CA1 or CA3 subregions, $EAAT2^{+}$ area fraction was decreased in DG, suggesting reduced coverage of glutamate transporters in this area (not shown, p=0.0241).

**CX43 expression is increased in MS+S CA3**

Connexins represent a group of pore-forming proteins permeable to cytoplasmic contents up to 1.5 kDa, including ions, metabolites, and purinergic signaling molecules(185). Disruption of GJs or aberrant hemichannel activity may contribute to diseases with seizure or excitotoxic manifestations(185). As the major astrocyte connexin isoform known to be affected by inflammatory and demyelinating disease, CX43 immunostaining was assessed in the HBSFRC cohort(185). CX43 intensity was comparable between MS & MS+S specimens in CA1 (**Figure 2.6A/D**) and DG (**Figure 2.6C/F**). In contrast, CX43 intensity was elevated in MS+S CA3 relative to MS only (**Figure 2.6B/E**). No difference was observed in immunoreactive area fraction in any region analyzed.

## 2.5 | DISCUSSION

In the current study, we sought to shed light on the pathogenesis of seizures in MS by examining hippocampi of MS and MS+S donors obtained from the UCLA HBSFRC. Specifically, we assessed changes to astrocytes that could lead to dysregulated neuronal excitation, including their expression of molecules associated with synaptic glutamate clearance and spatial $K^+$ buffering as well as response to inflammation or injury. We found that, although demyelinated lesion burden was comparable among the tissues acquired from the HBSFRC, astrocyte dysfunction in MS+S specimens relative to MS varied by hippocampal subregion (**Table 2.3**). Based on these findings, we constructed a model summarizing how our observations could contribute to neuronal hyperexcitability in MS (**Figure 2.7**).

Among the biomarkers assayed, the CA1 of MS+S specimens in the HBSFRC cohort displayed the greatest number of changes compared to the MS only group. In addition to $GFAP^+$ astrogliosis surpassing that seen in MS, both AQP4 and EAAT2 were less robustly expressed in the CA1 of MS+S tissues. The impact of these findings on seizure development or maintenance are twofold; EAAT2's activity accounts for roughly 95% of glutamate buffering in the adult mammalian CNS (190), acting quickly to clear glutamate during synaptic neurotransmission (191, 192). Underscoring the critical role it plays in regulating neuronal excitability, hypofunction mutations in the *SLC1A2* gene (which encodes EAAT2) are sufficient to generate severe pediatric epilepsy (193), with seizure severity depending on the site of lost EAAT2 performance (194). Although both neurons and glia express EAAT2 (195), genetic ablation from neurons results in no gross phenotype, while its loss from astrocytes produces severe behavioral abnormalities and lethal seizures (196). Thus, the reduced EAAT2 signal observed in the MS+S CA1 in the

present study may increase seizure susceptibility by abnormally bolstering synaptic glutamate concentrations (**Figure 2.7A**).

The second way that these data could contribute to seizure vulnerability in MS patients is inferred from the suppression of AQP4 expression seen in the MS+S CA1 & CA3. AQP4 is a passive water channel expressed primarily by astrocytes that is enriched in endfeet contacting blood vessels (197) which contributes to normal extracellular space volume, glymphatic solute clearance, and $K^+$ buffering (146, 198-200). Loss of perivascular AQP4 results in delayed $K^+$ clearance and protracted stimulation-evoked seizures (199, 200), potentially leading to hyperexcitability pursuant to loss of $K^+$ charge separation (201, 202) (**Figure 2.7B**). Indeed, AQP4 expression is perturbed throughout epileptic hippocampi, with loss of its normal perivascular distribution in the CA1 (134, 147, 186). These observations have parallels in results obtained from the HBSFRC cohort: in addition to the decreased expression noted, perivascular AQP4 expression was sparse in the MS+S CA1, hinting at a role for this molecular in seizure etiology in MS. Of note, seizures are less common in patients with neuromyelitis optica spectrum disorder (NMOSD), a demyelinating disease related to MS characterized by circulating anti-AQP4 IgG, than MS patients (6, 203-205). As internalization of perivascular AQP4 is also observed at astrocyte endfeet in NMOSD, the contribution of reduced AQP4 to the genesis of seizures in MS will likely require additional study (206, 207).

While the functional implications of these findings are not able to be gleaned from postmortem studies, these data hint at a possible mechanism of neuronal hyperexcitability in MS that involves two hits; persistently elevated extracellular $K^+$ concentration engendered by reduced perivascular AQP4 could lower seizure threshold by mildly depolarizing neurons. Simultaneously, reduced EAAT2 could suppress efficiency of

neurotransmission-released glutamate clearance, leading to stronger and more frequent ionotropic glutamate receptor mediated synaptic potentials. Thus, with more glutamatergic neurotransmission and less input needed to elicit an action potential in affected neurons, these data may represent one way that the MS+S CA1 is predisposed to seizure (**Figure 2.7C**). Considering that loss of inhibitory neuron populations is also observed in various brain regions during demyelinating disease, GABAergic containment of pathological excitation may be insufficient to stem its spread to neighboring structures (60, 82, 149, 208).

While these data point to one plausible means of propagating seizures in MS, the finding that CX43 expression is enhanced in the MS+S CA3 raises several questions regarding the nature of such upregulation. In the brain, glia are the foremost expressers of connexin proteins, which link astrocytes and oligodendrocytes into a glial syncytium (185). This network of interconnected cells facilitates spatial $K^+$ buffering and propagation of Ca2+ waves through gap junction-mediated direct cytoplasmic coupling (163, 209-212). Additionally, uncoupled connexin hemichannels facing the extracellular space are thought to modulate neurotransmission via release of so-called gliotransmitters, such as purines, D-serine, and glutamate (213-218). In the present study, CX43 expression was increased in MS+S CA3, which has parallels in epileptic brain tissue (219), however, whether this represents increased gap junction coupling or hemichannel mobilization cannot be inferred from this study (**Figure 2.7D**).

Despite this uncertainty, several scenarios are plausible given our understanding of the impact that inflammatory demyelination has on connexin expression and function. Both oligodendrocyte death and MS-induced inflammatory cytokines are known to diminish gap junction coupling and increase hemichannel open probability (220-225). If

the increased CX43 observed represents more abundant hemichannels, the proinflammatory cytokine milieu encountered by astrocytes could augment release of glutamatergic and purinergic signaling molecules (226). In such a case, hemichannel blockade could ameliorate seizures in MS+S, as similar interventions have proven to reduce seizure severity in animal models of epilepsy associated with greater hemichannel activity (220, 227, 228). See **Appendix D** for a thorough discussion of how gap junction pathology could contribute to seizures in demyelinating disease.

An alternative interpretation of increased CX43 pertains to increased gap junction coupling in the MS+S CA3. CX43+ gap junctions couple astrocytes to one another and to oligodendrocytes, thereby facilitating movement of $K^+$ from areas of depolarizing activity to blood vessels for removal (212, 229). This may, therefore, represent a compensatory mechanism in the seizure prone MS+S hippocampus to address chronically elevated extracellular $K^+$ concentrations. Lending credence to this possibility, changes to AQP4 expression, which was diminished in the CA3 of MS+S tissues, impacts CX43 expression (230, 231). However, recent reports have linked connexin-mediated astrocyte synchrony to hypersynchronous neuronal depolarization during seizures (232). To resolve this question, as well as the nature of CX43 upregulation in MS+S, further study that permits a greater degree of experimental manipulation is necessary.

Although limited in number, animal studies probing the mechanism by which demyelination leads to seizure using the chronic 0.2% dietary cuprizone (CPZ) model of MS have yielded insights into the mechanism of MS-induced seizures. CPZ-fed mice display tonic-clonic convulsive behavior, electrographic seizures, and elevated theta-range oscillation power that parallel observations made in humans (60, 105). These seizures are associated with reduced numbers of inhibitory neurons in the murine CA1,

specifically basket cells expressing the calcium binding molecule parvalbumin, mirroring postmortem human studies (82).

While the resulting disinhibition arising from loss of GABAergic neurons could feasibly lead to seizures in mice, these studies also revealed that astrocytes exhibit profound changes to their morphology as well as molecules known to be perturbed in TLE. Astrocytes from CPZ fed demyelinating mice exhibit loss of domain organization, membrane varicosities suggestive of energetic failure, and perturbed AQP4 & EAAT2 expression (60). As these biomarkers are analogously impacted in the hippocampi of MS+S patients, the CPZ model may represent a means of gaining further insight into the pathophysiology of MS+S as well as answering several of the questions presented herein.

Overall, even though MS+S patients represent a minority of the population with MS, the greater morbidity & mortality as well as decreased quality of life in this group behooves further investigation of the pathology, cellular and molecular mechanisms leading to seizures in these patients.

## 2.6 | FIGURES & LEGENDS

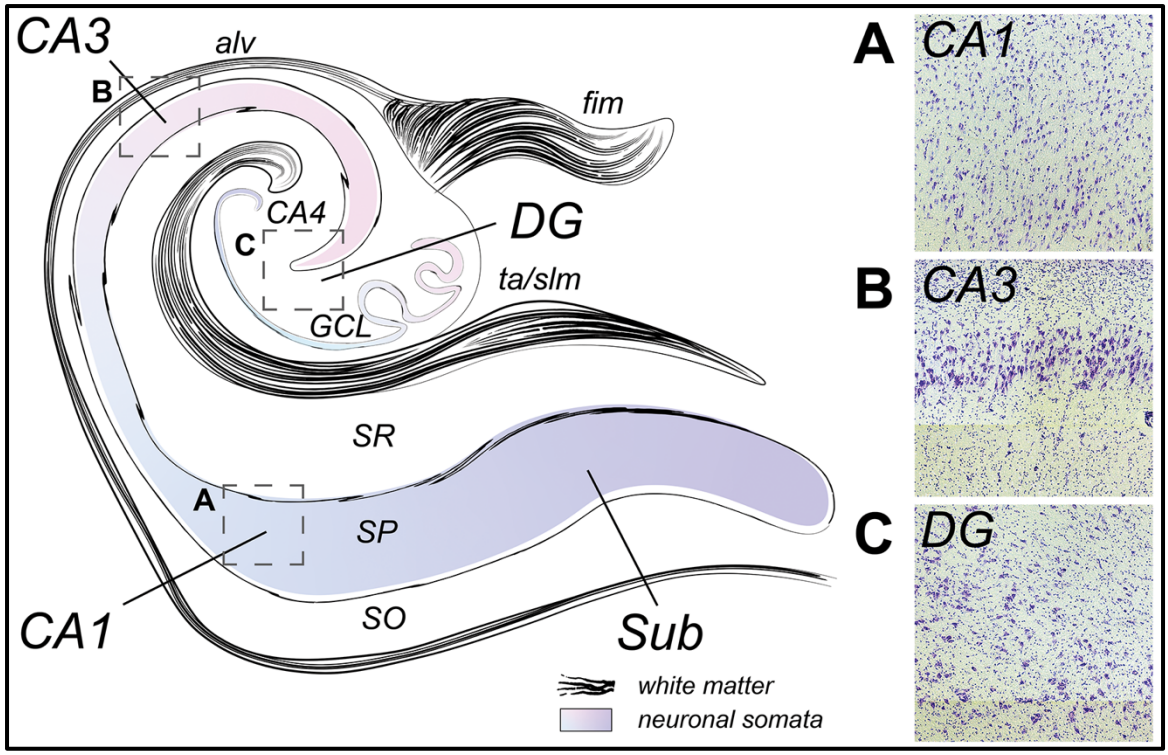


**Figure 2.1 |** *Illustrated human hippocampal anatomy and cytoarchitecture characteristic of CA1, CA3, & DG images used for analysis.* Diagram showing human hippocampus with subiculum (Sub), CA1, CA3, CA4, and dentate gyrus (DG) with strata oriens (SO), pyramidale (SP), radiatum (SR), and lacunosum-moleculare, as well as granule cell layer (GCL), noted. Dashed boxes correspond to representative 5X Nissl stained cytoarchitecture (shown in insets **A-C**) used to identify regions for confocal imaging.

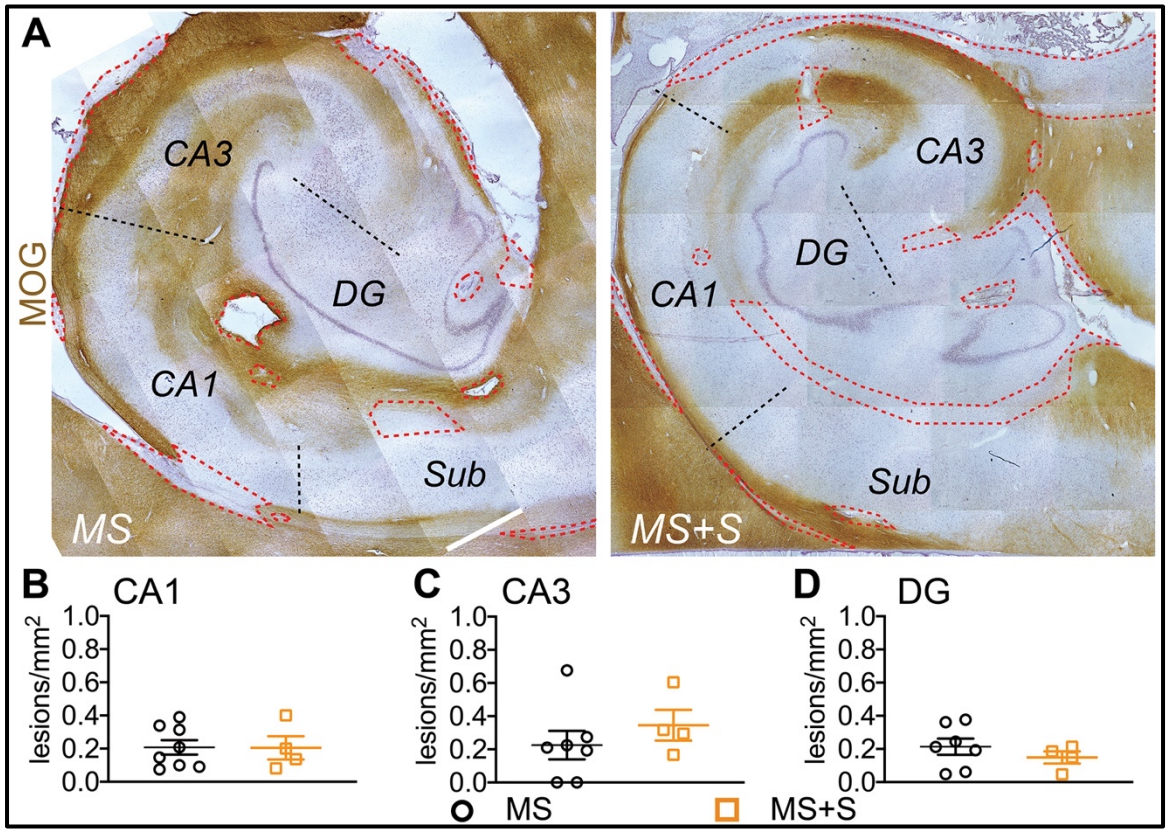


**Figure 2.2 |** *Demyelinated lesion burden is similar in the HBSFRC cohort.* **A)** Representative 5X stitched micrographs showing MOG immunoreactivity in MS & MS+S hippocampus visualized by HRP-DAB chromogen IHC with hematoxylin counterstain. CA1, CA3, DG, & Sub are indicated. Demyelinated lesions are traced by red dashed line. Black dashed lines represent divisions between subregions. **B-D)** Quantification of lesion distribution in MS & MS+S tissues. Comparison of demyelinated lesion density in CA1 (B), CA3 (C), and DG (D) revealed no significant difference in lesion burden between MS & MS+S specimens. Unpaired t-test.

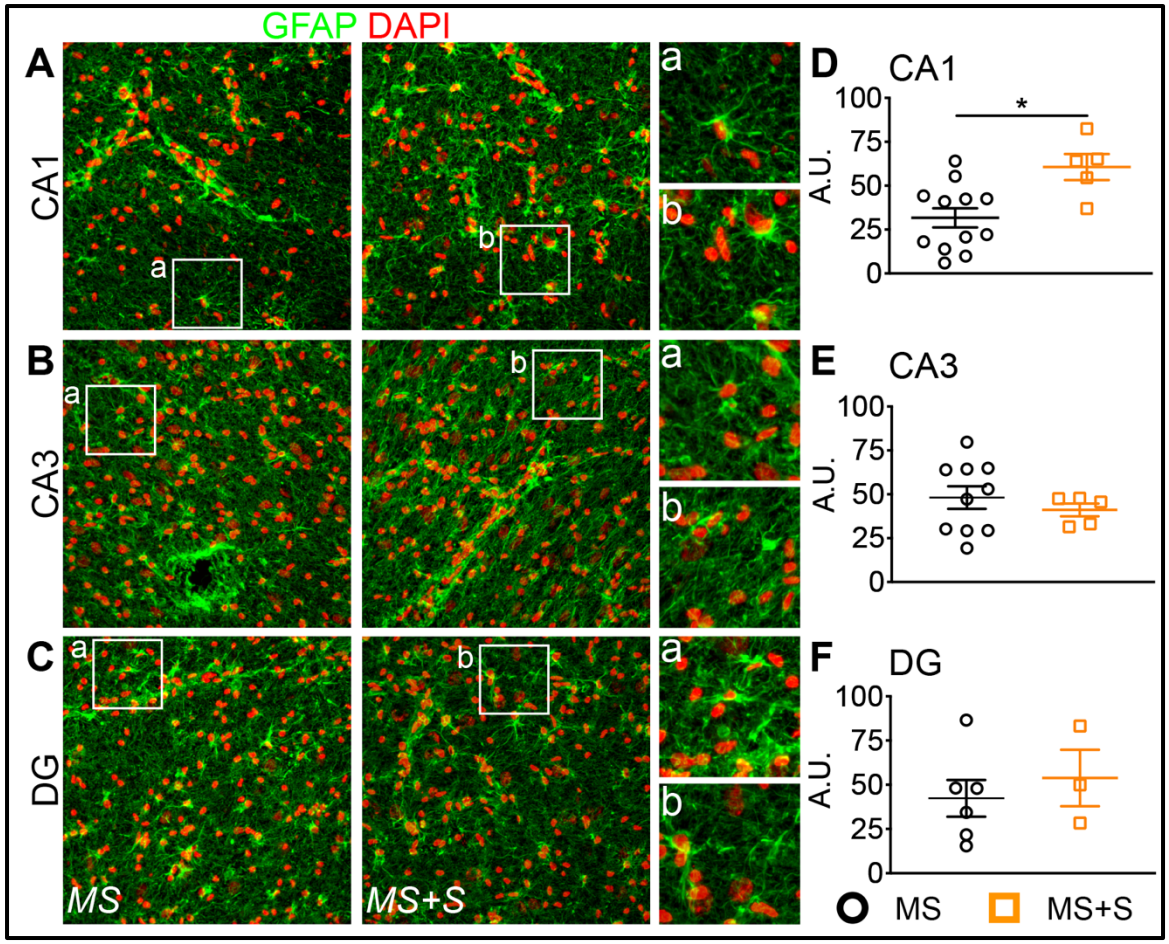


**Figure 2.3 |** *GFAP⁺ astrogliosis is more pronounced in the CA1 subfield of MS patients with seizures.* **A-C)** Representative 20X micrographs showing astrocytes (GFAP; green) with nuclear counterstain (DAPI; red) in CA1, CA3, & DG of MS & MS+S hippocampi. Insets a & b show digitally magnified area within dashed boxes for detail. **D-F)** Normalized GFAP immunoreactive signal intensity in MS & MS+S CA1 (D), CA3 (E), and DG in shown in arbitrary units (A.U.). Relative to MS, GFAP⁺ signal intensity was greater in CA1 of MS+S specimens. No difference was observed in CA3 or DG. Unpaired t test.

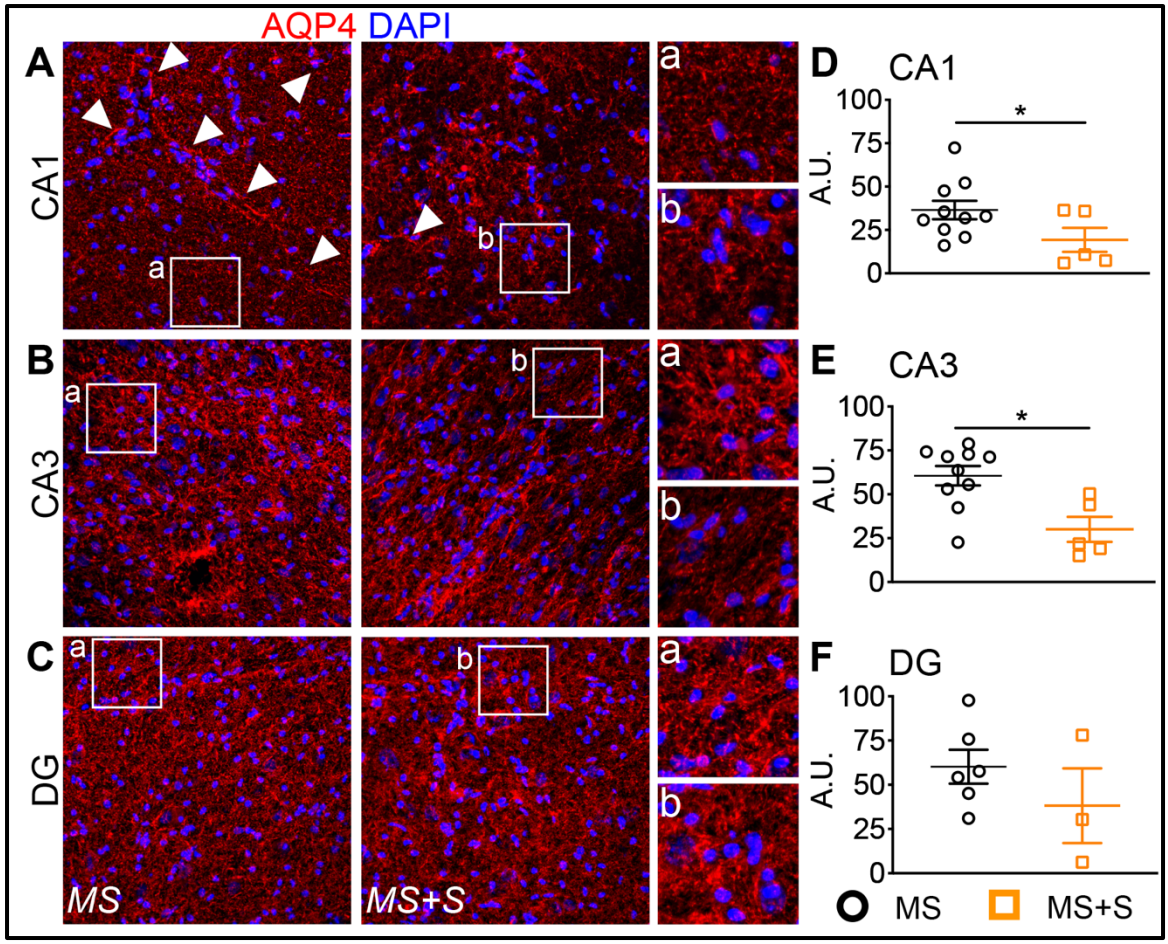


**Figure 2.4 |** *AQP4 expression is decreased in MS+S CA1 & CA3 subregions with loss of perivascular localization in the HBSFRC cohort.* **A-C)** Representative 20X micrographs showing AQP4 (red) with nuclear counterstain (DAPI; blue) in CA1, CA3, & DG of MS & MS+S hippocampi. Insets a & b show digitally magnified area within dashed boxes for detail. Note reduced perivascular AQP4 localization in MS+S CA1 (arrowheads). **D-F)** Normalized GFAP immunoreactive signal intensity in MS & MS+S CA1 (D), CA3 (E), and DG in shown in arbitrary units (A.U.). Relative to MS, AQP4 expression was reduced in MS+S CA1 & CA3. No difference was observed in DG. Unpaired t test.

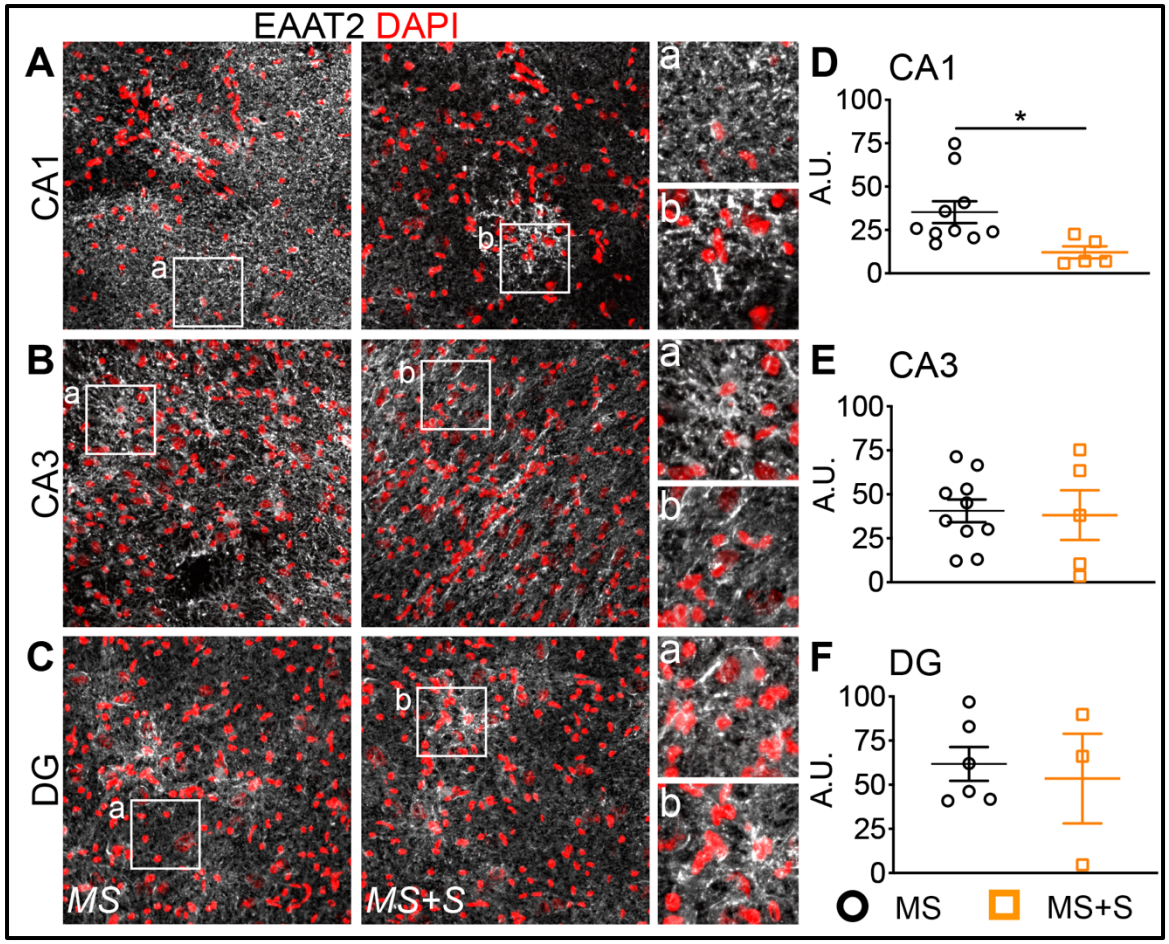


**Figure 2.5 |** *EAAT2 expression is reduced in the CA1 of MS+S specimens obtained from the HBSFRC.* **A-C)** Representative 20X micrographs showing EAAT2 (gray) with nuclear counterstain (DAPI; red) in CA1, CA3, & DG of MS & MS+S hippocampi. Insets a & b show digitally magnified area within dashed boxes for detail. **D-F)** Normalized EAAT2 immunoreactive signal intensity in MS & MS+S CA1 (D), CA3 (E), and DG in shown in arbitrary units (A.U.). Relative to MS, EAAT2+ signal intensity was greater in CA1 of MS+S specimens. No difference was observed in CA3 or DG. Unpaired t test.

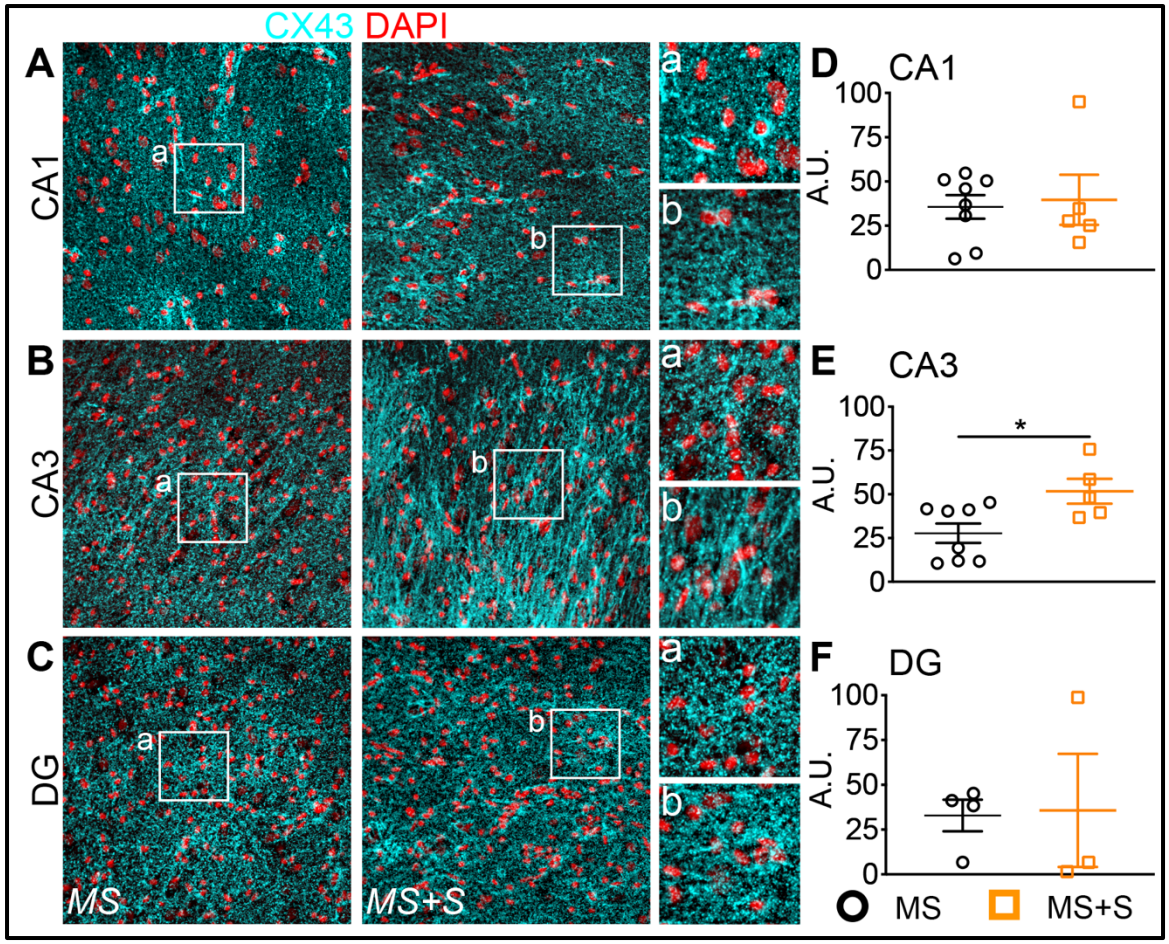


**Figure 2.6 |** *CX43 expression is enhanced in MS+S CA3 within the HBSFRC cohort.* **A-C)** Representative 20X micrographs showing CX43 (cyan) with nuclear counterstain (DAPI; red) in CA1, CA3, & DG of MS & MS+S hippocampi. Insets a & b show digitally magnified area within dashed boxes for detail. **D-F)** Normalized CX43 immunoreactive signal intensity in MS & MS+S CA1 (D), CA3 (E), and DG in shown in arbitrary units (A.U.). Relative to MS, CX43+ signal intensity was greater in CA3 of MS+S specimens. No difference was observed in CA3 or DG. Unpaired t test.

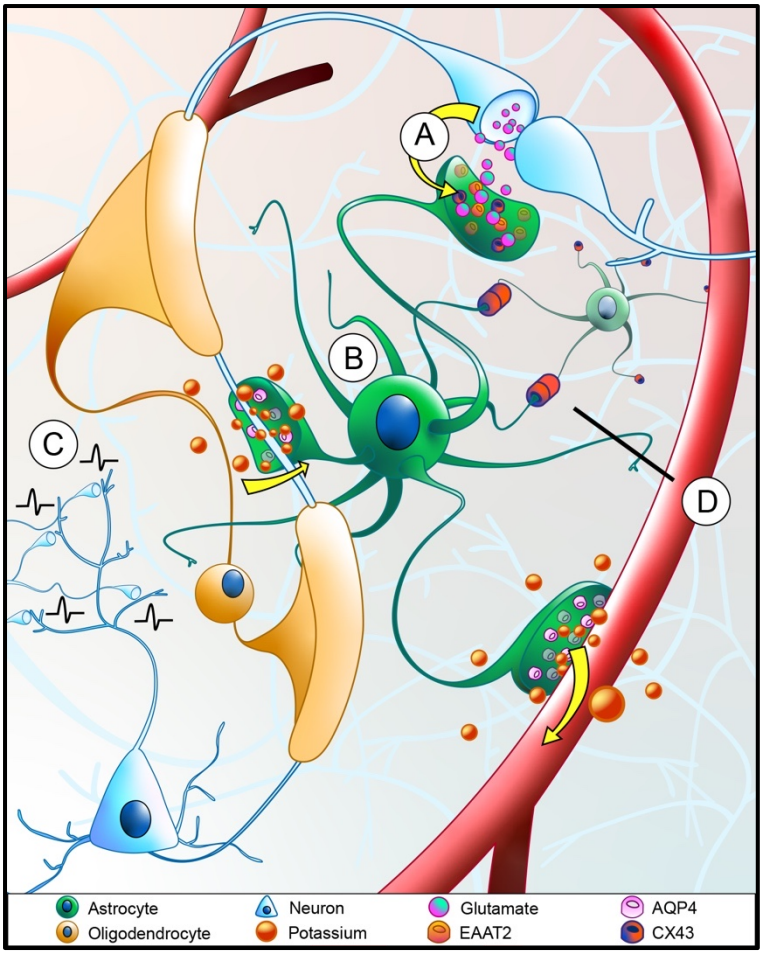


**Figure 2.7 |** *Model summarizing MS+S neuropathology differing from MS only and its impact on neuronal excitability.* **A)** Reduced EAAT2 expression suggests elevated synaptic glutamate concentration in MS+S, resulting in protracted, higher amplitude post-synaptic response. **B)** Decreased AQP4 expression and localization away from blood vessels in MS+S suggests compromised $K^+$ removal, elevated resting membrane potential (RMP), and lower depolarization threshold. **C)** Increased synaptic potential frequency leads to high amplitude excitatory events and seizure. **D)** Increased CX43 expression in CA3 may represent enhanced gap junction coupling among astrocytes or proliferation of uncoupled hemichannels, rendering its relevance unclear in the context of MS+S.

| | *n* | MS phenotype | Age at death (yrs±SD) | Autolysis time (hrs±SD) |
|---|---|---|---|---|
| MS only | 21 (12 ♀, 9 ♂) | MS, RRMS, SPMS | 65.6±9.3 | 16.4±7.5 |
| MS+S | 7 (4 ♀, 3 ♂) | MS, SPMS | 61.9±13.3 | 20.3±10.1 |

**Table 2.1 |** Summary of specimens acquired from HBSFRC/NIH NeuroBioBank.

| Antibody | Manufacturer | Catalogue # | Dilution |
|---|---|---|---|
| mouse anti-myelin oligodendrocyte glycoprotein (MOG) | Millipore Sigma | MAB5680 | 1:500 |
| chicken anti-glial fibrillary acidic protein (GFAP) | Millipore Sigma | AB5541 | 1:1000 |
| rabbit anti-aquaporin-4 (AQP4) | Millipore Sigma | AB2218 | 1:500 |
| guinea pig anti-glutamate transporter, glial (EAAT2) | Millipore Sigma | AB1783 | 1:1000 |
| rabbit anti-connexin 43 (CX43) | Millipore Sigma | C6219 | 1:500 |
| goat anti-mouse IgG (H+L), horseradish peroxidase | Millipore Sigma | AP308P | 1:500 |
| goat anti-chicken Ig (H+L), DyLight 650 | Invitrogen | SA5-10073 | 10 µg/mL |
| goat anti-rabbit IgG (H+L), Alexa Fluor +555 | Invitrogen | A32732 | 1:500 |
| goat anti-rabbit IgG (H+L), Alexa Fluor +488 | Invitrogen | A32731 | 1:500 |
| goat anti-rabbit IgG (H+L), Cy3 | Millipore Sigma | AP108C | 1:500 |

**Table 2.2 |** Antibodies used in the study included in [Chapter 2].

| | CA1 | CA3 | DG |
|---|---|---|---|
| Astrogliosis | ↑ | --- | --- |
| Water homeostasis | ↓ | ↓ | --- |
| Synaptic glutamate clearance | ↓ | --- | --- |
| Connexin expression | --- | ↑ | --- |

**Table 2.3 |** Visual summary of differences in markers indicated in MS+S hippocampal subregions relative to MS only. ↑ = increased expression; ↓ = decreased expression; --- = no difference.

**CHAPTER 3 |** Remodeling of GABAergic innervation and glutamatergic dysfunction may contribute to hyperexcitability and seizures in chronically demyelinated mice

Andrew S. Lapato[#,a,c], Carrie R. Jonak[#,a,c], Devin K. Binder[a,b,c], Seema K. Tiwari-Woodruff[a,b,c]

1. Division of Biomedical Sciences, UCR School of Medicine, Riverside, CA 92521
2. Neuroscience Graduate Program, UCR, Riverside, CA 92521
3. Center for Glia-Neuronal Interaction, UCR School of Medicine, Riverside, CA 92521

# Co-first authors

A version of this chapter was presented as a poster at the 2018 meeting of *The Society for Neuroscience*.

## 3.1 | ABSTRACT

Similar to MS patients with seizures, translational studies have identified tonic-clonic seizures and changes to EEG interneuron and AQP4 density in the hippocampal CA1, but the cause of seizures in demyelinating disease remain obscure. In the present study, we sought to identify functional and cytoarchitectural changes potentially etiologic to demyelination-induced seizures using multi-electrode array (MEA) electroencephalography (EEG) and immunohistochemistry. Elevated delta frequency band power (1-4 Hz) was observed in all cortical areas of 12 wk CPZ mice relative to normal, with right medial and temporal areas also exhibiting increased theta frequency band power (4-8 Hz). Notably, right medial and right frontal areas also exhibited reduced low gamma (30-55 Hz) and high gamma (65-100 Hz) frequency band power, respectively. In addition to cortical/white matter demyelination and commissural axon pathology, GABAergic cell numbers declined with concurrent reduction of GAD65 immunoreactivity in medial cortex and CA1 of 12 wk CPZ mice. These mice also displayed PV+ projections extending between the rostral cortex and striatum that were not seen in normal mice. These changes were accompanied by signs of perturbed glutamatergic system regulation, including enhanced GluA2+ AMPA receptor signal, reduced glutamate transporter signal, and reduced group 2 metabotropic glutamate receptor signal. Additionally, astrocytic $K^+$ handling is likely compromised due to loss of perivascular Kir4.1 localization, implicating impaired spatial $K^+$ buffering in mice with chronic demyelination-induced seizures. Aberrant cortical EEG, including reduction of PV+ neuron-mediated gamma frequency power white matter commissural axon pathology, plasticity of GABAergic innervation, and aberrant glutamatergic transmission likely contribute to demyelination-induced seizures.

## 3.2 | INTRODUCTION

Epileptic seizures are estimated to be up to six-fold more prevalent among the 2.3 million people affected by the autoimmune demyelinating disease multiple sclerosis (MS) than the overall population (62, 80, 94, 96, 233, 234). This patient subset is more likely to demonstrate a fulminant course of disease, proceed to disability more rapidly, and experience earlier mortality than other MS patients (82, 83). Furthermore, relapse-like symptoms are a frequent side-effect of traditional anti-epileptic drugs such as carbamazepine and gabapentin and intractable epilepsies are commonly observed (5, 87, 180). Yet while this group is at greater risk of developing seizures and suffers greater morbidity, epileptogenesis in MS remains poorly understood.

Analogous to epileptic brains, MS patients that develop seizures exhibit extensive astrogliosis, accumulation of inflammatory lesions in the hippocampus, and disappearance of GABAergic interneurons from temporal lobe structures involved in seizure initiation (82, 86, 103). Additionally, our previous work examining hippocampal pathology in the cuprizone (CPZ) model of demyelination-induced seizures revealed loss of parvalbumin (PV)+ inhibitory interneurons, widespread astrogliosis, and changes to aquaporin (AQP)4 in the CA1 subregion (60).

In the present study, we deploy in vivo multielectrode array (MEA) electroencephalography (EEG) monitoring to assess activity across multiple cortical areas in chronically demyelinated mice with spontaneous seizures. To identify cellular and molecular changes potentially etiologic to seizures, immunohistochemical analysis was subsequently performed in these regions as well as in the hippocampal CA1 subregion, which previously demonstrated similar electrographic disturbances in chronically demyelinated mice with seizures to examine molecular correlates of seizure activity (60).

## 3.3 | MATERIALS & METHODS

*Animals & cuprizone treatment* 8-12 week-old male C57BL6/J mice were obtained from the Jackson Laboratory (Bar Harbor, ME) and housed at the University of California Riverside (UCR) vivarium. Bis(cyclohexanone)oxaldihydrazone (cuprizone; CPZ) demyelination paradigm followed a previously described course (60). Briefly, cohorts received standard diet (Normal) or chow milled with 0.2% w/w CPZ for up to 12 weeks. At the end of recording, mice were euthanized and perfused for IHC. Animals were housed on a 12-hour light/dark cycle under pathogen-free conditions at UCR. Food and water were freely accessible throughout the duration of experiments. All procedures and experiments were conducted in accordance with the National Institutes of Health (NIH) Guide for the Care and Use of Laboratory Animal, s and approved by the Institutional Animal Care and Use Committee at UCR.

*Multi-electrode array (MEA) electroencephalography (EEG)* MEA EEG implantation and recording was performed following the protocol published in (235). Briefly, one week prior to recording, mice were anesthetized by IP ketamine/xylazine (80 mg/kg ketamine / 10 mg/kg xylazine). Anesthesia was monitored by hind limb withdrawal reflex & reapplied as necessary and body temperature was maintained at 37°C using a homeothermic pad during surgery. Scalp was prepared for implant by removing hair, disinfected, cleaned, and reflected symmetrically from a midline incision. Connective tissue was debrided from cranial surface and a NeuroNexus 30-contact MEA probe (Ann Arbor, MI), consisting of a 20μm-thick planar array of platinum electrodes, was applied to the surface of the skull to monitor resting state EEG was monitored (**Figure 3.1A)**. MEA probes were fixed to the head using dental cement (**Figure 3.1B**) and mice were allowed

unrestricted movement during recording by means of a communicating tether (**Figure 3,1C**). Spectral analysis was performed as previously published (236). Briefly, Fast Fourier transforms were performed on 1-second segments to determine power ($\mu V^2$/Hz). Values were divided into δ (1-4 Hz), θ (4-8 Hz), α (8-13 Hz), β (15-30 Hz), $\gamma^{low}$ (30-55 Hz), and $\gamma^{high}$ (65-100 Hz) frequency bands for additional analysis. Electrographic seizures were identified from recordings by experimenter observation of clusters of spike-wave complexes asymmetrically positioned over baseline.

*Immunohistochemistry (IHC)* 40 µm free-floating sagittal sections containing medial cortex and hippocampus were immunostained according to a previously reported protocol (60, 61, 136, 137). Information pertaining to antibodies & dilutions used in the present study are denoted in **Table 3.1**.

*Imaging and Quantification* Fluorescence intensity micrographs were acquired using an Olympus BX61 confocal microscope (Olympus America Inc., Center Valley, PA) at 20X & 60X objectives. ≤20 µm thick z-stack projections were compiled using SlideBook 6 software (Intelligent Imaging Innovations, Inc., Denver, CO) or Olympus cellSens software (Olympus America Inc.). Image analysis was carried out in Fiji software. Data points represent average values for two fields of view per area per donor sample.

*Statistical analysis* Statistical analysis was carried out as previously published using Prism 8 software (GraphPad Software, La Jolla, CA) (136, 184). P values are represented by the following symbols positioned above data sets: * = p≤ 0.05, ** = p≤0.01, *** = p≤0.001, **** = p≤0.0001. Differences were considered significant when p≤0.05. Statistical tests used are indicated in corresponding figure legends.

## 3.4 | RESULTS & DISCUSSION

### Electrographic seizures localize to temporal cortical areas in mice fed CPZ chronically.

Spontaneous and startle-induced seizures are a feature of chronic dietary administration of the toxic demyelinating agent CPZ, but the spatiotemporal characteristics of these seizures remain undefined (60, 105). To identify brain structures associated with CPZ-induced seizures, resting state EEGs were recorded from 8-12 week-old C57BL/6 male mice fed standard chow (Normal) or 0.2% w/w CPZ for 12 weeks (12 wk CPZ) using a 30-channel NeuroNexus surface MEA probe (**Figure 3.1A**).

Neither group demonstrated tonic-clonic seizures prior to, during, or after EEG acquisition, however, experimenters noted occasional periods of brief behavioral arrest in the 12 wk CPZ cohort (not quantified). Analysis of resting state EEG recordings revealed spontaneous epileptiform activity in several closely apposed channels in the 12 wk CPZ cohort while distal sites remained unaffected (**Figure 3.1D—F**, arrowheads; n=3). Channels exhibiting ictal events clustered to the temporal grouping of electrodes, suggesting involvement of these sites in CPZ-induced seizure pathology (**Figure 3.1G**).

### Slow cortical oscillation power is enhanced in mice with demyelination-induced seizures.

Our group previously reported that mice fed CPZ for 12 weeks develop generalized seizures associated with augmentation of specific hippocampal EEG frequencies (60). Analysis of the frequency contents comprising the EEG waveform can provide information regarding neuronal excitability, communication, and integration of afferent signals (237). Thus, electrodes were pooled following left/right temporal, medial, and frontal groupings

as in **Figure 3.1G** and waveforms were decomposed for spectral analysis as previously described (236).

In addition to electrographic seizures, EEG power was differentially impacted in 12 wk CPZ mice both regionally and by frequency band (**Figure 3.2A-C**). At the regional level, the medial grouping of electrodes recorded enhanced power across frequencies below 65 Hz (**Figure 3B-C)**. No other grouping detected similarly consistent elevation. In the frequency domain, compared to normal, slow oscillations within the delta (1-4 Hz) range were enhanced in all areas surveyed in the 12 wk CPZ cohort (**Figure 3.2B-C**). Outside of medial cortex, frequencies below 30 Hz (low gamma) were comparable between groups, aside from elevated right temporal theta (4-8 Hz) power in the 12 wk CPZ cohort. Within the gamma frequency range (30-100 Hz), which is generated by rhythmic activity of PV-expressing interneurons (238-240), $\gamma^{low}$ (30-55 Hz) power was elevated in 12 wk CPZ mice, suggesting suppression of PV interneuron activity (239, 241). In contrast, $\gamma^{hi}$ (65-100 Hz) power declined in the right frontal electrode grouping, feasibly also representing interneuron dysfunction (242, 243).

**Extensive demyelination of cortex, callosal fiber tracts, and hippocampus after 12 weeks of CPZ.**

The 0.2% dietary CPZ paradigm utilized in this study produces well characterized and consistent demyelination of the telencephalon, diencephalon, and brain stem (108). To confirm demyelination in the 12 wk CPZ cohort, myelin basic protein (MBP) immunoreactivity was assessed in right hemisphere sagittal sections approximately 2 mm lateral to midline (**Figure 3.3**). With respect to Normal controls, cortical, callosal, and hippocampal (CA1) MBP-reactive area fractions fell significantly in 12 wk CPZ mice

(**Figure B-D**). Demyelination was exceptionally profound in cortical gray matter, which fell to approximately 80% of normal coverage in 12 wk CPZ mice (**Figure 3.3B**).

**PV+ interneuron loss from cortex and hippocampus is associated with reduced presynaptic GABAergic marker intensity in 12 wk CPZ pyramidal cell layer.**

For unknown reason, PV-expressing neurons are selectively lost in various models of demyelinating disease (60, 149, 208). We previously reported declining PV+ interneuron density in the dorsal CA1 subfield of chronically CPZ-demyelinated mice after 12 weeks of CPZ (60). Here, we examine inhibitory innervation in the hippocampus and cortical gray matter proximal to regions displaying electrographic seizures.

PV+ cell density declined in 12 wk CPZ cortex, CA1 oriens (SO), pyramidal cell (SP), and radiatum strata (SR) relative to normal, consistent with previously published hippocampal data (**Figure 3.4A-B**) (60). These data suggest reduced inhibitory drive supplied by PV-expressing interneuron populations may contribute to demyelination-induced seizures (244-246). However, because PV expression exhibits remarkable plasticity in several disease models, the synaptic GABA synthetic enzyme, glutamate decarboxylase (GAD)65, was analyzed to determine the impact of chronic CPZ on GABAergic innervation (247-249).

Individual synaptic puncta were not reliably identifiable in 60X magnified optical sections taken form Z-stacked confocal micrographs acquired for this study (**Figure 3.4C**). Thus, signal intensity was analyzed in normal and 12 wk CPZ sagittal sections then normalized to the minimum and maximum values of the entire data set to identify relative differences in expression (**Figure 3.4D)**. Compared to Normal controls, GAD65 signal intensity declined in the 12 wk CPZ CA1 SP (**Figure 3.4D**). In contrast, cohorts displayed

comparable GAD65 signal intensity in the SR, suggesting specific compromise of perisomatic inhibition after 12 weeks of CPZ-demyelination (**Figure 3.4D**). Since both cholecystokinin- and PV-expressing provide GAD65+ synapses to pyramidal layer neurons, these data are consistent with loss of PV+ interneurons and the innervation they supply (250).

Normally, PV-expressing basket cells coordinate output behavior of large neuronal ensembles through high-frequency $GABA_A$-mediated phasic inhibition (251-253). In addition to their roles in information processing and generation of gamma oscillations, PV-expressing neurons impart physiologic resistance to seizures (254-256). To this point, ablation of PV+ cells, or even NMDA receptor-mediated afferents they receive yields severe recurrent seizures (155, 257, 258) Thus, the presumptive loss of GABAergic synapses from these sources could be epileptogenic in demyelination-induced seizures (120, 259-261). Together, these data support the hypothesis that reduced GABAergic innervation, driven by PV+ cell loss, may contribute to seizures during chronic demyelinating disease.

Notably, neither total inhibitory GAD67+ neurons nor somatostatin (SST)+ neurons changed significantly in the 12 wk CPZ cohort, suggesting selective loss of PV expressing cells (**Appendix B**). Differential loss of GABAergic neurons could arise for various reasons. The fast-spiking behavior of PV+ basket cells generates significant energetic demand, which is offset by coordinated action of voltage gated sodium ($Na_v$) and potassium ($K_v$)3.1 channels (262-269). Although PV+ interneuron sources of $K_v$3.1 has not been evaluated in MS or animal models to our knowledge, demyelinating disease produces changes in $K_v$3 and $Na_v$ expression (270, 271). Therefore, examination of PV-interneuron channel activity and mitochondrial dynamics may prove useful in determining

the reason for PV vulnerability in demyelinating disease. However, neocortical PV-expressing neurons are also extensively myelinated in the mammalian CNS, making a direct link between demyelination and PV+ cell loss and enticing target for future study (272-275).

## Novel PV expression within white matter tracts of chronically CPZ-fed mice with seizures.

Although PV+ interneuron somata density declined with chronic CPZ administration, experimenters noted unusual patterns of PV expression in the 12 wk CPZ cohort (**Figure 3.6**). In contrast to Normal controls (**Figure 3.6a-c**), 12 wk CPZ mice exhibited long ranging PV+ projection fibers extending between the cortex and diencephalon at least as far as the globus pallidus (Gp; **Figure 3.6a'-c'**). These fibers followed white matter tracts of the internal capsule and corpus callosum, but neither their cellular sources nor postsynaptic targets could be inferred from the data available. Furthermore, it is unclear from these studies whether the PV+ processes identified represents de novo expression by existing PV-negative axons or infiltration of PV-bearing fibers into demyelinated tracts. Studies are planned to address these questions, however, possible insight into their identity and function may be inferred by examining a different seizure disorder, tuberous sclerosis.

Tuberous sclerosis is a multi-system, autosomal dominant disorder caused by mutations in negative regulators of mTOR signal transduction, which produces CNS symptoms that include epileptic seizures and intellectual disability (276). When diencephalic neurons lack tuberous sclerosis complex (TSC)1, morphologically analogous PV+ projections are observed following striatal white matter (249). In TSC1 mutants,

these fibers issue from glutamatergic thalamic relay neurons that aberrantly express PV as a product of pathologically elevated mTOR signaling (249). The synapses formed by such fibers generate stronger, higher frequency action potentials than their wild type counterparts, feasibly driving excessive excitation at their post synaptic targets (249). If similar pathophysiology is responsible for the PV-expressing fibers observed here, elevated thalamocortical glutamatergic transmission could play a part in producing CPZ-induced seizures. In addition, mTOR signaling enhances excitatory transmission in the hippocampus, which is consistent with electrographic disturbances in 12 wk CPZ mice (60, 277). These data indicate that evaluating mTOR signal transduction may help resolve the molecular mechanisms driving demyelination-induced seizures.

**Dysregulated glutamate & $K^+$ handling may contribute to demyelination-induced seizures.**

Appreciation for the outsized role that astrocytes play in modulating neuronal excitation, both homeostatically and pathologically, continues to mount (185, 195, 278-281). Astrocyte-mediated synaptic clearance accounts for 90% of glutamate reuptake in the adult CNS, primarily via excitatory amino acid transporter (EAAT)2 (282, 283). In addition to controlling synaptic glutamate concentrations acutely, astrocyte-expressed EAAT2 plays a critical function in resisting seizures and suppressing network excitation (191, 192, 196, 284-286).

Cytokine-induced glutamatergic potentiation and down regulation of astrocytic glutamate transporters elevate brain glutamate in MS, which acts as one vector of neuronal and oligodendroglial cell death (121, 194, 223, 287-291). Additionally, our group finds reduced EAAT2 signal in MS+S hippocampi that outstrips that observed in MS only,

suggesting insufficient synaptic glutamate clearance may play a role in demyelination-induced seizures (61). Here, whether CPZ-induced seizures showcase similar perturbation to astrocyte glutamate transporter expression is examined in sagittal sections from Normal and 12 wk CPZ mice taken from the right hemisphere, approximately 2 mm from midline.

12 wk CPZ mice exhibited a trend toward reduced EAAT2 signal intensity in medial cortex relative to controls that reached statistical significance in the hippocampus CA1 (**Figure 3.6A-D**). This suggests that, similar to MS+S hippocampi, compromised astrocytic support of glutamatergic synapses could feasibly contribute to chronic CPZ-induced seizures (61). Functional studies are required to confirm this hypothesis as evidence suggests a surplus of glutamate transporter capacity exists under physiologic conditions (282, 292).

In addition to regulating excitability by controlling glutamate concentrations, astrocytes shape normal neurotransmission by maintaining extracellular [$K^+$] (185, 293). This is primarily accomplished by cellular uptake of $K^+$ released at the site of depolarizing activity by inward rectifier potassium channels (Kirs) composed of 4.1 & 5.1 isoforms, although Kir4.1 accounts for most inward $K^+$ current generated (294-296). These channels favor maximal $K^+$ permeability under hyperpolarizing conditions, contributing to the $I_H$ current described by Goldman, Hodgkin, & Katz (202). Although astrocytes are the primary source of brain Kir4.1, oligodendrocyte derived Kirs are increasingly recognized as essential to regulating both white and gray matter excitability by controlling extracellular $K^+$ accumulation (209, 297-300). Additionally, Kir4.1 and AQP4 frequently co-localize at the ultrastructural level, suggesting functional ties between two molecules (197, 301). Since loss of gray matter Kir4.1 immunoreactivity is a feature of neurological diseases with

seizures as a manifestation such as epilepsy and MS, Kir4.1 was evaluated in normal and 12 wk CPZ mice (302, 303).

Unexpectedly, Kir4.1 staining intensity rose in the demyelinated CA1, suggesting increased expression in 12 wk CPZ mice (**Figure 3.7F**). Because of the paucity of post-mitotic oligodendrocytes and oligodendrocyte precursors present in the CA1 by 12 weeks of CPZ intoxication, the expression observed here is putatively attributed to astrocytes (60). Of note, while Kir4.1 reactivity tracked small blood vessels in the Normal cohort, perivascular Kir4.1 was negatively attenuated in the 12 wk CPZ group (**Figure 3.7E-F**, arrowheads). To our knowledge, this is the first reported instance of Kir4.1 mislocalization not associated with glioblastoma (304-306). However, the complexity of Kir4.1 regulation and function renders interpretation of these results difficult without additional data (304-306).

In addition to generating a net inward $K^+$ current in response to action potentials, Kir4.1 kinetics reverse at the endfoot-vascular interface, leading to a net outward current at these sites (130). This function, termed spatial potassium buffering, is supported by extensive gap junction coupling among astrocytes, leading to rapid $K^+$ conduction away from active cells to be discarded into the circulatory system (229, 293, 307, 308). In the context of demyelination-induced seizures, reduced perivascular Kir4.1 could disrupt electrochemical homeostasis across various populations, thereby enhancing neuronal excitability as insufficient spatial $K^+$ buffering produces rising extracellular [$K^+$] (201, 202). Adding additional complexity, Kir4.1 gain-of-function mutations (which is feasible given **Figure 3.7E-F**), counterintuitively, produce epilepsy and intellectual impairment (309).

The cause of infracellular Kir4.1 redistribution is not established, but direct observation of glial Kir4.1 currents is warranted given the associated with loss of channel

function in neoplastic glia (304). Interestingly, β1-syntrophin, a component of the dystrophin-associated protein complex, anchors Kir4.1 in astrocyte endfeet to facilitate $K^+$ elimination (310, 311). Because AQP4 mislocalization in temporal epilepsy is thought to involve the related α1-syntrophin isoform, further study could elucidate whether the lost perivascular Kir4.1 observed involves similar cytoskeletal derangement (310-312). Thus, characterizing Kir4.1 function is necessary to disentangle the role of this channel in CPZ-induced seizures.

**Neuronal responsiveness to glutamate may be enhanced in demyelinated mice with seizures.**

Glutamatergic neurotransmission represents the principle means of excitatory communication in the adult mammalian CNS (313). This is largely accomplished by N-Methyl-d-aspartate (NMDA), kainic acid (KA), and α-amino-3-hydroxy-5-methyl-4-isoxazolepropionic acid (AMPA)-type ionotropic glutamate receptors, which convey essential excitatory information to their postsynaptic targets via phasic cation flux upon ligation (314). NMDA receptors are gated by both ligands and membrane potential and generate slow inward currents, whereas KA & AMPA-type receptors permit fast cation permeability (315) However, excessive activity of these receptors can lead to seizures and excitotoxic ell death due to swelling and unconstrained $Ca^{2+}$ signaling (315-318). As mice with demyelination-induced seizures exhibit signs of dysfunctional astrocytic control of synaptic glutamate, responsiveness to glutamate was assessed by evaluating immunolabeling for the most widely expressed AMPA receptor subunits in the CNS, GluA1 & GluA2 (319).

GluA1 signal was comparable between normal and 12 wk CPZ mice in all hippocampal regions analyzed (**Figure 3.7A-D**). In contrast, GluA2 signal intensity was elevated in both SR & SP of 12 wk CPZ CA1 (**Figure 3.7E-G**). These data suggest increased GluA2+ AMPA receptor composition and glutamatergic drive in chronically demyelinated mice with seizures. Whole-cell recordings are required to confirm the functional ramifications of these results, though, given the complex modifying influence of AMPA receptor-associated proteins on channel activity (319, 320). Of note, these studies did not GluA2 transcript editing, leaving the status of $Ca^{2+}$ gating uncertain (321-323). However, in vivo $Ca^{2+}$ imaging of hippocampal neurons in mice fed CPZ chronically supports the conclusion that posttranscriptional RNA editing is intact (324).

Although functional studies remain lacking, we examined PSD-95 immunoreactivity to identify whether rising GluA2 signal reflected recruitment to synaptic sites. PSD-95 tracked rising GluA2 signal intensity in the 12 wk CPZ cohort relative to normal (**Figure 3.7H**). PSD-95 is a postsynaptic, membrane-associated guanylate kinase that stabilizes ionotropic glutamate receptors and associated glutamatergic molecules at excitatory synapses in an activity-dependent fashion (325-327). In addition, experimentally expressing PSD-95 reduces silent synapse frequency and causes higher magnitude excitatory postsynaptic currents (325). Together, these data raise the likelihood that the elevated GluA2 signal seen in **Figure 3.7** corresponds to enhanced neuronal sensitivity to glutamatergic neurotransmission in chronically demyelinated mice with seizures.

In addition to eliciting depolarization of postsynaptic targets, glutamate provides inhibitory feedback to presynaptic neurons and suppresses $Ca^{2+}$ glia through $G_{i/o}$ coupled group 2 metabotropic glutamate receptor (mGlur)-mediated reduction of neurotransmitter release and (328). Our data point to remodeling of GABAergic innervation, deterioration of homeostatic synaptic glutamate regulation, and enhanced glutamatergic receptor signal in chronically demyelinated mice with seizures. As group 2 metabotropic receptors are reduced in animal models of epilepsy and correspond to attenuated control of excitatory amino acid signaling, mGlur2/3 immunoreactivity was analyzed in sagittal sections taken from normal and 12 wk CPZ mice (329-331). In addition, group 2 mGlurs were analyzed in mice fed CPZ for nine weeks that did not display tonic-clonic seizures (9 wk CPZ) to determine whether mGlur expression differed between chronically demyelinated mice with and without seizures.

mGlur2/3 immunoreactive signal was comparable in Normal controls and 9 wk CPZ animals in both CA1 SR & SLM (**Figure 3.8A-C**). 12 wk CPZ mice exhibited a different pattern of expression, with suppression of group 2 mGlur signal intensity in SR and elevation of SLM signal intensity (**Figure 3.8A-C**). This suggests that seizures during chronic demyelination may involve impairment of mGlur-mediated glutamatergic feedback inhibition. This hypothesis is supported by studies showing mGlur2/3 agonism reduces the severity of pilocarpine induced epilepsy (332)Furthermore, a major function of CA1 is to integrate polymodal sensory information arriving from temperoammonic fibers in SLM with perforant path afferents conveyed by Schaffer collaterals to proximal

dendrites in SR (333-335). Differential group 2 mGlur expression could therefore have implications for temporal and spatial summation of these afferents in addition to raising excitatory drive.

Astrocytes express both mGlur2 & 3, which participate in glutamate surveillance and modulate EAAT function as well as $Ca^{2+}$ wave propagation (331, 336-338). In these cells, ligation of group 2 mGlurs positively regulates glutamate transporter expression, possibly providing a link between these data and reduced EAAT expression observed in human and mouse models of MS+S (61). Together, these observations indicate that postsynaptic targets are more sensitive to glutamate and more glutamate is available at the synaptic cleft. Thus, neuronal excitability in CPZ-induced seizures likely involves dysregulation of glutamatergic system regulation.

**CONCLUSIONS**

In this report, we showed that mice fed CPZ chronically experience seizures as well as modified GABAergic innervation, dysregulation of glutamatergic neurotransmission, and interruption of normal potassium handling. Together, these data provide strong evidence for a hyperexcitable state in the demyelinated CNS that may predispose to seizures. Thus, direct observation is warranted to identify functional outcomes of the cellular and molecular changes described here. Exposing whether these elements are etiologic to seizures in MS will necessarily inform future studies aimed at mitigating the epileptic phenotype produced by demyelinating disease.

## 3.5 | FIGURES & LEGENDS

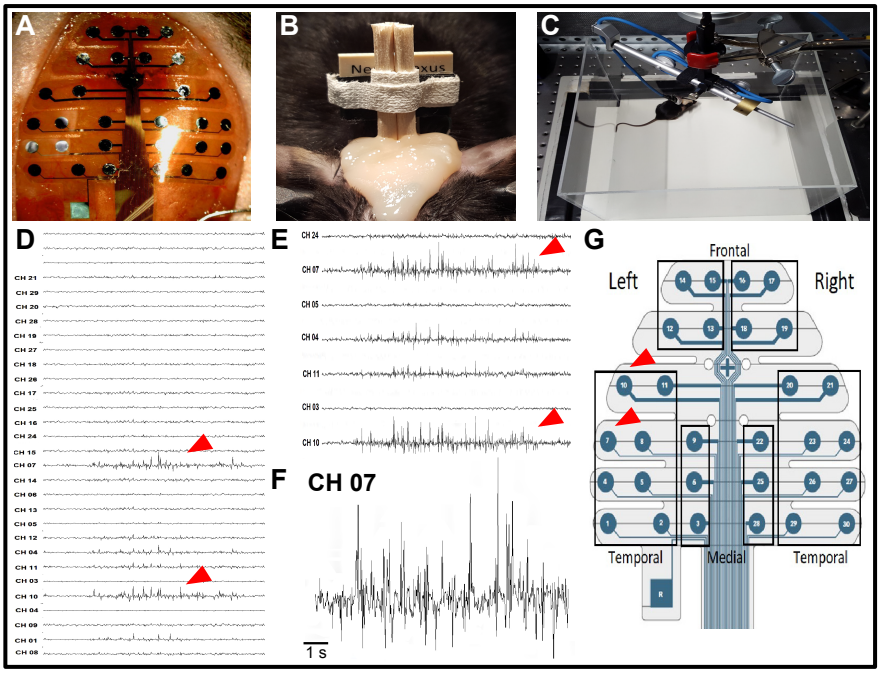


**Figure 3.1 |** *MEA EEG localizes electrographic seizures to temporal probe grouping in chronically cuprizone-demyelinated mice.* A) 30-channel NeuroNexus MEA probe in place on mouse skull surface. **B)** Mounted headstage for chronic recording in vivo. **C)** Chronic monitoring of awake, behaving mice with commutator. D) Example 30-channel MEA EEG recorded from mice fed CPZ for 12 weeks post. Red arrowheads indicate channels showing putative seizure-like events. E) Expanded view of (D) demonstrating spontaneous electrographic seizure activity in channels 7 & 10 (arrowheads). Seizure activity in this example was associated with behavioral arrest. F) Magnified trace recorded in channel (CH) 07 from (E) demonstrating synchronized electrographic seizure activity arising from channel 7. G) NeuroNexus probe electrode map showing location of channels 7 and 10 which display epileptiform activity which cluster over left temporal cortex. Note that EEGs are normal in simultaneously recorded channels at distal sites

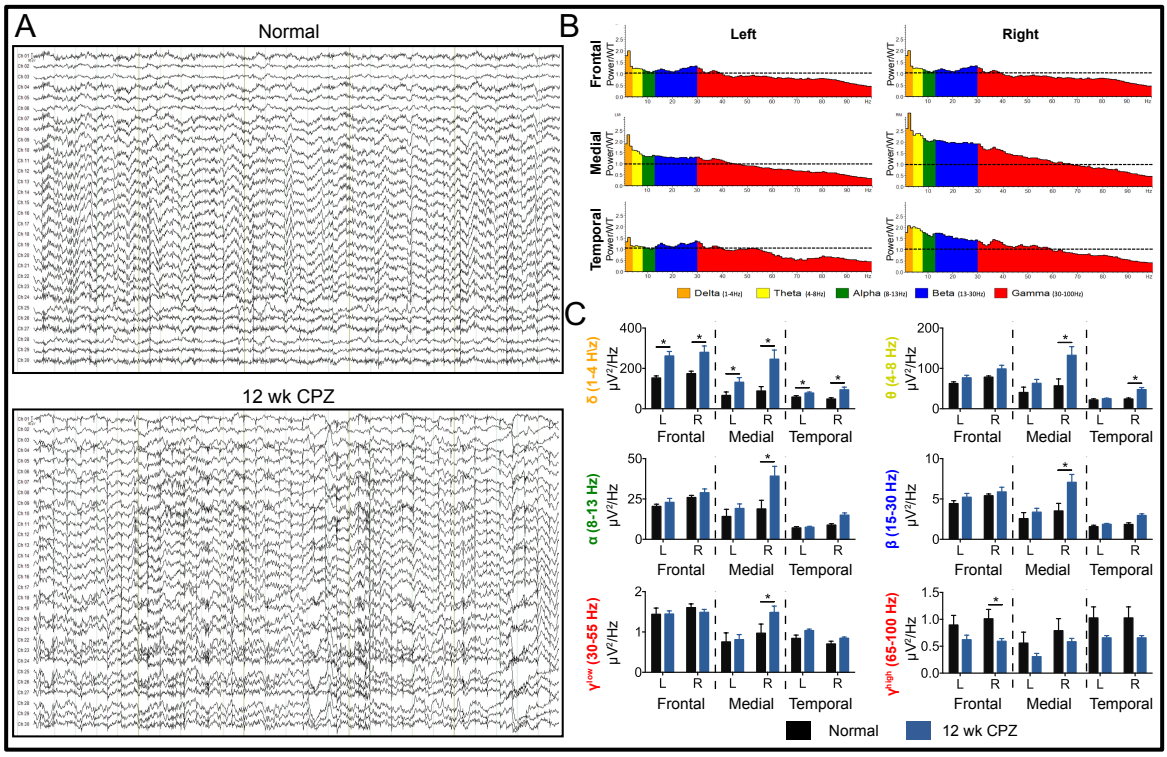


**Figure 3.2 |** *Slow oscillatory band power is enhanced in mice with demyelination-induced seizures.* A) Representative 30-channel MEA EEG traces from normal and 12 wk CPZ mice. B-C) Spectral analysis of data presented in (A). B) Ratio of EEG power in specific frequency bands in 12 wk CPZ mice relative to Normal at specified frequencies. Average power observed in Normal mice is represented by dashed black line (J) (quantified in K) demonstrates region and frequency band-specific alterations in EEG power in chronically demyelinated mice. Note augmented delta frequency power in all groupings as well as selective lateralization of medial grouping power enhancement. One-way ANOVA with Tukey's test for multiple comparisons. n=4-5/group.

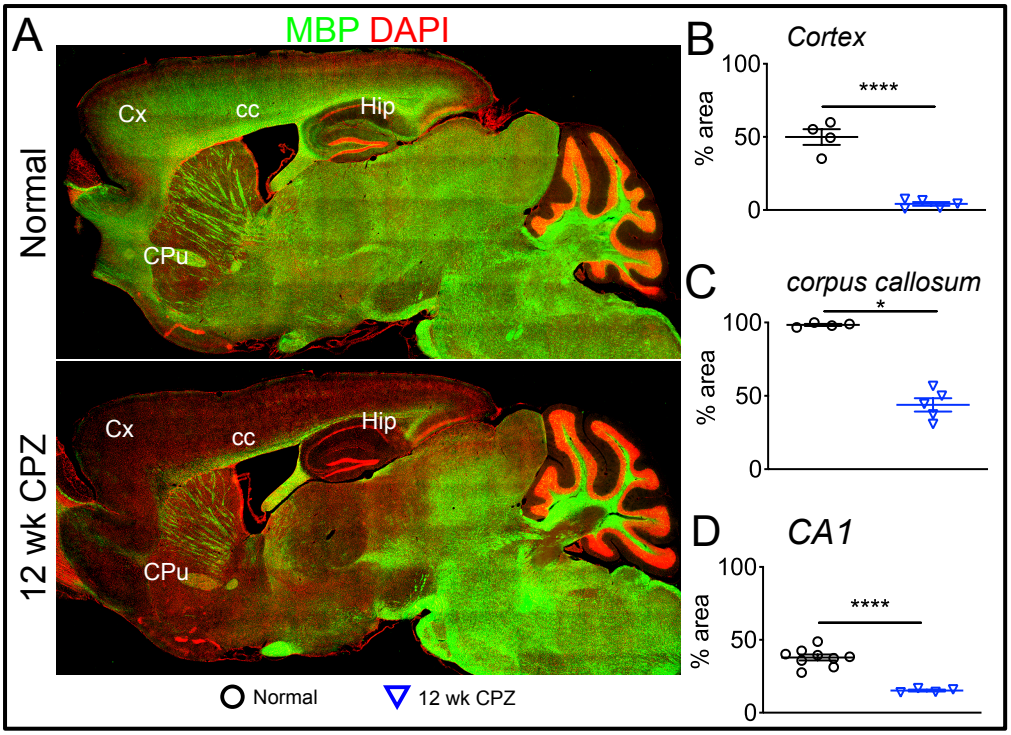


**Figure 3.3 |** *Cuprizone produces significant cortical, callosal, and hippocampal demyelination by 12 weeks of administration.* A) Representative 4X stitched fluorescence micrographs of myelin (MBP; green) immunolabeling with nuclear counterstain (DAPI; red) in sagittal sections taken from Normal (top) and 12 wk CPZ (bottom) mice. Cx = cortex, cc = corpus callosum. B-D) Cx, cc, and CA1 MBP immunoreactive area fraction in Normal and 12 wk CPZ animals. One-way ANOVA with Tukey's correction for multiple comparisons.

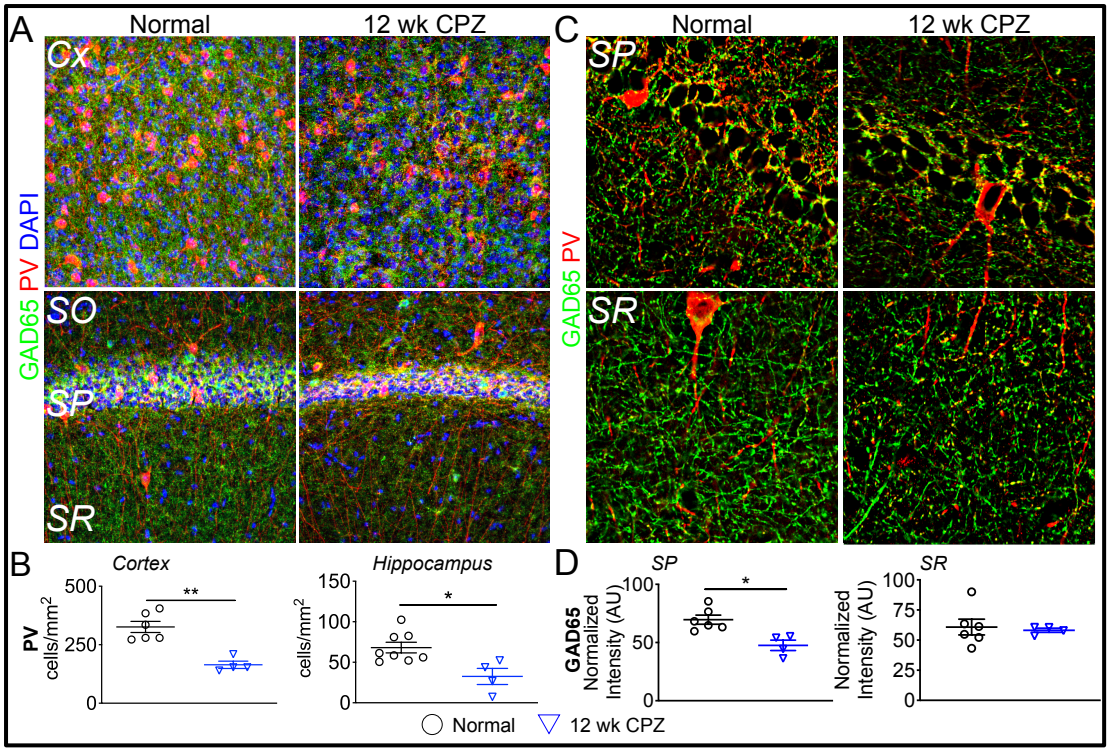


**Figure 3.4 |** *PV+ interneuron loss from cortex and hippocampus is associated with reduced presynaptic GABAergic marker intensity in 12 wk CPZ pyramidal cell layer.* A) Representative 20X confocal micrographs showing cortical (top) and hippocampal (bottom) GABAergic synaptic immunolabeling (GAD65; green) and PV-expressing neurons (red) with nuclear counterstain (DAPI; blue) in Normal (left column) and 12 wk CPZ mice (right column). SO = stratum oriens, SP = pyramidal cell layer, SR = stratum radiatum. Quantification of PV+ cell density in hippocampal CA1 subregion revealed decreased population size in medial cortex and CA1 of 12 wk CPZ animals. C) Representative 60X confocal micrographs showing putative GABAergic synapses (GAD65; green) and PV (red) in Normal and 12 wk CPZ CA1. D) Quantification of normalized GAD65 signal intensity from (C). GAD65+ signal was reduced in 12 wk CPZ animals relative to normal in SP but not SR. One-way ANOVA with Tukey's test for multiple comparisons.

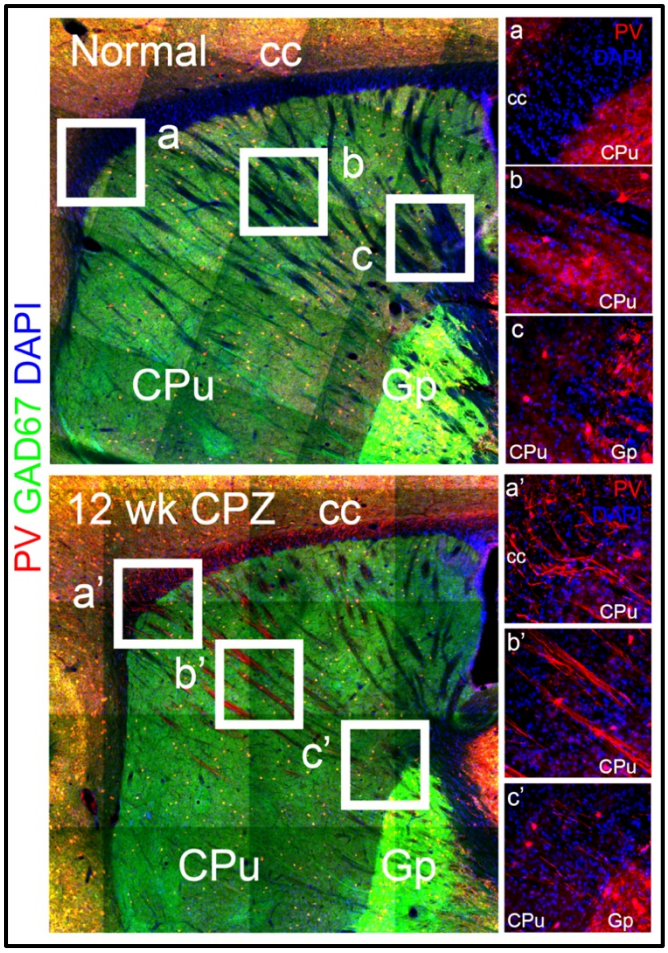


**Figure 3.5 |** *Novel PV expression in demyelinated white matter tracts of chronically CPZ-fed mice with seizures.* Distribution of GAD67 (green) and PV-interneuron (red) immunolabeling with nuclear counterstain (DAPI; blue) in representative 10X stitched sagittal micrographs from Normal (top) and 12 wk CPZ (bottom) mice. cc = corpus callosum, CPu = caudate putamen, Gp = globus pallidus. a-c) 20X micrographs showing PV immunolabeling restricted to diencephalon parenchyma representative of staining in Normal mice. a'-c') Representative 20X micrographs showing novel PV-immunostaining in 12 wk CPZ mice following internal capsule white matter between cortex and Gp with axonal morphology. Images were acquired from mediolaterally matched sections from right sagittal-cut hemispheres, approximately 1 mm from midline.

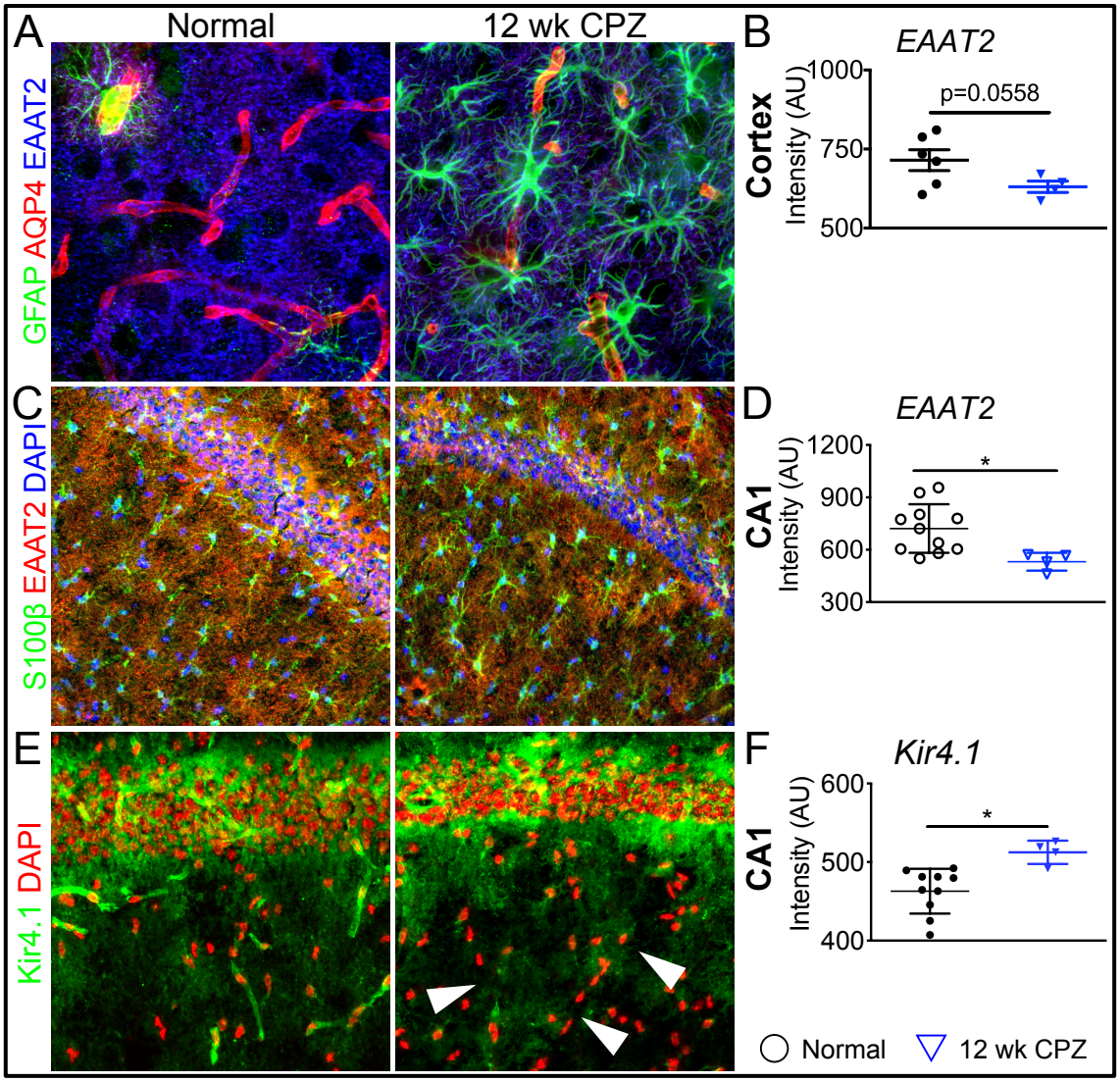


**Figure 3.6 |** *Astrocytes may contribute to neuronal hyperexcitability through altered $K^+$ and glutamate buffering in chronically demyelinated mice with seizures.* A-B) Representative 40X micrographs showing astrocytes (GFAP; green), glutamate transporters (EAAT2; blue), and AQP4 (red) in Normal and 12 wk CPZ medial cortex with EAAT2 signal quantification. EAAT2 intensity trended toward decline in 12 wk CPZ Cx relative to normal. C-D) Representative 20X micrographs showing astrocytes (S100β; green) and glutamate transporters (EAAT2; red) with nuclear counterstain (DAPI; blue) in

hippocampal CA1 of Normal and 12 wk CPZ mice with intensity quantified. EAAT2 signal was reduced in 12 wk CPZ mice compared to normal. E-F) Representative 20X micrographs demonstrating Kir4.1 immunoreactivity (green) with nuclear counterstain (DAPI; red) in Normal and 12 wk CPZ mice. Kir4.1 signal intensity (quantified in [F]), was elevated in CA1 of 12 wk CPZ mice compared to normal. However, perivascular Kir4.1 distribution was absent or less robust in 12 wk CPZ CA1, indicated by arrowheads. One-way ANOVA with Tukey's test for multiple comparisons.

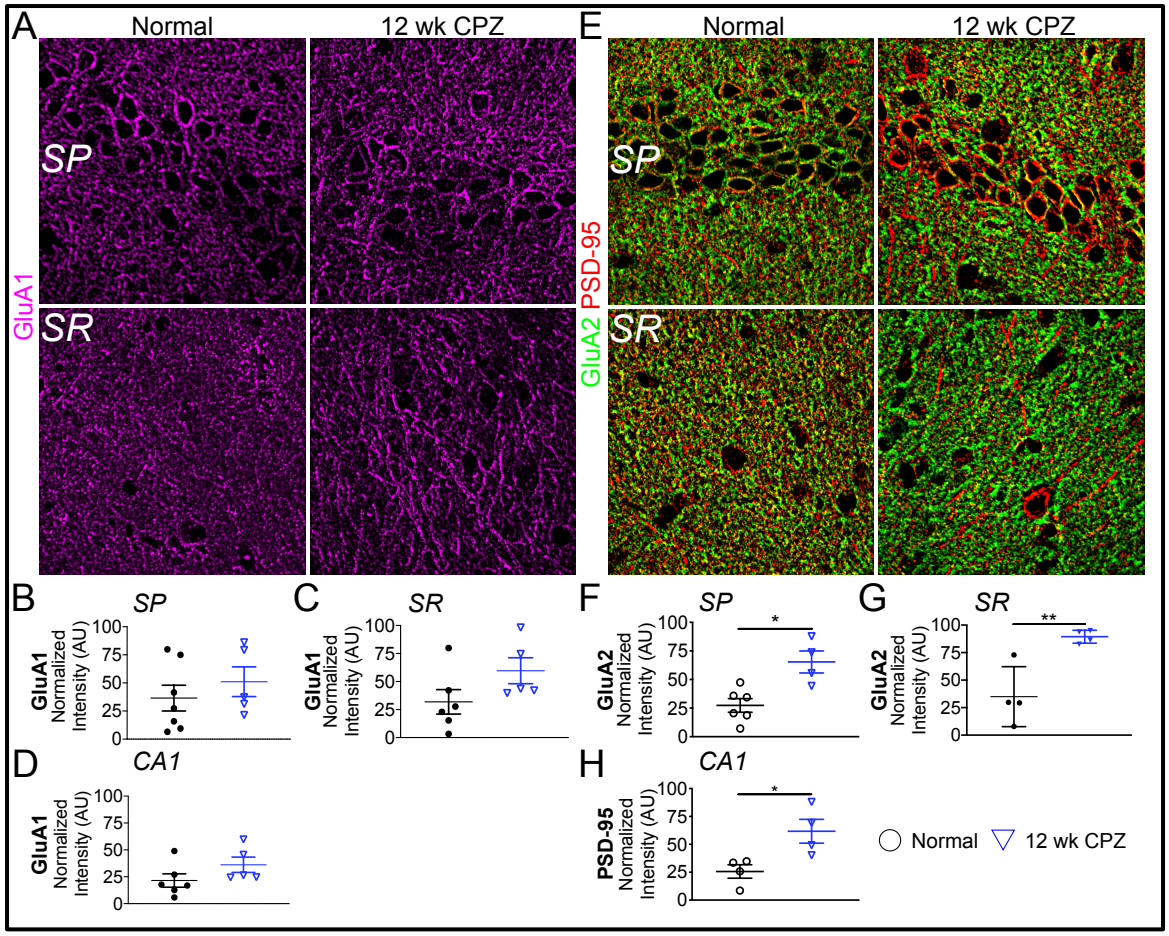


**Figure 3.7 |** *Shift toward greater GluA2+ AMPAR subunit composition in chronically demyelinated mice with seizures.* A) GluA1 immunolabeling in representative 60X micrographs acquired from Normal and 12 wk CPZ CA1 SP & SR. B-D) GluA1 signal intensity was comparable between groups in all regions of interest analyzed. E) GluA2 immunolabeling (green) with glutamatergic post-synaptic density (PSD) protein, PSD-95 (red), in Normal and 12 wk CPZ CA1 SP/SR. F-G) GluA2 signal intensity was elevated in all regions of interest analyzed relative to Normal. H) Increased 12 wk CPZ PSD-95 signal paralleled GluA2. One-way ANOVA with Tukey's test for multiple comparisons.

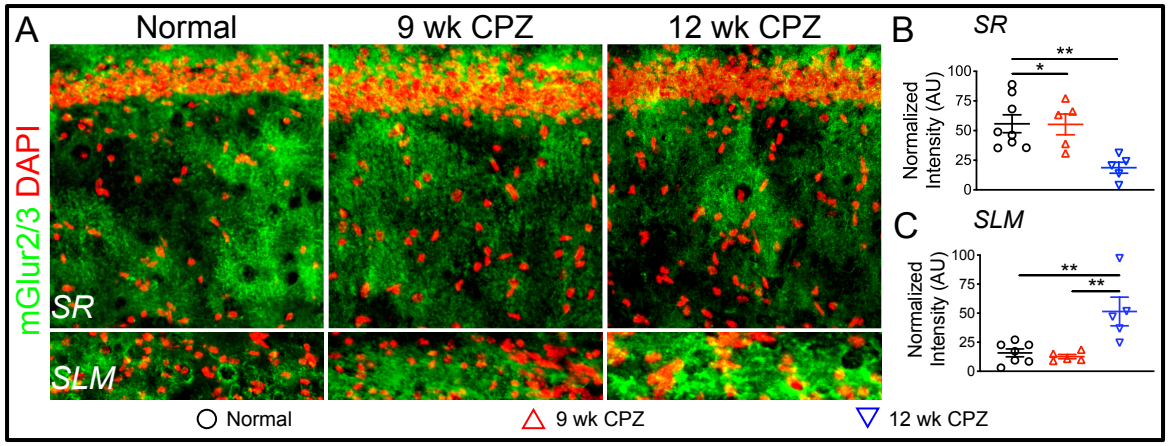


**Figure 3.8 |** *Hippocampal CA1 group 2 metabotropic glutamate receptor expression is differentially impacted in mice with demyelination-induced seizures.* A) Group 2 mGlur immunolabeling (mGlur2/3; green) with nuclear counterstain (DAPI; red) in representative 20X micrographs acquired from Normal, 9 wk CPZ, and 12 wk CPZ CA1 SR (top) & SLM (bottom). B) Normalized group 2 mGlur signal intensity was reduced in 12 wk CPZ relative to 9 wk CPZ and Normal cohorts. C) SLM mGlur signal intensity rose in 12 wk CPZ mice compared to other groups. all regions of interest analyzed. One-way ANOVA with Tukey's test for multiple comparisons.

| Antibody | Manufacturer | Catalogue # | RRID | Dilution |
|---|---|---|---|---|
| chicken anti-MBP | Millipore Sigma | AB9348 | AB_2140366 | 1:500 |
| chicken anti-GFAP | Millipore Sigma | AB5541 | AB_177521 | 1:1000 |
| rabbit anti-AQP4 | Millipore Sigma | AB2218 | AB_1163383 | 1:500 |
| guinea pig anti-EAAT2 | Millipore Sigma | AB1783 | AB_90949 | 1:1000 |
| mouse anti-non-phosphorylated 200 kDa neurofilament (SMI-32) | Millipore Sigma | NE1023 | AB_10682557 | 1:500 |
| rabbit anti-Kir4.1 | Alomone Labs | APC-035 | AB_2040120 | 1:500 |
| rabbit anti-PV | Abcam | ab11427 | AB_298032 | 1:500 |
| rabbit anti-GluA1 | Abcam | ab183797 | AB_2728702 | 1:500 |
| mouse anti-GluA2 | Millipore Sigma | MABN1189 | AB_2737079 | 1:500 |
| rabbit-anti-PSD-95 | Abcam | ab18258 | AB_444362 | 1:500 |
| rat-anti somatostatin (SST) | Millipore Sigma | MAB354 | AB_2255365 | 1:100 |
| mouse anti-glutamate decarboxylase (GAD)65 | Abcam | ab26113 | AB_448989 | 1:500 |
| rabbit anti-GAD67 | Millipore Sigma | MAB5406 | AB_2278725 | 1:500 |
| goat anti-chicken IgG (H+L), DyLight 650 | Invitrogen | SA5-10073 | AB_2556653 | 10 µg/mL |
| goat anti-rabbit IgG (H+L), Alexa Fluor +555 | Invitrogen | A32732 | AB_2633281 | 1:500 |
| goat anti-mouse IgG (H+L), Alexa Fluor +555 | Invitrogen | A32727 | AB_2633276 | 1:500 |
| goat anti-guinea pig IgG (H+L), Cy3 | Millipore Sigma | AP108C | AB_92422 | 1:1000 |
| goat anti-rabbit IgG (H+L), Alexa Fluor +488 | Invitrogen | A32731 | AB_2633280 | 1:500 |
| goat anti-rabbit IgG (H+L), Cy3 | Millipore Sigma | AP108C | AB_92422 | 1:500 |

**Table 3.1 |** *List of antibodies used in Chapter 3.*

## CONCLUDING REMARKS

Evidence for elevated CNS glutamate is abundant in MS, but only some patients experience epileptic seizures (189). GWAS may be useful in uncovering genetic risk factors, however, the data we present herein suggest cellular populations are impacted differently during demyelinating disease in putatively epileptogenic ways. In this manuscript, we identified that seizures in demyelinating disease are associated with electrographic and behavioral seizures, educed and modified GABAergic innervation, altered presynaptic and glial regulation of glutamatergic neurotransmission, and interruption of normal astrocyte $K^+$ handling. Additionally, the translational relevance of these findings was validated in postmortem hippocampal tissue from MS patients with seizures, which display analogous dysfunction in water, glutamate, and $K^+$ handling by astrocytes. As discussed previously, each of these perturbations feasibly reduces the input threshold necessary to elicit or contain seizures in the demyelinated CNS. However, when these data are considered within an excitation/inhibition imbalance framework of epileptogenesis, their summation favors uncompensated glutamatergic signaling as a driver of seizures in demyelinating disease (277) (**Summary Figure A-C**).

Although ostensibly multifactorial in their maintenance, future studies will determine the position of these phenomena within the etiology of demyelination-induced seizures. Notably, planned experiments (339) are designed to test whether the GABAergic PV+ cell loss observed in 12 wk CPZ mice is sufficient and necessary to produce seizures during chronic CPZ intoxication (**Summary Figure A**). There is reason to believe this is the case: unilaterally silencing hippocampal PV+ interneurons produces spontaneous recurrent ictal activity in otherwise healthy mice (340). Paralleling the histopathology seen both experimentally using CPZ and in postmortem human tissue,

seizures arising from PV silencing happen in the absence of widespread neurodegeneration (60, 61, 340).

The extent to which CPZ-induced PV+ cell loss recapitulates the AAV-mediated silencing paradigm deployed in Drexel et al., is not known, but targeting these cells therapeutically may be sufficient to avert epileptogenesis in MS (340). Indeed, a similar approach yields encouraging results in the APP/PS1 model of Alzheimer's disease (AD), which is associated with network hyperexcitability, subclinical epileptic waveforms, and PV+ interneuron dysfunction (341-343). Negatively modulating PV+ interneurons chemogenetically using Designer Receptors Exclusively Activated by Designer Drugs (DREADDs) demonstrates promise in preserving these cells in the otherwise hostile neurodegenerative environment of AD (343). Careful titration of such an intervention is required, however; similarly attenuating PV+ interneuron via the hM4Di DREADD, which reduces neuronal firing probability, reduces the threshold input necessary to elicit seizure (340, 344).

Although PV+ cell loss-induced disinhibition may be sufficiently epileptogenic, the astrocyte dysfunction reported feasibly contributes independently to network hyperexcitability during demyelinating disease (60, 61). Astrocytes and other macroglia maintain direct cytoplasmic linkage, effectively rendering them a syncytium through which metabolites and signaling molecules permeate (185). This state of cellular interconnectivity is critical to astrocyte control of neuronal excitation: spatial redistribution of potassium and control of synaptic glutamate availability are essential in constraining epileptiform discharges and constraining generalization (163, 209, 211, 281, 345, 346).

Glial glutamate transporters, inward rectifier potassium channels, water channels, and connexin subunits are all affected by demyelinating disease (**Summary Figure B**)

(60, 61). Although more study is required to confirm the functional impact of these data, impaired astrocytic excitoregulation is frequently indicted as epileptogenic (281, 303). Additionally, the CPZ-induced backdrop of lost oligodendrocyte potassium uptake, which is demonstrably ictogenic in its own right, may potentiate the deleterious effects caused by astrocyte dysfunction (300). Furthermore, astrocyte control of network excitation requires coupling between glial glutamate uptake by EAAT2 with GAT-3-mediated GABA efflux (280, 286, 347). Thus, the ramifications of compromised astrocytic support in demyelinated animals with seizures may extend beyond glutamate and potassium buffering, thereby behooving further investigation.

An important limitation to the model used in acquiring these data pertains to the minimal role of humoral immunity in producing CPZ pathology (348). Many of the cytokines released by lymphocytes within the context of MS potentiate glutamatergic transmission independently of their activity on specific glutamate receptors (289, 349-352). As cytokine milieu differs between adaptive models of MS, such as EAE, and CPZ, meaning the studies deployed here are unlikely to capture the contribution of cytokines to demyelination-induced seizures (108). However, because seizures are not reported in mice with EAE, alternative models are required. Notably, seizures are observed in mice exposed to the Theiler's murine encephalomyelitis virus model of MS, which exhibits robust lymphocyte infiltration (353). In this model, infiltration of peripheral macrophages exhibiting elevated production of TNF and IL-1β were required to elicit seizures (353). These data suggest the primacy of innate immunity in producing seizures during demyelinating disease but demand additional study to confirm.

In summary, the studies contained herein indicate that electrographically identifiable seizures appearing secondary to demyelinating disease involve disinhibition

of principle cell ensembles, augmented glutamate sensitivity, and suppressed metabolic support by astroglia. Planned studies will address the saliency of these elements to the pathophysiology contributing to seizures in MS with goal of identifying their core driver.

**SUMMARY FIGURE**

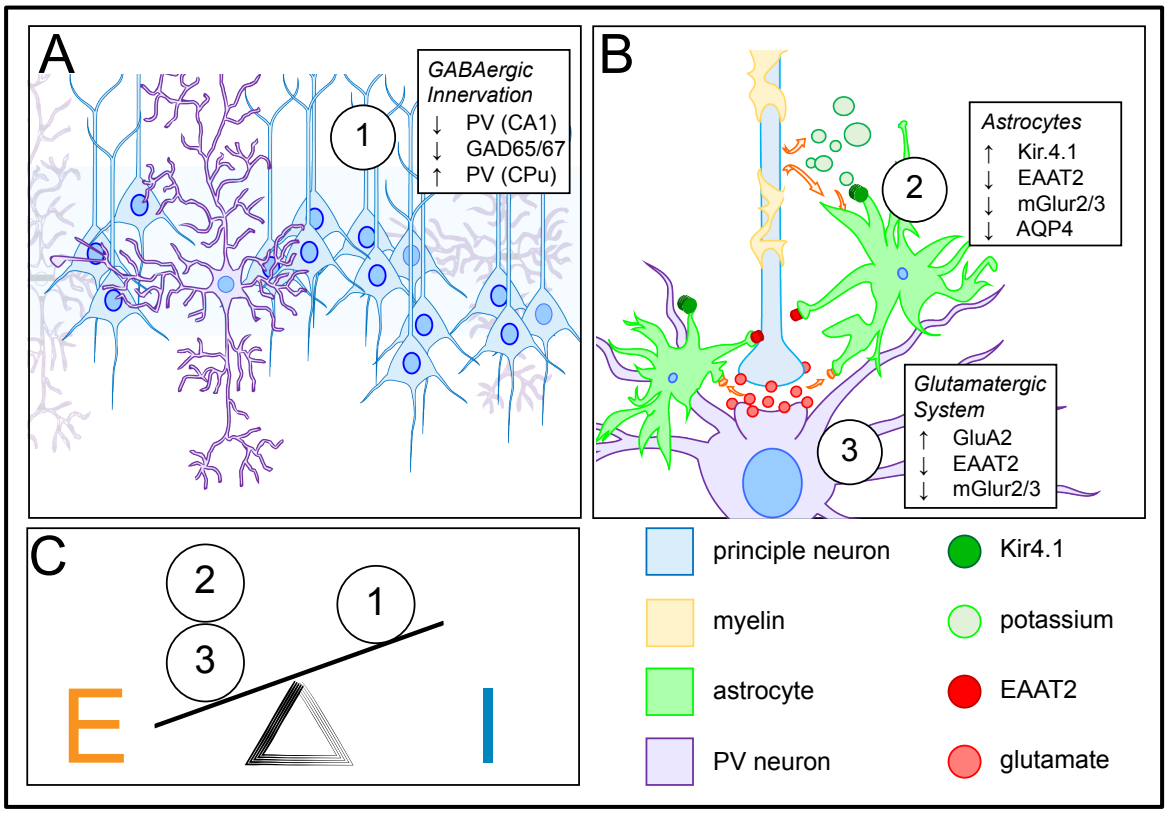


**Summary Figure** | *Visual summary of demyelination-induced changes and how they may contribute to seizures.* A) Loss and remodeling of PV-supplied GABAergic innervation (1) impairs inhibition-mediated resistance to seizures. B) Dysfunction of astrocytic glutamate & potassium handling (2) leads to more easily elicited and higher magnitude glutamatergic transmission (3). C) Potentiated excitatory neurotransmission (E, gold; 2 & 3) and reduced inhibitory tone (I, blue; 1) imbalances E/I axis, resulting in seizures.

**APPENDIX A** | Detailed HBSFRC clinical data.

| | ID | Age | Sex | Autolysis time (hrs) | Diagnoses | Stains: structures | Microscopic exam findings |
|---|---|---|---|---|---|---|---|
| MS | 2639 | 72 | F | 11.0 | RRMS | H&E: FC, PC, PVWM, Hip, TC. LFB: PVWM | PVWM shows moderately-well demarcated plaque consisting of decreased staining, extensive oligodendrocyte loss, and prominent gliosis. The myelin stain shows varying amounts of residual myelination with complete sparing of the subcortical U-fibers. There is mild focal perivascular cuffing by lymphocytes. Adjacent, uninvolved white matter shows mild thickening of the small vascular structures. The neocortex is normal. There is no hypercellularity and microglial nodules are not identified. Sections of FC show extensive necrosis, hemorrhage, perivascular lymphocytic infiltration and gliosis. The hippocampus shows rare neurofibrillary tangles and granulovacuolar degeneration. There is no evidence of neuritic plaque formation. |
| | 2660 | 50 | F | 17.0 | RRMS | H&E: WM, FC, Hip, CB, pons, thalamus, corpus striatum. LFB: WM | WM shows moderately well demarcated plaques consisting of complete demyelination and variable oligodendrocyte loss. The density of axons in these areas is decreased by 90%. There is no axonal hypertrophy and peripheral hypercellularity is not present. There is moderate associated gliosis. There are numerous examples of perivascular cuffing by lymphocytes. Adjacent WM shows rarefication and significant gliosis. An area of TC adjacent to the Hip shows numerous hyperchromatic, pyknotic neurons in a background of spongiosis and endothelial proliferation. There is a clear demarcation with adjacent, normal appearing cortex. The remaining sections are unremarkable. |
| | 3250 | 75 | M | 17.3 | SPMS | H&E & LFB: PVWM, BG | BG show a small focal region of minimal pathology in the transcapsular caudato-lenticular grey stria. The area is slightly rarefied, has minimal gliosis, and minimal lymphocytic infiltration. The area is difficult to see with the LFB myelin stain. The PVWM is unremarkable. |
| | 3289 | 54 | F | 29.0 | RRMS | H&E: PVWM | Demyelinating plaque formation with complete demyelination and axonal loss. There is near complete loss of oligodendrocytes. Scattered astrocytes are also present in the plaque with focal areas of very reactive gliosis at the plaque margin. Macrophages are generally absent although numerous examples of perivascular hemosiderin laden macrophages are present. Significant inflammation is not present. The adjacent WM shows a slight increase in cellularity with mild perivascular inflammation and perivascular hemosiderin laden macrophages. |
| | 3737 | 76 | F | 12.8 | SPMS | H&E & LFB: subcortical WM, posterior occipital WM | Partial periventricular rarefaction with 40% associated axonal loss, moderate demyelination, and mild oligodendrocyte loss. There is no evidence of macrophage activity or perivascular lymphocytic infiltration. |
| | 3835 | 65 | M | 29.4 | SPMS, melanoma, colon CA | H&E & LFB: PVWM | The section shows plaque formation with up to 90% axonal loss and 75% demyelination. There is a prominent decrease in oligodendrocyte density and associated gliosis is mild. There are numerous examples of macrophage activity and perivascular lymphocytic cuffing. |
| | 4212 | 50 | F | 18.9 | MS, hepatitis B, bed sore, chronic UTI | H&E: PVWM, Hip, TC. LFB: PVWM | PVWM sections show demyelinating plaque formation with up to 100% axonal loss and 100% demyelination. There is near-complete oligodendrocyte loss and prominent associated gliosis. There is no evidence of macrophage activity or perivascular lymphocytic cuffing. The TC shows normal neuronal cellularity. The Hip shows no evidence of neurodegenerative disease or hypoxia. |
| | 4750 | 83 | F | 19.4 | MS, Chronic MS plaque formation, stroke, extensuive atherosclerosis | H&E: PVWM, Hip, TC, Pu, centrum semiovali, pons. LFB: PVWM | PVWM shows a small area of demyelination with up to 50% axonal loss, 50% demyelination, and scattered corpora amylacea. Oligodendrocyte loss and gliosis are minimal and there is no associated macrophage activity or perivascular lymphocytic cuffing. The section of right centrum semiovali shows a very small focus of demyelination with up to 75% axonal loss, vacuolization, oligodendrocyte loss, and gliosis. An LFB myelin stain was not done on this section but demyelination appears from the H&E to be prominent. There is also associated macrophage activity and perivascular lymphocytic cuffing. The section of Left Pu contains an area of cavity formation secondary to liquefactive necrosis with scattered residual macrophages and adjacent gliosis. The section of pons is unremarkable. The section of TC shows normal neocortical neuronal cellularity and normal subcortical WM. The Hip is normal without evidence of neurodegeneration or hypoxia. |
| | 4803 | 57 | M | 29.7 | Depression, Hypertension, MS plaque formation | H&E: PVWM, Hip, TC. LFB: PVWM | PVWM shows demyelinating plaque formation with up to 50% axonal loss and 50% demyelination. There is a variable decrease in oligodendrocyte density. There is minimal associated gliosis. There are scattered distended macrophages and examples of perivascular lymphocytic cuffing. The neocortex contains normal neuronal cellularity. Hip contains scattered shrunken and hyperchromatic neurons. |
| | 4995 | 63 | F | 35.5 | SPMS, AD, chronic UTI | H&E: BS WM, Hip, TC. LFB: BS WM | CB shows a small focus of subcortical demyelinating plaque formation with up to 40% axonal loss and 60% demyelination. There is a mild decrease in oligodendrocyte density and minimal associated gliosis. There is no evidence of macrophage activity or perivascular lymphocytic cuffing. TC is normal. Hip is normal without evidence of neurodegeneration or hypoxia. |
| | 5022 | 71 | M | 6.0 | MS, pulmonary embolism, trigeminal neuralgia, left bundle branch block, recurrent UTI, laparoscopic cholecystectomy, unintelligible speech with inability to cough/clear throat/whistle when tired | Neurofilament/CD68 IHC & LFB-PAS: pons CB WM | Sections from the pons and cerebral WM confirm the presence of multiple, predominantly inactive MS plaques. There is evidence of focal myelin loss with relative preservation of axons, gliosis, and relatively scant, chronic inflammation. |
| | 5024 | 67 | F | 11.8 | MS, hypertension, lyperlipidemia, depression, restless leg syndrome, osteroporosis, UTI, anemia, hysterectomy and salpingo-oophorectomy secondary to fibrosis, fibroids and bleeding, GERD, hiatal hernia | Neurofilament/CD68 IHC & LFB: FC, BG, Hip, Midbrain, pons, medulla/spinal cord, CB, frontal WM, WM plaque | Sections show evidence of mild cerebral arteriosclerosis. Sections also show multiple inactive multiple sclerosis plaques. There is evidence of focal myelin loss with relative preservation of axons and gliosis. There is only very mild focal chronic inflammation. |
| | 5025 | 73 | M | 3.4 | SPMS, cerebral arteriosclerosis | Neurofilament/CD68 IHC & LFB: PVWM, FC, BG, Hip/WM plaque, midbrain, pons, medulla/spinal cord, CB | Sections show evidence of cerebral arteriosclerosis and MS. Sampled plaques show myelin loss, gliosis, relative preservation of axons and only moderate macrophagic infiltration at the margin of some of the lesion. |
| | 5068 | 62 | M | 10.7 | MS | H&E: PVWM, Hip, TC. LFB: PVWM | PVWM shows plaque formation with up to 90% axonal loss and 100% demyelination. There is 100% oligodendrocyte loss and associated gliosis. There is no evidence of macrophage activity or perivascular lymphocytic cuffing. The neocortex contains normal neuronal cellularity and normal subcortical WM. Hip is also normal without evidence of neurodegeneration or hypoxia. |
| | 5090 | 65 | M | 26.9 | MS, hypertension, chronic UTI, pneumonia, depression, sleep apnea | H&E: PVWM, Hip. LFB: PVWM | PVWM shows an irregular area of extensive myelin loss with relative axonal preservation. There is associated gliosis and occasional macrophages. There is no perivascular lymphocytic cuffing. Hip displays well populated pyramidal and granular cell layers without evidence of neurodegeneration or acute hypoxic/ischemic change. |
| | 5093 | 74 | M | 8.5 | SPMS, optic neuritis, aspiration pneumonia, sepsis, chronic UTI, hypertension, myocardial infarction, type II diabetes | H&E: PVWM, Amy. LFB: PVWM | PVWM shows small fairly well-defined foci of myelin loss with comparative preservation of axons and occasional reactive astrocytes. Those areas are highlighted by LFB stain and could be consistent with the clinical diagnosis of MS. Amy and adjacent TC show no significant neuropathologic changes on H&E. |

| | ID | Age | Sex | Autolysis time (hrs) | Diagnoses | Stains: structures | Microscopic exam findings |
|---|---|---|---|---|---|---|---|
| MS (cont.) | 5102 | 60 | F | 14.7 | RRMS, depression, celiac disease, headache, neurogenic bladder, chronic UTI, osteoporosis, insomnia | H&E: PVWM, Hip. LFB: PVWM | PVWM shows fairly well defined area of demyelination and relative preservation of axons with scattered macrophages. Pathologically similar lesion is present in the PVWM in Hip section. Hip displays well-populated pyramidal and granular cell layers without evidence of neurodegeneration or acute hypoxic/ischemic change |
| | 5115 | 68 | F | 24.0 | SPMS, acute renal failure, paraplegic, headache, sepsis, tobacco abuse, depression, neurogenic bladder, peripheral vascular disease | H&E: FC, PVWM, Hip. LFB: PVWM | Sections of neocortex show normal neuronal laminations and populations without significant hypoxic/ischemic neuron loss or fibrous gliosis. Section of the PVWM shows a large fairly well defined area of demyelination with comparative axonal preservation. Occasional foamy macrophages, hyperplastic astrocytes, and scant perivascular small lymphocytes are noted. LFB stain highlights area of myelin loss. These findings are consistent with a chronic plaque or MS. Section of the Hip shows well-populated pyramidal and granular cell layers without acute hypoxic/ischemic changes or Hip sclerosis. In the adjacent temporal PVWM there is a well-defined area of myelin loss similar to the one in the frontal WM. |
| | 5123 | 79 | F | 24.8 | RRMS, congestive heart failure, trigeminal neuralgia, asthma, AD (probable based on neuropathology exam) | H&E: FC, PVWM, Hip. LFB: PVWM | Neocortex shows well preserved neuronal laminations and populations without significant hypoxic/ischemic neuron loss or fibrous gliosis. The Hip shows granulovacuolar degeneration and occasional, intraneuronal and "ghost", neurofibrillary tangles in the pyramidal cell layer and entorhinal cortex. There also is focal myelin pallor of the adjacent PVWM. PVWM displays somewhat ill-defined areas of myelin pallor with relative axonal preservation which are highlighted by the LFB special stain. |
| | 5268 | 66 | M | 16.8 | MS | H&E: FC, posterior cingulate gyrus, occipital WM, pons | Neocortex shows normal neuronal laminations and populations. There are arteriosclerotic changes with microhemorrhages, could be consistent with hypertension. Posterior cingulate gyrus, occipital WM, and pons clearly show old demyelination [sic] plaques. |
| | 5292 | 70 | F | 16.0 | RRMS, early onset AD, metastatic CA | H&E & LFB: BG, parietal PVWM, pons | Old demyelination [sic] plaques are seen in BG and PVWM. The loss of myelin is supported by the loss of blue stain using LFB. |
| | 5308 | 54 | F | 9.3 | SPMS | H&E & LFB: frontal WM, thalamus, pontine tegmentum | Old demyelination [sic] plaques are seen in all sections. The LFB stain confirmed the loss of myelin. Some WM blood vessels show a mild degree of perivascular lymphocytic infiltrate. The CB cortex is normal. |
| | 5320 | 74 | F | 14.9 | MS, chronic UTI, neurogenic bladder, dysphagia, osteoarthritis, anemia, neuropathy, hypertension, depression (clinical), lacunar infarct | H&E: pontine tegmentum, CB WM, fronal PVWM, parietal gray matter. CD68 IHC: PVWM | Old demyelination [sic] plaques are seen in CB WM and PVWM. A CD68 stain of the frontal PVWM highlights the macrophages in the demyelination [sic] lesion. |
| | 5350 | 70 | F | 23.1 | MS | H&E: FC, Hip, parietal WM, pons, substantia nigra | Neocortex shows normal neuronal laminations and populations without significant hypoxic/ischemic neuron loss or fibrous gliosis. Sections of the parietal WM show a fairly well demarcated area of myelin loss with relative axonal preservation and surrounding mild reactive astrocytes. the hippocampus shows no significant neuropathologic changes. Substantia nigra is well populated with pigmented neurons. Sections of the pons show well populated locus coeruleus and normal fiber tracts in basis pontis. |
| | 5353 | 50 | M | 13.0 | MS, neurogenic bladder | H&E: FC, Hip, substantia nigra, PVWM pons | Neocortex shows normal neuronal laminations and populations without significant hypoxic/ischemic neuron loss or fibrous gliosis. The subcortical WM shows multiple fairly well demarcated areas of myelin loss with relative axonal preservation. Smaller areas of demyelination with reactive astrocytosis are seen in a section of the Hip. Hip shows no significant abnormalities. Substantia nigra is well populated with pigmented neurons. There is pallor of pontine fiber tracts, likely secondary to Wallerian degermation. |
| MS+S | 2966 | 55 | F | 15.0 | 3502 | PVWM (stains not indicated) | Section of the parietal PVWM shows extensive demyelination and axonal loss, reactive astrocytes, rare lipid-laden macrophages and sparse chronic perivascular inflammation consistent with MS. |
| | 3260 | 47 | F | 11.5 | SPMS, seizure disorder, obesity | H&E & LFB: PVWM, CB | PVWM shows demyelinating plaque formation with extensively decreased intra-plaque oligodendrocyte cellularity (90-100%), extensive axonal loss, and extensive adjacent associated gliosis. Macrophages and perivascular lymphocytic cuffing are not found. The LFB stain shows complete demyelination. The adjacent cortex and WM are unremarkable. The section of CB is also unremarkable. |
| | 3502 | 78 | M | 15.5 | SPMS, Stroke/CVA, Bell's Palsy, seizure disorder | H&E: periventricular plaque, BG, occipital subcortex. LFB: periventricular plaque | The demyelinating plaque shows complete oligodendrocyte loss, complete axonal dropout, and complete demyelination. There is moderate associated gliosis. There is minimal perivascular cuffing but macrophage activity is not observed. Adjacent cortex and WM are unremarkable. The occipital cortical sections show small areas of subcortical pallor. The section of BG shows no evidence of demyelination, infarction, or necrosis. Scattered small vascular structures show medial thickening. |
| | 4546 | 59 | M | 38.5 | MS, seizure disorder, dementia, depression, optic neuritis, aspiration pneumonia, dysphagia, COPD, hyperlipidemia, neurogenic bladder | H&E: WM plaque, TC, Hip, thalamus. LFB: WM plaque | WM plaque shows irregular foci of demyelination with up to 80% axonal loss and 100% demyelination. There is a marked decrease in oligodendrocyte density with moderate associated gliosis and scattered corpora amylacea. Significant macrophage activity and perivascular lymphocytic cuffing are absent. The adjacent uninvolved WM also shows scattered corpora amylacea but is otherwise normal. Thalamus shows a similar process but with less axonal loss and demyelination. Hip and TC are normal |
| | 4869 | 54 | F | 12.3 | Depression, Hypertension, seizure disorder | H&E: PVWM, FC, Hip, TC. LFB: PVWM | PVWM shows mild periventricular demyelinating plaque formation with up to 50% axonal loss and 50% demyelination. There is a variable decrease in oligodendrocyte density. Associated gliosis is mild. There is scattered evidence of macrophage activity and minimal perivascular lymphocytic cuffing. The neocortex shows normal neuronal cellularity and normal subcortical WM. The Hip is also normal without evidence of neurodegeneration or hypoxia. |

AD = Alzheimer's disease; Amy = amygdala; BG = basal ganglia; BS = brain stem; CA = cancer; CB = cerebellum; COPD = chronic obstructive pulmonary disease; CVA = cerebrovascular accident; FC = frontal cortex; H&E = hematoxylin & eosin stain; Hip = hippocampus; LFB = Luxol Fast Blue Stain; MS = multiple sclerosis; PAS = Periodic acid–Schiff; PC = parietal cortex; Pu = putamenPVWM = periventricular white matter; RRMS = relapsing-remitting MS; SPMS = secondary progressive MS; TC = temporal cortex; UTI = urinary tract infection; WM = white matter

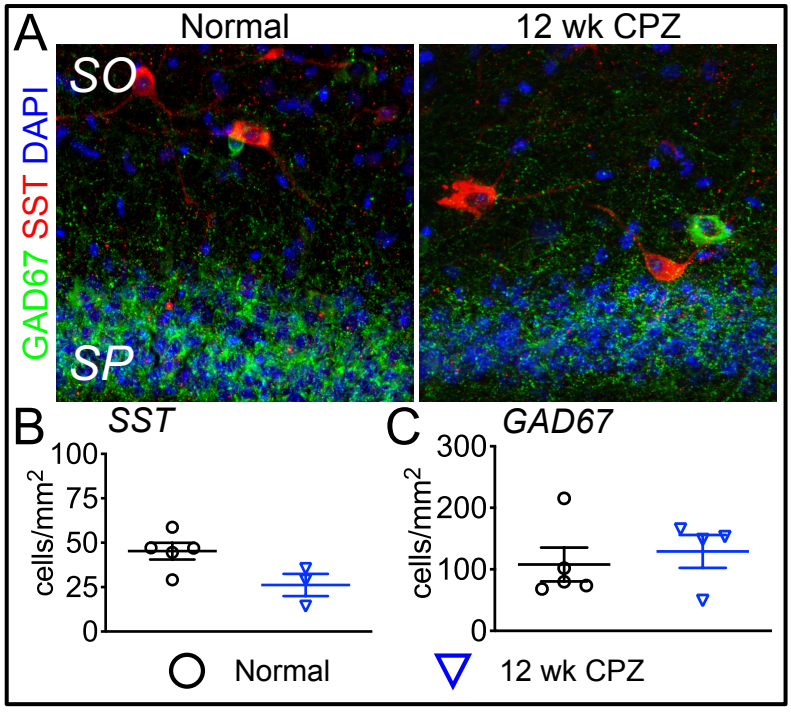


**Appendix B |** *CA1 somatostatin-expressing neurons are spared during cuprizone demyelination-induced epileptogenesis.* A) Representative 20X micrographs showing normal and 12 wk CPZ immunolabeling for SST+ interneurons (red) and total GABAergic neurons (GAD67; green) in CA1 SO & SP. B-C) Quantification of images shown in (A). Neither SST+ nor GAD67+ cell density changed significantly between normal and 12 wk CPZ animals. Ordinary one-way ANOVA with Tukey's correction for multiple comparisons.

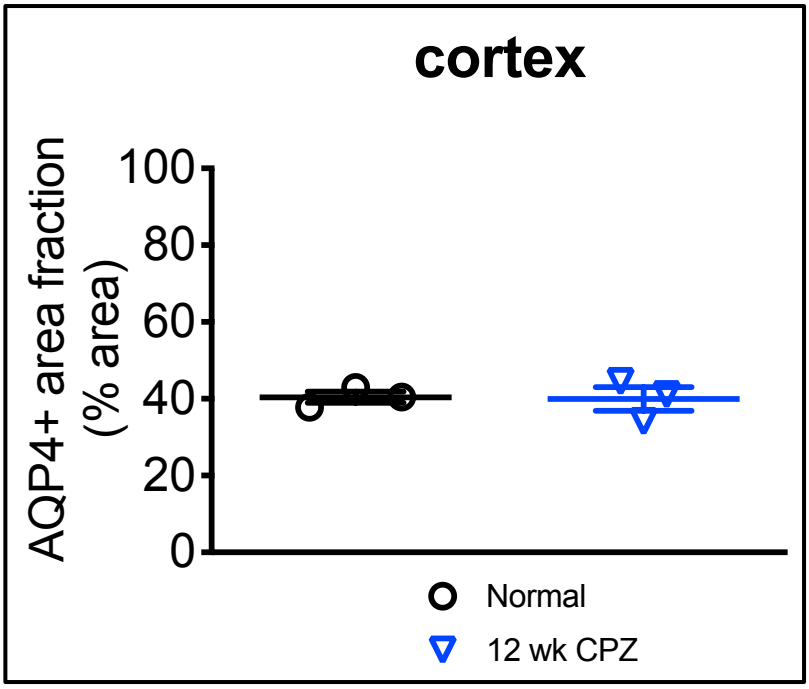


**Appendix C |** *Cortical AQP4 is comparable between Normal and 12 wk CPZ mice.* Quantification of cortical AQP4-immunoreactive area fraction in **Figure 3.6A** showed no statistically appreciable difference between Normal and 12 wk CPZ mice.

**APPENDIX D |** Connexins and pannexins: At the junction of neuro-glial homeostasis & disease.

Andrew S. Lapato[a,c] & Seema K. Tiwari-Woodruff[a,b,c]

a) Division of Biomedical Sciences, UCR School of Medicine, Riverside, CA 92521
b) Neuroscience Graduate Program, UCR, Riverside, CA 92521
c) Center for Glia-Neuronal Interaction, UCR School of Medicine, Riverside, CA 92521

A version of this section was published in *The Journal of Neuroscience Research*.

Lapato, A. S. & Tiwari-Woodruff, S. K. Connexins and pannexins: At the junction of neuro-glial homeostasis & disease. *J Neurosci Res* **96**, 31-44 (2018).

## Introduction

Accruing evidence indicates that connexin (Cx) and pannexin (Panx) transmembrane channels are crucial to the coordination and maintenance of physiologic CNS activity. In neurons, Cxs electrochemically couple neurons by electrical synapses (354), while glial Cxs mediate numerous functions ranging from K+ buffering to direct modulation of glutamatergic activity (209, 211, 226, 345). Alone, Cxs and Panxs represent a mechanism for robust autocrine and paracrine signaling through release of gliotransmitters, which are essential to synaptic strength and plasticity (355, 356). Dysregulation of Cx and Panx activity is implicated in neurodegenerative disease (357) and may be etiologic in some human epilepsy (281). In addition, Cx and Panx sensitivity to inflammatory mediators suggests that alteration in neuronal excitability may be present in a range of disease states. In the following sections, we will describe the structure, function, regulation, and distribution of CNS Cx and Panx molecules. We will also summarize evidence for their functions related to neuronal excitability under homeostatic conditions and examine their role as effectors of pathological glutamatergic transmission.

## Structure and function of connexins and pannexins

Structurally, the Cx and Panx family of proteins comprise a group of transmembrane pores that are permeable to ions, metabolites, second messengers, and purine signaling mediators up to 1.5 kDa (358) with divergent peptide sequences but homologous topology. Each channel forming complex is composed of six monomers containing four membrane-spanning domains linked by two extracellular loops that mediate docking with complimentary Cx hexamers (Figure 1). Post-translational modification of Cx monomers largely takes place at the site of the intracellular carboxyl tail (359) and is thought to regulate non-channel functions of Cxs such as adhesion,

migration (360, 361), and proliferation (362, 363). Adhesion and migration mediated by GJs are of particular importance in the developing CNS, where they facilitate neocortical neuron migration by providing points of contact with radial glia (364) and movement of subventricular zone-derived cells along the rostral migratory stream (365). Phosphorylation of the Cx intracellular tail plays a role in gating pore permeability, thereby allowing dynamic opening and closing under a range of conditions (366). However, Cx and Panx biology may extend beyond these functions into a variety of intracellular regulatory processes (367).

When uncoupled to a complimentary hexamer, these pores are termed hemichannels (HCs) and allow exchange of cellular contents with the extracellular space (368). Opening of Cx and Panx HCs has traditionally been thought of as deleterious to CNS homeostasis (369), occuring under pathological conditions leading to excitotoxic cell death such as ischemia (370, 371) and excessive depolarization (372, 373). More recent evidence, however, has shed light on Cx and Panx HC physiologic activities including their function as a platform for robust autocrine and paracrine signaling between and amongst glia and neurons (355, 374).

Gliotransmission continues to draw attention to Cx and Panx HCs, whereby paracrine signaling by purinergic mediators and a host of other gliotransmitters released by these channels have proven essential to synaptic strength and plasticity (217, 375, 376). When HCs are coupled with complementary HCs on adjacent cells, they form gap junctions (GJs), which act in pairs to facilitate direct intercellular communication of cytoplasmic molecules. Of note, Panx1 HCs have not been shown to form GJs in vivo without substantial manipulation (377-379), which is thought to be due to post-translational N-linked glycosylation of the second extracellular loop of each Panx subunit

(Figure 1). In neurons, GJs are the substrate of electrical synapses formation (380), while GJs among glia couple cells in the panglial network, which participates in buffering excitotoxic metabolites produced by depolarizing activity.

Regulation of GJ and HC open probability is affected by a variety of circumstances. Under homeostatic conditions, neuronal activity leading to decreased extracellular Ca2+ (210, 356) and increased K+ (381) encourages opening of HCs and autocrine purinergic signaling via adenosine triphosphate (ATP) release (382). However, pathological environments also open HCs and GJs aberrantly. Neurodegenerative diseases such as experimental autoimmune encephalomyelitis (357), multiple sclerosis (383), and epilepsy (281) cause uncoupling of pan-glial network GJs, with the resulting dysregulated gliotransmitter release contributing to abnormal neuronal activity (356). Inflammatory mediators, including the cytokines interleukin (IL)-1β and tumor necrosis factor (TNF)α drive HC open probability, as application of either cytokine or the toll-like receptor (TLR) 4 ligand lipopolysaccharide (LPS) induces increased hemichannel— mediated uptake of ethidium bromide in astrocytes both in vitro and slice (222, 227).

Expression of Cxs and Panxs is distributed throughout the CNS (Table 1) where they participate in a variety of functions. In addition to their channel activity which promotes metabolic coupling amongst macroglia (384), Cx GJs are critical to glial survival and stabilization of associated Cx HCs (163, 359). Mutations in oligodendrocyte-expressed Cx genes result in phenotypes indistinguishable from inherited hypomyelinating leukodystrophies, which are characterized by impairment of myelin sheath formation, inflammation, and sensorimotor neurological deficits (163, 359, 385). For example, a mutation in the Cx47 promoter results in Pelizaeus–Merzbacher-like disease (386), while

altered Cx32 expression leads to symptomology closely resembling Charcot-Marie-Tooth disease (387).

Further emphasizing the importance of glial coupling, astrocyte-oligodendrocyte coupling is reduced in Cx47—KO mice and is associated with myelin vacuolation in the optic nerve (388). Mice lacking Cx32 and Cx47 exhibit more pronounced myelin pathology, which is accompanied by loss of oligodendrocytes and action tremors progressing into tonic-clonic seizures and mortality by the sixth postnatal week (388, 389). Loss and activation of astrocytes, oligodendrocyte loss, myelin vacuolation, inflammation, and invasion of phagocytic cells are also common to disorders of GJ coupling (163, 359, 390), suggesting a role for intact pan-glial network GJ connections in supporting its members' survival and homeostatic functions. However, while non-channel properties of Cxs have been explored in the context of neuronal differentiation (362, 391) and glutamatergic transmission (213), the mechanism whereby Cxs support glial survival remains poorly understood.

**Connexins and pannexins in synaptic plasticity**

*Electrical synapses, excitability, and learning*

At the forefront of Cx and Panx neurobiology research is their role in neuronal excitability and their ability to modify synaptic activity. Neuronal GJs, which couple cells by electrical synapses, are numerous in the embryonic CNS, but become increasingly limited during development (392-400). In the adult mammalian brain, GJs are restricted primarily to inhibitory GABAergic networks and associated principle neurons (354, 401), with Cx36 becoming the predominant isoform expressed (392, 402). Cx36 GJs allow rapid electrochemical transmission and influence synchronization of interconnected neurons (403, 404). Coupled neurons of the reticular thalamic nucleus and suprachiasmatic

nucleus of the thalamus (SCN) display inherent Cx36-dependent desynchronizing properties (405, 406). While synchronization of SCN neurons is required for light-dark cycle detection and circadian rhythm, these examples illustrate the overriding strength of inhibitory networks coupled by GJs and hint at their physiologic role in resisting development of epileptiform synchronization.

Traditionally, GJ-mediated electrical synapses have been considered static structures. However, recent research casts doubt on this long-standing assumption. Like glutamatergic chemical synapses, GJ-mediated electrical synapses in the rat inferior olive also display activity dependent strengthening (407). In this study, the authors observed that the N-Methyl-D-aspartate receptor (NMDAR) NR1 subunit co-localized with neuropilar Cx36 GJs. Agonism of NMDARs resulted in increased coupled potential upon stimulation that was accompanied by elevated uptake of a tracer dye (407), indicating that GJ—NMDAR complexes are sensitive to synaptic activity and become upregulated or opened in response. As electrical synapses facilitate rapid and widespread inhibition, these data suggest that depolarizing inputs modify GJ strength to set a basal inhibitory tone on excitatory networks.

Unsurprisingly, in addition to their function in limiting excitability, neuronal GJs also play a major role in learning and memory. Knockout of Cx36 resulted in diminished novel object recognition that was exaggerated by environments containing complex stimuli (408). In addition, Cx36—KO mice exhibited impaired short-term and long-term memory in Y-maze testing, and reduced motor learning by rotorod (408). Interestingly, field excitatory post-synaptic potentials (fEPSPs) recorded from cornu ammonis 1 (CA1) hippocampal pyramidal neurons after Schaffer collateral stimulation were also decreased in Cx36—KO mice (409), suggesting coordinated GJ-coupled interneuron activity is an

essential component of LTP inducing events. This is supported by reports finding that the power of gamma and theta frequencies, which are thought to be mediated by GABAergic interneurons (410), are increased in the hippocampus following tetanic stimulation of Schaffer collaterals (411).

Similarly, knockout of Cx31.1, which is expressed in dopaminergic neurons of the substantia nigra pars compacta (412) and striatal output neurons (413) that play a role in sensory-motor control and novelty-induced exploration (414), resulted in elevated exploration of novel environments and impaired performance in novel object recognition tasks (415). Together, these studies point to a central role for neuronal coupling via GJs in memory formation and consolidation. This may be attributable to autoinhibition of GABAergic networks by remaining inhibitory chemical synapses and reduced long term potentiation (LTP), which is thought to represent the cellular substrate of learning (416).

*The pan-glial network: beyond buffering*

The most abundant source of GJs and HCs in the brain come from the highly interconnected lattice of glial cells interspersed throughout the CNS (Figure 2). Chief among the tasks of this syncytium of astrocytes, oligodendrocytes, and endothelial cells is the modification of neuronal excitation through the spatial buffering of ions and metabolites by GJ connected cells (163, 209, 211, 281, 345, 346, 417). In this model, inward K+ currents are generated by active uptake by astrocytes and oligodendrocytes near depolarizing cells and sustained by conduction of buffered K+ to blood vessels for elimination (Figure 2). Failure to remove sufficient K+ results in adequate change in resting membrane potential to allow spontaneous action potentials. However, while this activity is critical to physiologic excitatory activity, the pan-glial network exercises additional GJ and HC mediated effects on neuronal excitability both directly and indirectly.

Astrocyte Ca2+ waves are associated with neuronal activity and are conducted through astrocyte GJs and HCs (210). Glutamatergic activity induces decline in extracellular Ca2+ accompanied by rapid elevation of intracellular Ca2+ in both astrocytes and neurons. After a delay, astrocytes then exhibit a secondary “slow” intracellular Ca2+ wave initiated by ATP release by Panx1 HCs acting in an autocrine fashion (210). These waves are not attributable to glutamate signaling and require Cx30 and Cx43 GJs to travel between neighboring astrocytes (210). Importantly, astrocyte slow waves are associated with activation of the metabotropic purine receptor P2Y1 on nearby inhibitory interneurons, leading to increased inhibitory post synaptic currents (IPSCs) (210). This suggests that Ca2+ slow waves may be involved in augmenting feedback inhibition through purinergic signaling, expanding the ways that they modify glutamatergic transmission.

Additional modulation of excitatory activity is exerted by astrocytes through Cx dependent regulation of synaptic glutamate release. Interestingly, astrocyte expressed Cx isoforms appear to affect glutamatergic transmission by distinct mechanisms. Basal quantal release of glutamate is set by Cx43 at excitatory synapses without altering the threshold for depolarization or the activity of excitatory amino acid transporters (213). Instead, postsynaptic glutamate release is augmented by purinergic signaling mediated by astrocyte HCs (226). In contrast, Cx30 buffers synaptic glutamate through non-GJ mediated activities (361). Organotypic slices from Cx30—KO mice exhibit decreased glutamatergic activity independent of presynaptic quantal release or postsynaptic glutamate sensitivity. Instead, Cx30 regulates astrocyte process migration and glutamate transporter 1 (GLT-1) efficacy. In a 2014 study, Pannasch (361) observed that Cx30—KO astrocyte processes enriched in GLT-1 invade excitatory synapses more deeply than wild type astrocytes, thereby reducing glutamate within the synaptic cleft (361). This

activity is independent of Cx30's GJ function, possibly relying on regulation by proteins complexed to Cx30 GJs.

Oligodendrocytes are commonly overlooked in the composition of the pan-glial network, instead thought of as merely myelinating projection axons. However, emerging evidence indicates that oligodendrocytes are also essential to maintaining physiologic generation of action potentials independent of their myelinating function (418-420). Oligodendrocytes comprise a varying fraction of pan-glial network participants that form biocytin-permeable homotypic GJs with other oligodendrocytes and NG2+/Olig2+CNPase-oligodendrocyte precursors in white matter (421) as well as heterotypic GJs with astrocytes throughout the CNS (422).

In myelinated fiber tracts, oligodendrocytes participate in spatial K+ buffering at the level of periaxonal myelin, which conducts ions through reflexive Cx32 GJs within myelin layers closest to the axolemma and strings of Cx32 GJs connecting adjacent paranodal loops (345). Nearby astrocyte processes then siphon K+ from myelin and oligodendrocyte somata for elimination through heterotypic Cx47—43 and Cx32—30 GJs (345). In genetic ablation studies, mice lacking both Cx32 and Cx47 exhibit periaxonal myelin vacuolation in the optic nerve that is worsened by retinal ganglion activity (423). Interestingly, the authors of this study also found that mice lacking the inward rectifier K+ channel Kir4.1 deficient mice exhibited myelin vacuolation in spinal cord grey matter (423), possibly due to osmotic damage due to failure to disperse rising K+ concentration within the myelin sheath.

In a recent study from Battefeld et al., (209) satellite oligodendrocytes (424) associated with the axon initial segment of somatosensory cortex layer V pyramidal neurons were predicted to dampen neuronal bursting by computational modelling (209).

Their model was validated experimentally and found to be mediated by activity dependent inward rectifying K+ (Kir) currents in sOLs. Furthermore, GJ blockade using the non-specific Cx/ Panx inhibitor carbenoxolone (CBX) abolished Kir currents and reduced voltage coupling between sOLs and adjacent astrocytes (209). These findings support the importance of oligodendrocytes in maintaining homeostatic extracellular ion concentrations, with implications for disease states involving white matter injury, such as MS.

*Hemichannels and purinergic signaling in synaptic plasticity, learning, and memory*

Purinergic signaling molecules released by Cx and Panx HCs acting on neuronal and glial P2X and P2Y receptors comprise a fundamental component of synaptic plasticity (355, 356, 425, 426). Measurement of CA1 fEPSPs after CA3 Schaffer collateral tetanic stimulation shows that LTP is abnormally increased in mice lacking Panx1 HCs (Panx1—KO) (355, 427). Interestingly, in addition to elevated fEPSPs, stimulation of Panx1—KO Schaffer collateral projections results in absent long term depression (LTD) in CA1 pyramidal neurons (355, 427). Behaviorally, Panx1—KO mice also perform worse at novel object recognition and spatial recall tasks (355). Thus, purines released by Panx1 HCs represent a negative feedback mechanism dampening exaggerated LTP, which has been shown to impair spatial learning (428). Remarkably, physiologic LTP is restored in Panx1—KO mice when Schaffer collateral stimulation is accompanied by a mix of gliotransmitters including adenosine and ATP, possibly reflecting hyperpolarization through ATP-dependent K+ channels (429) or adenosine mediated inhibition through A1 and A2 receptors (430, 431).

Astrocyte HCs also participate in purinergic signaling and learning. In a 2014 study from Chever (226) blockade of Cx43 HCs with the Cx43 HC-specific inhibitor gap26

resulted in reduced fEPSPs recorded in CA1 neurons after Schaffer collateral stimulation (226). These results were replicated when Cx43 HCs were left intact, but P2 receptors were blocked using the P2 antagonists RB2 and PPADS (226), suggesting purinergic signaling molecules released by Cx43 HCs were responsible for modifying glutamatergic activity after stimulation. A similar in vivo study examining the role of Cx43 HCs in fear conditioning supports these findings. In a 2012 study by Stehberg  microinjection of the Cx43 HC specific blocking peptide TAT-Cx43L2 or gap27 into the basolateral amygdala resulted in amnesia to fear conditioning training (214). Interestingly, co-administration of these blocking peptides with a gliotransmitter cocktail including glutamate, glutamine, lactate, D- serine, glycine, and ATP restored fear conditioning memory. This effect was not observed when either peptide was injected several hours after training, indicating that Cx43 HCs participated in short term fear memory consolidation (214). While this study did not implicate a specific gliotransmitter in mediating the observed effects, it bolsters slice recording findings that implicate HCs in learning and memory.

**A little too excited: connexin and pannexin dysregulation and seizures**

*Electrical synapses in seizures*

Seizures are characterized by aberrant hypersynchronous excitatory activity that may be localized to a specific population of neurons or generalized throughout several brain regions. Classically, seizure development is thought to occur when inhibitory GABAergic transmission is compromised or overwhelmed by glutamatergic activity. Under homeostatic conditions, a range of mechanisms exist that confer resistance to seizures, including principle cell inhibition and desynchronizing activity of GABAergic networks (401, 403, 404). Damage to or dysfunction of these networks may be involved in seizure initiation and propagation (117, 120).

As the primary Cx isoform expressed in the adult CNS, Cx36 GJ-coupled GABAergic populations are critical for setting basal inhibitory tone in several brain regions (392, 403, 407, 412, 413), and may be indispensable to maintaining physiologic resistance to epileptiform activity. However, the contribution of Cx36—coupling to seizures remains uncertain due to disparate—and occasionally contrary—reporting. Studies utilizing global ablation of Cx36 GJs have yielded data indicating an anti-epileptogenic (432), pro-epileptogenic (433), and bystander (434, 435) role for these molecules.

In support of an anti-epileptogenic function, Cx36—KO mice exhibit increased susceptibility to seizure induction in the pentylenetetrazol (PTZ) model of epilepsy (432). Consistent with these findings, pharmacological GJ blockade by CBX or quinine, which preferentially inhibits Cx36 and Cx50 (436), resulted in increased cortical epileptiform activity in organotypic slice culture using the low-Mg2+ model of seizure induction (437). Jacobson  hypothesize that this phenomenon may be the result of autoinhibition of GABAergic Cx36-coupled neurons (432). In this study, the authors suggest that although the electrical synapses responsible for excitation of linked inhibitory networks would be absent in Cx36—KO animals, GABAergic chemical synapses on nearby inhibitory interneurons would remain. The resulting inhibition of inhibitory cells could feasibly give rise to aberrant excitatory activity by failing to suppress collateral excitation of surrounding pyramidal neurons or providing feedback inhibition (432). This hypothesis is supported by lines of evidence that indicate that in Cx36—KO mice, hippocampal epileptiform activity induced by kainate exposure may be partially attributable to reduced GABAA receptor activity (438).

In contrast, Maier  found that Cx36—KO hippocampi were less susceptible to seizures induced by the K+ channel inhibitor, 4-aminopyridine (4-AP)(433). Their

recordings from Cx36—KO slices showed less frequent spontaneous sharp wave events than wild type hippocampi with fewer and slower ripples. These data suggest that Cx36 GJs help coordinate the excitatory hypersynchronization thought to generate sharp wave-ripple complexes (439), with their activity becoming pathologic after 4-AP exposure. Surprisingly, while ongoing seizure-like events were reduced in Cx36—KO mice, a portion of the slices recorded from failed to exhibit any activity whatsoever in response to 100μM 4-AP, indicating that Cx36 blockade could represent an effective method of managing seizures. Corroborating this, relatively selective Cx36 GJ inhibition by quinine or CBX application after 4-AP-induced seizures suppressed the amplitude of epileptiform activity and reduced involvement of the contralateral cortex in vivo (440).

However, to qualify these results, although their summed ictal activity was lower than control animals, quinine treated rats displayed more frequent seizures of shorter duration. Additional complication in understanding Cx36-mediated activity in seizures comes from studies that find it dispensable to seizure initiation and resistance. Mefloquine, a quinine derivative inhibitor of Cx36 and Cx50 GJs at low doses (441), failed to elicit any change in seizure-like event amplitude, frequency, or duration in low Mg2+ and aconitine treated neocortical slice preparations from wild type mice compared control treated and Cx36—KOs (435). Similarly, in a 2011 study, Beaumont and Maccaferri (434) found that 4-AP treated CA1 interneurons of Cx36—KO mice exhibit no difference in epileptiform GABAergic currents relative to wild type despite uncoupling of interneurons across hippocampal strata (434). Furthermore, the authors demonstrated that CBX, but not mefloquine, inhibits GABAA receptors independently of the allosteric regulatory site of benzodiazepines, calling into question the use of CBX to study Cx contributions to seizures.

The use of Cx36—KO mice also presents an important limitation in the study of epilepsy. In the low Mg2+ model of seizure, slices from these mice exhibit a GJ-independent increase in picrotoxin-sensitive GABAergic augmentation (442). Wild type slices treated with mefloquine prior to seizure induction did not exhibit picrotoxin or etomidate-sensitive augmentation, indicating these effects were the result of compensatory changes in Cx36— KO animals. While differences in model may underlie the variegated findings in these reports, they also highlight the need for selective Cx36 inhibitors in the study of electrical synapse dysregulation and its contribution to neuronal hyperexcitability.

*Inflammation, seizure, and pan-glial network gap junction dysregulation*

Pan-glial network maintenance of a sufficiently high seizure threshold in the homeostatic CNS relies on various GJ and non-GJ functions (213, 361). Spatial buffering of K+ and other metabolites released during periods of increased neuronal depolarization is critical to constraining hypersynchronous excitatory activity and reducing generalization of epileptiform bursting when initiated (163, 209, 211, 281, 345, 346). Astrocytes are central to the pan-glial network's ability to carry out this function and recent evidence illustrates that dysregulation of astrocyte Cx43 GJs may drive the pathogenesis of some human temporal lobe epilepsy.

In a 2015 study from Bedner et al. (281), hippocampal astrocytes from surgical specimens of sclerotic hippocampi from epileptic patient anomalously expressed ionotropic glutamate receptors, but not glutamate transporters (281). In addition, dye loading experiments in these astrocytes revealed severely restricted diffusion of biocytin into neighboring cells, suggesting they had become uncoupled from the pan-glial network

(281). These results were replicated in vivo using the 3 month post- intrahippocampal kainate (KA) injection mouse model of epileptogenesis (281).

In the same study, Cx43-eYFP labeled astrocyte uncoupling was induced by a single injection of KA and persisted for at least six months and preceded neuronal apoptosis (281). Astrocyte uncoupling was recapitulated in organotypic slice and in vivo by application of tumor necrosis factor α (TNFα), and interleukin (IL)-1β (281), which have been identified in serum and cerebrospinal fluid of epileptic patients (443). Interestingly, another study using 7 days post-intrahippocampal KA injection model showed an increase in dye coupling of hippocampal reactive astrocytes and an increase in GFAP and Cx43 protein (164), indicating time-dependent changes in coupling of astrocyte GJs after seizure.

Seizure activity could also be due to loss of oligodendrocyte Cxs and reduction of Cx43 expression as observed in inimmune-mediated mouse models of MS (357, 444). Furthermore, demyelinating MS lesions show evidence of GJ dysregulation, where inflamed white matter tracts and adjacent normal appearing tissue exhibit decreased Cx43 expression and oligodendrocyte uncoupling from reactive astrocytes (224, 225). In addition, MS patients are three to six times more likely to develop epilepsy than the overall population (62). While the mechanism that predisposes a subset of these patients to seizures remains unclear, a recent study identified altered expression of the astrocytic water channel implicated in epileptogenesis, aquaporin (AQP)4 (445), and extensive infiltration of microglia/macrophages into the CA1 of mice that experienced seizures following chronic cuprizone (CPZ)-induced demyelination (60). However, although Cx47 redistribution has been noted in CPZ demyelination (446), whether GJ dysfunction is etiologic in seizure development in this model is still unknown.

Transcriptomic analysis of Cx and Panx expression following seizure induction using a cobalt ($Co^{2+}$) model of seizure genesis demonstrated significant upregulation of Panx1, Panx2, and Cx43 mRNAs and post-translational phosphorylation of Cx43 (447), which is associated with increased GJ open probability and seizure (366). Protein and mRNA changes were independent of $Co^{2+}$ administration and required epileptiform discharges, since $Co^{2+}$ application in the presence of tetrodotoxin, a voltage gated $Na^{+}$ channel blocker, ablated transcriptome changes (447).

Intracellular $Ca^{2+}$ slow wave propagation and HC mediated purinergic signaling amongst GJ coupled astrocytes also influences seizure development (210, 232). In the low $Mg^{2+}$ model of seizure, slow $Ca^{2+}$ waves become synchronized across nearby astrocytes, which become paired to synchronized neurons during seizure-like events (232). This aberrant neuron-glial synchrony is GJ dependent, as CBX and anti-Cx43 antibodies reduce epileptiform activity-induced $Ca^{2+}$ slow wave coordination, increased interictal periods, and completely ablated seizures in a number of trials (232). However, this study does not distinguish between Cx43 GJs and HCs, so whether the observed anti-epileptic effects of these molecules is due to inhibited $Ca^{2+}$ second messenger exchange across coupled astrocytes or impaired gliotransmitter release remains to be demonstrated.

*Microglia, hemichannels, and inflammation*

Microglia express Cx32 and Cx36 under homeostatic conditions, but because microglia do not form heterotypic or homotypic GJs (448), their physiologic role remains unclear (449, 450). Research investigating microglial Cx and Panx HC function often occurs in the context of disease, where they have been implicated in excitotoxic glutamatergic signaling (223, 289, 451-453). Using organotypic slices, Adubara demonstrated that LPS application augments astrocyte Cx43 HC opening, resulting in

enhanced synaptic glutamate (223). The authors identified TLR4 activation by LPS, which triggers secretion of inflammatory mediators such as TNFα, inducible nitric oxide synthase, and IL-1β (454), was required for HC dependent glutamate release. Interestingly, fEPSP amplitude was suppressed in LPS treated slices despite increased synaptic glutamate, but was restored by blockade of Cx43 by gap26 or TNFα/IL-1β inhibitors IL-1RA and sTNF-αR1 (223). While decreased glutamatergic transmission and its recovery following IL-1RA administration may partially be explained by IL-1β's dampening effect on post-synaptic glutamate sensitivity (289), this study illustrates how microglia modify neuronal activity in pathology.

Microglial Panx1 and Cx HCs also release purinergic signaling molecules under inflammatory conditions. In a 2015 report by Orellana et al., restraint stress increased hippocampal microglial, astrocyte, and neuronal ethidium bromide uptake, which was abrogated by application of the Panx1 HC blocking peptide 10panx1 but not Cx43 HC blockers (455). These changes in dye uptake were abolished by application of ionotropic purinergic receptor P2X7 and NMDAR antagonists, but not metabotropic purinergic P2Y1 receptor blockade, and were accompanied by increased extracellular glutamate and ATP (455). This suggests that ionotropic purinergic signaling downstream of Panx1-mediated gliotransmitter release may be a vehicle of microglial HC dysfunction during inflammation, such as those generated by chronic stress (456).

In addition to TLR4 ligands, microglial HCs open in response to inflammatory cytokines. Application of LPS or TNFα to primary microglia in vitro results in upregulation of glutaminase and glutamate release (453). Furthermore, supernatant from glutamate—releasing microglial cultures induces downregulation of the astrocyte glutamate aspartate transporter, GLAST (452). Together, these results indicate that microglial HCs alter

extracellular glutamate concentration and astrocyte-dependent glutamate buffering in pathology. However, because in vitro models often lack the complex regulatory environment of the CNS, in vivo studies are required to validate these findings.

*Gap junction-mediated purinergic signaling in epilepsy*

Like Cx and Panx HCs, the P2X7 ionotropic purinergic receptor is a relatively large, ATP- gated transmembrane channel permeable to molecules 800 kDa or smaller, including low to medium weight cations such as K+ and Ca2+ (457) and cytokines (i.e. IL-1β) (458). Activation of NMDARs results in a burst of ATP release by synaptic and astrocyte-derived Panx1 and Cx43 HCs, respectively, that amplify depolarization (355, 356, 425). Activity dependent ATP signaling is facilitated by Panx1 coupling to P2X7 in membrane complexes (459, 460), thereby ensuring that NMDAR activation is augmented by the ensuing purinergic drive.

Dysregulation of this interaction has been implicated in the pathogenesis of seizure, but evidence is highly model dependent. Increased Panx1 protein expression was detected in lobectomy specimens from epileptic patients, while Panx2 was decreased (461), indicating that purinergic signaling dysregulation may occur in these patients. Organotypic slice studies support this finding, showing that in the low Mg2+ model of seizure, blockade of Panx1 by CBX and NMDAR antagonists attenuated epileptiform burst frequency and amplitude (356). This suggests that feed-forward augmentation of NMDAR currents can initiate runaway seizure like activity. However, while the putative mechanism of epileptiform bursting is NMDAR activation in this model, synchronization of principle neurons GABAergic interneuron populations may have contributed to neuronal hyper synchronization through low Mg2+ sensitive Cx36 GJs (462). Thus, selective inhibition of

Panx1 HCs may be required to untangle specific contribution of Panx1 to seizures in this model.

Alternatively, P2X7—KO mice display augmented seizure susceptibility when challenged with the muscarinic agonist pilocarpine that is not attributable to changes in glutamatergic or GABAergic transmission (425). P2X7 or Panx1 blockade in wild type mice reproduced the decreased seizure threshold observed in knockout animals (425). Physiologic seizure resistance was restored in P2X7—KO mice by inhibition of intracellular Ca2+ release by the ryanodine receptor antagonist dantrolene (425). In contrast, P2X7 antagonism by JNJ-42253432 resulted in a less severe seizure profile in the kainate model of epilepsy, with decreased seizure severity, but not frequency in Sprague-Dawley rats (463). These studies suggest that purinergic signaling in epilepsy may be complicated by the choice of model and potentially species examined. Further research is required to fully illuminate how Panx1 function in seizures relates to the complex neuropathology observed in the epileptic CNS.

**Concluding remarks**

Evidence increasingly indicates that Cx and Panx GJs and HCs are critical to maintaining physiologic neuronal excitability, resistance to seizure, and may be central to hippocampus and amygdala based learning (209, 214, 355, 401). In GABAergic interneurons, Cx36 GJs allow for rapid and expansive inhibition via electrically coupled inhibitory syncytia that are calibrated to depolarizing activity (401, 403, 407). In glia, GJs link participants in the pan-glial network, which supports physiologic resting membrane potential through spatial buffering of K+ and constrains epileptiform bursting (163, 209, 211, 281, 345, 346). Purinergic and glutamatergic gliotransmission, which continues to

accrue attention for its role in modifying neuronal activity, relies heavily on autocrine and paracrine signaling by Cx and Panx HCs (356, 425, 464).

Inflammation-induced dysregulation of Cx GJs not only impacts glutamatergic neurotransmission (117, 120, 223, 289, 452, 453), but also underlies disorders of excitation, such as epilepsy (281). However, the role of Cx and Panx HCs in purinergic signaling and excitotoxicity remains conflicted, exhibiting a model-dependent effect on the result of ionotropic purinergic receptor activation (356, 425, 463). Furthermore, the contribution of microglial Cxs and Panxs to homeostatic or disease processes remains largely unknown. Apart from a handful of studies (223, 455), existing evidence regarding microglial HC and GJ function in pathology is restricted to in vitro work and focuses on TLR4 signaling (452, 453), which may produce artifacts not seen in vivo (448).

An important limitation to many studies of individual Cx and Panx function is the lack of selective and specific GJ and HC inhibitors. Mimetic peptides and antibodies that inhibit Panx1 (10panx1) and Cx43 (gap26, gap27, and TAT-Cx43L2) HCs with relatively high selectivity are now available (Table 2). However, many of these peptides also inhibit GJs, making blockade of HCs or GJs alone difficult in situ (465). Additionally, peptides targeting other Cx and Panx isoforms have not been developed, making their study more arduous and reliant on knockout models. However, as the tools available for their study become more varied and available, the study of Cxs and Panxs is likely to more easily uncover the homeostatic and pathological properties of HCs and GJs.

**Acknowledgments**

This work was generously supported by the National Multiple Sclerosis Society Grants NMSS-RG-4853A3/2 and NIH R01-7R01NS081141 Grants to S.K.T.-W.

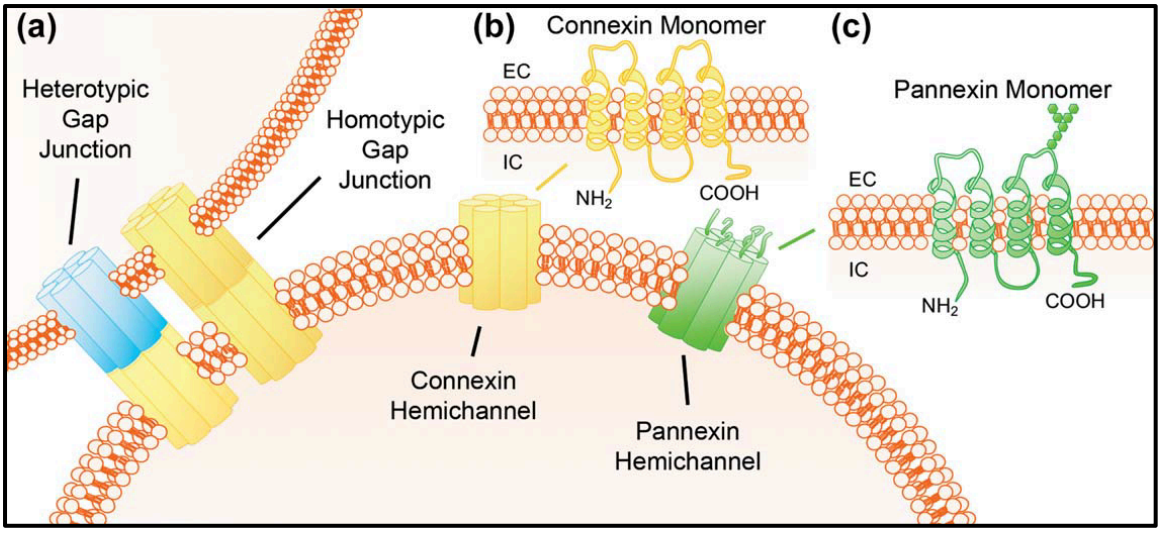


**Figure 1 | Connexin and pannexin structure and organization** A) Connexin and pannexin hemichannels are hexamers composed of six isoform subunits. Connexin hemichannels may be paired with homotypic or heterotypic hemichannels on adjacent cells to allow exchange of cytoplasmic contents up to 1.5 kDa as gap junctions. Pannexin hemichannels are not thought to form gap junctions due to N-linked glycosylation patterns. B, C) Connexins and pannexins are structurally and functionally homologous but have distinct amino acid sequences. Each subunit possesses four transmembrane domains linked by one intracellular and two extracellular loops. The carboxyl and amine terminals extend into the cytoplasm. The carboxyl tail is the site of regulatory modification and phosphorylation. C**)** Pannexin monomers are structurally related to connexins but glycosylation of the extracellular loop closest to the carboxyl terminal prohibits pannexin hemichannel assembly into functional gap junctions.

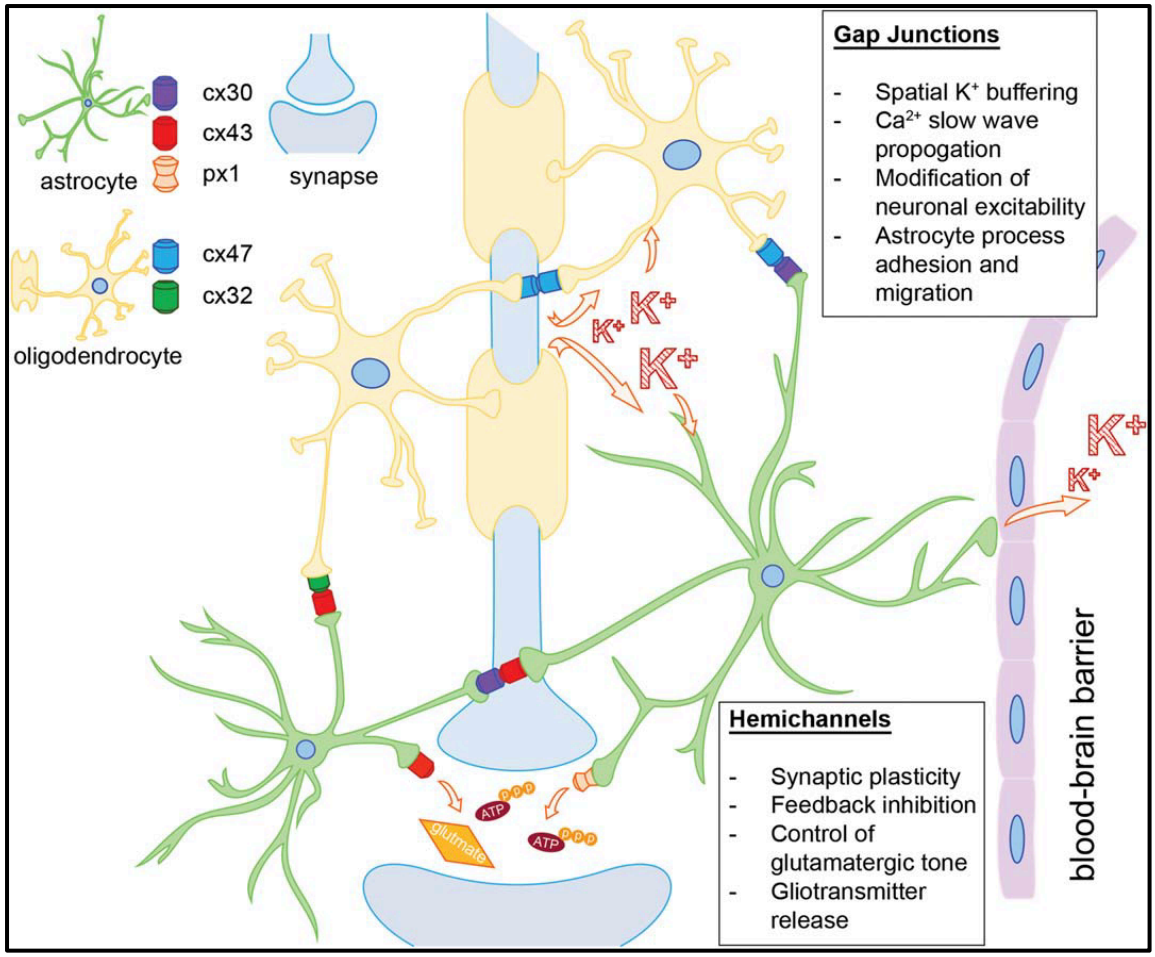


**Figure 2 | The pan-glial network participates in regulating excitatory neuronal transmission through gap junction and hemichannel-mediated functions**. Connexin gap junctions control glutamatergic activity indirectly through generation of inward K+ currents & spatial K+ buffering, activity-dependent astrocyte Ca2+ slow wave propagation, and regulation of synaptic invasion by GLT-1 enriched astrocyte process. Model depicts coupling partners for homotypic and heterotypic glial GJs and their cellular expression. Cx43 and Panx1 HCs contribute to synaptic plasticity, inhibitory feedback, and glutamatergic tone by autocrine and paracrine release of synaptic gliotransmitters, including glutamate and ATP.

**TABLE 1** Cellular distribution of Cx and Panx isoforms expressed by glia and neurons in the adult mammalian CNS

| Cell Type | Connexins | Pannexins | References |
|---|---|---|---|
| Astrocytes | Cx26, Cx30, Cx43, | Panx1 | Dermietzel et al., 1989, Nagy et al., 2001, Zoidl et al., 2007 |
| Microglia | Cx32a, Cx36, Cx43a | Panx1 | Orellana et al., 2015, Dobrenis et al., 2005, Eugenin et al., 2001, Takeuchi et al., 2006 |
| Oligodendrocytes | Cx29, Cx32, Cx47 | Panx1 | Dermietzel et al., 1989, Domercq et al., 2010, Nagy et al., 2003 |
| Neurons | Cx30.2, Cx31.1, Cx32, Cx36, Cx40, Cx45, Cx50 | Panx1, Panx2 | Bruzzone et al., 2003, Dere et al., 2008, Kreuzberg et al., 2008, Rash et al., 2000, Rozental et al., 1998, Schutte et al., 1998, Vis et al., 1998, Weickert et al., 2005 |

[a] expressed by activated microglia

**Table 1 |** Cellular distribution of Cx and Panx isoforms expressed by glia and neurons in the adult mammalian CNS. Astrocyte expressed Cx isoforms participate in HC-mediated gliotransmission and astrocyte-oligodendrocyte GJs within the pan-glial network. Cx36 HCs are expressed by microglia under homeostatic conditions, while Cx32 and Cx43 are upregulated in response to inflammation. Oligodendrocyte Cx isoforms contribute to GJ coupling with pan-glial network members and between myelin layers. Neuronal Cx heterogeneity reflects CNS regional specialization. Panx1 HCs are found in all CNS populations listed, but Panx2 is only identified in neurons.

| Manipulation | | Mechanism | Outcomes | References |
|---|---|---|---|---|
| Cx30 | KO | genetic ablation | ↓ CA1 fEPSPs after Schaffer collateral stimulation, ↓ LTP; ↓ astrocyte/astrocyte dye coupling | Abudara et al., 2015, Pannasch et al., 2014 |
| Cx31.1 | KO | genetic ablation | ↓ novel object recognition, ↑ novel environment exploration | Dere et al., 2008 |
| Cx36 | KO | genetic ablation | absent interneuron voltage coupling, ↓ IPSP amplitude; ↓ novel object recognition, ↓ short-term memory by Y-maze, ↓ motor learning by Rotarod; ↑ seizures w/ PTZ induction; ↓ CA1 fEPSPs after Schaffer collateral stimulation | Apostolides, 2013, Deans et al., 2001 Frisch et al., 2005, Jacobson et al., 2010, Wang and Belousov, 2011 |
| Cx43 | Astrocyte KO | GFAP:Cre $Cx43^{fl/fl}$ | ↓ dye coupling, hypertrophic astrocytes, ↓ vesicular glutamate release | Chever et al., 2014b |
| | gap26/27 | EC loop mimetic peptide; HC inhibitor | ↓ Ethidium bromide uptake, ↓ excitatory post synaptic current amplitude, ↓ ATP release; ↑ fEPSP amplitude after LPS | Abudara et al., 2015, Chever et al., 2014a |
| | TAT-Cx43L2 | tail mimetic peptide; HC inhibitor | ↓ fear conditioning memory with intra-amygdala injection | Stehberg et al., 2012 |
| | anti-Cx43 antibodies | HC blockade | ↓ Ca2 + slow wave synchronization, ↓ seizure number & frequency | Kekesi et al., 2015 |
| Cx30 + Cx43 | Cx30 + astrocyte Cx43 DKO | Cx30−KO + GFAP:Cre $Cx43^{fl/fl}$ | ↑ astrocyte intracellular $Ca^{2+}$ after LPS, ↓ dye uptake after LPS; ↓ $Ca^{2+}$ slow waves | Abudara et al., 2015, Torres et al., 2012 |
| Panx1 | KO | genetic ablation | absent LTD; ↑ CA1 fEPSPs after Schaffer collateral stimulation, ↑ LTP, ↓ novel object recognition, ↓ spatial memory recall | Ardiles et al., 2014, Prochnow et al., 2012 |
| | $^{10}$panx1 | EC loop mimetic peptide; Panx1 HC inhibitor | After chronic restraint stress: ↓ ethidium bromide uptake, ↓ glutamate release, ↓ ATP release | Orellana et al., 2015 |

**Table 2** | Summary of genetic and pharmacologic manipulations used to identify the function of specific Cx and Panx isoforms. Key results are indicated beside manipulation. Note that selective inhibitors are only available for HCs, but many will also block GJs over time (228).

**BIBLIOGRAPHY**


1. Wallin MT, Culpepper WJ, Campbell JD, Nelson LM, Langer-Gould A, Marrie RA, Cutter GR, Kaye WE, Wagner L, Tremlett H, Buka SL, Dilokthornsakul P, Topol B, Chen LH, LaRocca NG, Workgroup USMSP. The prevalence of MS in the United States: A population-based estimate using health claims data. Neurology. 2019;92(10):e1029-e40. Epub 2019/02/17. doi: 10.1212/WNL.0000000000007035. PubMed PMID: 30770430; PMCID: PMC6442006.

2. Goldenberg MM. Multiple sclerosis review. P T. 2012;37(3):175-84. Epub 2012/05/19. PubMed PMID: 22605909; PMCID: PMC3351877.

3. Frohman EM, Racke MK, Raine CS. Multiple sclerosis--the plaque and its pathogenesis. N Engl J Med. 2006;354(9):942-55. Epub 2006/03/03. doi: 10.1056/NEJMra052130. PubMed PMID: 16510748.

4. Reich DS, Lucchinetti CF, Calabresi PA. Multiple Sclerosis. N Engl J Med. 2018;378(2):169-80. Epub 2018/01/11. doi: 10.1056/NEJMra1401483. PubMed PMID: 29320652; PMCID: PMC6942519.

5. Koch M, Uyttenboogaart M, Polman S, De Keyser J. Seizures in multiple sclerosis. Epilepsia. 2008;49(6):948-53. Epub 2008/03/14. doi: 10.1111/j.1528-1167.2008.01565.x. PubMed PMID: 18336559.

6. Rosenthal JF, Hoffman BM, Tyor WR. CNS inflammatory demyelinating disorders: MS, NMOSD and MOG antibody associated disease. J Investig Med. 2020;68(2):321-30. Epub 2019/10/05. doi: 10.1136/jim-2019-001126. PubMed PMID: 31582425.

7. Lublin FD, Reingold SC, Cohen JA, Cutter GR, Sorensen PS, Thompson AJ, Wolinsky JS, Balcer LJ, Banwell B, Barkhof F, Bebo B, Jr., Calabresi PA, Clanet M, Comi G, Fox RJ, Freedman MS, Goodman AD, Inglese M, Kappos L, Kieseier BC, Lincoln JA, Lubetzki C, Miller AE, Montalban X, O'Connor PW, Petkau J, Pozzilli C, Rudick RA, Sormani MP, Stuve O, Waubant E, Polman CH. Defining the clinical course of multiple sclerosis: the 2013 revisions. Neurology. 2014;83(3):278-86. Epub 2014/05/30. doi: 10.1212/WNL.0000000000000560. PubMed PMID: 24871874; PMCID: PMC4117366.

8. Mahad DH, Trapp BD, Lassmann H. Pathological mechanisms in progressive multiple sclerosis. Lancet Neurol. 2015;14(2):183-93. Epub 2015/03/17. doi: 10.1016/S1474-4422(14)70256-X. PubMed PMID: 25772897.

9. Kaunzner UW, Gauthier SA. MRI in the assessment and monitoring of multiple sclerosis: an update on best practice. Ther Adv Neurol Disord. 2017;10(6):247-61. Epub 2017/06/14. doi: 10.1177/1756285617708911. PubMed PMID: 28607577; PMCID: PMC5453402.

10. Thompson AJ, Banwell BL, Barkhof F, Carroll WM, Coetzee T, Comi G, Correale J, Fazekas F, Filippi M, Freedman MS, Fujihara K, Galetta SL, Hartung HP, Kappos L, Lublin FD, Marrie RA, Miller AE, Miller DH, Montalban X, Mowry EM, Sorensen PS, Tintore M, Traboulsee AL, Trojano M, Uitdehaag BMJ, Vukusic S, Waubant E, Weinshenker BG, Reingold SC, Cohen JA. Diagnosis of multiple sclerosis: 2017 revisions of the McDonald criteria. Lancet Neurol. 2018;17(2):162-73. Epub 2017/12/26. doi: 10.1016/S1474-4422(17)30470-2. PubMed PMID: 29275977.

11. Ramagopalan SV, Dyment DA, Ebers GC. Genetic epidemiology: the use of old and new tools for multiple sclerosis. Trends Neurosci. 2008;31(12):645-52. Epub 2008/10/28. doi: 10.1016/j.tins.2008.09.001. PubMed PMID: 18952304.

12. Ramagopalan SV, Knight JC, Ebers GC. Multiple sclerosis and the major histocompatibility complex. Curr Opin Neurol. 2009;22(3):219-25. Epub 2009/04/24. doi: 10.1097/WCO.0b013e32832b5417. PubMed PMID: 19387341.

13. Jones EY, Fugger L, Strominger JL, Siebold C. MHC class II proteins and disease: a structural perspective. Nat Rev Immunol. 2006;6(4):271-82. Epub 2006/03/25. doi: 10.1038/nri1805. PubMed PMID: 16557259.

14. Roche PA, Furuta K. The ins and outs of MHC class II-mediated antigen processing and presentation. Nat Rev Immunol. 2015;15(4):203-16. Epub 2015/02/28. doi: 10.1038/nri3818. PubMed PMID: 25720354; PMCID: PMC6314495.

15. Neefjes J, Jongsma ML, Paul P, Bakke O. Towards a systems understanding of MHC class I and MHC class II antigen presentation. Nat Rev Immunol. 2011;11(12):823-36. Epub 2011/11/15. doi: 10.1038/nri3084. PubMed PMID: 22076556.

16. Rock KL, Reits E, Neefjes J. Present Yourself! By MHC Class I and MHC Class II Molecules. Trends Immunol. 2016;37(11):724-37. Epub 2016/09/12. doi: 10.1016/j.it.2016.08.010. PubMed PMID: 27614798; PMCID: PMC5159193.

17. Dustin ML. The immunological synapse. Cancer Immunol Res. 2014;2(11):1023-33. Epub 2014/11/05. doi: 10.1158/2326-6066.CIR-14-0161. PubMed PMID: 25367977; PMCID: PMC4692051.

18. Handunnetthi L, Ramagopalan SV, Ebers GC, Knight JC. Regulation of major histocompatibility complex class II gene expression, genetic variation and disease. Genes Immun. 2010;11(2):99-112. Epub 2009/11/06. doi: 10.1038/gene.2009.83. PubMed PMID: 19890353; PMCID: PMC2987717.

19. Alcina A, Abad-Grau Mdel M, Fedetz M, Izquierdo G, Lucas M, Fernandez O, Ndagire D, Catala-Rabasa A, Ruiz A, Gayan J, Delgado C, Arnal C, Matesanz F. Multiple sclerosis risk variant HLA-DRB1*1501 associates with high expression of DRB1 gene in

different human populations. PLoS One. 2012;7(1):e29819. Epub 2012/01/19. doi: 10.1371/journal.pone.0029819. PubMed PMID: 22253788; PMCID: PMC3258250.

20. Madsen LS, Andersson EC, Jansson L, Krogsgaard M, Andersen CB, Engberg J, Strominger JL, Svejgaard A, Hjorth JP, Holmdahl R, Wucherpfennig KW, Fugger L. A humanized model for multiple sclerosis using HLA-DR2 and a human T-cell receptor. Nature Genetics. 1999;23(3):343-7. PubMed PMID: WOS:000083792200026.

21. Ramagopalan SV, Dobson R, Meier UC, Giovannoni G. Multiple sclerosis: risk factors, prodromes, and potential causal pathways. Lancet Neurol. 2010;9(7):727-39. Epub 2010/07/09. doi: 10.1016/S1474-4422(10)70094-6. PubMed PMID: 20610348.

22. Gregory AP, Dendrou CA, Attfield KE, Haghikia A, Xifara DK, Butter F, Poschmann G, Kaur G, Lambert L, Leach OA, Promel S, Punwani D, Felce JH, Davis SJ, Gold R, Nielsen FC, Siegel RM, Mann M, Bell JI, McVean G, Fugger L. TNF receptor 1 genetic risk mirrors outcome of anti-TNF therapy in multiple sclerosis. Nature. 2012;488(7412):508-11. Epub 2012/07/18. doi: 10.1038/nature11307. PubMed PMID: 22801493; PMCID: PMC4268493.

23. Gregory SG, Schmidt S, Seth P, Oksenberg JR, Hart J, Prokop A, Caillier SJ, Ban M, Goris A, Barcellos LF, Lincoln R, McCauley JL, Sawcer SJ, Compston DA, Dubois B, Hauser SL, Garcia-Blanco MA, Pericak-Vance MA, Haines JL, Multiple Sclerosis Genetics G. Interleukin 7 receptor alpha chain (IL7R) shows allelic and functional association with multiple sclerosis. Nat Genet. 2007;39(9):1083-91. Epub 2007/07/31. doi: 10.1038/ng2103. PubMed PMID: 17660817.

24. Maier LM, Anderson DE, Severson CA, Baecher-Allan C, Healy B, Liu DV, Wittrup KD, De Jager PL, Hafler DA. Soluble IL-2RA levels in multiple sclerosis subjects and the effect of soluble IL-2RA on immune responses. J Immunol. 2009;182(3):1541-7. Epub 2009/01/22. doi: 10.4049/jimmunol.182.3.1541. PubMed PMID: 19155502; PMCID: PMC3992946.

25. International Multiple Sclerosis Genetics C, Hafler DA, Compston A, Sawcer S, Lander ES, Daly MJ, De Jager PL, de Bakker PI, Gabriel SB, Mirel DB, Ivinson AJ, Pericak-Vance MA, Gregory SG, Rioux JD, McCauley JL, Haines JL, Barcellos LF, Cree B, Oksenberg JR, Hauser SL. Risk alleles for multiple sclerosis identified by a genomewide study. N Engl J Med. 2007;357(9):851-62. Epub 2007/07/31. doi: 10.1056/NEJMoa073493. PubMed PMID: 17660530.

26. Cavanillas ML, Alcina A, Nunez C, de las Heras V, Fernandez-Arquero M, Bartolome M, de la Concha EG, Fernandez O, Arroyo R, Matesanz F, Urcelay E. Polymorphisms in the IL2, IL2RA and IL2RB genes in multiple sclerosis risk. Eur J Hum Genet. 2010;18(7):794-9. Epub 2010/02/25. doi: 10.1038/ejhg.2010.15. PubMed PMID: 20179739; PMCID: PMC2987360.

27. Arenas-Ramirez N, Woytschak J, Boyman O. Interleukin-2: Biology, Design and Application. Trends Immunol. 2015;36(12):763-77. Epub 2015/11/18. doi: 10.1016/j.it.2015.10.003. PubMed PMID: 26572555.

28. Bassiri H, Carding SR. A requirement for IL-2/IL-2 receptor signaling in intrathymic negative selection. J Immunol. 2001;166(10):5945-54. Epub 2001/05/09. doi: 10.4049/jimmunol.166.10.5945. PubMed PMID: 11342609.

29. Malek TR, Bayer AL. Tolerance, not immunity, crucially depends on IL-2. Nat Rev Immunol. 2004;4(9):665-74. Epub 2004/09/03. doi: 10.1038/nri1435. PubMed PMID: 15343366.

30. Nizri E, Irony-Tur-Sinai M, Lory O, Orr-Urtreger A, Lavi E, Brenner T. Activation of the cholinergic anti-inflammatory system by nicotine attenuates neuroinflammation via suppression of Th1 and Th17 responses. J Immunol. 2009;183(10):6681-8. Epub 2009/10/23. doi: 10.4049/jimmunol.0902212. PubMed PMID: 19846875.

31. Yu A, Snowhite I, Vendrame F, Rosenzwajg M, Klatzmann D, Pugliese A, Malek TR. Selective IL-2 responsiveness of regulatory T cells through multiple intrinsic mechanisms supports the use of low-dose IL-2 therapy in type 1 diabetes. Diabetes. 2015;64(6):2172-83. Epub 2015/01/13. doi: 10.2337/db14-1322. PubMed PMID: 25576057.

32. Liao W, Lin JX, Leonard WJ. Interleukin-2 at the crossroads of effector responses, tolerance, and immunotherapy. Immunity. 2013;38(1):13-25. Epub 2013/01/29. doi: 10.1016/j.immuni.2013.01.004. PubMed PMID: 23352221; PMCID: PMC3610532.

33. Yang ZZ, Grote DM, Ziesmer SC, Manske MK, Witzig TE, Novak AJ, Ansell SM. Soluble IL-2Ralpha facilitates IL-2-mediated immune responses and predicts reduced survival in follicular B-cell non-Hodgkin lymphoma. Blood. 2011;118(10):2809-20. Epub 2011/07/02. doi: 10.1182/blood-2011-03-340885. PubMed PMID: 21719603; PMCID: PMC3172797.

34. Cerosaletti K, Schneider A, Schwedhelm K, Frank I, Tatum M, Wei S, Whalen E, Greenbaum C, Kita M, Buckner J, Long SA. Multiple autoimmune-associated variants confer decreased IL-2R signaling in CD4+ CD25(hi) T cells of type 1 diabetic and multiple sclerosis patients. PLoS One. 2013;8(12):e83811. Epub 2014/01/01. doi: 10.1371/journal.pone.0083811. PubMed PMID: 24376757; PMCID: PMC3871703.

35. Viglietta V, Baecher-Allan C, Weiner HL, Hafler DA. Loss of functional suppression by CD4+CD25+ regulatory T cells in patients with multiple sclerosis. J Exp Med. 2004;199(7):971-9. Epub 2004/04/07. doi: 10.1084/jem.20031579. PubMed PMID: 15067033; PMCID: PMC2211881.

36. Damoiseaux J. The IL-2 - IL-2 receptor pathway in health and disease: The role of the soluble IL-2 receptor. Clin Immunol. 2020;218:108515. Epub 2020/07/04. doi: 10.1016/j.clim.2020.108515. PubMed PMID: 32619646.

37. Hartmann FJ, Khademi M, Aram J, Ammann S, Kockum I, Constantinescu C, Gran B, Piehl F, Olsson T, Codarri L, Becher B. Multiple sclerosis-associated IL2RA polymorphism controls GM-CSF production in human TH cells. Nat Commun. 2014;5:5056. Epub 2014/10/04. doi: 10.1038/ncomms6056. PubMed PMID: 25278028.

38. Lotfi N, Thome R, Rezaei N, Zhang GX, Rezaei A, Rostami A, Esmaeil N. Roles of GM-CSF in the Pathogenesis of Autoimmune Diseases: An Update. Front Immunol. 2019;10:1265. Epub 2019/07/06. doi: 10.3389/fimmu.2019.01265. PubMed PMID: 31275302; PMCID: PMC6593264.

39. Chinen T, Kannan AK, Levine AG, Fan X, Klein U, Zheng Y, Gasteiger G, Feng Y, Fontenot JD, Rudensky AY. An essential role for the IL-2 receptor in Treg cell function. Nat Immunol. 2016;17(11):1322-33. Epub 2016/10/21. doi: 10.1038/ni.3540. PubMed PMID: 27595233; PMCID: PMC5071159.

40. Danikowski KM, Jayaraman S, Prabhakar BS. Regulatory T cells in multiple sclerosis and myasthenia gravis. J Neuroinflammation. 2017;14(1):117. Epub 2017/06/11. doi: 10.1186/s12974-017-0892-8. PubMed PMID: 28599652; PMCID: PMC5466736.

41. De Jager PL, Baecher-Allan C, Maier LM, Arthur AT, Ottoboni L, Barcellos L, McCauley JL, Sawcer S, Goris A, Saarela J, Yelensky R, Price A, Leppa V, Patterson N, de Bakker PI, Tran D, Aubin C, Pobywajlo S, Rossin E, Hu X, Ashley CW, Choy E, Rioux JD, Pericak-Vance MA, Ivinson A, Booth DR, Stewart GJ, Palotie A, Peltonen L, Dubois B, Haines JL, Weiner HL, Compston A, Hauser SL, Daly MJ, Reich D, Oksenberg JR, Hafler DA. The role of the CD58 locus in multiple sclerosis. Proc Natl Acad Sci U S A. 2009;106(13):5264-9. Epub 2009/02/25. doi: 10.1073/pnas.0813310106. PubMed PMID: 19237575; PMCID: PMC2664005.

42. Mackall CL, Fry TJ, Gress RE. Harnessing the biology of IL-7 for therapeutic application. Nat Rev Immunol. 2011;11(5):330-42. Epub 2011/04/22. doi: 10.1038/nri2970. PubMed PMID: 21508983; PMCID: PMC7351348.

43. Lundstrom W, Highfill S, Walsh ST, Beq S, Morse E, Kockum I, Alfredsson L, Olsson T, Hillert J, Mackall CL. Soluble IL7Ralpha potentiates IL-7 bioactivity and promotes autoimmunity. Proc Natl Acad Sci U S A. 2013;110(19):E1761-70. Epub 2013/04/24. doi: 10.1073/pnas.1222303110. PubMed PMID: 23610432; PMCID: PMC3651437.

44. Mazzucchelli R, Durum SK. Interleukin-7 receptor expression: intelligent design. Nat Rev Immunol. 2007;7(2):144-54. Epub 2007/01/30. doi: 10.1038/nri2023. PubMed PMID: 17259970.

45. International Multiple Sclerosis Genetics C, Wellcome Trust Case Control C, Sawcer S, Hellenthal G, Pirinen M, Spencer CC, Patsopoulos NA, Moutsianas L, Dilthey A, Su Z, Freeman C, Hunt SE, Edkins S, Gray E, Booth DR, Potter SC, Goris A, Band G, Oturai AB, Strange A, Saarela J, Bellenguez C, Fontaine B, Gillman M, Hemmer B, Gwilliam R, Zipp F, Jayakumar A, Martin R, Leslie S, Hawkins S, Giannoulatou E, D'Alfonso S, Blackburn H, Martinelli Boneschi F, Liddle J, Harbo HF, Perez ML, Spurkland A, Waller MJ, Mycko MP, Ricketts M, Comabella M, Hammond N, Kockum I, McCann OT, Ban M, Whittaker P, Kemppinen A, Weston P, Hawkins C, Widaa S, Zajicek J, Dronov S, Robertson N, Bumpstead SJ, Barcellos LF, Ravindrarajah R, Abraham R, Alfredsson L, Ardlie K, Aubin C, Baker A, Baker K, Baranzini SE, Bergamaschi L, Bergamaschi R, Bernstein A, Berthele A, Boggild M, Bradfield JP, Brassat D, Broadley SA, Buck D, Butzkueven H, Capra R, Carroll WM, Cavalla P, Celius EG, Cepok S, Chiavacci R, Clerget-Darpoux F, Clysters K, Comi G, Cossburn M, Cournu-Rebeix I, Cox MB, Cozen W, Cree BA, Cross AH, Cusi D, Daly MJ, Davis E, de Bakker PI, Debouverie M, D'Hooghe M B, Dixon K, Dobosi R, Dubois B, Ellinghaus D, Elovaara I, Esposito F, Fontenille C, Foote S, Franke A, Galimberti D, Ghezzi A, Glessner J, Gomez R, Gout O, Graham C, Grant SF, Guerini FR, Hakonarson H, Hall P, Hamsten A, Hartung HP, Heard RN, Heath S, Hobart J, Hoshi M, Infante-Duarte C, Ingram G, Ingram W, Islam T, Jagodic M, Kabesch M, Kermode AG, Kilpatrick TJ, Kim C, Klopp N, Koivisto K, Larsson M, Lathrop M, Lechner-Scott JS, Leone MA, Leppa V, Liljedahl U, Bomfim IL, Lincoln RR, Link J, Liu J, Lorentzen AR, Lupoli S, Macciardi F, Mack T, Marriott M, Martinelli V, Mason D, McCauley JL, Mentch F, Mero IL, Mihalova T, Montalban X, Mottershead J, Myhr KM, Naldi P, Ollier W, Page A, Palotie A, Pelletier J, Piccio L, Pickersgill T, Piehl F, Pobywajlo S, Quach HL, Ramsay PP, Reunanen M, Reynolds R, Rioux JD, Rodegher M, Roesner S, Rubio JP, Ruckert IM, Salvetti M, Salvi E, Santaniello A, Schaefer CA, Schreiber S, Schulze C, Scott RJ, Sellebjerg F, Selmaj KW, Sexton D, Shen L, Simms-Acuna B, Skidmore S, Sleiman PM, Smestad C, Sorensen PS, Sondergaard HB, Stankovich J, Strange RC, Sulonen AM, Sundqvist E, Syvanen AC, Taddeo F, Taylor B, Blackwell JM, Tienari P, Bramon E, Tourbah A, Brown MA, Tronczynska E, Casas JP, Tubridy N, Corvin A, Vickery J, Jankowski J, Villoslada P, Markus HS, Wang K, Mathew CG, Wason J, Palmer CN, Wichmann HE, Plomin R, Willoughby E, Rautanen A, Winkelmann J, Wittig M, Trembath RC, Yaouanq J, Viswanathan AC, Zhang H, Wood NW, Zuvich R, Deloukas P, Langford C, Duncanson A, Oksenberg JR, Pericak-Vance MA, Haines JL, Olsson T, Hillert J, Ivinson AJ, De Jager PL, Peltonen L, Stewart GJ, Hafler DA, Hauser SL, McVean G, Donnelly P, Compston A. Genetic risk and a primary role for cell-mediated immune mechanisms in multiple sclerosis. Nature. 2011;476(7359):214-9. Epub 2011/08/13. doi: 10.1038/nature10251. PubMed PMID: 21833088; PMCID: PMC3182531.

46. Dobson R, Giovannoni G. Multiple sclerosis - a review. Eur J Neurol. 2019;26(1):27-40. Epub 2018/10/10. doi: 10.1111/ene.13819. PubMed PMID: 30300457.

47. Gale CR, Martyn CN. Migrant studies in multiple sclerosis. Prog Neurobiol. 1995;47(4-5):425-48. Epub 1995/11/01. doi: Doi 10.1016/0301-0082(95)00033-X. PubMed PMID: 8966212.

48. Munger KL, Zhang SM, O'Reilly E, Hernan MA, Olek MJ, Willett WC, Ascherio A. Vitamin D intake and incidence of multiple sclerosis. Neurology. 2004;62(1):60-5. Epub 2004/01/14. doi: 10.1212/01.wnl.0000101723.79681.38. PubMed PMID: 14718698.

49. Cantorna MT, Zhu Y, Froicu M, Wittke A. Vitamin D status, 1,25-dihydroxyvitamin D3, and the immune system. Am J Clin Nutr. 2004;80(6 Suppl):1717S-20S. Epub 2004/12/09. doi: 10.1093/ajcn/80.6.1717S. PubMed PMID: 15585793.

50. Rezk SA, Zhao X, Weiss LM. Epstein-Barr virus (EBV)-associated lymphoid proliferations, a 2018 update. Hum Pathol. 2018;79:18-41. Epub 2018/06/10. doi: 10.1016/j.humpath.2018.05.020. PubMed PMID: 29885408.

51. Ascherio A, Munger KL. Epidemiology of Multiple Sclerosis: From Risk Factors to Prevention-An Update. Semin Neurol. 2016;36(2):103-14. Epub 2016/04/27. doi: 10.1055/s-0036-1579693. PubMed PMID: 27116717.

52. Langer-Gould A, Wu J, Lucas R, Smith J, Gonzales E, Amezcua L, Haraszti S, Chen LH, Quach H, James JA, Barcellos LF, Xiang AH. Epstein-Barr virus, cytomegalovirus, and multiple sclerosis susceptibility: A multiethnic study. Neurology. 2017;89(13):1330-7. Epub 2017/09/01. doi: 10.1212/WNL.0000000000004412. PubMed PMID: 28855411; PMCID: PMC5649756.

53. Laurence M, Benito-Leon J. Epstein-Barr virus and multiple sclerosis: Updating Pender's hypothesis. Mult Scler Relat Disord. 2017;16:8-14. Epub 2017/08/02. doi: 10.1016/j.msard.2017.05.009. PubMed PMID: 28755684.

54. Sundstrom P, Nystrom M, Ruuth K, Lundgren E. Antibodies to specific EBNA-1 domains and HLA DRB1*1501 interact as risk factors for multiple sclerosis. J Neuroimmunol. 2009;215(1-2):102-7. Epub 2009/09/08. doi: 10.1016/j.jneuroim.2009.08.004. PubMed PMID: 19733917.

55. Heydarpour P, Amini H, Khoshkish S, Seidkhani H, Sahraian MA, Yunesian M. Potential impact of air pollution on multiple sclerosis in Tehran, Iran. Neuroepidemiology. 2014;43(3-4):233-8. Epub 2014/12/17. doi: 10.1159/000368553. PubMed PMID: 25501708.

56. Degelman ML, Herman KM. Smoking and multiple sclerosis: A systematic review and meta-analysis using the Bradford Hill criteria for causation. Mult Scler Relat Disord. 2017;17:207-16. Epub 2017/10/23. doi: 10.1016/j.msard.2017.07.020. PubMed PMID: 29055459.

57. Rosso M, Chitnis T. Association Between Cigarette Smoking and Multiple Sclerosis: A Review. JAMA Neurol. 2019. Epub 2019/12/17. doi: 10.1001/jamaneurol.2019.4271. PubMed PMID: 31841592.

58. Olsson T, Barcellos LF, Alfredsson L. Interactions between genetic, lifestyle and environmental risk factors for multiple sclerosis. Nat Rev Neurol. 2017;13(1):25-36. Epub 2016/12/10. doi: 10.1038/nrneurol.2016.187. PubMed PMID: 27934854.

59. Hedstrom AK, Baarnhielm M, Olsson T, Alfredsson L. Tobacco smoking, but not Swedish snuff use, increases the risk of multiple sclerosis. Neurology. 2009;73(9):696-701. Epub 2009/09/02. doi: 10.1212/WNL.0b013e3181b59c40. PubMed PMID: 19720976.

60. Lapato AS, Szu JI, Hasselmann JPC, Khalaj AJ, Binder DK, Tiwari-Woodruff SK. Chronic demyelination-induced seizures. Neuroscience. 2017;346:409-22. Epub 2017/02/06. doi: 10.1016/j.neuroscience.2017.01.035. PubMed PMID: 28153692; PMCID: PMC5394933.

61. Lapato AS, Thompson SM, Parra K, Tiwari-Woodruff SK. Astrocyte glutamate uptake and water homeostasis are dysregulated in the hippocampus of multiple sclerosis patients with seizures. ASN Neuro (accepted pending revision). 2020.

62. Poser CM, Brinar VV. Epilepsy and multiple sclerosis. Epilepsy Behav. 2003;4(1):6-12. Epub 2003/03/01. doi: 10.1016/s1525-5050(02)00646-7. PubMed PMID: 12609222.

63. Catenoix H, Marignier R, Ritleng C, Dufour M, Mauguiere F, Confavreux C, Vukusic S. Multiple sclerosis and epileptic seizures. Mult Scler. 2011;17(1):96-102. Epub 2010/09/24. doi: 10.1177/1352458510382246. PubMed PMID: 20861180.

64. Lassmann H. Multiple Sclerosis Pathology. Cold Spring Harb Perspect Med. 2018;8(3). Epub 2018/01/24. doi: 10.1101/cshperspect.a028936. PubMed PMID: 29358320; PMCID: PMC5830904.

65. Zalc B. One hundred and fifty years ago Charcot reported multiple sclerosis as a new neurological disease. Brain. 2018;141(12):3482-8. Epub 2018/11/22. doi: 10.1093/brain/awy287. PubMed PMID: 30462211; PMCID: PMC6262215.

66. Kornek B, Storch MK, Weissert R, Wallstroem E, Stefferl A, Olsson T, Linington C, Schmidbauer M, Lassmann H. Multiple sclerosis and chronic autoimmune encephalomyelitis: a comparative quantitative study of axonal injury in active, inactive, and remyelinated lesions. Am J Pathol. 2000;157(1):267-76. Epub 2000/07/06. doi: 10.1016/S0002-9440(10)64537-3. PubMed PMID: 10880396; PMCID: PMC1850217.

67. Maysami S, Nguyen D, Zobel F, Heine S, Hopfner M, Stangel M. Oligodendrocyte precursor cells express a functional chemokine receptor CCR3: implications for myelination. J Neuroimmunol. 2006;178(1-2):17-23. Epub 2006/07/11. doi: 10.1016/j.jneuroim.2006.05.021. PubMed PMID: 16828880.

68. Franklin RJ, Ffrench-Constant C. Remyelination in the CNS: from biology to therapy. Nat Rev Neurosci. 2008;9(11):839-55. Epub 2008/10/22. doi: 10.1038/nrn2480. PubMed PMID: 18931697.

69. Boyd A, Zhang H, Williams A. Insufficient OPC migration into demyelinated lesions is a cause of poor remyelination in MS and mouse models. Acta Neuropathol. 2013;125(6):841-59. Epub 2013/04/19. doi: 10.1007/s00401-013-1112-y. PubMed PMID: 23595275; PMCID: PMC3661931.

70. Kirby L, Jin J, Cardona JG, Smith MD, Martin KA, Wang J, Strasburger H, Herbst L, Alexis M, Karnell J, Davidson T, Dutta R, Goverman J, Bergles D, Calabresi PA. Oligodendrocyte precursor cells present antigen and are cytotoxic targets in inflammatory demyelination. Nat Commun. 2019;10(1):3887. Epub 2019/08/31. doi: 10.1038/s41467-019-11638-3. PubMed PMID: 31467299; PMCID: PMC6715717.

71. Trapp BD, Peterson J, Ransohoff RM, Rudick R, Mork S, Bo L. Axonal transection in the lesions of multiple sclerosis. N Engl J Med. 1998;338(5):278-85. Epub 1998/01/29. doi: 10.1056/NEJM199801293380502. PubMed PMID: 9445407.

72. Nave KA, Trapp BD. Axon-glial signaling and the glial support of axon function. Annu Rev Neurosci. 2008;31:535-61. Epub 2008/06/19. doi: 10.1146/annurev.neuro.30.051606.094309. PubMed PMID: 18558866.

73. Meyer N, Richter N, Fan Z, Siemonsmeier G, Pivneva T, Jordan P, Steinhauser C, Semtner M, Nolte C, Kettenmann H. Oligodendrocytes in the Mouse Corpus Callosum Maintain Axonal Function by Delivery of Glucose. Cell Rep. 2018;22(9):2383-94. Epub 2018/03/01. doi: 10.1016/j.celrep.2018.02.022. PubMed PMID: 29490274.

74. Bjartmar C, Wujek JR, Trapp BD. Axonal loss in the pathology of MS: consequences for understanding the progressive phase of the disease. Journal of the neurological sciences. 2003;206(2):165-71. Epub 2003/02/01. doi: 10.1016/s0022-510x(02)00069-2. PubMed PMID: 12559505.

75. Peterson JW, Bo L, Mork S, Chang A, Trapp BD. Transected neurites, apoptotic neurons, and reduced inflammation in cortical multiple sclerosis lesions. Ann Neurol. 2001;50(3):389-400. Epub 2001/09/18. doi: 10.1002/ana.1123. PubMed PMID: 11558796.

76. Berret E, Kim SE, Lee SY, Kushmerick C, Kim JH. Functional and structural properties of ion channels at the nerve terminal depends on compact myelin. J Physiol. 2016;594(19):5593-609. Epub 2016/05/12. doi: 10.1113/JP272205. PubMed PMID: 27168396; PMCID: PMC5043032.

77. Cambron M, D'Haeseleer M, Laureys G, Clinckers R, Debruyne J, De Keyser J. White-matter astrocytes, axonal energy metabolism, and axonal degeneration in multiple sclerosis. J Cereb Blood Flow Metab. 2012;32(3):413-24. Epub 2012/01/05. doi: 10.1038/jcbfm.2011.193. PubMed PMID: 22214904; PMCID: PMC3293127.

78. Lassmann H, Bruck W, Lucchinetti CF. The immunopathology of multiple sclerosis: an overview. Brain Pathol. 2007;17(2):210-8. Epub 2007/03/29. doi: 10.1111/j.1750-3639.2007.00064.x. PubMed PMID: 17388952.

79. Langenbruch L, Kramer J, Guler S, Moddel G, Gessner S, Melzer N, Elger CE, Wiendl H, Budde T, Meuth SG, Kovac S. Seizures and epilepsy in multiple sclerosis: epidemiology and prognosis in a large tertiary referral center. J Neurol. 2019. Epub 2019/05/10. doi: 10.1007/s00415-019-09332-x. PubMed PMID: 31069528.

80. Evans C, Beland SG, Kulaga S, Wolfson C, Kingwell E, Marriott J, Koch M, Makhani N, Morrow S, Fisk J, Dykeman J, Jette N, Pringsheim T, Marrie RA. Incidence and prevalence of multiple sclerosis in the Americas: a systematic review. Neuroepidemiology. 2013;40(3):195-210. Epub 2013/02/01. doi: 10.1159/000342779. PubMed PMID: 23363936.

81. Kinnunen E, Wikstrom J. Prevalence and prognosis of epilepsy in patients with multiple sclerosis. Epilepsia. 1986;27(6):729-33. Epub 1986/11/01. doi: 10.1111/j.1528-1157.1986.tb03602.x. PubMed PMID: 3780609.

82. Nicholas R, Magliozzi R, Campbell G, Mahad D, Reynolds R. Temporal lobe cortical pathology and inhibitory GABA interneuron cell loss are associated with seizures in multiple sclerosis. Mult Scler. 2016;22(1):25-35. Epub 2015/04/30. doi: 10.1177/1352458515579445. PubMed PMID: 25921040; PMCID: PMC4702245.

83. Martinez-Juarez IE, Lopez-Meza E, Gonzalez-Aragon Mdel C, Ramirez-Bermudez J, Corona T. Epilepsy and multiple sclerosis: Increased risk among progressive forms. Epilepsy Res. 2009;84(2-3):250-3. Epub 2009/03/31. doi: 10.1016/j.eplepsyres.2009.01.009. PubMed PMID: 19329280.

84. Striano P, Orefice G, Brescia Morra V, Boccella P, Sarappa C, Lanzillo R, Vacca G, Striano S. Epileptic seizures in multiple sclerosis: clinical and EEG correlations. Neurol Sci. 2003;24(5):322-8. Epub 2004/01/13. doi: 10.1007/s10072-003-0183-2. PubMed PMID: 14716527.

85. Ghezzi A, Montanini R, Basso PF, Zaffaroni M, Massimo E, Cazzullo CL. Epilepsy in multiple sclerosis. Eur Neurol. 1990;30(4):218-23. Epub 1990/01/01. doi: 10.1159/000117350. PubMed PMID: 2209677.

86. Martinez-Lapiscina EH, Ayuso T, Lacruz F, Gurtubay IG, Soriano G, Otano M, Bujanda M, Bacaicoa MC. Cortico-juxtacortical involvement increases risk of epileptic seizures in multiple sclerosis. Acta Neurol Scand. 2013;128(1):24-31. Epub 2013/01/08. doi: 10.1111/ane.12064. PubMed PMID: 23289848.

87. Moreau T, Sochurkova D, Lemesle M, Madinier G, Billiar T, Giroud M, Dumas R. Epilepsy in patients with multiple sclerosis: radiological-clinical correlations. Epilepsia. 1998;39(8):893-6. Epub 1998/08/13. doi: 10.1111/j.1528-1157.1998.tb01187.x. PubMed PMID: 9701383.

88. Cendrowski W, Majkowski J. Epilepsy in multiple sclerosis. Journal of the neurological sciences. 1972;17(4):389-98. Epub 1972/12/01. doi: http://dx.doi.org/10.1016/0022-510X(72)90151-7. PubMed PMID: 5086256.

89. Calabrese M, De Stefano N, Atzori M, Bernardi V, Mattisi I, Barachino L, Rinaldi L, Morra A, McAuliffe MM, Perini P, Battistin L, Gallo P. Extensive cortical inflammation is associated with epilepsy in multiple sclerosis. J Neurol. 2008;255(4):581-6. Epub 2008/01/30. doi: 10.1007/s00415-008-0752-7. PubMed PMID: 18227989.

90. Calabrese M, Grossi P, Favaretto A, Romualdi C, Atzori M, Rinaldi F, Perini P, Saladini M, Gallo P. Cortical pathology in multiple sclerosis patients with epilepsy: a 3 year longitudinal study. J Neurol Neurosurg Psychiatry. 2012;83(1):49-54. Epub 2011/09/06. doi: 10.1136/jnnp-2011-300414. PubMed PMID: 21890577.

91. Calabrese M, Castellaro M, Bertoldo A, De Luca A, Pizzini FB, Ricciardi GK, Pitteri M, Zimatore S, Magliozzi R, Benedetti MD, Manganotti P, Montemezzi S, Reynolds R, Gajofatto A, Monaco S. Epilepsy in multiple sclerosis: The role of temporal lobe damage. Mult Scler. 2017;23(3):473-82. Epub 2016/06/05. doi: 10.1177/1352458516651502. PubMed PMID: 27260699.

92. de Lanerolle NC, Lee TS, Spencer DD. Histopathology of Human Epilepsy. In: th, Noebels JL, Avoli M, Rogawski MA, Olsen RW, Delgado-Escueta AV, editors. Jasper's Basic Mechanisms of the Epilepsies. 4th ed. Bethesda (MD): National Center for Biotechnology Information (US); 2012.

93. Huusko N, Romer C, Ndode-Ekane XE, Lukasiuk K, Pitkanen A. Loss of hippocampal interneurons and epileptogenesis: a comparison of two animal models of acquired epilepsy. Brain Struct Funct. 2015;220(1):153-91. Epub 2013/10/08. doi: 10.1007/s00429-013-0644-1. PubMed PMID: 24096381.

94. Browne P, Chandraratna D, Angood C, Tremlett H, Baker C, Taylor BV, Thompson AJ. Atlas of Multiple Sclerosis 2013: A growing global problem with widespread inequity. Neurology. 2014;83(11):1022-4. Epub 2014/09/10. doi: 10.1212/WNL.0000000000000768. PubMed PMID: 25200713; PMCID: PMC4162299.

95. Ropper AH, Samuels MA, Klein JP. Chapter 36. Multiple Sclerosis and Other Inflammatory Demyelinating Diseases. Adams and Victor's Principles of Neurology, 10e. New York, NY: The McGraw-Hill Companies; 2014.

96. Lund C, Nakken KO, Edland A, Celius EG. Multiple sclerosis and seizures: incidence and prevalence over 40 years. Acta Neurol Scand. 2014;130(6):368-73. Epub 2014/09/12. doi: 10.1111/ane.12276. PubMed PMID: 25209977.

97. Marrie RA, Reider N, Cohen J, Trojano M, Sorensen PS, Cutter G, Reingold S, Stuve O. A systematic review of the incidence and prevalence of sleep disorders and seizure disorders in multiple sclerosis. Mult Scler. 2015;21(3):342-9. Epub 2014/12/24. doi: 10.1177/1352458514564486. PubMed PMID: 25533301; PMCID: PMC4429167.

98. Engelsen BA, Grønning M. Epileptic seizures in patients with multiple sclerosis. Is the prognosis of epilepsy underestimated? Seizure. 1997;6(5):377-82. doi: 10.1016/s1059-1311(97)80037-4.

99. Allen AN, Seminog OO, Goldacre MJ. Association between multiple sclerosis and epilepsy: large population-based record-linkage studies. Bmc Neurol. 2013;13(1):189. Epub 2013/12/07. doi: 10.1186/1471-2377-13-189. PubMed PMID: 24304488; PMCID: PMC4235201.

100. Uribe-San-Martin R, Ciampi-Diaz E, Suarez-Hernandez F, Vasquez-Torres M, Godoy-Fernandez J, Carcamo-Rodriguez C. Prevalence of epilepsy in a cohort of patients with multiple sclerosis. Seizure. 2014;23(1):81-3. Epub 2013/10/09. doi: 10.1016/j.seizure.2013.09.008. PubMed PMID: 24099836.

101. Babiloni C, Del Percio C, Capotosto P, Noce G, Infarinato F, Muratori C, Marcotulli C, Bellagamba G, Righi E, Soricelli A, Onorati P, Lupattelli T. Cortical sources of resting state electroencephalographic rhythms differ in relapsing-remitting and secondary progressive multiple sclerosis. Clin Neurophysiol. 2016;127(1):581-90. Epub 2015/06/27. doi: 10.1016/j.clinph.2015.05.029. PubMed PMID: 26111485.

102. Cawley N, Solanky BS, Muhlert N, Tur C, Edden RA, Wheeler-Kingshott CA, Miller DH, Thompson AJ, Ciccarelli O. Reduced gamma-aminobutyric acid concentration is associated with physical disability in progressive multiple sclerosis. Brain. 2015;138(Pt 9):2584-95. Epub 2015/08/26. doi: 10.1093/brain/awv209. PubMed PMID: 26304151; PMCID: PMC4643627.

103. Kutzelnigg A, Lucchinetti CF, Stadelmann C, Bruck W, Rauschka H, Bergmann M, Schmidbauer M, Parisi JE, Lassmann H. Cortical demyelination and diffuse white matter injury in multiple sclerosis. Brain. 2005;128(Pt 11):2705-12. Epub 2005/10/19. doi: 10.1093/brain/awh641. PubMed PMID: 16230320.

104. Zivadinov R, Uher T, Hagemeier J, Vaneckova M, Ramasamy DP, Tyblova M, Bergsland N, Seidl Z, Dwyer MG, Krasensky J, Havrdova E, Horakova D. A serial 10-year follow-up study of brain atrophy and disability progression in RRMS patients. Mult Scler. 2016;22(13):1709-18. Epub 2016/02/18. doi: 10.1177/1352458516629769. PubMed PMID: 26883943.

105. Hoffmann K, Lindner M, Groticke I, Stangel M, Loscher W. Epileptic seizures and hippocampal damage after cuprizone-induced demyelination in C57BL/6 mice. Exp Neurol. 2008;210(2):308-21. Epub 2007/12/22. doi: 10.1016/j.expneurol.2007.11.005. PubMed PMID: 18096162.

106. McCarthy DP, Richards MH, Miller SD. Mouse models of multiple sclerosis: experimental autoimmune encephalomyelitis and Theiler's virus-induced demyelinating disease. Methods Mol Biol. 2012;900:381-401. Epub 2012/08/31. doi: 10.1007/978-1-60761-720-4_19. PubMed PMID: 22933080; PMCID: PMC3583382.

107. Merrill JE. In vitro and in vivo pharmacological models to assess demyelination and remyelination. Neuropsychopharmacology. 2009;34(1):55-73. Epub 2008/09/19. doi: 10.1038/npp.2008.145. PubMed PMID: 18800062; PMCID: PMC7100020.

108. Praet J, Guglielmetti C, Berneman Z, Van der Linden A, Ponsaerts P. Cellular and molecular neuropathology of the cuprizone mouse model: clinical relevance for multiple sclerosis. Neurosci Biobehav Rev. 2014;47:485-505. Epub 2014/12/03. doi: 10.1016/j.neubiorev.2014.10.004. PubMed PMID: 25445182.

109. Matsushima GK, Morell P. The neurotoxicant, cuprizone, as a model to study demyelination and remyelination in the central nervous system. Brain Pathol. 2001;11(1):107-16. Epub 2001/01/06. doi: 10.1111/j.1750-3639.2001.tb00385.x. PubMed PMID: 11145196.

110. Lucchinetti C, Bruck W, Parisi J, Scheithauer B, Rodriguez M, Lassmann H. Heterogeneity of multiple sclerosis lesions: implications for the pathogenesis of demyelination. Ann Neurol. 2000;47(6):707-17. Epub 2000/06/14. doi: 10.1002/1531-8249(200006)47:6<707::aid-ana3>3.0.co;2-q. PubMed PMID: 10852536.

111. Manrique-Hoyos N, Jurgens T, Gronborg M, Kreutzfeldt M, Schedensack M, Kuhlmann T, Schrick C, Bruck W, Urlaub H, Simons M, Merkler D. Late motor decline after accomplished remyelination: impact for progressive multiple sclerosis. Ann Neurol.

2012;71(2):227-44. Epub 2012/03/01. doi: 10.1002/ana.22681. PubMed PMID: 22367995.

112. Kim JY, Shen S, Dietz K, He Y, Howell O, Reynolds R, Casaccia P. HDAC1 nuclear export induced by pathological conditions is essential for the onset of axonal damage. Nat Neurosci. 2010;13(2):180-9. Epub 2009/12/29. doi: 10.1038/nn.2471. PubMed PMID: 20037577; PMCID: PMC2829989.

113. Franco-Pons N, Torrente M, Colomina MT, Vilella E. Behavioral deficits in the cuprizone-induced murine model of demyelination/remyelination. Toxicol Lett. 2007;169(3):205-13. Epub 2007/02/24. doi: 10.1016/j.toxlet.2007.01.010. PubMed PMID: 17317045.

114. Kesterson JW, Carlton WW. Aqueductal stenosis as the cause of hydrocephalus in mice fed the substituted hydrazine, cuprizone. Experimental and Molecular Pathology. 1970;13(3):281-94. doi: 10.1016/0014-4800(70)90091-2.

115. Kesterson JW, Carlton WW. Cuprizone toxicosis in mice—Attempts to antidote the toxicity. Toxicology and Applied Pharmacology. 1972;22(1):6-13. doi: 10.1016/0041-008x(72)90220-7.

116. Geurts JJ, Bo L, Roosendaal SD, Hazes T, Daniels R, Barkhof F, Witter MP, Huitinga I, van der Valk P. Extensive hippocampal demyelination in multiple sclerosis. J Neuropathol Exp Neurol. 2007;66(9):819-27. Epub 2007/09/07. doi: 10.1097/nen.0b013e3181461f54. PubMed PMID: 17805012.

117. Toyoda I, Fujita S, Thamattoor AK, Buckmaster PS. Unit Activity of Hippocampal Interneurons before Spontaneous Seizures in an Animal Model of Temporal Lobe Epilepsy. J Neurosci. 2015;35(16):6600-18. Epub 2015/04/24. doi: 10.1523/JNEUROSCI.4786-14.2015. PubMed PMID: 25904809; PMCID: PMC4405565.

118. Ellender TJ, Raimondo JV, Irkle A, Lamsa KP, Akerman CJ. Excitatory effects of parvalbumin-expressing interneurons maintain hippocampal epileptiform activity via synchronous afterdischarges. J Neurosci. 2014;34(46):15208-22. Epub 2014/11/14. doi: 10.1523/JNEUROSCI.1747-14.2014. PubMed PMID: 25392490; PMCID: PMC4228130.

119. Liu YQ, Yu F, Liu WH, He XH, Peng BW. Dysfunction of hippocampal interneurons in epilepsy. Neurosci Bull. 2014;30(6):985-98. doi: 10.1007/s12264-014-1478-4. PubMed PMID: 25370443.

120. Schwaller B, Tetko IV, Tandon P, Silveira DC, Vreugdenhil M, Henzi T, Potier MC, Celio MR, Villa AE. Parvalbumin deficiency affects network properties resulting in increased susceptibility to epileptic seizures. Mol Cell Neurosci. 2004;25(4):650-63. Epub 2004/04/15. doi: 10.1016/j.mcn.2003.12.006. PubMed PMID: 15080894.

121. Rossi S, Studer V, Motta C, De Chiara V, Barbieri F, Bernardi G, Centonze D. Inflammation inhibits GABA transmission in multiple sclerosis. Mult Scler. 2012;18(11):1633-5. Epub 2012/03/16. doi: 10.1177/1352458512440207. PubMed PMID: 22419673.

122. Norkute A, Hieble A, Braun A, Johann S, Clarner T, Baumgartner W, Beyer C, Kipp M. Cuprizone treatment induces demyelination and astrocytosis in the mouse hippocampus. J Neurosci Res. 2008. Epub 2008/11/21. doi: 10.1002/jnr.21946. PubMed PMID: 19021291.

123. Gudi V, Gingele S, Skripuletz T, Stangel M. Glial response during cuprizone-induced de- and remyelination in the CNS: lessons learned. Front Cell Neurosci. 2014;8:73. Epub 2014/03/25. doi: 10.3389/fncel.2014.00073. PubMed PMID: 24659953; PMCID: PMC3952085.

124. Skripuletz T, Hackstette D, Bauer K, Gudi V, Pul R, Voss E, Berger K, Kipp M, Baumgartner W, Stangel M. Astrocytes regulate myelin clearance through recruitment of microglia during cuprizone-induced demyelination. Brain. 2013;136(Pt 1):147-67. Epub 2012/12/26. doi: 10.1093/brain/aws262. PubMed PMID: 23266461.

125. Clarner T, Janssen K, Nellessen L, Stangel M, Skripuletz T, Krauspe B, Hess FM, Denecke B, Beutner C, Linnartz-Gerlach B, Neumann H, Vallieres L, Amor S, Ohl K, Tenbrock K, Beyer C, Kipp M. CXCL10 triggers early microglial activation in the cuprizone model. J Immunol. 2015;194(7):3400-13. Epub 2015/03/01. doi: 10.4049/jimmunol.1401459. PubMed PMID: 25725102.

126. Rodriguez-Cruces R, Concha L. White matter in temporal lobe epilepsy: clinico-pathological correlates of water diffusion abnormalities. Quant Imaging Med Surg. 2015;5(2):264-78. Epub 2015/04/09. doi: 10.3978/j.issn.2223-4292.2015.02.06. PubMed PMID: 25853084; PMCID: PMC4379316.

127. Anderson G, Rodriguez M. Multiple sclerosis, seizures, and antiepileptics: role of IL-18, IDO, and melatonin. Eur J Neurol. 2011;18(5):680-5. Epub 2010/12/02. doi: 10.1111/j.1468-1331.2010.03257.x. PubMed PMID: 21118329.

128. Oberheim NA, Tian GF, Han X, Peng W, Takano T, Ransom B, Nedergaard M. Loss of astrocytic domain organization in the epileptic brain. J Neurosci. 2008;28(13):3264-76. Epub 2008/03/28. doi: 10.1523/JNEUROSCI.4980-07.2008. PubMed PMID: 18367594; PMCID: PMC6670598.

129. Binder DK, Nagelhus EA, Ottersen OP. Aquaporin-4 and epilepsy. Glia. 2012;60(8):1203-14. doi: 10.1002/glia.22317.

130. Nwaobi SE, Cuddapah VA, Patterson KC, Randolph AC, Olsen ML. The role of glial-specific Kir4.1 in normal and pathological states of the CNS. Acta Neuropathol. 2016;132(1):1-21. Epub 2016/03/11. doi: 10.1007/s00401-016-1553-1. PubMed PMID: 26961251; PMCID: PMC6774634.

131. Feng G, Mellor RH, Bernstein M, Keller-Peck C, Nguyen QT, Wallace M, Nerbonne JM, Lichtman JW, Sanes JR. Imaging neuronal subsets in transgenic mice expressing multiple spectral variants of GFP. Neuron. 2000;28(1):41-51. Epub 2000/11/22. doi: S0896-6273(00)00084-2 [pii]. PubMed PMID: 11086982.

132. Crawford DK, Mangiardi M, Tiwari-Woodruff SK. Assaying the functional effects of demyelination and remyelination: revisiting field potential recordings. J Neurosci Meth. 2009;182(1):25-33. Epub 2009/06/02. doi: 10.1016/j.jneumeth.2009.05.013. PubMed PMID: 19481113.

133. Paxinos G, Franklin KBJ. The Mouse Brain in Stereotaxic Coordinates: Elsevier Academic Press; 2004.

134. Lee DJ, Hsu MS, Seldin MM, Arellano JL, Binder DK. Decreased expression of the glial water channel aquaporin-4 in the intrahippocampal kainic acid model of epileptogenesis. Exp Neurol. 2012;235(1):246-55. Epub 2012/03/01. doi: 10.1016/j.expneurol.2012.02.002. PubMed PMID: 22361023; PMCID: PMC3334411.

135. Moore SM, Khalaj AJ, Kumar S, Winchester Z, Yoon J, Yoo T, Martinez-Torres L, Yasui N, Katzenellenbogen JA, Tiwari-Woodruff SK. Multiple functional therapeutic effects of the estrogen receptor β agonist indazole-Cl in a mouse model of multiple sclerosis. Proc Natl Acad Sci U S A. 2014;111(50):18061-6. doi: 10.1073/pnas.1411294111. PubMed PMID: 25453074; PMCID: PMC4273334.

136. Tiwari-Woodruff S, Morales LB, Lee R, Voskuhl RR. Differential neuroprotective and antiinflammatory effects of estrogen receptor (ER)alpha and ERbeta ligand treatment. Proc Natl Acad Sci U S A. 2007;104(37):14813-8. Epub 2007/09/06. doi: 10.1073/pnas.0703783104. PubMed PMID: 17785421; PMCID: PMC1976208.

137. Mangiardi M, Crawford DK, Xia X, Du S, Simon-Freeman R, Voskuhl RR, Tiwari-Woodruff SK. An animal model of cortical and callosal pathology in multiple sclerosis. Brain Pathol. 2011;21(3):263-78. Epub 2010/10/30. doi: 10.1111/j.1750-3639.2010.00444.x. PubMed PMID: 21029240; PMCID: PMC5233755.

138. Crawford DK, Mangiardi M, Song B, Patel R, Du S, Sofroniew MV, Voskuhl RR, Tiwari-Woodruff SK. Oestrogen receptor beta ligand: a novel treatment to enhance endogenous functional remyelination. Brain : a journal of neurology. 2010;133(10):2999-3016. Epub 2010/09/23. doi: 10.1093/brain/awq237. PubMed PMID: 20858739; PMCID: 2947430.

139. Mahad D, Ziabreva I, Lassmann H, Turnbull D. Mitochondrial defects in acute multiple sclerosis lesions. Brain. 2008;131(Pt 7):1722-35. Epub 2008/06/03. doi: 10.1093/brain/awn105. PubMed PMID: 18515320; PMCID: PMC2442422.

140. Meijer DH, Kane MF, Mehta S, Liu H, Harrington E, Taylor CM, Stiles CD, Rowitch DH. Separated at birth? The functional and molecular divergence of OLIG1 and OLIG2. Nat Rev Neurosci. 2012;13(12):819-31. Epub 2012/11/21. doi: 10.1038/nrn3386. PubMed PMID: 23165259; PMCID: PMC3733228.

141. Lang J, Maeda Y, Bannerman P, Xu J, Horiuchi M, Pleasure D, Guo F. Adenomatous polyposis coli regulates oligodendroglial development. J Neurosci. 2013;33(7):3113-30. Epub 2013/02/15. doi: 10.1523/JNEUROSCI.3467-12.2013. PubMed PMID: 23407966; PMCID: PMC3711764.

142. Porter AG, Janicke RU. Emerging roles of caspase-3 in apoptosis. Cell Death Differ. 1999;6(2):99-104. Epub 1999/04/14. doi: 10.1038/sj.cdd.4400476. PubMed PMID: 10200555.

143. Ito D, Imai Y, Ohsawa K, Nakajima K, Fukuuchi Y, Kohsaka S. Microglia-specific localisation of a novel calcium binding protein, Iba1. Brain Res Mol Brain Res. 1998;57(1):1-9. Epub 1998/06/19. doi: 10.1016/s0169-328x(98)00040-0. PubMed PMID: 9630473.

144. Domingues HS, Portugal CC, Socodato R, Relvas JB. Oligodendrocyte, Astrocyte, and Microglia Crosstalk in Myelin Development, Damage, and Repair. Front Cell Dev Biol. 2016;4:71. Epub 2016/08/24. doi: 10.3389/fcell.2016.00071. PubMed PMID: 27551677; PMCID: PMC4923166.

145. Robel S. Astroglial Scarring and Seizures: A Cell Biological Perspective on Epilepsy. Neuroscientist. 2016;1(17). doi: 10.1177/1073858416645498. PubMed PMID: 27118807.

146. Nagelhus EA, Ottersen OP. Physiological roles of aquaporin-4 in brain. Physiol Rev. 2013;93(4):1543-62. Epub 2013/10/19. doi: 10.1152/physrev.00011.2013. PubMed PMID: 24137016; PMCID: PMC3858210.

147. Lee TS, Eid T, Mane S, Kim JH, Spencer DD, Ottersen OP, de Lanerolle NC. Aquaporin-4 is increased in the sclerotic hippocampus in human temporal lobe epilepsy. Acta Neuropathol. 2004;108(6):493-502. Epub 2004/11/02. doi: 10.1007/s00401-004-0910-7. PubMed PMID: 15517312.

148. Lesort M, Terro F, Esclaire F, Hugon J. Neuronal APP accumulates in toxic membrane blebbings. J Neural Transm (Vienna). 1997;104(4-5):497-513. Epub 1997/01/01. doi: 10.1007/BF01277667. PubMed PMID: 9295181.

149. Ziehn MO, Avedisian AA, Tiwari-Woodruff S, Voskuhl RR. Hippocampal CA1 atrophy and synaptic loss during experimental autoimmune encephalomyelitis, EAE. Lab Invest. 2010;90(5):774-86. Epub 2010/02/17. doi: 10.1038/labinvest.2010.6. PubMed PMID: 20157291; PMCID: PMC3033772.

150. Mullen RJ, Buck CR, Smith AM. NeuN, a neuronal specific nuclear protein in vertebrates. Development. 1992;116(1):201-11. Epub 1992/09/01. PubMed PMID: 1483388.

151. Rao MS, Shetty AK. Efficacy of doublecortin as a marker to analyse the absolute number anddendritic growth of newly generated neurons in the adult dentate gyrus. European Journal of Neuroscience. 2004;19(2):234-46. doi: 10.1111/j.1460-9568.2003.03123.x. PubMed PMID: WOS:000188224800002.

152. Kee N, Sivalingam S, Boonstra R, Wojtowicz JM. The utility of Ki-67 and BrdU as proliferative markers of adult neurogenesis. J Neurosci Meth. 2002;115(1):97-105. doi: Pii S0165-0270(02)00007-9
Doi 10.1016/S0165-0270(02)00007-9. PubMed PMID: WOS:000175018000011.

153. Arabadzisz D, Antal K, Parpan F, Emri Z, Fritschy JM. Epileptogenesis and chronic seizures in a mouse model of temporal lobe epilepsy are associated with distinct EEG patterns and selective neurochemical alterations in the contralateral hippocampus. Exp Neurol. 2005;194(1):76-90. Epub 2005/05/19. doi: 10.1016/j.expneurol.2005.01.029. PubMed PMID: 15899245.

154. Martinez-Lapiscina EH, Ayuso T, Lacruz F, Gurtubay IG, Soriano G, Otano M, Bujanda M, Bacaicoa MC. Cortico-juxtacortical involvement increases risk of epileptic seizures in multiple sclerosis. Acta Neurol Scand. 2013;128(1):24-31. doi: 10.1111/ane.12064. PubMed PMID: 23289848.

155. Wolf DC, Bueno-Junior LS, Lopes-Aguiar C, Do Val Da Silva RA, Kandratavicius L, Leite JP. The frequency of spontaneous seizures in rats correlates with alterations in sensorimotor gating, spatial working memory, and parvalbumin expression throughout limbic regions. Neuroscience. 2016;312:86-98. Epub 2015/11/20. doi: 10.1016/j.neuroscience.2015.11.008. PubMed PMID: 26582750.

156. Houser CR. Do structural changes in GABA neurons give rise to the epileptic state? Adv Exp Med Biol. 2014;813:151-60. Epub 2014/07/12. doi: 10.1007/978-94-017-8914-1_12. PubMed PMID: 25012374; PMCID: PMC4634888.

157. Hernandez-Lain A, Hedley-Whyte ET, Hariri LP, Molyneaux B, Nagle KJ, Cole AJ, Kilbride R. Pathology of bilateral pulvinar degeneration following long duration status epilepticus. Seizure. 2013;22(10):901-4. Epub 2013/08/22. doi: 10.1016/j.seizure.2013.07.012. PubMed PMID: 23962521.

158. Kohus Z, Kali S, Rovira-Esteban L, Schlingloff D, Papp O, Freund TF, Hajos N, Gulyas AI. Properties and dynamics of inhibitory synaptic communication within the CA3 microcircuits of pyramidal cells and interneurons expressing parvalbumin or cholecystokinin. J Physiol. 2016;594(13):3745-74. Epub 2016/04/03. doi: 10.1113/JP272231. PubMed PMID: 27038232; PMCID: PMC4929320.

159. Dewar D, Underhill SM, Goldberg MP. Oligodendrocytes and ischemic brain injury. J Cereb Blood Flow Metab. 2003;23(3):263-74. Epub 2003/03/07. doi: 10.1097/01.WCB.0000053472.41007.F9. PubMed PMID: 12621301.

160. Marrif H, Juurlink BHJ. Differential vulnerability of oligodendrocytes and astrocytes to hypoxic–ischemic stresses. Advances in Molecular and Cell Biology: Elsevier; 2003. p. 857-67.

161. Gouix E, Buisson A, Nieoullon A, Kerkerian-Le Goff L, Tauskela JS, Blondeau N, Had-Aissouni L. Oxygen glucose deprivation-induced astrocyte dysfunction provokes neuronal death through oxidative stress. Pharmacol Res. 2014;87:8-17. Epub 2014/06/15. doi: 10.1016/j.phrs.2014.06.002. PubMed PMID: 24928737.

162. Lemasters JJ, DiGuiseppi J, Nieminen AL, Herman B. Blebbing, free Ca2+ and mitochondrial membrane potential preceding cell death in hepatocytes. Nature. 1987;325(6099):78-81. Epub 1987/01/01. doi: 10.1038/325078a0. PubMed PMID: 3099216.

163. Magnotti LM, Goodenough DA, Paul DL. Deletion of oligodendrocyte Cx32 and astrocyte Cx43 causes white matter vacuolation, astrocyte loss and early mortality. Glia. 2011;59(7):1064-74. Epub 2011/05/04. doi: 10.1002/glia.21179. PubMed PMID: 21538560; PMCID: PMC3094483.

164. Takahashi DK, Vargas JR, Wilcox KS. Increased coupling and altered glutamate transport currents in astrocytes following kainic-acid-induced status epilepticus. Neurobiol Dis. 2010;40(3):573-85. Epub 2010/08/10. doi: 10.1016/j.nbd.2010.07.018. PubMed PMID: 20691786; PMCID: PMC3031166.

165. Alvestad S, Hammer J, Hoddevik EH, Skare O, Sonnewald U, Amiry-Moghaddam M, Ottersen OP. Mislocalization of AQP4 precedes chronic seizures in the kainate model of temporal lobe epilepsy. Epilepsy Res. 2013;105(1-2):30-41. Epub 2013/01/30. doi: 10.1016/j.eplepsyres.2013.01.006. PubMed PMID: 23357720.

166. Hubbard JA, Szu JI, Yonan JM, Binder DK. Regulation of astrocyte glutamate transporter-1 (GLT1) and aquaporin-4 (AQP4) expression in a model of epilepsy. Exp Neurol. 2016;283(Pt A):85-96. Epub 2016/05/08. doi: 10.1016/j.expneurol.2016.05.003. PubMed PMID: 27155358; PMCID: PMC4992641.

167. Zhang B, Zou J, Han L, Rensing N, Wong M. Microglial activation during epileptogenesis in a mouse model of tuberous sclerosis complex. Epilepsia. 2016;57(8):1317-25. Epub 2016/06/07. doi: 10.1111/epi.13429. PubMed PMID: 27263494; PMCID: PMC4972670.

168. Eyo UB, Murugan M, Wu LJ. Microglia-Neuron Communication in Epilepsy. Glia. 2017;65(1):5-18. Epub 2016/05/18. doi: 10.1002/glia.23006. PubMed PMID: 27189853; PMCID: PMC5116010.

169. Hu QP, Mao DA. Histone deacetylase inhibitor SAHA attenuates post-seizure hippocampal microglia TLR4/MYD88 signaling and inhibits TLR4 gene expression via histone acetylation. BMC Neurosci. 2016;17(1):22. Epub 2016/05/20. doi: 10.1186/s12868-016-0264-9. PubMed PMID: 27193049; PMCID: PMC4872358.

170. Zhou M, Wang CM, Yang WL, Wang P. Microglial CD14 activated by iNOS contributes to neuroinflammation in cerebral ischemia. Brain Res. 2013;1506:105-14. Epub 2013/02/19. doi: 10.1016/j.brainres.2013.02.010. PubMed PMID: 23416151; PMCID: PMC3615048.

171. Nyquist PA, Cascino GD, Rodriguez M. Seizures in patients with multiple sclerosis seen at Mayo Clinic, Rochester, Minn, 1990-1998. Mayo Clin Proc. 2001;76(10):983-6. Epub 2001/10/19. doi: 10.4065/76.10.983. PubMed PMID: 11605699.

172. Shaygannejad V, Ashtari F, Zare M, Ghasemi M, Norouzi R, Maghzi H. Seizure characteristics in multiple sclerosis patients. J Res Med Sci. 2013;18(Suppl 1):S74-7. Epub 2013/08/21. PubMed PMID: 23961293; PMCID: PMC3743327.

173. Spatt J, Chaix R, Mamoli B. Epileptic and non-epileptic seizures in multiple sclerosis. J Neurol. 2001;248(1):2-9. Epub 2001/03/27. doi: 10.1007/s004150170262. PubMed PMID: 11266015.

174. Spatt J, Goldenberg G, Mamoli B. Simple dysphasic seizures as the sole manifestation of relapse in multiple sclerosis. Epilepsia. 1994;35(6):1342-5. Epub 1994/11/01. doi: 10.1111/j.1528-1157.1994.tb01809.x. PubMed PMID: 7988531.

175. Primavera A, Gianelli MV, Bandini F. Aphasic status epilepticus in multiple sclerosis. Eur Neurol. 1996;36(6):374-7. Epub 1996/01/01. doi: 10.1159/000117296. PubMed PMID: 8954306.

176. Newman P, Saunders M. A unique case of musicogenic epilepsy. Arch Neurol. 1980;37(4):244-5. Epub 1980/04/01. doi: 10.1001/archneur.1980.00500530082016. PubMed PMID: 7362491.

177. Kelley BJ, Rodriguez M. Seizures in patients with multiple sclerosis: epidemiology, pathophysiology and management. CNS Drugs. 2009;23(10):805-15. Epub 2009/09/11. doi: 10.2165/11310900-000000000-00000. PubMed PMID: 19739692; PMCID: PMC2748351.

178. Colasanti A, Guo Q, Giannetti P, Wall MB, Newbould RD, Bishop C, Onega M, Nicholas R, Ciccarelli O, Muraro PA, Malik O, Owen DR, Young AH, Gunn RN, Piccini P, Matthews PM, Rabiner EA. Hippocampal Neuroinflammation, Functional Connectivity, and Depressive Symptoms in Multiple Sclerosis. Biol Psychiatry. 2016;80(1):62-72. Epub 2016/01/27. doi: 10.1016/j.biopsych.2015.11.022. PubMed PMID: 26809249; PMCID: PMC4918731.

179. Burman J, Zelano J. Epilepsy in multiple sclerosis: A nationwide population-based register study. Neurology. 2017;89(24):2462-8. Epub 2017/11/10. doi: 10.1212/WNL.0000000000004740. PubMed PMID: 29117950.

180. Solaro C, Brichetto G, Battaglia MA, Messmer Uccelli M, Mancardi GL. Antiepileptic medications in multiple sclerosis: adverse effects in a three-year follow-up study. Neurol Sci. 2005;25(6):307-10. Epub 2005/02/25. doi: 10.1007/s10072-004-0362-9. PubMed PMID: 15729492.

181. Wojtowicz JM. Adult neurogenesis. From circuits to models. Behav Brain Res. 2012;227(2):490-6. Epub 2011/09/07. doi: 10.1016/j.bbr.2011.08.013. PubMed PMID: 21893104.

182. Preibisch S, Saalfeld S, Tomancak P. Globally optimal stitching of tiled 3D microscopic image acquisitions. Bioinformatics. 2009;25(11):1463-5. Epub 2009/04/07. doi: 10.1093/bioinformatics/btp184. PubMed PMID: 19346324; PMCID: PMC2682522.

183. Schindelin J, Arganda-Carreras I, Frise E, Kaynig V, Longair M, Pietzsch T, Preibisch S, Rueden C, Saalfeld S, Schmid B, Tinevez JY, White DJ, Hartenstein V, Eliceiri K, Tomancak P, Cardona A. Fiji: an open-source platform for biological-image analysis. Nat Methods. 2012;9(7):676-82. Epub 2012/06/30. doi: 10.1038/nmeth.2019. PubMed PMID: 22743772; PMCID: PMC3855844.

184. Crawford DK, Mangiardi M, Song B, Patel R, Du S, Sofroniew MV, Voskuhl RR, Tiwari-Woodruff SK. Oestrogen receptor beta ligand: a novel treatment to enhance endogenous functional remyelination. Brain. 2010;133(10):2999-3016. Epub 2010/09/23. doi: 10.1093/brain/awq237. PubMed PMID: 20858739; PMCID: PMC2947430.

185. Lapato AS, Tiwari-Woodruff SK. Connexins and pannexins: At the junction of neuro-glial homeostasis & disease. J Neurosci Res. 2018;96(1):31-44. Epub 2017/06/06. doi: 10.1002/jnr.24088. PubMed PMID: 28580666; PMCID: PMC5749981.

186. Eid T, Lee TS, Thomas MJ, Amiry-Moghaddam M, Bjornsen LP, Spencer DD, Agre P, Ottersen OP, de Lanerolle NC. Loss of perivascular aquaporin 4 may underlie deficient water and K+ homeostasis in the human epileptogenic hippocampus. Proc Natl Acad Sci U S A. 2005;102(4):1193-8. Epub 2005/01/20. doi: 10.1073/pnas.0409308102. PubMed PMID: 15657133; PMCID: PMC545857.

187. Lehre KP, Danbolt NC. The number of glutamate transporter subtype molecules at glutamatergic synapses: Chemical and stereological quantification in young adult rat brain. Journal of Neuroscience. 1998;18(21):8751-7. doi: DOI 10.1523/jneurosci.18-21-08751.1998. PubMed PMID: WOS:000076616600020.

188. Mathern GW, Mendoza D, Lozada A, Pretorius JK, Dehnes Y, Danbolt NC, Nelson N, Leite JP, Chimelli L, Born DE, Sakamoto AC, Assirati JA, Fried I, Peacock WJ, Ojemann GA, Adelson PD. Hippocampal GABA and glutamate transporter immunoreactivity in patients with temporal lobe epilepsy. Neurology. 1999;52(3):453-72. Epub 1999/02/20. doi: 10.1212/wnl.52.3.453. PubMed PMID: 10025773.

189. Azevedo CJ, Kornak J, Chu P, Sampat M, Okuda DT, Cree BA, Nelson SJ, Hauser SL, Pelletier D. In vivo evidence of glutamate toxicity in multiple sclerosis. Ann Neurol. 2014;76(2):269-78. Epub 2014/07/22. doi: 10.1002/ana.24202. PubMed PMID: 25043416; PMCID: PMC4142752.

190. Tanaka K, Watase K, Manabe T, Yamada K, Watanabe M, Takahashi K, Iwama H, Nishikawa T, Ichihara N, Kikuchi T, Okuyama S, Kawashima N, Hori S, Takimoto M, Wada K. Epilepsy and exacerbation of brain injury in mice lacking the glutamate transporter GLT-1. Science. 1997;276(5319):1699-702. Epub 1997/06/13. doi: 10.1126/science.276.5319.1699. PubMed PMID: 9180080.

191. Bergles DE, Jahr CE. Synaptic activation of glutamate transporters in hippocampal astrocytes. Neuron. 1997;19(6):1297-308. Epub 1998/01/14. doi: 10.1016/s0896-6273(00)80420-1. PubMed PMID: 9427252.

192. Bergles DE, Jahr CE. Glial contribution to glutamate uptake at Schaffer collateral-commissural synapses in the hippocampus. Journal of Neuroscience. 1998;18(19):7709-16. PubMed PMID: WOS:000076060100009.

193. Guella I, McKenzie MB, Evans DM, Buerki SE, Toyota EB, Van Allen MI, Epilepsy Genomics S, Suri M, Elmslie F, Deciphering Developmental Disorders S, Simon MEH, van Gassen KLI, Heron D, Keren B, Nava C, Connolly MB, Demos M, Farrer MJ. De Novo Mutations in YWHAG Cause Early-Onset Epilepsy. Am J Hum Genet. 2017;101(2):300-10. Epub 2017/08/05. doi: 10.1016/j.ajhg.2017.07.004. PubMed PMID: 28777935; PMCID: PMC5544417.

194. Sugimoto J, Tanaka M, Sugiyama K, Ito Y, Aizawa H, Soma M, Shimizu T, Mitani A, Tanaka K. Region-specific deletions of the glutamate transporter GLT1 differentially affect seizure activity and neurodegeneration in mice. Glia. 2018;66(4):777-88. Epub 2017/12/08. doi: 10.1002/glia.23281. PubMed PMID: 29214672.

195. Danbolt NC, Furness DN, Zhou Y. Neuronal vs glial glutamate uptake: Resolving the conundrum. Neurochem Int. 2016;98:29-45. Epub 2016/05/29. doi: 10.1016/j.neuint.2016.05.009. PubMed PMID: 27235987.

196. Petr GT, Sun Y, Frederick NM, Zhou Y, Dhamne SC, Hameed MQ, Miranda C, Bedoya EA, Fischer KD, Armsen W, Wang J, Danbolt NC, Rotenberg A, Aoki CJ, Rosenberg PA. Conditional deletion of the glutamate transporter GLT-1 reveals that astrocytic GLT-1 protects against fatal epilepsy while neuronal GLT-1 contributes significantly to glutamate uptake into synaptosomes. J Neurosci. 2015;35(13):5187-201. Epub 2015/04/04. doi: 10.1523/JNEUROSCI.4255-14.2015. PubMed PMID: 25834045; PMCID: PMC4380995.

197. Nagelhus EA, Mathiisen TM, Ottersen OP. Aquaporin-4 in the central nervous system: cellular and subcellular distribution and coexpression with KIR4.1. Neuroscience. 2004;129(4):905-13. Epub 2004/11/25. doi: 10.1016/j.neuroscience.2004.08.053. PubMed PMID: 15561407.

198. Mestre H, Hablitz LM, Xavier AL, Feng W, Zou W, Pu T, Monai H, Murlidharan G, Castellanos Rivera RM, Simon MJ, Pike MM, Pla V, Du T, Kress BT, Wang X, Plog BA, Thrane AS, Lundgaard I, Abe Y, Yasui M, Thomas JH, Xiao M, Hirase H, Asokan A, Iliff JJ, Nedergaard M. Aquaporin-4-dependent glymphatic solute transport in the rodent brain. Elife. 2018;7. Epub 2018/12/19. doi: 10.7554/eLife.40070. PubMed PMID: 30561329; PMCID: PMC6307855.

199. Binder DK, Yao X, Zador Z, Sick TJ, Verkman AS, Manley GT. Increased seizure duration and slowed potassium kinetics in mice lacking aquaporin-4 water channels. Glia. 2006;53(6):631-6. Epub 2006/02/14. doi: 10.1002/glia.20318. PubMed PMID: 16470808.

200. Strohschein S, Huttmann K, Gabriel S, Binder DK, Heinemann U, Steinhauser C. Impact of aquaporin-4 channels on K+ buffering and gap junction coupling in the hippocampus. Glia. 2011;59(6):973-80. Epub 2011/03/30. doi: 10.1002/glia.21169. PubMed PMID: 21446052.

201. Goldman DE. Potential, Impedance, and Rectification in Membranes. J Gen Physiol. 1943;27(1):37-60. Epub 1943/09/20. doi: 10.1085/jgp.27.1.37. PubMed PMID: 19873371; PMCID: PMC2142582.

202. Hodgkin AL, Katz B. The effect of sodium ions on the electrical activity of giant axon of the squid. J Physiol. 1949;108(1):37-77. Epub 1949/03/03. doi: 10.1113/jphysiol.1949.sp004310. PubMed PMID: 18128147; PMCID: PMC1392331.

203. Hamid SHM, Whittam D, Saviour M, Alorainy A, Mutch K, Linaker S, Solomon T, Bhojak M, Woodhall M, Waters P, Appleton R, Duddy M, Jacob A. Seizures and Encephalitis in Myelin Oligodendrocyte Glycoprotein IgG Disease vs Aquaporin 4 IgG Disease. JAMA Neurol. 2018;75(1):65-71. Epub 2017/11/14. doi: 10.1001/jamaneurol.2017.3196. PubMed PMID: 29131884; PMCID: PMC5833490.

204. Akaishi T, Takahashi T, Himori N, Fujihara K, Misu T, Abe M, Ishii T, Nakazawa T, Aoki M, Nakashima I. Serum AQP4-IgG level is associated with the phenotype of the first attack in neuromyelitis optica spectrum disorders. J Neuroimmunol. 2020;340:577168. Epub 2020/01/28. doi: 10.1016/j.jneuroim.2020.577168. PubMed PMID: 31986374.

205. Hillebrand S, Schanda K, Nigritinou M, Tsymala I, Bohm D, Peschl P, Takai Y, Fujihara K, Nakashima I, Misu T, Reindl M, Lassmann H, Bradl M. Circulating AQP4-specific auto-antibodies alone can induce neuromyelitis optica spectrum disorder in the rat. Acta Neuropathol. 2019;137(3):467-85. Epub 2018/12/20. doi: 10.1007/s00401-018-1950-8. PubMed PMID: 30564980; PMCID: PMC6514074.

206. Hinson SR, Romero MF, Popescu BF, Lucchinetti CF, Fryer JP, Wolburg H, Fallier-Becker P, Noell S, Lennon VA. Molecular outcomes of neuromyelitis optica (NMO)-IgG binding to aquaporin-4 in astrocytes. Proc Natl Acad Sci U S A. 2012;109(4):1245-50. Epub 2011/12/01. doi: 10.1073/pnas.1109980108. PubMed PMID: 22128336; PMCID: PMC3268278.

207. Hinson SR, Clift IC, Luo N, Kryzer TJ, Lennon VA. Autoantibody-induced internalization of CNS AQP4 water channel and EAAT2 glutamate transporter requires astrocytic Fc receptor. Proc Natl Acad Sci U S A. 2017;114(21):5491-6. Epub 2017/05/04. doi: 10.1073/pnas.1701960114. PubMed PMID: 28461494; PMCID: PMC5448211.

208. Falco A, Pennucci R, Brambilla E, de Curtis I. Reduction in parvalbumin-positive interneurons and inhibitory input in the cortex of mice with experimental autoimmune encephalomyelitis. Exp Brain Res. 2014;232(7):2439-49. Epub 2014/04/29. doi: 10.1007/s00221-014-3944-7. PubMed PMID: 24770856; PMCID: PMC4055863.

209. Battefeld A, Klooster J, Kole MH. Myelinating satellite oligodendrocytes are integrated in a glial syncytium constraining neuronal high-frequency activity. Nat Commun. 2016;7:11298. Epub 2016/05/11. doi: 10.1038/ncomms11298. PubMed PMID: 27161034; PMCID: PMC4866043.

210. Torres A, Wang F, Xu Q, Fujita T, Dobrowolski R, Willecke K, Takano T, Nedergaard M. Extracellular Ca(2)(+) acts as a mediator of communication from neurons

to glia. Sci Signal. 2012;5(208):ra8. Epub 2012/01/26. doi: 10.1126/scisignal.2002160. PubMed PMID: 22275221; PMCID: PMC3548660.

211. Kofuji P, Newman EA. Potassium buffering in the central nervous system. Neuroscience. 2004;129(4):1045-56. Epub 2004/11/25. doi: 10.1016/j.neuroscience.2004.06.008. PubMed PMID: 15561419; PMCID: PMC2322935.

212. Fasciani I, Pluta P, Gonzalez-Nieto D, Martinez-Montero P, Molano J, Paino CL, Millet O, Barrio LC. Directional coupling of oligodendrocyte connexin-47 and astrocyte connexin-43 gap junctions. Glia. 2018;66(11):2340-52. Epub 2018/08/26. doi: 10.1002/glia.23471. PubMed PMID: 30144323.

213. Chever O, Pannasch U, Ezan P, Rouach N. Astroglial connexin 43 sustains glutamatergic synaptic efficacy. Philos Trans R Soc Lond B Biol Sci. 2014;369(1654):20130596. Epub 2014/09/17. doi: 10.1098/rstb.2013.0596. PubMed PMID: 25225090; PMCID: PMC4173282.

214. Stehberg J, Moraga-Amaro R, Salazar C, Becerra A, Echeverria C, Orellana JA, Bultynck G, Ponsaerts R, Leybaert L, Simon F, Saez JC, Retamal MA. Release of gliotransmitters through astroglial connexin 43 hemichannels is necessary for fear memory consolidation in the basolateral amygdala. FASEB J. 2012;26(9):3649-57. Epub 2012/06/06. doi: 10.1096/fj.11-198416. PubMed PMID: 22665389.

215. Parpura V, Basarsky TA, Liu F, Jeftinija K, Jeftinija S, Haydon PG. Glutamate-mediated astrocyte-neuron signalling. Nature. 1994;369(6483):744-7. Epub 1994/06/30. doi: 10.1038/369744a0. PubMed PMID: 7911978.

216. Nedergaard M. Direct signaling from astrocytes to neurons in cultures of mammalian brain cells. Science. 1994;263(5154):1768-71. Epub 1994/03/25. doi: 10.1126/science.8134839. PubMed PMID: 8134839.

217. Stout CE, Costantin JL, Naus CC, Charles AC. Intercellular calcium signaling in astrocytes via ATP release through connexin hemichannels. J Biol Chem. 2002;277(12):10482-8. Epub 2002/01/16. doi: 10.1074/jbc.M109902200. PubMed PMID: 11790776.

218. Meunier C, Wang N, Yi C, Dallerac G, Ezan P, Koulakoff A, Leybaert L, Giaume C. Contribution of Astroglial Cx43 Hemichannels to the Modulation of Glutamatergic Currents by D-Serine in the Mouse Prefrontal Cortex. J Neurosci. 2017;37(37):9064-75. Epub 2017/08/20. doi: 10.1523/JNEUROSCI.2204-16.2017. PubMed PMID: 28821660; PMCID: PMC6596802.

219. Wu XL, Tang YC, Lu QY, Xiao XL, Song TB, Tang FR. Astrocytic Cx 43 and Cx 40 in the mouse hippocampus during and after pilocarpine-induced status epilepticus. Exp

Brain Res. 2015;233(5):1529-39. Epub 2015/02/19. doi: 10.1007/s00221-015-4226-8. PubMed PMID: 25690864.

220. Walrave L, Pierre A, Albertini G, Aourz N, De Bundel D, Van Eeckhaut A, Vinken M, Giaume C, Leybaert L, Smolders I. Inhibition of astroglial connexin43 hemichannels with TAT-Gap19 exerts anticonvulsant effects in rodents. Glia. 2018;66(8):1788-804. Epub 2018/04/24. doi: 10.1002/glia.23341. PubMed PMID: 29683209.

221. Meme W, Calvo CF, Froger N, Ezan P, Amigou E, Koulakoff A, Giaume C. Proinflammatory cytokines released from microglia inhibit gap junctions in astrocytes: potentiation by beta-amyloid. FASEB J. 2006;20(3):494-6. Epub 2006/01/21. doi: 10.1096/fj.05-4297fje. PubMed PMID: 16423877.

222. Retamal MA, Froger N, Palacios-Prado N, Ezan P, Saez PJ, Saez JC, Giaume C. Cx43 hemichannels and gap junction channels in astrocytes are regulated oppositely by proinflammatory cytokines released from activated microglia. J Neurosci. 2007;27(50):13781-92. Epub 2007/12/14. doi: 10.1523/JNEUROSCI.2042-07.2007. PubMed PMID: 18077690; PMCID: PMC6673621.

223. Abudara V, Roux L, Dallerac G, Matias I, Dulong J, Mothet JP, Rouach N, Giaume C. Activated microglia impairs neuroglial interaction by opening Cx43 hemichannels in hippocampal astrocytes. Glia. 2015;63(5):795-811. Epub 2015/02/04. doi: 10.1002/glia.22785. PubMed PMID: 25643695.

224. Markoullis K, Sargiannidou I, Schiza N, Roncaroli F, Reynolds R, Kleopa KA. Oligodendrocyte gap junction loss and disconnection from reactive astrocytes in multiple sclerosis gray matter. J Neuropathol Exp Neurol. 2014;73(9):865-79. Epub 2014/08/08. doi: 10.1097/NEN.0000000000000106. PubMed PMID: 25101702.

225. Markoullis K, Sargiannidou I, Schiza N, Hadjisavvas A, Roncaroli F, Reynolds R, Kleopa KA. Gap junction pathology in multiple sclerosis lesions and normal-appearing white matter. Acta Neuropathol. 2012;123(6):873-86. Epub 2012/04/10. doi: 10.1007/s00401-012-0978-4. PubMed PMID: 22484441.

226. Chever O, Lee CY, Rouach N. Astroglial connexin43 hemichannels tune basal excitatory synaptic transmission. J Neurosci. 2014;34(34):11228-32. Epub 2014/08/22. doi: 10.1523/JNEUROSCI.0015-14.2014. PubMed PMID: 25143604; PMCID: PMC6615508.

227. Froger N, Orellana JA, Calvo CF, Amigou E, Kozoriz MG, Naus CC, Saez JC, Giaume C. Inhibition of cytokine-induced connexin43 hemichannel activity in astrocytes is neuroprotective. Mol Cell Neurosci. 2010;45(1):37-46. Epub 2010/08/05. doi: 10.1016/j.mcn.2010.05.007. PubMed PMID: 20684043.

228. Samoilova M, Wentlandt K, Adamchik Y, Velumian AA, Carlen PL. Connexin 43 mimetic peptides inhibit spontaneous epileptiform activity in organotypic hippocampal slice cultures. Exp Neurol. 2008;210(2):762-75. Epub 2008/02/21. doi: 10.1016/j.expneurol.2008.01.005. PubMed PMID: 18284929.

229. Bazzigaluppi P, Weisspapir I, Stefanovic B, Leybaert L, Carlen PL. Astrocytic gap junction blockade markedly increases extracellular potassium without causing seizures in the mouse neocortex. Neurobiol Dis. 2017;101:1-7. Epub 2016/12/23. doi: 10.1016/j.nbd.2016.12.017. PubMed PMID: 28007587.

230. Katoozi S, Skauli N, Rahmani S, Camassa LMA, Boldt HB, Ottersen OP, Amiry-Moghaddam M. Targeted deletion of Aqp4 promotes the formation of astrocytic gap junctions. Brain Struct Funct. 2017;222(9):3959-72. Epub 2017/05/30. doi: 10.1007/s00429-017-1448-5. PubMed PMID: 28551776.

231. Jullienne A, Fukuda AM, Ichkova A, Nishiyama N, Aussudre J, Obenaus A, Badaut J. Modulating the water channel AQP4 alters miRNA expression, astrocyte connectivity and water diffusion in the rodent brain. Sci Rep. 2018;8(1):4186. Epub 2018/03/10. doi: 10.1038/s41598-018-22268-y. PubMed PMID: 29520011; PMCID: PMC5843607.

232. Kekesi O, Ioja E, Szabo Z, Kardos J, Heja L. Recurrent seizure-like events are associated with coupled astroglial synchronization. Front Cell Neurosci. 2015;9:215. Epub 2015/07/08. doi: 10.3389/fncel.2015.00215. PubMed PMID: 26150770; PMCID: PMC4471369.

233. Engelsen BA, Grønning M. Epileptic seizures in patients with multiple sclerosis. Is the prognosis of epilepsy underestimated? Seizure. 1997;6(5):377-82.

234. Marrie RA, Reider N, Cohen J, Trojano M, Sorensen PS, Cutter G, Reingold S, Stuve O. A systematic review of the incidence and prevalence of sleep disorders and seizure disorders in multiple sclerosis. Mult Scler2015. p. 342-9.

235. Jonak CR, Lovelace JW, Ethell IM, Razak KA, Binder DK. Reusable Multielectrode Array Technique for Electroencephalography in Awake Freely Moving Mice. Front Integr Neurosci. 2018;12:53. Epub 2018/11/13. doi: 10.3389/fnint.2018.00053. PubMed PMID: 30416434; PMCID: PMC6213968.

236. Lovelace JW, Ethell IM, Binder DK, Razak KA. Translation-relevant EEG phenotypes in a mouse model of Fragile X Syndrome. Neurobiol Dis. 2018;115:39-48. Epub 2018/04/02. doi: 10.1016/j.nbd.2018.03.012. PubMed PMID: 29605426; PMCID: PMC5969806.

237. Cole SR, Voytek B. Brain Oscillations and the Importance of Waveform Shape. Trends Cogn Sci. 2017;21(2):137-49. Epub 2017/01/09. doi: 10.1016/j.tics.2016.12.008. PubMed PMID: 28063662.

238. Bartos M, Vida I, Jonas P. Synaptic mechanisms of synchronized gamma oscillations in inhibitory interneuron networks. Nat Rev Neurosci. 2007;8(1):45-56. Epub 2006/12/21. doi: 10.1038/nrn2044. PubMed PMID: 17180162.

239. Chen G, Zhang Y, Li X, Zhao X, Ye Q, Lin Y, Tao HW, Rasch MJ, Zhang X. Distinct Inhibitory Circuits Orchestrate Cortical beta and gamma Band Oscillations. Neuron. 2017;96(6):1403-18 e6. Epub 2017/12/22. doi: 10.1016/j.neuron.2017.11.033. PubMed PMID: 29268099; PMCID: PMC5864125.

240. Sohal VS, Zhang F, Yizhar O, Deisseroth K. Parvalbumin neurons and gamma rhythms enhance cortical circuit performance. Nature. 2009;459(7247):698-702. Epub 2009/04/28. doi: 10.1038/nature07991. PubMed PMID: 19396159; PMCID: PMC3969859.

241. Kim T, Thankachan S, McKenna JT, McNally JM, Yang C, Choi JH, Chen L, Kocsis B, Deisseroth K, Strecker RE, Basheer R, Brown RE, McCarley RW. Cortically projecting basal forebrain parvalbumin neurons regulate cortical gamma band oscillations. Proc Natl Acad Sci U S A. 2015;112(11):3535-40. Epub 2015/03/04. doi: 10.1073/pnas.1413625112. PubMed PMID: 25733878; PMCID: PMC4371918.

242. Darvas F, Rao RP, Murias M. Localized high gamma motor oscillations respond to perceived biologic motion. J Clin Neurophysiol. 2013;30(3):299-307. Epub 2013/06/05. doi: 10.1097/WNP.0b013e3182872f40. PubMed PMID: 23733096; PMCID: PMC3675661.

243. Buzsaki G, Wang XJ. Mechanisms of gamma oscillations. Annu Rev Neurosci. 2012;35:203-25. Epub 2012/03/27. doi: 10.1146/annurev-neuro-062111-150444. PubMed PMID: 22443509; PMCID: PMC4049541.

244. Pelkey KA, Chittajallu R, Craig MT, Tricoire L, Wester JC, McBain CJ. Hippocampal GABAergic Inhibitory Interneurons. Physiol Rev. 2017;97(4):1619-747. Epub 2017/09/29. doi: 10.1152/physrev.00007.2017. PubMed PMID: 28954853; PMCID: PMC6151493.

245. Rudy B, Fishell G, Lee S, Hjerling-Leffler J. Three groups of interneurons account for nearly 100% of neocortical GABAergic neurons. Dev Neurobiol. 2011;71(1):45-61. Epub 2010/12/15. doi: 10.1002/dneu.20853. PubMed PMID: 21154909; PMCID: PMC3556905.

246. Tremblay R, Lee S, Rudy B. GABAergic Interneurons in the Neocortex: From Cellular Properties to Circuits. Neuron. 2016;91(2):260-92. Epub 2016/08/02. doi: 10.1016/j.neuron.2016.06.033. PubMed PMID: 27477017; PMCID: PMC4980915.

247. Kaufman DL, Houser CR, Tobin AJ. Two forms of the gamma-aminobutyric acid synthetic enzyme glutamate decarboxylase have distinct intraneuronal distributions and cofactor interactions. J Neurochem. 1991;56(2):720-3. Epub 1991/02/01. doi: 10.1111/j.1471-4159.1991.tb08211.x. PubMed PMID: 1988566.

248. Filice F, Vorckel KJ, Sungur AO, Wohr M, Schwaller B. Reduction in parvalbumin expression not loss of the parvalbumin-expressing GABA interneuron subpopulation in genetic parvalbumin and shank mouse models of autism. Mol Brain. 2016;9:10. Epub 2016/01/29. doi: 10.1186/s13041-016-0192-8. PubMed PMID: 26819149; PMCID: PMC4729132.

249. Normand EA, Crandall SR, Thorn CA, Murphy EM, Voelcker B, Browning C, Machan JT, Moore CI, Connors BW, Zervas M. Temporal and mosaic Tsc1 deletion in the developing thalamus disrupts thalamocortical circuitry, neural function, and behavior. Neuron. 2013;78(5):895-909. Epub 2013/05/15. doi: 10.1016/j.neuron.2013.03.030. PubMed PMID: 23664552; PMCID: PMC4529124.

250. Veres JM, Nagy GA, Hajos N. Perisomatic GABAergic synapses of basket cells effectively control principal neuron activity in amygdala networks. Elife. 2017;6. Epub 2017/01/07. doi: 10.7554/eLife.20721. PubMed PMID: 28060701; PMCID: PMC5218536.

251. Pouille F, Marin-Burgin A, Adesnik H, Atallah BV, Scanziani M. Input normalization by global feedforward inhibition expands cortical dynamic range. Nat Neurosci. 2009;12(12):1577-85. Epub 2009/11/03. doi: 10.1038/nn.2441. PubMed PMID: 19881502.

252. Willems JGP, Wadman WJ, Cappaert NLM. Parvalbumin interneuron mediated feedforward inhibition controls signal output in the deep layers of the perirhinal-entorhinal cortex. Hippocampus. 2018;28(4):281-96. Epub 2018/01/18. doi: 10.1002/hipo.22830. PubMed PMID: 29341361; PMCID: PMC5900730.

253. Bartos M, Elgueta C. Functional characteristics of parvalbumin- and cholecystokinin-expressing basket cells. J Physiol. 2012;590(4):669-81. Epub 2012/01/18. doi: 10.1113/jphysiol.2011.226175. PubMed PMID: 22250212; PMCID: PMC3381301.

254. Calin A, Stancu M, Zagrean AM, Jefferys JGR, Ilie AS, Akerman CJ. Chemogenetic Recruitment of Specific Interneurons Suppresses Seizure Activity. Front Cell Neurosci. 2018;12:293. Epub 2018/09/21. doi: 10.3389/fncel.2018.00293. PubMed PMID: 30233328; PMCID: PMC6134067.

255. Hu H, Gan J, Jonas P. Interneurons. Fast-spiking, parvalbumin(+) GABAergic interneurons: from cellular design to microcircuit function. Science. 2014;345(6196):1255263. Epub 2014/08/02. doi: 10.1126/science.1255263. PubMed PMID: 25082707.

256. Wohr M, Orduz D, Gregory P, Moreno H, Khan U, Vorckel KJ, Wolfer DP, Welzl H, Gall D, Schiffmann SN, Schwaller B. Lack of parvalbumin in mice leads to behavioral deficits relevant to all human autism core symptoms and related neural morphofunctional abnormalities. Transl Psychiatry. 2015;5:e525. Epub 2015/03/11. doi: 10.1038/tp.2015.19. PubMed PMID: 25756808; PMCID: PMC4354349.

257. Billingslea EN, Tatard-Leitman VM, Anguiano J, Jutzeler CR, Suh J, Saunders JA, Morita S, Featherstone RE, Ortinski PI, Gandal MJ, Lin R, Liang Y, Gur RE, Carlson GC, Hahn CG, Siegel SJ. Parvalbumin cell ablation of NMDA-R1 causes increased resting network excitability with associated social and self-care deficits. Neuropsychopharmacology. 2014;39(7):1603-13. Epub 2014/02/15. doi: 10.1038/npp.2014.7. PubMed PMID: 24525709; PMCID: PMC4023157.

258. Dinocourt C, Petanjek Z, Freund TF, Ben-Ari Y, Esclapez M. Loss of interneurons innervating pyramidal cell dendrites and axon initial segments in the CA1 region of the hippocampus following pilocarpine-induced seizures. J Comp Neurol. 2003;459(4):407-25. Epub 2003/04/11. doi: 10.1002/cne.10622. PubMed PMID: 12687707.

259. Pouille F, Watkinson O, Scanziani M, Trevelyan AJ. The contribution of synaptic location to inhibitory gain control in pyramidal cells. Physiol Rep. 2013;1(5):e00067. Epub 2013/12/05. doi: 10.1002/phy2.67. PubMed PMID: 24303159; PMCID: PMC3841021.

260. Bischop DP, Orduz D, Lambot L, Schiffmann SN, Gall D. Control of neuronal excitability by calcium binding proteins: a new mathematical model for striatal fast-spiking interneurons. Front Mol Neurosci. 2012;5:78. Epub 2012/07/13. doi: 10.3389/fnmol.2012.00078. PubMed PMID: 22787441; PMCID: PMC3392946.

261. Soukupova M, Binaschi A, Falcicchia C, Zucchini S, Roncon P, Palma E, Magri E, Grandi E, Simonato M. Impairment of GABA release in the hippocampus at the time of the first spontaneous seizure in the pilocarpine model of temporal lobe epilepsy. Exp Neurol. 2014;257:39-49. Epub 2014/04/29. doi: 10.1016/j.expneurol.2014.04.014. PubMed PMID: 24768627.

262. Amilhon B, Huh CY, Manseau F, Ducharme G, Nichol H, Adamantidis A, Williams S. Parvalbumin Interneurons of Hippocampus Tune Population Activity at Theta Frequency. Neuron. 2015;86(5):1277-89. Epub 2015/06/08. doi: 10.1016/j.neuron.2015.05.027. PubMed PMID: 26050044.

263. Bohannon AS, Hablitz JJ. Optogenetic dissection of roles of specific cortical interneuron subtypes in GABAergic network synchronization. J Physiol. 2018;596(5):901-19. Epub 2017/12/24. doi: 10.1113/JP275317. PubMed PMID: 29274075; PMCID: PMC5830415.

264. Hu H, Roth FC, Vandael D, Jonas P. Complementary Tuning of Na(+) and K(+) Channel Gating Underlies Fast and Energy-Efficient Action Potentials in GABAergic Interneuron Axons. Neuron. 2018;98(1):156-65 e6. Epub 2018/04/06. doi: 10.1016/j.neuron.2018.02.024. PubMed PMID: 29621485; PMCID: PMC5896255.

265. Hu H, Jonas P. A supercritical density of Na(+) channels ensures fast signaling in GABAergic interneuron axons. Nat Neurosci. 2014;17(5):686-93. Epub 2014/03/25. doi: 10.1038/nn.3678. PubMed PMID: 24657965; PMCID: PMC4286295.

266. Inan M, Zhao M, Manuszak M, Karakaya C, Rajadhyaksha AM, Pickel VM, Schwartz TH, Goldstein PA, Manfredi G. Energy deficit in parvalbumin neurons leads to circuit dysfunction, impaired sensory gating and social disability. Neurobiol Dis. 2016;93:35-46. Epub 2016/04/24. doi: 10.1016/j.nbd.2016.04.004. PubMed PMID: 27105708.

267. Cabungcal JH, Steullet P, Morishita H, Kraftsik R, Cuenod M, Hensch TK, Do KQ. Perineuronal nets protect fast-spiking interneurons against oxidative stress. Proc Natl Acad Sci U S A. 2013;110(22):9130-5. Epub 2013/05/15. doi: 10.1073/pnas.1300454110. PubMed PMID: 23671099; PMCID: PMC3670388.

268. Chow A, Erisir A, Farb C, Nadal MS, Ozaita A, Lau D, Welker E, Rudy B. K(+) channel expression distinguishes subpopulations of parvalbumin- and somatostatin-containing neocortical interneurons. J Neurosci. 1999;19(21):9332-45. Epub 1999/10/26. PubMed PMID: 10531438.

269. Lien CC, Jonas P. Kv3 potassium conductance is necessary and kinetically optimized for high-frequency action potential generation in hippocampal interneurons. Journal of Neuroscience. 2003;23(6):2058-68. PubMed PMID: WOS:000181776900011.

270. Jukkola P, Gu Y, Lovett-Racke AE, Gu C. Suppression of Inflammatory Demyelinaton and Axon Degeneration through Inhibiting Kv3 Channels. Front Mol Neurosci. 2017;10:344. Epub 2017/11/11. doi: 10.3389/fnmol.2017.00344. PubMed PMID: 29123469; PMCID: PMC5662905.

271. Waxman SG, Craner MJ, Black JA. Na+ channel expression along axons in multiple sclerosis and its models. Trends Pharmacol Sci. 2004;25(11):584-91. Epub 2004/10/20. doi: 10.1016/j.tips.2004.09.001. PubMed PMID: 15491781.

272. Micheva KD, Wolman D, Mensh BD, Pax E, Buchanan J, Smith SJ, Bock DD. A large fraction of neocortical myelin ensheathes axons of local inhibitory neurons. Elife. 2016;5. Epub 2016/07/08. doi: 10.7554/eLife.15784. PubMed PMID: 27383052; PMCID: PMC4972537.

273. Stedehouder J, Couey JJ, Brizee D, Hosseini B, Slotman JA, Dirven CMF, Shpak G, Houtsmuller AB, Kushner SA. Fast-spiking Parvalbumin Interneurons are Frequently Myelinated in the Cerebral Cortex of Mice and Humans. Cereb Cortex. 2017;27(10):5001-13. Epub 2017/09/20. doi: 10.1093/cercor/bhx203. PubMed PMID: 28922832.

274. Stedehouder J, Brizee D, Shpak G, Kushner SA. Activity-Dependent Myelination of Parvalbumin Interneurons Mediated by Axonal Morphological Plasticity. J Neurosci. 2018;38(15):3631-42. Epub 2018/03/07. doi: 10.1523/JNEUROSCI.0074-18.2018. PubMed PMID: 29507147.

275. Micheva KD, Chang EF, Nana AL, Seeley WW, Ting JT, Cobbs C, Lein E, Smith SJ, Weinberg RJ, Madison DV. Distinctive Structural and Molecular Features of Myelinated Inhibitory Axons in Human Neocortex. eNeuro. 2018;5(5). Epub 2018/11/09. doi: 10.1523/ENEURO.0297-18.2018. PubMed PMID: 30406183; PMCID: PMC6220577.

276. Henske EP, Jozwiak S, Kingswood JC, Sampson JR, Thiele EA. Tuberous sclerosis complex. Nat Rev Dis Primers. 2016;2:16035. Epub 2016/05/27. doi: 10.1038/nrdp.2016.35. PubMed PMID: 27226234.

277. Bateup HS, Johnson CA, Denefrio CL, Saulnier JL, Kornacker K, Sabatini BL. Excitatory/inhibitory synaptic imbalance leads to hippocampal hyperexcitability in mouse models of tuberous sclerosis. Neuron. 2013;78(3):510-22. Epub 2013/05/15. doi: 10.1016/j.neuron.2013.03.017. PubMed PMID: 23664616; PMCID: PMC3690324.

278. Binder DK. Astrocytes: Stars of the Sacred Disease. Epilepsy Curr. 2018;18(3):172-9. Epub 2018/06/29. doi: 10.5698/1535-7597.18.3.172. PubMed PMID: 29950942; PMCID: PMC6017684.

279. Amiri M, Bahrami F, Janahmadi M. Functional contributions of astrocytes in synchronization of a neuronal network model. J Theor Biol. 2012;292:60-70. Epub 2011/10/08. doi: 10.1016/j.jtbi.2011.09.013. PubMed PMID: 21978738.

280. Heja L, Nyitrai G, Kekesi O, Dobolyi A, Szabo P, Fiath R, Ulbert I, Pal-Szenthe B, Palkovits M, Kardos J. Astrocytes convert network excitation to tonic inhibition of neurons. BMC Biol. 2012;10:26. Epub 2012/03/17. doi: 10.1186/1741-7007-10-26. PubMed PMID: 22420899; PMCID: PMC3342137.

281. Bedner P, Dupper A, Huttmann K, Muller J, Herde MK, Dublin P, Deshpande T, Schramm J, Haussler U, Haas CA, Henneberger C, Theis M, Steinhauser C. Astrocyte

uncoupling as a cause of human temporal lobe epilepsy. Brain. 2015;138(Pt 5):1208-22. Epub 2015/03/15. doi: 10.1093/brain/awv067. PubMed PMID: 25765328; PMCID: PMC5963418.

282. Diamond JS, Jahr CE. Synaptically released glutamate does not overwhelm transporters on hippocampal astrocytes during high-frequency stimulation. Journal of Neurophysiology. 2000;83(5):2835-43.

283. Rimmele TS, Rosenberg PA. GLT-1: The elusive presynaptic glutamate transporter. Neurochem Int. 2016;98:19-28. Epub 2016/05/01. doi: 10.1016/j.neuint.2016.04.010. PubMed PMID: 27129805; PMCID: PMC5070539.

284. Deemyad T, Luthi J, Spruston N. Astrocytes integrate and drive action potential firing in inhibitory subnetworks. Nat Commun. 2018;9(1):4336. Epub 2018/10/20. doi: 10.1038/s41467-018-06338-3. PubMed PMID: 30337521; PMCID: PMC6194108.

285. Domercq M, Etxebarria E, Perez-Samartin A, Matute C. Excitotoxic oligodendrocyte death and axonal damage induced by glutamate transporter inhibition. Glia. 2005;52(1):36-46. Epub 2005/05/14. doi: 10.1002/glia.20221. PubMed PMID: 15892126.

286. Heja L, Barabas P, Nyitrai G, Kekesi KA, Lasztoczi B, Toke O, Tarkanyi G, Madsen K, Schousboe A, Dobolyi A, Palkovits M, Kardos J. Glutamate uptake triggers transporter-mediated GABA release from astrocytes. PLoS One. 2009;4(9):e7153. Epub 2009/09/25. doi: 10.1371/journal.pone.0007153. PubMed PMID: 19777062; PMCID: PMC2744931.

287. Rossi S, Furlan R, De Chiara V, Motta C, Studer V, Mori F, Musella A, Bergami A, Muzio L, Bernardi G, Battistini L, Martino G, Centonze D. Interleukin-1beta causes synaptic hyperexcitability in multiple sclerosis. Ann Neurol. 2012;71(1):76-83. Epub 2012/01/26. doi: 10.1002/ana.22512. PubMed PMID: 22275254.

288. Papageorgiou IE, Lewen A, Galow LV, Cesetti T, Scheffel J, Regen T, Hanisch UK, Kann O. TLR4-activated microglia require IFN-gamma to induce severe neuronal dysfunction and death in situ. Proc Natl Acad Sci U S A. 2016;113(1):212-7. Epub 2015/12/25. doi: 10.1073/pnas.1513853113. PubMed PMID: 26699475; PMCID: PMC4711883.

289. Mandolesi G, Musella A, Gentile A, Grasselli G, Haji N, Sepman H, Fresegna D, Bullitta S, De Vito F, Musumeci G, Di Sanza C, Strata P, Centonze D. Interleukin-1beta alters glutamate transmission at purkinje cell synapses in a mouse model of multiple sclerosis. J Neurosci. 2013;33(29):12105-21. Epub 2013/07/19. doi: 10.1523/JNEUROSCI.5369-12.2013. PubMed PMID: 23864696; PMCID: PMC6794065.

290. Werner P, Pitt D, Raine CS. Multiple sclerosis: altered glutamate homeostasis in lesions correlates with oligodendrocyte and axonal damage. Ann Neurol. 2001;50(2):169-80. Epub 2001/08/17. doi: 10.1002/ana.1077. PubMed PMID: 11506399.

291. Fang J, Han D, Hong J, Tan Q, Tian Y. The chemokine, macrophage inflammatory protein-2gamma, reduces the expression of glutamate transporter-1 on astrocytes and increases neuronal sensitivity to glutamate excitotoxicity. J Neuroinflammation. 2012;9:267. Epub 2012/12/14. doi: 10.1186/1742-2094-9-267. PubMed PMID: 23234294; PMCID: PMC3545864.

292. Otis TS, Kavanaugh MP. Isolation of current components and partial reaction cycles in the glial glutamate transporter EAAT2. J Neurosci. 2000;20(8):2749-57. Epub 2001/02/07. PubMed PMID: 10751425; PMCID: PMC6772199.

293. Wallraff A, Kohling R, Heinemann U, Theis M, Willecke K, Steinhauser C. The impact of astrocytic gap junctional coupling on potassium buffering in the hippocampus. J Neurosci. 2006;26(20):5438-47. Epub 2006/05/19. doi: 10.1523/JNEUROSCI.0037-06.2006. PubMed PMID: 16707796; PMCID: PMC6675300.

294. Hibino H, Fujita A, Iwai K, Yamada M, Kurachi Y. Differential assembly of inwardly rectifying K+ channel subunits, Kir4.1 and Kir5.1, in brain astrocytes. J Biol Chem. 2004;279(42):44065-73. Epub 2004/08/18. doi: 10.1074/jbc.M405985200. PubMed PMID: 15310750.

295. Tanemoto M, Kittaka N, Inanobe A, Kurachi Y. In vivo formation of a proton-sensitive Kþ channel by heteromeric subunit assembly of Kir5.1 with Kir4.1. J Physiol. 2000;525(3):587-92.

296. Seifert G, Huttmann K, Binder DK, Hartmann C, Wyczynski A, Neusch C, Steinhauser C. Analysis of astroglial K+ channel expression in the developing hippocampus reveals a predominant role of the Kir4.1 subunit. J Neurosci. 2009;29(23):7474-88. Epub 2009/06/12. doi: 10.1523/JNEUROSCI.3790-08.2009. PubMed PMID: 19515915; PMCID: PMC6665420.

297. Brasko C, Hawkins V, De La Rocha IC, Butt AM. Expression of Kir4.1 and Kir5.1 inwardly rectifying potassium channels in oligodendrocytes, the myelinating cells of the CNS. Brain Struct Funct. 2017;222(1):41-59. Epub 2016/02/18. doi: 10.1007/s00429-016-1199-8. PubMed PMID: 26879293; PMCID: PMC5225165.

298. Schirmer L, Mobius W, Zhao C, Cruz-Herranz A, Ben Haim L, Cordano C, Shiow LR, Kelley KW, Sadowski B, Timmons G, Probstel AK, Wright JN, Sin JH, Devereux M, Morrison DE, Chang SM, Sabeur K, Green AJ, Nave KA, Franklin RJ, Rowitch DH. Oligodendrocyte-encoded Kir4.1 function is required for axonal integrity. Elife. 2018;7.

Epub 2018/09/12. doi: 10.7554/eLife.36428. PubMed PMID: 30204081; PMCID: PMC6167053.

299. Neusch C, Rozengurt N, Jacobs RE, Lester HA, Kofuji P. Kir4.1 potassium channel subunit is crucial for oligodendrocyte development and in vivo myelination. Journal of Neuroscience. 2001;21(15):5429-38. PubMed PMID: WOS:000170108900008.

300. Larson VA, Mironova Y, Vanderpool KG, Waisman A, Rash JE, Agarwal A, Bergles DE. Oligodendrocytes control potassium accumulation in white matter and seizure susceptibility. Elife. 2018;7. Epub 2018/03/30. doi: 10.7554/eLife.34829. PubMed PMID: 29596047; PMCID: PMC5903864.

301. Amiry-Moghaddam M, Williamson A, Palomba M, Eid T, de Lanerolle NC, Nagelhus EA, Adams ME, Froehner SC, Agre P, Ottersen OP. Delayed K+ clearance associated with aquaporin-4 mislocalization: phenotypic defects in brains of alpha-syntrophin-null mice. Proc Natl Acad Sci U S A. 2003;100(23):13615-20. Epub 2003/11/05. doi: 10.1073/pnas.2336064100. PubMed PMID: 14597704; PMCID: PMC263862.

302. Schirmer L, Srivastava R, Kalluri SR, Bottinger S, Herwerth M, Carassiti D, Srivastava B, Gempt J, Schlegel J, Kuhlmann T, Korn T, Reynolds R, Hemmer B. Differential loss of KIR4.1 immunoreactivity in multiple sclerosis lesions. Ann Neurol. 2014;75(6):810-28. Epub 2014/04/30. doi: 10.1002/ana.24168. PubMed PMID: 24777949.

303. Bedner P, Steinhauser C. Altered Kir and gap junction channels in temporal lobe epilepsy. Neurochem Int. 2013;63(7):682-7. Epub 2013/01/30. doi: 10.1016/j.neuint.2013.01.011. PubMed PMID: 23357483.

304. Olsen ML, Sontheimer H. Mislocalization of Kir channels in malignant glia. Glia. 2004;46(1):63-73. Epub 2004/03/05. doi: 10.1002/glia.10346. PubMed PMID: 14999814; PMCID: PMC2548404.

305. Zurolo E, de Groot M, Iyer A, Anink J, van Vliet EA, Heimans JJ, Reijneveld JC, Gorter JA, Aronica E. Regulation of Kir4.1 expression in astrocytes and astrocytic tumors: a role for interleukin-1 beta. J Neuroinflammation. 2012;9:280. Epub 2012/12/29. doi: 10.1186/1742-2094-9-280. PubMed PMID: 23270518; PMCID: PMC3538650.

306. Olsen ML, Sontheimer H. Functional implications for Kir4.1 channels in glial biology: from K+ buffering to cell differentiation. J Neurochem. 2008;107(3):589-601. Epub 2008/08/12. doi: 10.1111/j.1471-4159.2008.05615.x. PubMed PMID: 18691387; PMCID: PMC2581639.

307. Steinhauser C, Seifert G, Bedner P. Astrocyte dysfunction in temporal lobe epilepsy: K+ channels and gap junction coupling. Glia. 2012;60(8):1192-202. Epub 2012/02/14. doi: 10.1002/glia.22313. PubMed PMID: 22328245.

308. Ma B, Buckalew R, Du Y, Kiyoshi CM, Alford CC, Wang W, McTigue DM, Enyeart JJ, Terman D, Zhou M. Gap junction coupling confers isopotentiality on astrocyte syncytium. Glia. 2016;64(2):214-26. Epub 2015/10/06. doi: 10.1002/glia.22924. PubMed PMID: 26435164; PMCID: PMC4595908.

309. Sicca F, Ambrosini E, Marchese M, Sforna L, Servettini I, Valvo G, Brignone MS, Lanciotti A, Moro F, Grottesi A, Catacuzzeno L, Baldini S, Hasan S, D'Adamo MC, Franciolini F, Molinari P, Santorelli FM, Pessia M. Gain-of-function defects of astrocytic Kir4.1 channels in children with autism spectrum disorders and epilepsy. Sci Rep. 2016;6:34325. Epub 2016/09/30. doi: 10.1038/srep34325. PubMed PMID: 27677466; PMCID: PMC5039625.

310. Rao SB, Katoozi S, Skauli N, Froehner SC, Ottersen OP, Adams ME, Amiry-Moghaddam M. Targeted deletion of beta1-syntrophin causes a loss of Kir 4.1 from Muller cell endfeet in mouse retina. Glia. 2019;67(6):1138-49. Epub 2019/02/26. doi: 10.1002/glia.23600. PubMed PMID: 30803043; PMCID: PMC6462228.

311. Constantin B. Dystrophin complex functions as a scaffold for signalling proteins. Biochim Biophys Acta. 2014;1838(2):635-42. Epub 2013/09/12. doi: 10.1016/j.bbamem.2013.08.023. PubMed PMID: 24021238.

312. Amiry-Moghaddam M, Otsuka T, Hurn PD, Traystman RJ, Haug FM, Froehner SC, Adams ME, Neely JD, Agre P, Ottersen OP, Bhardwaj A. An alpha-syntrophin-dependent pool of AQP4 in astroglial end-feet confers bidirectional water flow between blood and brain. Proc Natl Acad Sci U S A. 2003;100(4):2106-11. Epub 2003/02/13. doi: 10.1073/pnas.0437946100. PubMed PMID: 12578959; PMCID: PMC149966.

313. Ben-Ari Y, Khalilov I, Kahle KT, Cherubini E. The GABA excitatory/inhibitory shift in brain maturation and neurological disorders. Neuroscientist. 2012;18(5):467-86. Epub 2012/05/02. doi: 10.1177/1073858412438697. PubMed PMID: 22547529.

314. Traynelis SF, Wollmuth LP, McBain CJ, Menniti FS, Vance KM, Ogden KK, Hansen KB, Yuan H, Myers SJ, Dingledine R. Glutamate receptor ion channels: structure, regulation, and function. Pharmacol Rev. 2010;62(3):405-96. Epub 2010/08/19. doi: 10.1124/pr.109.002451. PubMed PMID: 20716669; PMCID: PMC2964903.

315. Barker-Haliski M, White HS. Glutamatergic Mechanisms Associated with Seizures and Epilepsy. Cold Spring Harb Perspect Med. 2015;5(8):a022863. Epub 2015/06/24. doi: 10.1101/cshperspect.a022863. PubMed PMID: 26101204; PMCID: PMC4526718.

316. Lau A, Tymianski M. Glutamate receptors, neurotoxicity and neurodegeneration. Pflugers Arch. 2010;460(2):525-42. Epub 2010/03/17. doi: 10.1007/s00424-010-0809-1. PubMed PMID: 20229265.

317. Olloquequi J, Cornejo-Cordova E, Verdaguer E, Soriano FX, Binvignat O, Auladell C, Camins A. Excitotoxicity in the pathogenesis of neurological and psychiatric disorders: Therapeutic implications. J Psychopharmacol. 2018;32(3):265-75. Epub 2018/02/16. doi: 10.1177/0269881118754680. PubMed PMID: 29444621.

318. Hernandez DE, Salvadores NA, Moya-Alvarado G, Catalan RJ, Bronfman FC, Court FA. Axonal degeneration induced by glutamate excitotoxicity is mediated by necroptosis. J Cell Sci. 2018;131(22). Epub 2018/10/20. doi: 10.1242/jcs.214684. PubMed PMID: 30333135.

319. Twomey EC, Yelshanskaya MV, Grassucci RA, Frank J, Sobolevsky AI. Channel opening and gating mechanism in AMPA-subtype glutamate receptors. Nature. 2017;549(7670):60-5. Epub 2017/07/25. doi: 10.1038/nature23479. PubMed PMID: 28737760; PMCID: PMC5743206.

320. Jacobi E, von Engelhardt J. Diversity in AMPA receptor complexes in the brain. Curr Opin Neurobiol. 2017;45:32-8. Epub 2017/04/05. doi: 10.1016/j.conb.2017.03.001. PubMed PMID: 28376410.

321. Geiger JRP, Melcher T, Koh DS, Sakmann B, Seeburg PH, Jonas P, Monyer H. Relative abundance of subunit mRNAs determines gating and Ca2+ permeability of AMPA receptors in principal neurons and interneurons in rat CNS. Neuron. 1995;15(1):193-204. doi: 10.1016/0896-6273(95)90076-4.

322. Bochet P, Audinat E, Lambolez B, Crépel F, Rossier J, Iino M, Tsuzuki K, Ozawa S. Subunit composition at the single-cell level explains functional properties of a glutamate-gated channel. Neuron. 1994;12(2):383-8. doi: 10.1016/0896-6273(94)90279-8.

323. Jonas P, Racca C, Sakmann B, Seeburg PH, Monyer H. Differences in Ca2+ permeability of AMPA-type glutamate receptor channels in neocortical neurons caused by differential GluR-B subunit expression. Neuron. 1994;12(6):1281-9. Epub 1994/06/01. doi: 10.1016/0896-6273(94)90444-8. PubMed PMID: 8011338.

324. Das A, Bastian C, Trestan L, Suh J, Dey T, Trapp BD, Baltan S, Dana H. Reversible Loss of Hippocampal Function in a Mouse Model of Demyelination/Remyelination. Front Cell Neurosci. 2019;13:588. Epub 2020/02/11. doi: 10.3389/fncel.2019.00588. PubMed PMID: 32038176; PMCID: PMC6987410.

325. Chen X, Levy JM, Hou A, Winters C, Azzam R, Sousa AA, Leapman RD, Nicoll RA, Reese TS. PSD-95 family MAGUKs are essential for anchoring AMPA and NMDA receptor complexes at the postsynaptic density. Proc Natl Acad Sci U S A. 2015;112(50):E6983-92. Epub 2015/11/26. doi: 10.1073/pnas.1517045112. PubMed PMID: 26604311; PMCID: PMC4687590.

326. Chen X, Nelson CD, Li X, Winters CA, Azzam R, Sousa AA, Leapman RD, Gainer H, Sheng M, Reese TS. PSD-95 is required to sustain the molecular organization of the postsynaptic density. J Neurosci. 2011;31(17):6329-38. Epub 2011/04/29. doi: 10.1523/JNEUROSCI.5968-10.2011. PubMed PMID: 21525273; PMCID: PMC3099547.

327. Jeong J, Pandey S, Li Y, Badger JD, 2nd, Lu W, Roche KW. PSD-95 binding dynamically regulates NLGN1 trafficking and function. Proc Natl Acad Sci U S A. 2019;116(24):12035-44. Epub 2019/05/30. doi: 10.1073/pnas.1821775116. PubMed PMID: 31138690; PMCID: PMC6575593.

328. Niswender CM, Conn PJ. Metabotropic glutamate receptors: physiology, pharmacology, and disease. Annu Rev Pharmacol Toxicol. 2010;50:295-322. Epub 2010/01/09. doi: 10.1146/annurev.pharmtox.011008.145533. PubMed PMID: 20055706; PMCID: PMC2904507.

329. Pacheco Otalora LF, Couoh J, Shigamoto R, Zarei MM, Garrido Sanabria ER. Abnormal mGluR2/3 expression in the perforant path termination zones and mossy fibers of chronically epileptic rats. Brain Res. 2006;1098(1):170-85. Epub 2006/06/24. doi: 10.1016/j.brainres.2006.04.124. PubMed PMID: 16793029.

330. Ohishi H, Ogawa-Meguro R, Shigemoto R, Kaneko T, Nakanishi S, Mizuno N. Immunohistochemical localization of metabotropic glutamate receptors, mGluR2 and mGluR3, in rat cerebellar cortex. Neuron. 1994;13(1):55-66. Epub 1994/07/01. PubMed PMID: 8043281; PMCID: 8043281.

331. Jin LE, Wang M, Yang ST, Yang Y, Galvin VC, Lightbourne TC, Ottenheimer D, Zhong Q, Stein J, Raja A, Paspalas CD, Arnsten AFT. mGluR2/3 mechanisms in primate dorsolateral prefrontal cortex: evidence for both presynaptic and postsynaptic actions. Mol Psychiatry. 2017;22(11):1615-25. Epub 2016/08/10. doi: 10.1038/mp.2016.129. PubMed PMID: 27502475; PMCID: PMC5298940.

332. Caulder EH, Riegle MA, Godwin DW. Activation of group 2 metabotropic glutamate receptors reduces behavioral and electrographic correlates of pilocarpine induced status epilepticus. Epilepsy Res. 2014;108(2):171-81. Epub 2013/12/07. doi: 10.1016/j.eplepsyres.2013.10.009. PubMed PMID: 24305700; PMCID: PMC4378620.

333. Stevenson RF, Reagh ZM, Chun AP, Murray EA, Yassa MA. Pattern Separation and Source Memory Engage Distinct Hippocampal and Neocortical Regions during

Retrieval. J Neurosci. 2020;40(4):843-51. Epub 2019/11/22. doi: 10.1523/JNEUROSCI.0564-19.2019. PubMed PMID: 31748377; PMCID: PMC6975302.

334. Leal SL, Yassa MA. Integrating new findings and examining clinical applications of pattern separation. Nat Neurosci. 2018;21(2):163-73. Epub 2018/01/27. doi: 10.1038/s41593-017-0065-1. PubMed PMID: 29371654; PMCID: PMC5898810.

335. Montchal ME, Reagh ZM, Yassa MA. Precise temporal memories are supported by the lateral entorhinal cortex in humans. Nat Neurosci. 2019;22(2):284-8. Epub 2019/01/16. doi: 10.1038/s41593-018-0303-1. PubMed PMID: 30643291; PMCID: PMC6592045.

336. Tang W, Szokol K, Jensen V, Enger R, Trivedi CA, Hvalby O, Helm PJ, Looger LL, Sprengel R, Nagelhus EA. Stimulation-evoked Ca2+ signals in astrocytic processes at hippocampal CA3-CA1 synapses of adult mice are modulated by glutamate and ATP. J Neurosci. 2015;35(7):3016-21. Epub 2015/02/24. doi: 10.1523/JNEUROSCI.3319-14.2015. PubMed PMID: 25698739; PMCID: PMC4331625.

337. Huang YH, Sinha SR, Tanaka K, Rothstein JD, Bergles DE. Astrocyte glutamate transporters regulate metabotropic glutamate receptor-mediated excitation of hippocampal interneurons. J Neurosci. 2004;24(19):4551-9. Epub 2004/05/14. doi: 10.1523/JNEUROSCI.5217-03.2004. PubMed PMID: 15140926; PMCID: PMC6729403.

338. Sun W, McConnell E, Pare JF, Xu Q, Chen M, Peng W, Lovatt D, Han X, Smith Y, Nedergaard M. Glutamate-dependent neuroglial calcium signaling differs between young and adult brain. Science. 2013;339(6116):197-200. Epub 2013/01/12. doi: 10.1126/science.1226740. PubMed PMID: 23307741; PMCID: PMC3569008.

339. Lapato AS. (but postponed due to coronavirus pandemic)2020.

340. Drexel M, Romanov RA, Wood J, Weger S, Heilbronn R, Wulff P, Tasan RO, Harkany T, Sperk G. Selective Silencing of Hippocampal Parvalbumin Interneurons Induces Development of Recurrent Spontaneous Limbic Seizures in Mice. J Neurosci. 2017;37(34):8166-79. Epub 2017/07/25. doi: 10.1523/JNEUROSCI.3456-16.2017. PubMed PMID: 28733354.

341. Styr B, Slutsky I. Imbalance between firing homeostasis and synaptic plasticity drives early-phase Alzheimer's disease. Nat Neurosci. 2018;21(4):463-73. Epub 2018/02/07. doi: 10.1038/s41593-018-0080-x. PubMed PMID: 29403035; PMCID: PMC6533171.

342. Vossel KA, Ranasinghe KG, Beagle AJ, Mizuiri D, Honma SM, Dowling AF, Darwish SM, Van Berlo V, Barnes DE, Mantle M, Karydas AM, Coppola G, Roberson ED, Miller BL, Garcia PA, Kirsch HE, Mucke L, Nagarajan SS. Incidence and impact of

subclinical epileptiform activity in Alzheimer's disease. Ann Neurol. 2016;80(6):858-70. Epub 2016/10/04. doi: 10.1002/ana.24794. PubMed PMID: 27696483; PMCID: PMC5177487.

343. Hijazi S, Heistek TS, Scheltens P, Neumann U, Shimshek DR, Mansvelder HD, Smit AB, van Kesteren RE. Early restoration of parvalbumin interneuron activity prevents memory loss and network hyperexcitability in a mouse model of Alzheimer's disease. Mol Psychiatry. 2019. Epub 2019/08/23. doi: 10.1038/s41380-019-0483-4. PubMed PMID: 31431685.

344. Roth BL. DREADDs for Neuroscientists. Neuron. 2016;89(4):683-94. Epub 2016/02/20. doi: 10.1016/j.neuron.2016.01.040. PubMed PMID: 26889809; PMCID: PMC4759656.

345. Kamasawa N, Sik A, Morita M, Yasumura T, Davidson KG, Nagy JI, Rash JE. Connexin-47 and connexin-32 in gap junctions of oligodendrocyte somata, myelin sheaths, paranodal loops and Schmidt-Lanterman incisures: implications for ionic homeostasis and potassium siphoning. Neuroscience. 2005;136(1):65-86. Epub 2005/10/06. doi: 10.1016/j.neuroscience.2005.08.027. PubMed PMID: 16203097; PMCID: PMC1550704.

346. Wasseff SK, Scherer SS. Cx32 and Cx47 mediate oligodendrocyte:astrocyte and oligodendrocyte:oligodendrocyte gap junction coupling. Neurobiol Dis. 2011;42(3):506-13. Epub 2011/03/15. doi: 10.1016/j.nbd.2011.03.003. PubMed PMID: 21396451; PMCID: PMC3773476.

347. Benedetti B, Matyash V, Kettenmann H. Astrocytes control GABAergic inhibition of neurons in the mouse barrel cortex. J Physiol. 2011;589(Pt 5):1159-72. Epub 2011/01/13. doi: 10.1113/jphysiol.2010.203224. PubMed PMID: 21224221; PMCID: PMC3060594.

348. Guglielmetti C, Le Blon D, Santermans E, Salas-Perdomo A, Daans J, De Vocht N, Shah D, Hoornaert C, Praet J, Peerlings J, Kara F, Bigot C, Mai Z, Goossens H, Hens N, Hendrix S, Verhoye M, Planas AM, Berneman Z, van der Linden A, Ponsaerts P. Interleukin-13 immune gene therapy prevents CNS inflammation and demyelination via alternative activation of microglia and macrophages. Glia. 2016;64(12):2181-200. Epub 2016/10/21. doi: 10.1002/glia.23053. PubMed PMID: 27685637.

349. Ho YH, Lin YT, Wu CW, Chao YM, Chang AY, Chan JY. Peripheral inflammation increases seizure susceptibility via the induction of neuroinflammation and oxidative stress in the hippocampus. J Biomed Sci. 2015;22(1):46. Epub 2015/06/24. doi: 10.1186/s12929-015-0157-8. PubMed PMID: 26100815; PMCID: PMC4477313.

350. Auvin S, Shin D, Mazarati A, Sankar R. Inflammation induced by LPS enhances epileptogenesis in immature rat and may be partially reversed by IL1RA. Epilepsia. 2010;51 Suppl 3:34-8. Epub 2010/07/22. doi: 10.1111/j.1528-1167.2010.02606.x. PubMed PMID: 20618397; PMCID: PMC2910518.

351. Vezzani A, Balosso S, Ravizza T. The role of cytokines in the pathophysiology of epilepsy. Brain Behav Immun. 2008;22(6):797-803. Epub 2008/05/23. doi: 10.1016/j.bbi.2008.03.009. PubMed PMID: 18495419.

352. Mohebiany AN, Schneider R. Glutamate excitotoxicity in the cerebellum mediated by IL-1beta. J Neurosci. 2013;33(47):18353-5. Epub 2013/11/22. doi: 10.1523/JNEUROSCI.3946-13.2013. PubMed PMID: 24259559.

353. Cusick MF, Libbey JE, Patel DC, Doty DJ, Fujinami RS. Infiltrating macrophages are key to the development of seizures following virus infection. J Virol. 2013;87(3):1849-60. Epub 2012/12/14. doi: 10.1128/JVI.02747-12. PubMed PMID: 23236075; PMCID: PMC3554195.

354. Galarreta M, Hestrin S. A network of fast-spiking cells in the neocortex connected by electrical synapses. Nature. 1999;402(6757):72-5. Epub 1999/11/26. doi: 10.1038/47029. PubMed PMID: 10573418.

355. Prochnow N, Abdulazim A, Kurtenbach S, Wildforster V, Dvoriantchikova G, Hanske J, Petrasch-Parwez E, Shestopalov VI, Dermietzel R, Manahan-Vaughan D, Zoidl G. Pannexin1 stabilizes synaptic plasticity and is needed for learning. PLoS One. 2012;7(12):e51767. Epub 2013/01/04. doi: 10.1371/journal.pone.0051767. PubMed PMID: 23284764; PMCID: PMC3527502.

356. Thompson RJ, Jackson MF, Olah ME, Rungta RL, Hines DJ, Beazely MA, MacDonald JF, MacVicar BA. Activation of pannexin-1 hemichannels augments aberrant bursting in the hippocampus. Science. 2008;322(5907):1555-9. Epub 2008/12/06. doi: 10.1126/science.1165209. PubMed PMID: 19056988.

357. Markoullis K, Sargiannidou I, Gardner C, Hadjisavvas A, Reynolds R, Kleopa KA. Disruption of oligodendrocyte gap junctions in experimental autoimmune encephalomyelitis. Glia. 2012;60(7):1053-66. Epub 2012/03/31. doi: 10.1002/glia.22334. PubMed PMID: 22461072.

358. Loewenstein WR. Junctional intercellular communication: the cell-to-cell membrane channel. Physiol Rev. 1981;61(4):829-913. Epub 1981/10/01. doi: 10.1152/physrev.1981.61.4.829. PubMed PMID: 6270711.

359. May D, Tress O, Seifert G, Willecke K. Connexin47 protein phosphorylation and stability in oligodendrocytes depend on expression of Connexin43 protein in astrocytes. J

Neurosci. 2013;33(18):7985-96. Epub 2013/05/03. doi: 10.1523/JNEUROSCI.5874-12.2013. PubMed PMID: 23637189; PMCID: PMC6618970.

360. Giepmans BN, Verlaan I, Hengeveld T, Janssen H, Calafat J, Falk MM, Moolenaar WH. Gap junction protein connexin-43 interacts directly with microtubules. Curr Biol. 2001;11(17):1364-8. Epub 2001/09/13. doi: 10.1016/s0960-9822(01)00424-9. PubMed PMID: 11553331.

361. Pannasch U, Freche D, Dallerac G, Ghezali G, Escartin C, Ezan P, Cohen-Salmon M, Benchenane K, Abudara V, Dufour A, Lubke JH, Deglon N, Knott G, Holcman D, Rouach N. Connexin 30 sets synaptic strength by controlling astroglial synapse invasion. Nat Neurosci. 2014;17(4):549-58. Epub 2014/03/04. doi: 10.1038/nn.3662. PubMed PMID: 24584052.

362. Cheng A, Tang H, Cai J, Zhu M, Zhang X, Rao M, Mattson MP. Gap junctional communication is required to maintain mouse cortical neural progenitor cells in a proliferative state. Dev Biol. 2004;272(1):203-16. Epub 2004/07/10. doi: 10.1016/j.ydbio.2004.04.031. PubMed PMID: 15242801.

363. Santiago MF, Alcami P, Striedinger KM, Spray DC, Scemes E. The carboxyl-terminal domain of connexin43 is a negative modulator of neuronal differentiation. J Biol Chem. 2010;285(16):11836-45. Epub 2010/02/19. doi: 10.1074/jbc.M109.058750. PubMed PMID: 20164188; PMCID: PMC2852920.

364. Elias LA, Wang DD, Kriegstein AR. Gap junction adhesion is necessary for radial migration in the neocortex. Nature. 2007;448(7156):901-7. Epub 2007/08/24. doi: 10.1038/nature06063. PubMed PMID: 17713529.

365. Marins M, Xavier AL, Viana NB, Fortes FS, Froes MM, Menezes JR. Gap junctions are involved in cell migration in the early postnatal subventricular zone. Dev Neurobiol. 2009;69(11):715-30. Epub 2009/07/01. doi: 10.1002/dneu.20737. PubMed PMID: 19565626.

366. Zador Z, Weiczner R, Mihaly A. Long-lasting dephosphorylation of connexin 43 in acute seizures is regulated by NMDA receptors in the rat cerebral cortex. Mol Med Rep. 2008;1(5):721-7. Epub 2008/09/01. doi: 10.3892/mmr_00000019. PubMed PMID: 21479476.

367. Esseltine JL, Laird DW. Next-Generation Connexin and Pannexin Cell Biology. Trends Cell Biol. 2016;26(12):944-55. Epub 2016/06/25. doi: 10.1016/j.tcb.2016.06.003. PubMed PMID: 27339936.

368. Simard M, Nedergaard M. The neurobiology of glia in the context of water and ion homeostasis. Neuroscience. 2004;129(4):877-96. Epub 2004/11/25. doi: 10.1016/j.neuroscience.2004.09.053. PubMed PMID: 15561405.

369. Paul DL, Ebihara L, Takemoto LJ, Swenson KI, Goodenough DA. Connexin46, a novel lens gap junction protein, induces voltage-gated currents in nonjunctional plasma membrane of Xenopus oocytes. J Cell Biol. 1991;115(4):1077-89. Epub 1991/11/01. doi: 10.1083/jcb.115.4.1077. PubMed PMID: 1659572; PMCID: PMC2289939.

370. John SA, Kondo R, Wang SY, Goldhaber JI, Weiss JN. Connexin-43 hemichannels opened by metabolic inhibition. J Biol Chem. 1999;274(1):236-40. Epub 1998/12/29. doi: 10.1074/jbc.274.1.236. PubMed PMID: 9867835.

371. Kondo RP, Wang SY, John SA, Weiss JN, Goldhaber JI. Metabolic inhibition activates a non-selective current through connexin hemichannels in isolated ventricular myocytes. J Mol Cell Cardiol. 2000;32(10):1859-72. Epub 2000/10/03. doi: 10.1006/jmcc.2000.1220. PubMed PMID: 11013130.

372. Ebihara L, Steiner E. Properties of a nonjunctional current expressed from a rat connexin46 cDNA in Xenopus oocytes. J Gen Physiol. 1993;102(1):59-74. Epub 1993/07/01. doi: 10.1085/jgp.102.1.59. PubMed PMID: 7690837; PMCID: PMC2229167.

373. Valiunas V, Weingart R. Electrical properties of gap junction hemichannels identified in transfected HeLa cells. Pflugers Arch. 2000;440(3):366-79. Epub 2000/08/23. doi: 10.1007/s004240000294. PubMed PMID: 10954323.

374. Klaassen LJ, Sun Z, Steijaert MN, Bolte P, Fahrenfort I, Sjoerdsma T, Klooster J, Claassen Y, Shields CR, Ten Eikelder HM, Janssen-Bienhold U, Zoidl G, McMahon DG, Kamermans M. Synaptic transmission from horizontal cells to cones is impaired by loss of connexin hemichannels. PLoS Biol. 2011;9(7):e1001107. Epub 2011/08/04. doi: 10.1371/journal.pbio.1001107. PubMed PMID: 21811399; PMCID: PMC3139627.

375. Cherian PP, Siller-Jackson AJ, Gu S, Wang X, Bonewald LF, Sprague E, Jiang JX. Mechanical strain opens connexin 43 hemichannels in osteocytes: a novel mechanism for the release of prostaglandin. Mol Biol Cell. 2005;16(7):3100-6. Epub 2005/04/22. doi: 10.1091/mbc.e04-10-0912. PubMed PMID: 15843434; PMCID: PMC1165395.

376. Montero TD, Orellana JA. Hemichannels: new pathways for gliotransmitter release. Neuroscience. 2015;286:45-59. Epub 2014/12/06. doi: 10.1016/j.neuroscience.2014.11.048. PubMed PMID: 25475761.

377. MacVicar BA, Thompson RJ. Non-junction functions of pannexin-1 channels. Trends Neurosci. 2010;33(2):93-102. Epub 2009/12/22. doi: 10.1016/j.tins.2009.11.007. PubMed PMID: 20022389.

378. Penuela S, Bhalla R, Gong XQ, Cowan KN, Celetti SJ, Cowan BJ, Bai D, Shao Q, Laird DW. Pannexin 1 and pannexin 3 are glycoproteins that exhibit many distinct characteristics from the connexin family of gap junction proteins. J Cell Sci. 2007;120(Pt 21):3772-83. Epub 2007/10/11. doi: 10.1242/jcs.009514. PubMed PMID: 17925379.

379. Sosinsky GE, Boassa D, Dermietzel R, Duffy HS, Laird DW, MacVicar B, Naus CC, Penuela S, Scemes E, Spray DC, Thompson RJ, Zhao HB, Dahl G. Pannexin channels are not gap junction hemichannels. Channels (Austin). 2011;5(3):193-7. Epub 2011/05/03. doi: 10.4161/chan.5.3.15765. PubMed PMID: 21532340; PMCID: PMC3704572.

380. Pereda AE, Curti S, Hoge G, Cachope R, Flores CE, Rash JE. Gap junction-mediated electrical transmission: regulatory mechanisms and plasticity. Biochim Biophys Acta. 2013;1828(1):134-46. Epub 2012/06/05. doi: 10.1016/j.bbamem.2012.05.026. PubMed PMID: 22659675; PMCID: PMC3437247.

381. Santiago MF, Veliskova J, Patel NK, Lutz SE, Caille D, Charollais A, Meda P, Scemes E. Targeting pannexin1 improves seizure outcome. PLoS One. 2011;6(9):e25178. Epub 2011/09/29. doi: 10.1371/journal.pone.0025178. PubMed PMID: 21949881; PMCID: PMC3175002.

382. Kawamura M, Jr., Ruskin DN, Masino SA. Metabolic autocrine regulation of neurons involves cooperation among pannexin hemichannels, adenosine receptors, and KATP channels. J Neurosci. 2010;30(11):3886-95. Epub 2010/03/20. doi: 10.1523/JNEUROSCI.0055-10.2010. PubMed PMID: 20237259; PMCID: PMC2872120.

383. Masaki K. Early disruption of glial communication via connexin gap junction in multiple sclerosis, Balo's disease and neuromyelitis optica. Neuropathology. 2015;35(5):469-80. Epub 2015/05/29. doi: 10.1111/neup.12211. PubMed PMID: 26016402.

384. Niu J, Li T, Yi C, Huang N, Koulakoff A, Weng C, Li C, Zhao CJ, Giaume C, Xiao L. Connexin-based channels contribute to metabolic pathways in the oligodendroglial lineage. J Cell Sci. 2016;129(9):1902-14. Epub 2016/03/24. doi: 10.1242/jcs.178731. PubMed PMID: 27006115.

385. Schiza N, Sargiannidou I, Kagiava A, Karaiskos C, Nearchou M, Kleopa KA. Transgenic replacement of Cx32 in gap junction-deficient oligodendrocytes rescues the phenotype of a hypomyelinating leukodystrophy model. Hum Mol Genet. 2015;24(7):2049-64. Epub 2014/12/20. doi: 10.1093/hmg/ddu725. PubMed PMID: 25524707.

386. Gotoh L, Inoue K, Helman G, Mora S, Maski K, Soul JS, Bloom M, Evans SH, Goto YI, Caldovic L, Hobson GM, Vanderver A. GJC2 promoter mutations causing Pelizaeus-

Merzbacher-like disease. Mol Genet Metab. 2014;111(3):393-8. Epub 2014/01/01. doi: 10.1016/j.ymgme.2013.12.001. PubMed PMID: 24374284; PMCID: PMC4183365.

387. Sargiannidou I, Kim GH, Kyriakoudi S, Eun BL, Kleopa KA. A start codon CMT1X mutation associated with transient encephalomyelitis causes complete loss of Cx32. Neurogenetics. 2015;16(3):193-200. Epub 2015/03/17. doi: 10.1007/s10048-015-0442-4. PubMed PMID: 25771809.

388. Odermatt B, Wellershaus K, Wallraff A, Seifert G, Degen J, Euwens C, Fuss B, Bussow H, Schilling K, Steinhauser C, Willecke K. Connexin 47 (Cx47)-deficient mice with enhanced green fluorescent protein reporter gene reveal predominant oligodendrocytic expression of Cx47 and display vacuolized myelin in the CNS. J Neurosci. 2003;23(11):4549-59. Epub 2003/06/14. PubMed PMID: 12805295; PMCID: PMC6740816.

389. Menichella DM, Goodenough DA, Sirkowski E, Scherer SS, Paul DL. Connexins are critical for normal myelination in the CNS. J Neurosci. 2003;23(13):5963-73. Epub 2003/07/05. PubMed PMID: 12843301; PMCID: PMC6741267.

390. Tress O, Maglione M, May D, Pivneva T, Richter N, Seyfarth J, Binder S, Zlomuzica A, Seifert G, Theis M, Dere E, Kettenmann H, Willecke K. Panglial gap junctional communication is essential for maintenance of myelin in the CNS. J Neurosci. 2012;32(22):7499-518. Epub 2012/06/01. doi: 10.1523/JNEUROSCI.0392-12.2012. PubMed PMID: 22649229; PMCID: PMC6703577.

391. Kunze A, Congreso MR, Hartmann C, Wallraff-Beck A, Huttmann K, Bedner P, Requardt R, Seifert G, Redecker C, Willecke K, Hofmann A, Pfeifer A, Theis M, Steinhauser C. Connexin expression by radial glia-like cells is required for neurogenesis in the adult dentate gyrus. Proc Natl Acad Sci U S A. 2009;106(27):11336-41. Epub 2009/06/25. doi: 10.1073/pnas.0813160106. PubMed PMID: 19549869; PMCID: PMC2700144.

392. Belluardo N, Mudo G, Trovato-Salinaro A, Le Gurun S, Charollais A, Serre-Beinier V, Amato G, Haefliger JA, Meda P, Condorelli DF. Expression of connexin36 in the adult and developing rat brain. Brain Res. 2000;865(1):121-38. Epub 2000/05/18. doi: 10.1016/s0006-8993(00)02300-3. PubMed PMID: 10814742.

393. Bruzzone R, Hormuzdi SG, Barbe MT, Herb A, Monyer H. Pannexins, a family of gap junction proteins expressed in brain. Proc Natl Acad Sci U S A. 2003;100(23):13644-9. Epub 2003/11/05. doi: 10.1073/pnas.2233464100. PubMed PMID: 14597722; PMCID: PMC263867.

394. Kreuzberg MM, Deuchars J, Weiss E, Schober A, Sonntag S, Wellershaus K, Draguhn A, Willecke K. Expression of connexin30.2 in interneurons of the central nervous

system in the mouse. Mol Cell Neurosci. 2008;37(1):119-34. Epub 2007/10/19. doi: 10.1016/j.mcn.2007.09.003. PubMed PMID: 17942321.

395. Rash JE, Staines WA, Yasumura T, Patel D, Furman CS, Stelmack GL, Nagy JI. Immunogold evidence that neuronal gap junctions in adult rat brain and spinal cord contain connexin-36 but not connexin-32 or connexin-43. Proc Natl Acad Sci U S A. 2000;97(13):7573-8. Epub 2000/06/22. doi: 10.1073/pnas.97.13.7573. PubMed PMID: 10861019; PMCID: PMC16587.

396. Rozental R, Morales M, Mehler MF, Urban M, Kremer M, Dermietzel R, Kessler JA, Spray DC. Changes in the properties of gap junctions during neuronal differentiation of hippocampal progenitor cells. J Neurosci. 1998;18(5):1753-62. Epub 1998/03/07. PubMed PMID: 9465000; PMCID: PMC6792627.

397. Schutte M, Chen S, Buku A, Wolosin JM. Connexin50, a gap junction protein of macrogliaP6n the mammalian retina and visual pathway. Exp Eye Res. 1998;66(5):605-13. Epub 1998/06/17. doi: 10.1006/exer.1997.0460. PubMed PMID: 9628808.

398. Swayne LA, Bennett SA. Connexins and pannexins in neuronal development and adult neurogenesis. BMC Cell Biol. 2016;17 Suppl 1(1):10. Epub 2016/05/28. doi: 10.1186/s12860-016-0089-5. PubMed PMID: 27230672; PMCID: PMC4896249.

399. Vis JC, Nicholson LF, Faull RL, Evans WH, Severs NJ, Green CR. Connexin expression in Huntington's diseased human brain. Cell Biol Int. 1998;22(11-12):837-47. Epub 2000/06/30. doi: 10.1006/cbir.1998.0388. PubMed PMID: 10873295.

400. Weickert S, Ray A, Zoidl G, Dermietzel R. Expression of neural connexins and pannexin1 in the hippocampus and inferior olive: a quantitative approach. Brain Res Mol Brain Res. 2005;133(1):102-9. Epub 2005/01/22. doi: 10.1016/j.molbrainres.2004.09.026. PubMed PMID: 15661370.

401. Apostolides PF, Trussell LO. Regulation of interneuron excitability by gap junction coupling with principal cells. Nat Neurosci. 2013;16(12):1764-72. Epub 2013/11/05. doi: 10.1038/nn.3569. PubMed PMID: 24185427; PMCID: PMC3963432.

402. Condorelli DF, Belluardo N, Trovato-Salinaro A, Mudo G. Expression of Cx36 in mammalian neurons. Brain Res Brain Res Rev. 2000;32(1):72-85. Epub 2000/04/07. doi: 10.1016/s0165-0173(99)00068-5. PubMed PMID: 10751658.

403. Deans MR, Gibson JR, Sellitto C, Connors BW, Paul DL. Synchronous activity of inhibitory networks in neocortex requires electrical synapses containing connexin36. Neuron. 2001;31(3):477-85. Epub 2001/08/23. doi: 10.1016/s0896-6273(01)00373-7. PubMed PMID: 11516403.

404. Landisman CE, Long MA, Beierlein M, Deans MR, Paul DL, Connors BW. Electrical synapses in the thalamic reticular nucleus. J Neurosci. 2002;22(3):1002-9. Epub 2002/02/05. PubMed PMID: 11826128; PMCID: PMC6758490.

405. Sevetson J, Haas JS. Asymmetry and modulation of spike timing in electrically coupled neurons. J Neurophysiol. 2015;113(6):1743-51. Epub 2014/12/30. doi: 10.1152/jn.00843.2014. PubMed PMID: 25540226.

406. Wang MH, Chen N, Wang JH. The coupling features of electrical synapses modulate neuronal synchrony in hypothalamic superachiasmatic nucleus. Brain Res. 2014;1550:9-17. Epub 2014/01/21. doi: 10.1016/j.brainres.2014.01.007. PubMed PMID: 24440632.

407. Turecek J, Yuen GS, Han VZ, Zeng XH, Bayer KU, Welsh JP. NMDA receptor activation strengthens weak electrical coupling in mammalian brain. Neuron. 2014;81(6):1375-88. Epub 2014/03/25. doi: 10.1016/j.neuron.2014.01.024. PubMed PMID: 24656255; PMCID: PMC4266555.

408. Frisch C, De Souza-Silva MA, Sohl G, Guldenagel M, Willecke K, Huston JP, Dere E. Stimulus complexity dependent memory impairment and changes in motor performance after deletion of the neuronal gap junction protein connexin36 in mice. Behav Brain Res. 2005;157(1):177-85. Epub 2004/12/25. doi: 10.1016/j.bbr.2004.06.023. PubMed PMID: 15617784.

409. Wang Y, Belousov AB. Deletion of neuronal gap junction protein connexin 36 impairs hippocampal LTP. Neurosci Lett. 2011;502(1):30-2. Epub 2011/07/30. doi: 10.1016/j.neulet.2011.07.018. PubMed PMID: 21798314; PMCID: PMC3159746.

410. Lasztoczi B, Klausberger T. Layer-specific GABAergic control of distinct gamma oscillations in the CA1 hippocampus. Neuron. 2014;81(5):1126-39. Epub 2014/03/13. doi: 10.1016/j.neuron.2014.01.021. PubMed PMID: 24607232.

411. Bikbaev A, Manahan-Vaughan D. Relationship of hippocampal theta and gamma oscillations to potentiation of synaptic transmission. Front Neurosci. 2008;2(1):56-63. Epub 2008/11/05. doi: 10.3389/neuro.01.010.2008. PubMed PMID: 18982107; PMCID: PMC2570077.

412. Vandecasteele M, Glowinski J, Venance L. Connexin mRNA expression in single dopaminergic neurons of substantia nigra pars compacta. Neurosci Res. 2006;56(4):419-26. Epub 2006/10/04. doi: 10.1016/j.neures.2006.08.013. PubMed PMID: 17014920.

413. Venance L, Glowinski J, Giaume C. Electrical and chemical transmission between striatal GABAergic output neurones in rat brain slices. J Physiol. 2004;559(Pt 1):215-30.

Epub 2004/07/06. doi: 10.1113/jphysiol.2004.065672. PubMed PMID: 15235091; PMCID: PMC1665072.

414. Leussis MP, Bolivar VJ. Habituation in rodents: a review of behavior, neurobiology, and genetics. Neurosci Biobehav Rev. 2006;30(7):1045-64. Epub 2006/06/16. doi: 10.1016/j.neubiorev.2006.03.006. PubMed PMID: 16774787.

415. Dere E, Zheng-Fischhofer Q, Viggiano D, Gironi Carnevale UA, Ruocco LA, Zlomuzica A, Schnichels M, Willecke K, Huston JP, Sadile AG. Connexin31.1 deficiency in the mouse impairs object memory and modulates open-field exploration, acetylcholine esterase levels in the striatum, and cAMP response element-binding protein levels in the striatum and piriform cortex. Neuroscience. 2008;153(2):396-405. Epub 2008/04/04. doi: 10.1016/j.neuroscience.2008.01.077. PubMed PMID: 18384970.

416. Morris RG, Moser EI, Riedel G, Martin SJ, Sandin J, Day M, O'Carroll C. Elements of a neurobiological theory of the hippocampus: the role of activity-dependent synaptic plasticity in memory. Philos Trans R Soc Lond B Biol Sci. 2003;358(1432):773-86. Epub 2003/05/15. doi: 10.1098/rstb.2002.1264. PubMed PMID: 12744273; PMCID: PMC1693159.

417. Nagy JI, Li X, Rempel J, Stelmack G, Patel D, Staines WA, Yasumura T, Rash JE. Connexin26 in adult rodent central nervous system: demonstration at astrocytic gap junctions and colocalization with connexin30 and connexin43. J Comp Neurol. 2001;441(4):302-23. Epub 2001/12/18. doi: 10.1002/cne.1414. PubMed PMID: 11745652.

418. Dermietzel R, Traub O, Hwang TK, Beyer E, Bennett MV, Spray DC, Willecke K. Differential expression of three gap junction proteins in developing and mature brain tissues. Proc Natl Acad Sci U S A. 1989;86(24):10148-52. Epub 1989/12/01. doi: 10.1073/pnas.86.24.10148. PubMed PMID: 2557621; PMCID: PMC298664.

419. Domercq M, Perez-Samartin A, Aparicio D, Alberdi E, Pampliega O, Matute C. P2X7 receptors mediate ischemic damage to oligodendrocytes. Glia. 2010;58(6):730-40. Epub 2009/12/24. doi: 10.1002/glia.20958. PubMed PMID: 20029962.

420. Nagy JI, Ionescu AV, Lynn BD, Rash JE. Coupling of astrocyte connexins Cx26, Cx30, Cx43 to oligodendrocyte Cx29, Cx32, Cx47: Implications from normal and connexin32 knockout mice. Glia. 2003;44(3):205-18. Epub 2003/11/07. doi: 10.1002/glia.10278. PubMed PMID: 14603462; PMCID: PMC1852517.

421. Maglione M, Tress O, Haas B, Karram K, Trotter J, Willecke K, Kettenmann H. Oligodendrocytes in mouse corpus callosum are coupled via gap junction channels formed by connexin47 and connexin32. Glia. 2010;58(9):1104-17. Epub 2010/05/15. doi: 10.1002/glia.20991. PubMed PMID: 20468052.

422. Griemsmann S, Hoft SP, Bedner P, Zhang J, von Staden E, Beinhauer A, Degen J, Dublin P, Cope DW, Richter N, Crunelli V, Jabs R, Willecke K, Theis M, Seifert G, Kettenmann H, Steinhauser C. Characterization of Panglial Gap Junction Networks in the Thalamus, Neocortex, and Hippocampus Reveals a Unique Population of Glial Cells. Cereb Cortex. 2015;25(10):3420-33. Epub 2014/07/20. doi: 10.1093/cercor/bhu157. PubMed PMID: 25037920; PMCID: PMC4585496.

423. Menichella DM, Majdan M, Awatramani R, Goodenough DA, Sirkowski E, Scherer SS, Paul DL. Genetic and physiological evidence that oligodendrocyte gap junctions contribute to spatial buffering of potassium released during neuronal activity. J Neurosci. 2006;26(43):10984-91. Epub 2006/10/27. doi: 10.1523/JNEUROSCI.0304-06.2006. PubMed PMID: 17065440; PMCID: PMC6674647.

424. Nualart-Marti A, Solsona C, Fields RD. Gap junction communication in myelinating glia. Biochim Biophys Acta. 2013;1828(1):69-78. Epub 2012/02/14. doi: 10.1016/j.bbamem.2012.01.024. PubMed PMID: 22326946; PMCID: PMC4474145.

425. Kim JE, Kang TC. The P2X7 receptor-pannexin-1 complex decreases muscarinic acetylcholine receptor-mediated seizure susceptibility in mice. J Clin Invest. 2011;121(5):2037-47. Epub 2011/04/21. doi: 10.1172/JCI44818. PubMed PMID: 21505260; PMCID: PMC3083785.

426. Zoidl G, Petrasch-Parwez E, Ray A, Meier C, Bunse S, Habbes HW, Dahl G, Dermietzel R. Localization of the pannexin1 protein at postsynaptic sites in the cerebral cortex and hippocampus. Neuroscience. 2007;146(1):9-16. Epub 2007/03/24. doi: 10.1016/j.neuroscience.2007.01.061. PubMed PMID: 17379420.

427. Ardiles AO, Flores-Munoz C, Toro-Ayala G, Cardenas AM, Palacios AG, Munoz P, Fuenzalida M, Saez JC, Martinez AD. Pannexin 1 regulates bidirectional hippocampal synaptic plasticity in adult mice. Front Cell Neurosci. 2014;8:326. Epub 2014/11/02. doi: 10.3389/fncel.2014.00326. PubMed PMID: 25360084; PMCID: PMC4197765.

428. Moser EI, Krobert KA, Moser MB, Morris RG. Impaired spatial learning after saturation of long-term potentiation. Science. 1998;281(5385):2038-42. Epub 1998/09/25. doi: 10.1126/science.281.5385.2038. PubMed PMID: 9748165.

429. Kawamura M, Gachet C, Inoue K, Kato F. Direct excitation of inhibitory interneurons by extracellular ATP mediated by P2Y1 receptors in the hippocampal slice. J Neurosci. 2004;24(48):10835-45. Epub 2004/12/03. doi: 10.1523/JNEUROSCI.3028-04.2004. PubMed PMID: 15574734; PMCID: PMC6730213.

430. Boison D, Aronica E. Comorbidities in Neurology: Is adenosine the common link? Neuropharmacology. 2015;97:18-34. Epub 2015/05/17. doi: 10.1016/j.neuropharm.2015.04.031. PubMed PMID: 25979489; PMCID: PMC4537378.

431. Diogenes MJ, Neves-Tome R, Fucile S, Martinello K, Scianni M, Theofilas P, Lopatar J, Ribeiro JA, Maggi L, Frenguelli BG, Limatola C, Boison D, Sebastiao AM. Homeostatic control of synaptic activity by endogenous adenosine is mediated by adenosine kinase. Cereb Cortex. 2014;24(1):67-80. Epub 2012/09/22. doi: 10.1093/cercor/bhs284. PubMed PMID: 22997174; PMCID: PMC3862265.

432. Jacobson GM, Voss LJ, Melin SM, Mason JP, Cursons RT, Steyn-Ross DA, Steyn-Ross ML, Sleigh JW. Connexin36 knockout mice display increased sensitivity to pentylenetetrazol-induced seizure-like behaviors. Brain Res. 2010;1360:198-204. Epub 2010/09/14. doi: 10.1016/j.brainres.2010.09.006. PubMed PMID: 20833151.

433. Maier N, Guldenagel M, Sohl G, Siegmund H, Willecke K, Draguhn A. Reduction of high-frequency network oscillations (ripples) and pathological network discharges in hippocampal slices from connexin 36-deficient mice. J Physiol. 2002;541(Pt 2):521-8. Epub 2002/06/04. doi: 10.1113/jphysiol.2002.017624. PubMed PMID: 12042356; PMCID: PMC2290340.

434. Beaumont M, Maccaferri G. Is connexin36 critical for GABAergic hypersynchronization in the hippocampus? J Physiol. 2011;589(Pt 7):1663-80. Epub 2011/02/09. doi: 10.1113/jphysiol.2010.201491. PubMed PMID: 21300748; PMCID: PMC3099022.

435. Voss LJ, Mutsaerts N, Sleigh JW. Connexin36 gap junction blockade is ineffective at reducing seizure-like event activity in neocortical mouse slices. Epilepsy Res Treat. 2010;2010:310753. Epub 2010/01/01. doi: 10.1155/2010/310753. PubMed PMID: 22937225; PMCID: PMC3428610.

436. Srinivas M, Hopperstad MG, Spray DC. Quinine blocks specific gap junction channel subtypes. Proc Natl Acad Sci U S A. 2001;98(19):10942-7. Epub 2001/09/06. doi: 10.1073/pnas.191206198. PubMed PMID: 11535816; PMCID: PMC58578.

437. Voss LJ, Jacobson G, Sleigh JW, Steyn-Ross A, Steyn-Ross M. Excitatory effects of gap junction blockers on cerebral cortex seizure-like activity in rats and mice. Epilepsia. 2009;50(8):1971-8. Epub 2009/06/03. doi: 10.1111/j.1528-1167.2009.02087.x. PubMed PMID: 19486358.

438. Pais I, Hormuzdi SG, Monyer H, Traub RD, Wood IC, Buhl EH, Whittington MA, LeBeau FE. Sharp wave-like activity in the hippocampus in vitro in mice lacking the gap junction protein connexin 36. J Neurophysiol. 2003;89(4):2046-54. Epub 2003/04/11. doi: 10.1152/jn.00549.2002. PubMed PMID: 12686578.

439. Schlingloff D, Kali S, Freund TF, Hajos N, Gulyas AI. Mechanisms of sharp wave initiation and ripple generation. J Neurosci. 2014;34(34):11385-98. Epub 2014/08/22. doi: 10.1523/JNEUROSCI.0867-14.2014. PubMed PMID: 25143618; PMCID: PMC6615505.

440. Gajda Z, Szupera Z, Blazso G, Szente M. Quinine, a blocker of neuronal cx36 channels, suppresses seizure activity in rat neocortex in vivo. Epilepsia. 2005;46(10):1581-91. Epub 2005/09/30. doi: 10.1111/j.1528-1167.2005.00254.x. PubMed PMID: 16190928.

441. Cruikshank SJ, Hopperstad M, Younger M, Connors BW, Spray DC, Srinivas M. Potent block of Cx36 and Cx50 gap junction channels by mefloquine. Proc Natl Acad Sci U S A. 2004;101(33):12364-9. Epub 2004/08/07. doi: 10.1073/pnas.0402044101. PubMed PMID: 15297615; PMCID: PMC514481.

442. Voss LJ, Melin S, Jacobson G, Sleigh JW. GABAergic compensation in connexin36 knock-out mice evident during low-magnesium seizure-like event activity. Brain Res. 2010;1360:49-55. Epub 2010/09/14. doi: 10.1016/j.brainres.2010.09.002. PubMed PMID: 20831861.

443. Vezzani A, French J, Bartfai T, Baram TZ. The role of inflammation in epilepsy. Nat Rev Neurol. 2011;7(1):31-40. Epub 2010/12/08. doi: 10.1038/nrneurol.2010.178. PubMed PMID: 21135885; PMCID: PMC3378051.

444. Brand-Schieber E, Werner P, Iacobas DA, Iacobas S, Beelitz M, Lowery SL, Spray DC, Scemes E. Connexin43, the major gap junction protein of astrocytes, is down-regulated in inflamed white matter in an animal model of multiple sclerosis. J Neurosci Res. 2005;80(6):798-808. Epub 2005/05/18. doi: 10.1002/jnr.20474. PubMed PMID: 15898103; PMCID: PMC1226319.

445. Binder DK, Nagelhus EA, Ottersen OP. Aquaporin-4 and epilepsy. Glia. 2012;60(8):1203-14. Epub 2012/03/02. doi: 10.1002/glia.22317. PubMed PMID: 22378467.

446. Parenti R, Cicirata F, Zappala A, Catania A, La Delia F, Cicirata V, Tress O, Willecke K. Dynamic expression of Cx47 in mouse brain development and in the cuprizone model of myelin plasticity. Glia. 2010;58(13):1594-609. Epub 2010/06/26. doi: 10.1002/glia.21032. PubMed PMID: 20578039.

447. Mylvaganam S, Zhang L, Wu C, Zhang ZJ, Samoilova M, Eubanks J, Carlen PL, Poulter MO. Hippocampal seizures alter the expression of the pannexin and connexin transcriptome. J Neurochem. 2010;112(1):92-102. Epub 2009/10/21. doi: 10.1111/j.1471-4159.2009.06431.x. PubMed PMID: 19840216.

448. Wasseff SK, Scherer SS. Activated microglia do not form functional gap junctions in vivo. J Neuroimmunol. 2014;269(1-2):90-3. Epub 2014/03/04. doi: 10.1016/j.jneuroim.2014.02.005. PubMed PMID: 24582000; PMCID: PMC4048983.

449. Dobrenis K, Chang HY, Pina-Benabou MH, Woodroffe A, Lee SC, Rozental R, Spray DC, Scemes E. Human and mouse microglia express connexin36, and functional gap junctions are formed between rodent microglia and neurons. J Neurosci Res. 2005;82(3):306-15. Epub 2005/10/08. doi: 10.1002/jnr.20650. PubMed PMID: 16211561; PMCID: PMC2583240.

450. Maezawa I, Jin LW. Rett syndrome microglia damage dendrites and synapses by the elevated release of glutamate. J Neurosci. 2010;30(15):5346-56. Epub 2010/04/16. doi: 10.1523/JNEUROSCI.5966-09.2010. PubMed PMID: 20392956; PMCID: PMC5533099.

451. Eugenin EA, Eckardt D, Theis M, Willecke K, Bennett MV, Saez JC. Microglia at brain stab wounds express connexin 43 and in vitro form functional gap junctions after treatment with interferon-gamma and tumor necrosis factor-alpha. Proc Natl Acad Sci U S A. 2001;98(7):4190-5. Epub 2001/03/22. doi: 10.1073/pnas.051634298. PubMed PMID: 11259646; PMCID: PMC31201.

452. Takaki J, Fujimori K, Miura M, Suzuki T, Sekino Y, Sato K. L-glutamate released from activated microglia downregulates astrocytic L-glutamate transporter expression in neuroinflammation: the 'collusion' hypothesis for increased extracellular L-glutamate concentration in neuroinflammation. J Neuroinflammation. 2012;9:275. Epub 2012/12/25. doi: 10.1186/1742-2094-9-275. PubMed PMID: 23259598; PMCID: PMC3575281.

453. Takeuchi H, Jin S, Wang J, Zhang G, Kawanokuchi J, Kuno R, Sonobe Y, Mizuno T, Suzumura A. Tumor necrosis factor-alpha induces neurotoxicity via glutamate release from hemichannels of activated microglia in an autocrine manner. J Biol Chem. 2006;281(30):21362-8. Epub 2006/05/25. doi: 10.1074/jbc.M600504200. PubMed PMID: 16720574.

454. Akira S, Takeda K. Toll-like receptor signalling. Nat Rev Immunol. 2004;4(7):499-511. Epub 2004/07/02. doi: 10.1038/nri1391. PubMed PMID: 15229469.

455. Orellana JA, Moraga-Amaro R, Diaz-Galarce R, Rojas S, Maturana CJ, Stehberg J, Saez JC. Restraint stress increases hemichannel activity in hippocampal glial cells and neurons. Front Cell Neurosci. 2015;9:102. Epub 2015/04/18. doi: 10.3389/fncel.2015.00102. PubMed PMID: 25883550; PMCID: PMC4382970.

456. Walker FR, Nilsson M, Jones K. Acute and chronic stress-induced disturbances of microglial plasticity, phenotype and function. Curr Drug Targets. 2013;14(11):1262-76. Epub 2013/09/12. doi: 10.2174/13894501113149990208. PubMed PMID: 24020974; PMCID: PMC3788324.

457. Sperlagh B, Illes P. P2X7 receptor: an emerging target in central nervous system diseases. Trends Pharmacol Sci. 2014;35(10):537-47. Epub 2014/09/17. doi: 10.1016/j.tips.2014.08.002. PubMed PMID: 25223574.

458. Monif M, Reid CA, Powell KL, Drummond KJ, O'Brien TJ, Williams DA. Interleukin-1beta has trophic effects in microglia and its release is mediated by P2X7R pore. J Neuroinflammation. 2016;13(1):173. Epub 2016/07/02. doi: 10.1186/s12974-016-0621-8. PubMed PMID: 27364756; PMCID: PMC4929731.

459. Bravo D, Maturana CJ, Pelissier T, Hernandez A, Constandil L. Interactions of pannexin 1 with NMDA and P2X7 receptors in central nervous system pathologies: Possible role on chronic pain. Pharmacol Res. 2015;101:86-93. Epub 2015/07/28. doi: 10.1016/j.phrs.2015.07.016. PubMed PMID: 26211949.

460. Pan HC, Chou YC, Sun SH. P2X7 R-mediated Ca(2+) -independent d-serine release via pannexin-1 of the P2X7 R-pannexin-1 complex in astrocytes. Glia. 2015;63(5):877-93. Epub 2015/01/30. doi: 10.1002/glia.22790. PubMed PMID: 25630251.

461. Jiang T, Long H, Ma Y, Long L, Li Y, Li F, Zhou P, Yuan C, Xiao B. Altered expression of pannexin proteins in patients with temporal lobe epilepsy. Mol Med Rep. 2013;8(6):1801-6. Epub 2013/10/23. doi: 10.3892/mmr.2013.1739. PubMed PMID: 24146091.

462. Palacios-Prado N, Hoge G, Marandykina A, Rimkute L, Chapuis S, Paulauskas N, Skeberdis VA, O'Brien J, Pereda AE, Bennett MV, Bukauskas FF. Intracellular magnesium-dependent modulation of gap junction channels formed by neuronal connexin36. J Neurosci. 2013;33(11):4741-53. Epub 2013/03/15. doi: 10.1523/JNEUROSCI.2825-12.2013. PubMed PMID: 23486946; PMCID: PMC3635812.

463. Amhaoul H, Ali I, Mola M, Van Eetveldt A, Szewczyk K, Missault S, Bielen K, Kumar-Singh S, Rech J, Lord B, Ceusters M, Bhattacharya A, Dedeurwaerdere S. P2X7 receptor antagonism reduces the severity of spontaneous seizures in a chronic model of temporal lobe epilepsy. Neuropharmacology. 2016;105:175-85. Epub 2016/01/19. doi: 10.1016/j.neuropharm.2016.01.018. PubMed PMID: 26775823.

464. Mika T, Prochnow N. Functions of connexins and large pore channels on microglial cells: the gates to environment. Brain Res. 2012;1487:16-24. Epub 2012/07/31. doi: 10.1016/j.brainres.2012.07.020. PubMed PMID: 22842527.

465. Giaume C, Leybaert L, Naus CC, Saez JC. Connexin and pannexin hemichannels in brain glial cells: properties, pharmacology, and roles. Front Pharmacol. 2013;4:88. Epub 2013/07/25. doi: 10.3389/fphar.2013.00088. PubMed PMID: 23882216; PMCID: PMC3713369.